



HAL
open science

Polymer and surface modifications for antibacterial purposes

Thi Phuong Thu Nguyen

► **To cite this version:**

Thi Phuong Thu Nguyen. Polymer and surface modifications for antibacterial purposes. Polymers. Université Paris Saclay (COmUE), 2019. English. NNT : 2019SACLS449 . tel-03505878

HAL Id: tel-03505878

<https://theses.hal.science/tel-03505878>

Submitted on 1 Jan 2022

HAL is a multi-disciplinary open access archive for the deposit and dissemination of scientific research documents, whether they are published or not. The documents may come from teaching and research institutions in France or abroad, or from public or private research centers.

L'archive ouverte pluridisciplinaire **HAL**, est destinée au dépôt et à la diffusion de documents scientifiques de niveau recherche, publiés ou non, émanant des établissements d'enseignement et de recherche français ou étrangers, des laboratoires publics ou privés.

Polymer and surface modifications for antibacterial purposes

Thèse de doctorat de l'Université Paris-Saclay
préparé à l'Université Paris-Sud

École doctorale n°571 Molécules, Matériaux, Instrumentation et
Biosystèmes (2MIB)
Spécialité de doctorat: Chimie

Thèse présentée et soutenue à Orsay, le 28 Novembre, par

Thi Phuong Thu Nguyen

Composition du Jury :

Sophie Monge-Darcos	Rapporteur
Professeur, Université de Montpellier (UMR 5253)	
Yvette Tran	Rapporteur
Maitre de Conférences, ESPCI Paris (UMR 7615)	
Nadine Aubry-Barroca,	Examinatrice
Maitre de Conférences, Université Paris Sud (UMR 8182)	
Anne-Chantal Gouget-Laemmel	Examinatrice
Chargée de Recherche, École Polytechnique (UMR 7643)	
Philippe Guégan	Président
Professeur, Sorbonne Université (UMR 8232)	
Philippe Roger	Directeur de thèse
Professeur, Université Paris Sud (UMR 8182)	

Acknowledgement

Now the storm was over but the road is still long ahead. And me, I will always treasure the three years I have spent as a doctoral student in Equipe SM₂B at ICMMO, Université Paris Sud, Université Paris Saclay.

First and foremost, I'd like to express my most sincere gratitude to my supervisors – Prof. Philippe Roger and Dr. Nadine Aubry-Barroca – for their instructions and guidance during the course of my PhD. Without Philippe's expertise in polymer and Nadine's ultimate force in organic chemistry, this dissertation would have never been completed. As one of the side-effects of doing a PhD, at (many) times I was distracted and lost, these side-effects would have been irreversible without my supervisors' kindness, sympathy and encouragements.

Secondly, I'm deeply acknowledged the rest of my thesis committee: Prof. Sophie Monge-Darcos, Dr. Yvette Tran, Dr. Anne-Chantal Gouget-Laemmel and Prof. Philippe Guegan for their insightful discussions during the defense as well as their suggestions and comments for the improvement of this thesis.

I am also thankful for the countless scientific and emotional supports that I have received from other members of the team SM₂B. My heartfelt appreciation goes towards Dr. Caroline Aymes-Chodur and Dr. Hanène Salmi for being there whenever I have a problem technically or personally. To Mohamad, thank you so much for all the discussions we had together and your kind instruction when I was still a newbie to SARA-ATRP (as you preferred). Thank you, Ludovic, for passing all of my polymers despite the issues we had encountered with the SEC. I am grateful for the help from Dr. Yann Bourdreux, Dr. Gilles Doisneau and Ludovic (again) for the synthesis of “glucose × sesamol”. My profound appreciation is given to Dr. Christophe Regnard of Institute de Biologie Integrative de la Cellule (I2BC) – Université Paris Sud and his students for their time carrying out the biological tests on my surfaces. Furthermore, a great deal of work in this thesis contains the assistance from technical platform of ICMMO, notably Dr. Diana Dragoie for our endless discussion on XPS results.

These years have passed so rapidly with so many fun and memories thanks to the friendly environment on the floor as well as many coffee breaks that I have enjoyed with Marisol, Marie, Mélanie, Nacim Manon, Junjun, Shu Han, Abdel-Wahab, Aurélien, Jérôme, Pauline, Christine, David, and so on. Mon français avait amélioré énormément grâce à vous.

My endless gratitude is given to my boyfriend for being by my side since I was a bachelor student till now when I'm becoming a doctor. I'm so thankful to have you, but the score is 1-1 now, isn't it? And - you know it's your turn, Anny - thank you for always being a keen listener and an amazing friend. I am also blessed to have the support from my friends not only in Vietnam, in France, but also from other corners of the world whose names would take several pages to complete.

I'd like to send my deepest acknowledgement to my parents and my sister, who always (and always will) support and respect my decisions even though such decisions took me so far away from home. Without their trust in me, I could have never come this far, done this much and become the person I am today. Thanks to them, I know that no matter what I do, how hard I fall, how weak and small I am, I still can achieve what I want because I have their DNAs – that's my secret internal force.

Lastly, to me of today, thank you for never giving up because no matter where life will lead us to, we will certainly never regret this!

Sceaux, December 16, 2019

Vive le polymère.

Table of Contents

Table of Contents	1
Abbreviation	5
General Introduction	7
Chapter 1. Bibliography	9
<i>1.1. Antibacterial surfaces.....</i>	9
1.1.1. The needs of new antibacterial surfaces	9
1.1.2. Mechanisms and examples of antimicrobial surfaces	10
<i>1.2. Poly(ethylene terephthalate) (PET) as template for post-modification</i>	16
1.2.1. PET: a material of excellence	16
1.2.2. Surface-modification of PET	18
<i>1.3. Reversible Deactivation Radical Polymerization and Surface-initiated Polymerization</i>	21
1.3.1. Reversible Addition–Fragmentation Chain Transfer Polymerization	24
1.3.2. Nitroxide-Mediated Polymerization (NMP).....	26
1.3.3. Atom Transfer Radical Polymerization (ATRP)	28
1.3.4. Cu(0)-mediated RDRP	32
<i>1.4. Polymer Post-modification</i>	36
1.4.1. N-hydroxysuccinimide esters	37
1.4.2. Pentafluorophenyl (meth)acrylates	39
<i>1.5. Conclusion</i>	45
Chapter 2. Polymerization of active esters in solution	47
<i>2.1. Cu(0)-mediated Reversible Deactivation Radical Polymerization of PFPMA.....</i>	47
2.1.1. A note on synthesis of PFPMA	47
2.1.2. Determination of refractive index increment for SEC analysis.....	50
2.1.3. Influence of solvent	50
2.1.4. Synergic influence of ligand and initiator	55
2.1.5. Influence of zero valent copper	59
2.1.1. Kinetics of Cu(0)-mediated RDRP under optimal conditions.....	60

2.2. End-chain analysis	62
2.2.2. Chain extension of PFPMA-Br as macro-initiator	67
2.2.3. Termination or immortality: “In the long run we are all dead”	68
2.2.4. Characterization of PFPMA by other analyses	69
2.2.5. Conclusion	72
2.3. Cu(0)-mediated Reversible Deactivation Radical Polymerization of NPMA	73
2.4. Cu(0)-mediated Reversible Deactivation Radical Copolymerization.....	76
2.4.1. NMR analysis: total conversion, solubility and composition.....	77
2.4.2. FTIR analysis: chemical environment analysis	82
2.4.3. X-ray Photon Spectroscopy: details on composition of copolymers.....	85
2.4.4. Thermal properties of copolymers.....	90
2.4.5. Conclusion	92
2.5. Conclusion	93
Chapter 3. Surface-initiated polymerization of active esters	95
3.1. Immobilization of initiator onto PET films	95
3.2. PET-initiated Cu(0)-mediated RDRP of PFPMA	100
3.2.1. Water contact angle	101
3.2.2. ATR FTIR.....	103
3.2.3. XPS analysis	104
3.2.4. Surface topology by AFM and SEM	106
3.2.5. Conclusion	108
3.3. PET-initiated Cu(0)-mediated RDRP of NPMA	108
3.4. PET-initiated Cu(0)-mediated RDRP of NPMA and PFPMA	113
3.5. Conclusion	117
Chapter 4. Post-modification of reactive polyesters in solution.....	119
4.1. Post-modification of PFPMA	119
4.1.1. Post-modification with amines	119
4.1.2. Post-modification with essential oils.....	124
4.1.3. Post-modification with sugars and their derivatives.....	144
4.1.1. Conclusion	150
4.2. Post-modification of PNPMA.....	151

4.2.1.	Post-modification with amines	151
4.2.2.	Reduction of nitro groups	152
4.2.3.	Conclusion	154
4.3.	<i>Post-modification of copolymers</i>	155
4.4.	<i>Conclusion</i>	157
Chapter 5. Post-modification of PET-g-PPFPMA and bacterial adhesion on functionalized PET films		159
5.1.	<i>Post-modification of PET-g-PPFPMA</i>	159
5.1.1.	Post-modification of PET-g-PPFPMA with geraniol	159
5.1.2.	Post-modification of PET-g-PPFPMA with citronellol.....	163
5.1.3.	Post-modification of PET-g-PPFPMA with sesamol	166
5.2.	<i>Bacterial adhesion on functionalized PET films</i>	169
5.2.1.	Adhesion of bacteria on PET-g-PCiMA.....	170
5.2.2.	Adhesion of bacteria on PET-g-PSeMA	170
5.3.	<i>Conclusion</i>	172
Chapter 6. Conclusions and Perspectives.....		173
Materials and Methods		175
Experimental.....		178
References		183

Abbreviations

4VP	<i>p</i> -vinyl pyridine
AFM	atomic force microscope
AIBN	azobisisobutyronitrile
AMR	antimicrobial resistance
ATR FTIR	attenuated total reflection fourier transform infrared spectroscopy
ATRP	atom transfer radical polymerization
BE	binding energy
BzCl	benzyl chloride
CDC13	deuterated chloroform
CFU	colony-forming unit
CPS	count per second
CTA	chain transfer agent
Đ	dispersity
DBU	1,8-diazabicyclo [5.4.0]undec-7-ene
DMAEMA	dimethylaminoethyl acrylate
DMAP	4-dimethylaminopyridine
DMF	dimethylformamide
DMSO	dimethylsulfoxide
dn/dc	refractive index increment
dnNbpv	4,4'-dinonyl-2,2'-dipyridyl
DP	degree of polymerization
DSC	differential scanning calorimetry
eBiB	ethyl α -bromoisobutyrate
EBPA	ethyl α -bromophenylacetate
Et ₃ N/TEA	triethylamine
FWHM	full width half maxima
HMTETA	1,1,4,7,10,10-hexamethyltriethylenetetramine
HPMA	<i>N</i> -(2-hydroxypropyl) methacrylamide
HSQC	heteronuclear single quantum coherence spectroscopy
IUPAC	international union of pure and applied chemistry
k_{act}	activation constant
k_{app}	apparent kinetic constant
K_{ATRP}	ATRP equilibrium constant
k_{deact}	deactivation constant
LAMA	2-lactobionamidoethyl methacrylate
LB	lysogeny/Luria broth
LMCT	ligand to metal charge transfer
MA	methyl acrylate
MALDI-ToF	matrix-assisted laser desorption/ionization time-of-flight
MALS	multi-angle light scattering
MBPA	methyl α -bromophenylacetate
Me ₆ TREN	tris [2-(dimethylamino)ethyl]amine
MeOH	methanol
MMA	methyl methacrylate
M_n	number-average molecular weight
$M_{n,NMR}$	number-average molecular weight determined from nmr
$M_{n,SEC}$	number-average molecular weight obtained from sec
$M_{n,theo}$	theretical number-average molecular weight
M_w	weight-average molecular weight
NHS	<i>N</i> -hydroxysuccinimide
NHS(M)A	<i>N</i> -hydroxysuccinimide (meth)acrylate

NIPAM	<i>N</i> -isopropylacrylamide
NIR	near infrared
NMP	nitroxide-mediated polymerization
NMR	nuclear magnetic resonance
NPMA	p-nitrophenyl methacrylate
PBMAm	poly(<i>n</i> -butyl methacrylamide)
PCarMA	poly(carvacryl methacrylate)
PCiMA	poly(citronellyl methacrylate)
PDA	polydopamine
PEG	polyethylene glycol
PEI	polyethyleneimine
PET	poly(ethylene terephthalate)
PFP4VB	pentafluorophenyl 4-vinylbenzoate
PFPMA	pentafluorophenyl methacrylate
PGeMA	poly(geranyl methacrylate)
PMDETA	<i>N, N, N', N'', N'''</i> -pentamethyldiethylenetriamine
PMGluMA	poly(methyl α - <i>D</i> -glucopyranosyl methacrylate)
PMMA	polymethylmethacrylate
PMYMA	poly(myrtenyl methacrylate)
PS	polystyrene
PSeGluMA	poly(sesamyl <i>b</i> - <i>D</i> -glucopyranosyl methacrylate)
PSeMA	poly(sesamyl methacrylate)
PVaMAm	poly(vanillyl methacrylamide)
RAFT	reversible addition-fragmentation chain-transfer
RDRP	reversible deactivation radical polymerization
RI	refractive index
RMS	root mean square roughness
SARA ATRP	supplemental activator and reducing agent atom transfer radical polymerization
SEC	size exclusion chromatography
SEM	scanning electron microscopy
SET-LRP	single electron transfer living radical polymerization
SFRP	stable free radical polymerization
SI	surface initiated
T_d	degradation temperature
TEMPO	(2,2,6,6-tetramethylpiperidin-1-yl)oxyl
T_g	glass transition temperature
TGA	thermal gravimetric analysis
THF	tetrahydrofuran
ToF-SIMS	time-of-flight secondary ion mass spectrometry
TPMA	tris(2-pyridylmethyl)amine
UV	ultra violet
WCA	water contact angle
WHO	world health organization
XPS	x-ray photon spectroscopy

General Introduction

The contact of bacteria with a surface either in suspension or in air may eventually lead to bacterial contamination of a surface. Surface contaminated by bacterial may create several problems like degradation or reduced in performance. Furthermore, if the bacterium is pathogenic, the spoiled surfaces might become a new source of disease transmission to humans and other living species. Therefore, the preparation of new antimicrobial surfaces is a major concern in different areas.

Functionalization of existing polymeric material surfaces is an attractive solution for the development of new antibacterial materials in which the surface functionalized with covalently grafted antimicrobial polymers represents an ideal solution. In our lab, many studies in the last decade have demonstrated promising results on model bacterial strains like *Bacillus subtilis*, *Listeria monocytogenes* and *Staphylococcus aureus*. These projects often involved the use of polymers containing essential oil derivatives because essential oils themselves are known to be natural antibacterial agents. Additionally, the nature origin of essential oils is favored over synthetic products also for their toxicity is expected to be lower. In general, these work required case-study in controlled polymerization in solution of an essential oil-containing monomer, which would then be applied to surface-initiated polymerization. Thus, the possibility to obtain a surface with a cocktail of biomolecules was quite challenging. To overcome that issue, the preparation of a reactive polymer template which can be modified easily with various bioactive molecules, whose antibacterial efficacies are strain-dependent, is of great interest. This approach will then allow the introduction on supporting surface numerous bioactive molecules to combine their additive or synergistic antibacterial effects. On that matter, polymer of active esters like pentafluorophenyl methacrylate (PFPMA) or *p*-nitrophenyl methacrylate (NPMA) attracted our interest. However, controlled polymerization of both monomers is often carried out by reversible addition-fragmentation chain transfer (RAFT) polymerization and traditional atom transfer radical polymerization (ATRP). Both techniques possess disadvantages for surface-initiated polymerization, hence, another polymerization technique that is easier to perform like Cu-mediated reversible deactivation radical polymerization (RDRP) presented to be a great choice over classical approaches.

Standing from those points of view, this project has been implemented in several stages which are going to be presented and discussed in the six chapters of this dissertation.

The first chapter covers an overview on the need of new antibacterial surfaces, state-of-the-art in preparation of such materials, the choice of supporting surface, a brief discussion on controlled polymerization, and finally the introduction of polymer post-modification as well as its impact on this dissertation.

The second chapter presents results obtained in the study of Cu(0)-mediated RDRP of PFPMA, NPMA and their copolymerization in solution. This chapter will focus mainly on the optimization to obtain controlled poly(pentafluorophenyl methacrylate) (PPFPMA) by the technique of interest. Homopolymerization of NPMA and copolymerization of the two active esters are also demonstrated and investigated but with less attention.

The third chapter deals with surface-initiated (co)polymerization of PFPMA and NPMA from poly(ethylene terephthalate) (PET). In the same manner as that of chapter two, the majority of this chapter will be on the study of PFPMA as the amount of work dedicated for NPMA and copolymerization process was less pronounced.

The fourth chapter focuses on the post-modification of reactive polymers. Herein, polymethacrylate derivatives of various essential oils were obtained by different modification approaches including single molecule substitution, sequential substitution and dual substitution of PFPMA. The post-modification of PNPMA and copolymers of NPMA and PFPMA is also going to be discussed.

Chapter 5 is about the post-modification of PFPMA grafted on PET substrates as well as their characterization. Some of these obtained functionalized surfaces have been tested for their adhesion properties which are also going to be discussed in this chapter.

The last chapter will summarize achievements of this research as well as perspectives for future work.

Chapter 1. Bibliography

This chapter presents an overview on different aspects of the research, where there will be discussion on the following parts: 1) the current status and the need of new antibacterial surfaces, 2) the choice of PET surfaces as the substrate of interest, 3) an introduction on Reversible Deactivation Radical Polymerization (RDRP) in solution and from surface, and 4) the polymer post-modification.

1.1. Antibacterial surfaces

1.1.1. The needs of new antibacterial surfaces

Infectious diseases have always been one of the leading causes among unnatural causes of death in human-being. Among several different types of infections, microbial infection has become an emerging issue. There are a wide range of diseases caused by microbial infection, yet difficulty in treatment of such illnesses due to the rise in antimicrobial resistance (AMR). This phenomenon has been considered one of the biggest health challenges worldwide in recent years by WHO. In 2013, the report entitled “Antibiotic Resistance Threats in the United States” stated that each year in the U.S., at least 2 million people get an antibiotic-resistant infection, nearly 23000 deaths would be caused by AMR infections. According to European Center for Disease Prevention and Control, in 2007, there have been 386 100 bacterial multi-resistance infections in Europe with 25 100 deaths.

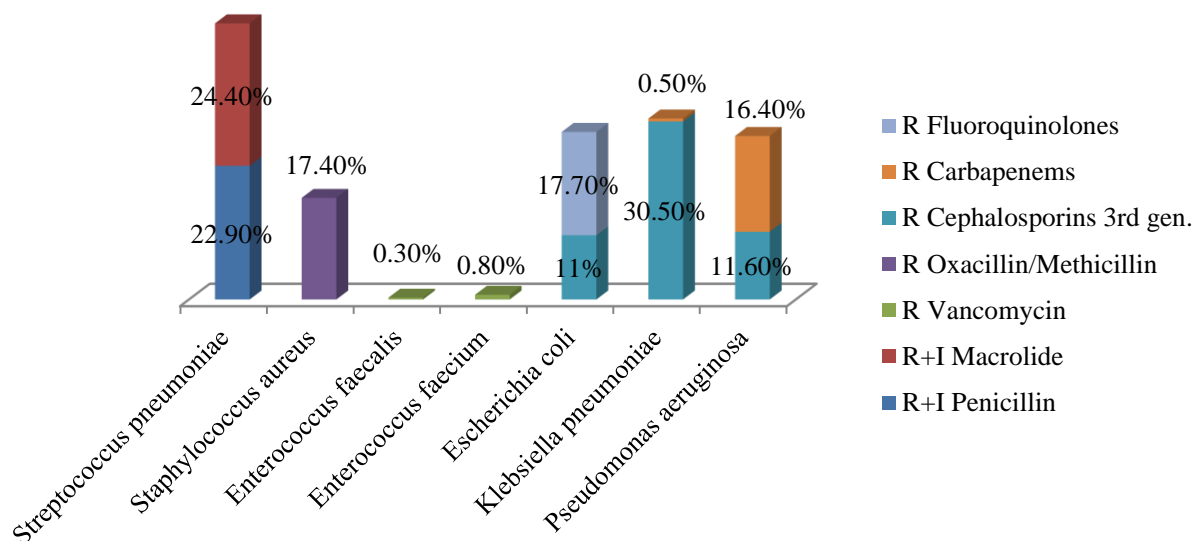


Figure 1. Resistance (R) and Insusceptibility (I) of some bacteria against common antibiotics - the French case (EARS-Net, 2015).

In France, 158 000 multidrug-resistant bacteria infections have been reported in 2012, causing 12 500 deaths. Figure 1 summarizes data of 2015 on the resistance (R) and insusceptibility (I) of some antibiotics against several bacteria.

Furthermore, as stated by the French Agency for the Safety of Health Products (l'Agence Nationale de Sécurité du Médicament et des Produits de Santé), due to the withdrawal of 34 substances in contrast to the commercialization of only 12 new products, there was a 20% decrease (from 103 to 79) in the number of available antibiotic substances in France between 2000 and 2015 [1]. On the other hand, the success in developing brand new medicines is time-consuming as well as huge financial and labor efforts; thus, the first and better resolution for infectious diseases is to prevent the incidence of infection. Several bacterial transmission mechanisms are known, but the contact with infected sources is the most common cause. Therefore, the preparation of surface that can efficiently reduce the adhesion of bacteria has been one of the subjects that attract attention of researcher all over the world.

1.1.2. Mechanisms and examples of antimicrobial surfaces

1.1.2.1. Adhesion of bacteria onto surface and the biofilm formation

Bacteria tend to adhere to surface as they may gain several advantages such as the increase in local concentrations of nutrients and the possibility to gain necessary metabolites and co-factors from the surface. Furthermore, bacteria attached to surface would gradually grow to form biofilm (Figure 2), which can be defined as a microbial community composed of “microbial cells that is enclosed in an extracellular polymeric substance matrix” [2], where their resistance enhances significantly thanks to several protective mechanisms [3]. However, adhered bacteria benefit from resistance not until the full formation of biofilm but right after cells attach to surface. Such resistance is related to the reduction in net charge and the enhanced stability of membrane.

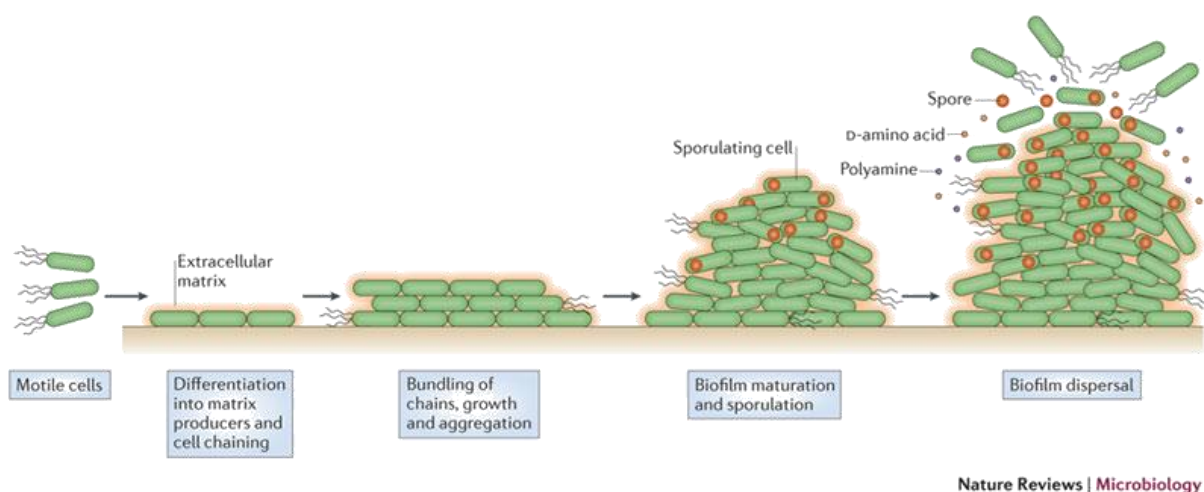


Figure 2. Different stages of biofilm formation, *Bacillus subtilis* example [4]

Compared to planktonic bacteria – floating single cells in water – biofilms might be said to be survival storages for microorganisms as they possess slower growth rate, better stress resistance, higher rate of horizontal transfer of antimicrobial genes, the production of extracellular polymeric substances and specific phenotypes.

In general, manmade materials are incapable of self-defense against attachment of microbial like natural surface such as taro or lotus leaves or insect wings. While taro and lotus leaves can resist bacterial fouling when immersed in water due to the presence of nanostructure on its surface [5], insect wings can be bactericidal due to the presence of well-organized nanopillar arrays on its surface which can disrupt the integrity of bacterial membranes [6]. Therefore, to prevent the microbial contamination is an utter need for long-term usage of synthetic materials. One of the easiest methods is to keep the surface sterile by using disinfectants like hypochlorite, hydrogen peroxide, silver salts, quaternary ammonium compounds or alcohols. Unfortunately, the effect of disinfectants does not last long and can even create environmental problems as in the case of triclosan [7, 8] or lead to the formation of resistant microbial strains [9-12]. Thus, the preparation of antimicrobial surfaces that can prevent the formation of biofilms is considered as a promising alternative.

In this research, the utilization of antimicrobial polymeric molecules is the major concern due to their several advantages compared to smaller molecules. They often provide better initial adsorption, stronger binding yet causing better disruption and disintegration with bacterial membrane, and additionally, they can be grafted from or to supporting surface. As the properties of motile free cells and microbes involved in biofilm are well differentiated due to the great complexity of biofilm. Antimicrobial surfaces often target at reducing the event of attachment of motile cells on surface to prevent the accumulation of cells and the growth of biofilm. As shown in Figure 3, antimicrobial substrates can inhibit the initial attachment of cells by either repelling cells approaching surface (antifouling/antiadhesion mechanism) or killing cell from the surroundings (antibacterial mechanism).

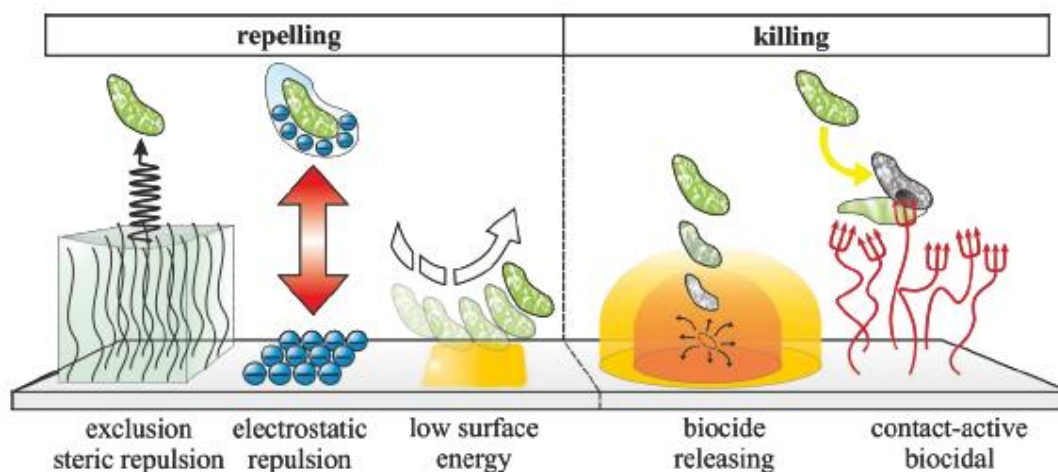


Figure 3. General principles of antimicrobial surfaces [13]

1.1.2.2. Antifouling surfaces

Antifouling surfaces can either exhibit repellent properties or affect biofilm architecture. This type of surface is often based on (1) hydrophilic polymers like poly(oxyethylene) or

previously called polyethylene glycol (PEG) or glycopolymers, (2) zwitterionic materials and (3) superhydrophobic surfaces.

a) Surface functionalized with hydrophilic polymers

PEG and their derivatives are polymers that show high biocompatibility towards human beings [14]. The introduction of PEGs to a surface is believed to reduce protein adsorption due to the repulsive electric forces resulted from the compression of polymer chains [14]. Interestingly, the chain length of PEG has been identified to have a certain influence on the bovine serum albumin antiadhesive properties [15], where it is remarked that the longer chain has tendency to aggregate onto surface due to intermolecular interaction, hence leading to lower antiadhesion against the protein because of increasing in surface energy. Results from other studies on the same subject but different substrates [16-18] also agree with the antifouling effect of surface grafted with PEG. For example, the graft of PEG to polyamide and PET surface *via* plasma polymerization helps to reduce 96% of *L. monocytogenes* compared to non-modified surface [16]. In another study, the incorporation of silane-PEG layer onto stainless steel has reduced the non-specific binding of avidin and fibronectin proteins by approximately 70% and the attachment of *E. coli* by more than 65% [17]. PEG coating on hydrogel-based materials also results in excellent antiadhesion effect in laboratory-scale towards marine and freshwater fouling organisms [18]. However, PEG is limited from long-term usage due to its rapid auto-oxidation in the presence of oxygen, metal ions or reductant enzymes [19].

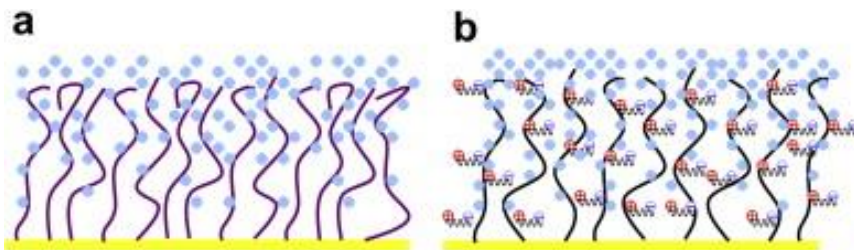


Figure 4. Illustration of chain hydration and chain flexibility of (a) hydrophilic polymers, (b) zwitterionic polymers, which attribute to antifouling properties [23]

Glycopolymer is another type of hydrophilic polymers that have been of great use in preparation of antifouling surface. Glycopolymers are known for their affinity in physiological molecules and its low toxicity, but the graft of these polymers on supporting surface can also reduce the attachment of cells onto surface due to the formation of hydration layer, as in the case of PEG, which creates a strong steric repulsion against living cells. Glycopolymers have been immobilized to several different substrates to enhance the surface's proteins antiadhesion and/or antibacterial properties. For instance, poly(D-glucoamidoethyl methacrylate) grafted on gold surface shows low non-specific BSA adhesion [20]. As another example, chitosan grafted from PET surface provides >99.9% inhibition of *E. coli* adhesion [21]. A study has reported that the increase in glycosyl side chains compared to methyl counterparts of copolymers coated on supporting surface can prevent protein adhesion,

suppress bacterial adherence yet enhance mammalian cell adhesion with excellent biocompatibility [22].

b) Surface functionalized with zwitterionic polymers

Zwitterionic polymers possess interesting chemical composition as they contain both positive and negative charges, which make them stable under atmospheric conditions and resistant to interaction with proteins and antifouling properties against bacteria. These polymers are often derived from betaines (phosphobetaine, carboxybetaine, sulfobetaine), phospholipids and amino acids. Many studies on the immobilization of zwitterionic polymers on various supporting surfaces have shown the effectiveness of the polymer in reducing adhesion of protein and bacteria. Gold surface grafted with poly((3-(methacryloylamino)propyl)-dimethyl(3-sulfopropyl)ammonium hydroxide) shows impressive reduction in protein adsorption towards different proteins [24]. Adhesion of *S. aureus*, *E. coli* and *P. fluorescens* is reduced completely on polypropylene membrane coated with polysulfobetaine methacrylate at grafting density of $560 \mu\text{g}/\text{cm}^2$ [25]. Another study on the use of amino acid-based polymers describes that the presence of these polymers on gold surface suppress ~99% *E. coli* adherence compared to bare surface [26].

It is suggested that the repellent properties of hydrophilic and zwitterionic polymers are originated from the hydration layer formed near the surface, as illustrated in Figure 4. The role of this hydration layer is believed to create a physical and energetic barrier to prevent adsorption of protein on the surface [27, 28], which is a key factor in adhesion of bacteria to surface. Besides, the flexibility of polymer chains also plays a significant role in protein resistance. The approach of protein to a surface may compress polymer chain, which then causes steric repulsion due to unfavorable decrease in entropy [14, 29]. It is suggested that the best nonfouling ability of polymers can only be achieved in presence of both hydration and steric repulsion [23].

c) Superhydrophobic surfaces

The application of superhydrophobic surface for antiadhesion properties has come from the so-called lotus effect, *i.e.* the self-cleaning properties due to the hierarchical micro/nanostructures and the hydrophobic wax on top of the lotus leaf. Though the idea is relatively new, several studies have proven its promising future. It is reported that the adhesion of pathogenic *S. aureus* and *P. aeruginosa* was reduced significantly on fluorinated silica-colloid-based superhydrophobic surfaces [30]. Anti-adhesive superhydrophobic stainless steel was also obtained by electrodeposition of hydrophobic polymers with controlled topographical features [31]. Another study presents that shrink-induced superhydrophobic surfaces coated with polystyrene, polycarbonate and polyethylene can reduce the adhesion of *E. coli* compared to surface without induction in hydrophobicity [32]. In addition, inorganic laser ablated superhydrophobic Ti surface shows inhibition in *P.*

aeruginosa adherence but colonization of *S. aureus* because of the difference in cellular structure of the two bacteria [33].

1.1.2.3. Antibacterial surfaces

a) Cationic polymers

Cationic polymers have been proved to have excellent antibacterial properties and polyethyleneimine (PEI) derivatives are the first example of these cationic polymers. The graft of PEI, either alkylated or quaternized, on surface have been extensively studied to improve the surface's antibacterial properties [34-41]. A recent publication on silicon surface coated with ultrathin layer (3.5 nm) of branched PEI showed 95% reduction in adhesion of *S. aureus* and 80% reduction in case of *P. aeruginosa*, however, the duration of activity was different for the two bacteria [42]. Another study involving the use of brush-like PEI grafted on polyurethane ureteral stent surfaces presented potential antibacterial activity as such surfaces have reduced the adherence of *K. pneumonia*, *E. coli* and *P. mirabilis* up to 2 order of magnitude [43]. *N*-alkylated immobilized PEI on surface indicated more than 90% antibacterial efficiency against both airborne and waterborne *S. aureus*, *S. epidermidis*, *P. aeruginosa*, and *E. coli* [37]. Sequential PEI crosslinking with terephthalaldehyde enabled the preparation of 10 layers on glass surfaces that kills up to 90% of *E. coli* and 50% of *S. aureus* upon contact, and more interestingly, the incorporation of silver nanoparticles into this system enhanced the contact kill with more than 99% killed both bacterial cells observed on modified surface [38]. A recent work has shown that surfaces obtained by the co-deposition of catechol/PEI, then the graft and *N*-alkylation of another layer of PEI possessed not only 95% antibacterial efficiency against *S. aureus* but also antifouling behavior [40].

In addition, cationic quaternary ammonium containing polymers are also great candidates for antibacterial properties. Cellulose paper grafted with 1-bromooctane quaternized polymer of 2-(dimethylamino)ethyl methacrylate showed impressive killing efficiency against *E. coli* [44]; this polymer has also been extensively studied for its antibacterial properties in other studies [45-48]. As another example, a method proposed to functionalize surfaces of various common synthetic materials with poly(vinyl-*N*-pyridium bromide) reported drastic decrease in the number of both *E. coli* and *S. aureus* in contact with examined surface in both dry and wet state [49]. Polymer surfaces covalently grafted with copolymers of diallyldimethylammonium chloride have also presented to be able to significantly reduce the settlement of *M. luteus* and *E. coli* [50]. More interestingly, a recent study has evaluated the antibacterial properties of cationic polymers with the charge located either on the side chain or on the main chain. The same study mentioned that main-chain cationic polymers showed higher antibacterial effects compared to side-chain cationic polymers and small molecule cationic compounds [51]. In addition, the improvement in activity between cationic polymers and small cationic compounds lies in the relatively concentrated charge and longer chain lengths, which induce stronger electrostatic and hydrophobic effects. On the other hand, the divergent activity of main-chain and side-chain cationic polymers is due to the difference in charge distribution along polymer chain. The alternating distribution of hydrophobic and

hydrophilic moieties in main-chain cationic polymer backbone provides better insertion of hydrophobic segments into phospholipid bilayers of bacterial cells. In contrast, in side-chain cationic polymer, the distribution of positive charges is rather local, hence, requires higher charge density as well as additional hydrophobic groups for a biocidal effect.

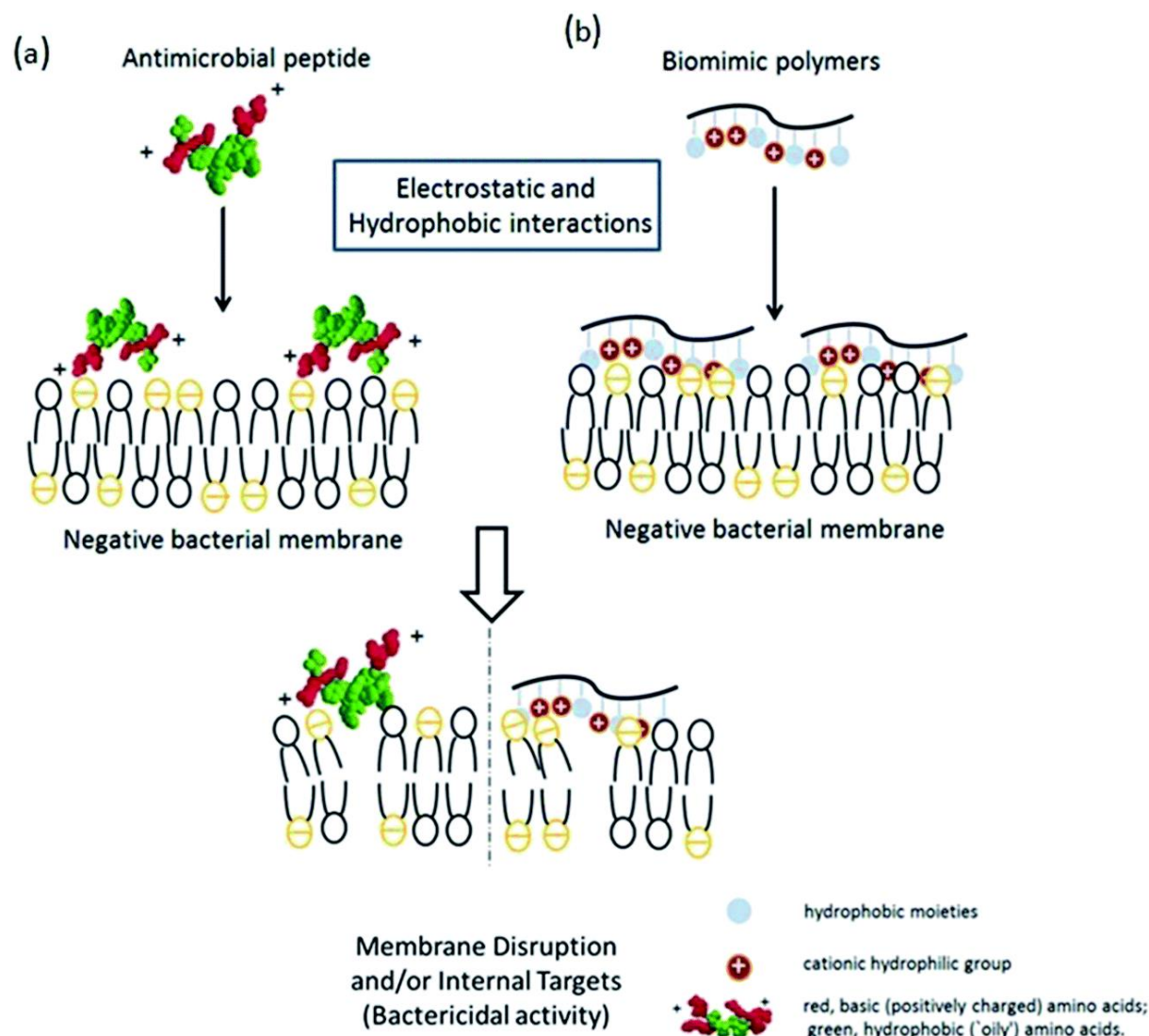


Figure 5. Interaction of cationic polymers with bacterial membrane [52]

The design of cationic polymer is inspired from the interaction with the membrane of natural antimicrobial peptides. As seen in Figure 5, similar to antimicrobial peptides, the positive charges located on the polymers can interact *via* electrostatic interaction with the global negative charge bacterial membrane. Additionally, the neutral hydrophobic characteristic elsewhere in the polymers leads to the hydrophobic interaction with the membrane. The combinations of these two interactions eventually result in the disruption of bacterial membrane, hence, killing the bacteria.

b) Polymer derived from essential oils

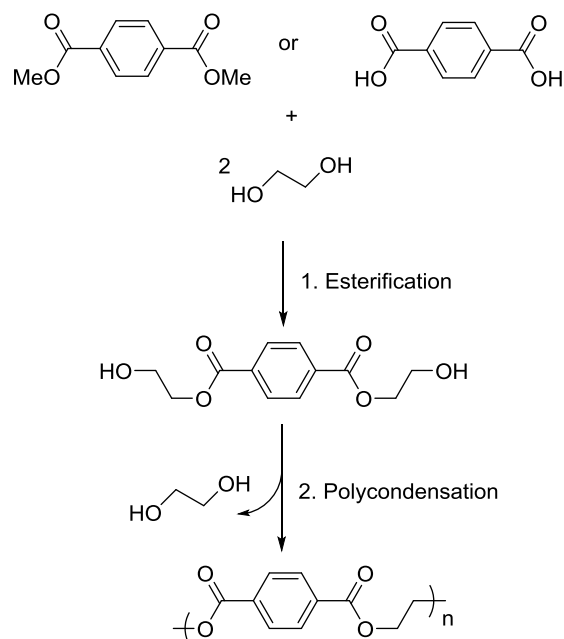
Many essential oils are known for their antibacterial properties [53-58]. Not only that surface encapsulating essential oils may reduce the adhesion or proliferation of bacteria [59-65], several studies from our lab on polymers derived from essential oils have presented interesting results for the preparation of antibacterial surfaces. For example, poly(myrtenyl methacrylate) adsorbed on glass was demonstrated to reduce adhesion of *B. subtilis* [66]. Furthermore, the grafting-from of poly(thymyl methacrylate) on PET reduced 91%, 98% and 99% adhesion of *P. aeruginosa*, *L. monocytogenes* and *S. aureus*, respectively [67]. Notably, this type of surface presented to be efficient in inhibiting formation of *S. aureus* biofilm. Recently, vanillin-derived monomer was successfully polymerized from PET surface by UV-induced grafting from polymerization strategy [68]. The grafted polymer helped reduce 85% adhesion of *R. wratislaviensis* and 97% adhesion of *S. aureus*. Outside studies have also insisted the same approach, such as the immobilization of polymer derived from eugenol, thymol or carvacrol on silica nanoparticles [69]. Additionally, the research on polyborneolacrylates with different chirality coated on PMMA surface shows important inhibition in bacterial adhesion against *E. coli* and *S. aureus* even after 60 hours of incubation [70].

1.2. Poly(ethylene terephthalate) (PET) as template for post-modification

1.2.1. PET: a material of excellence

PET is synthetic recyclable thermoplastic polyester with excellent properties. This material has been using greatly in industry, especially as beverage packaging, sheet and films, consumer goods, food packaging, and so on.

PET can be synthesized in industrial scale by two steps including pre-polymerization to obtain bis-(2-hydroxyethyl) terephthalate followed by polycondensation of the pre-polymer (Scheme 1) [71]. The first step may be done by either the esterification of ethylene glycol and terephthalic acid or the trans-esterification between dimethyl terephthalate and ethylene glycol .



Scheme 1. Synthesis of PET in manufacturing industry

During the industrial processing and thermal treatment, depending on conditions, resulted PET often exists in either amorphous (clear, transparent) or semi-crystalline (opaque, off white) state with its properties change accordingly. In general, the melting temperature of this polymer is in the range of 250-265 °C. At amorphous state the glass temperature of PET is 65 °C, while at its semi-crystalline state the glass temperature comes to 81 °C [71]. However, at any form, PET has a fairly good chemical resistance, especially against organic solvents, as summarized in Figure 6.

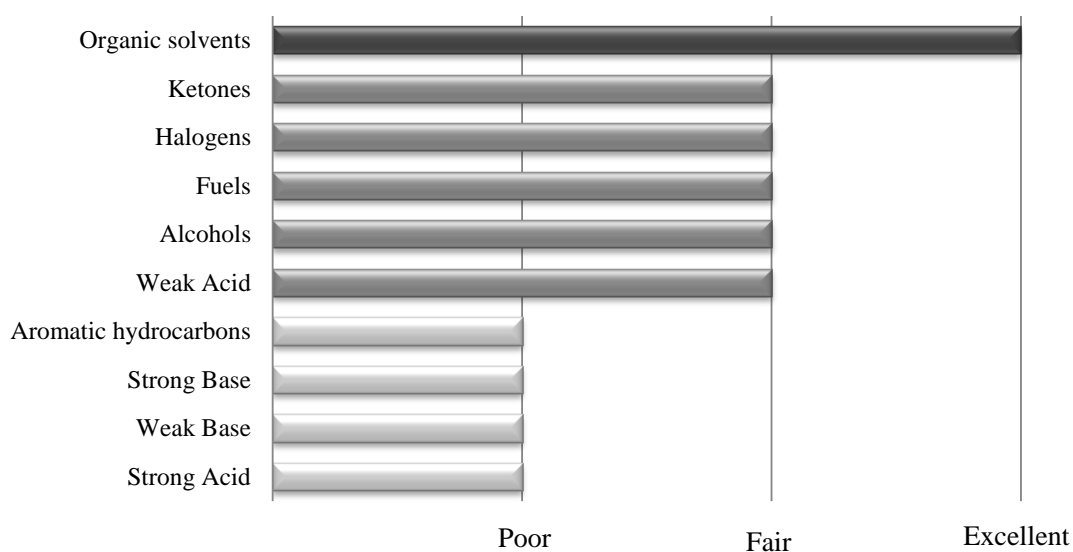


Figure 6. Level of PET resistance towards different chemicals

Regarding PET production and consumption, Smither Pira published in 2016 a report entitled “The Future of PET Packaging to 2021” in which it is forecasted that the consumption of PET for packaging would reach 21.1 million tons by 2021 with the annual market growth of 3.8% [72].

However, there are certain properties that hold PET back from widely employed in biomedical: its hydrophobicity nature, its low surface energy which causing problems in contact with microorganisms, finally the bacterial colonization on PET surface may also lead to the degradation of the material. Therefore, surface modification of PET to enhance these limitations and expand the use of the polyester is of interest.

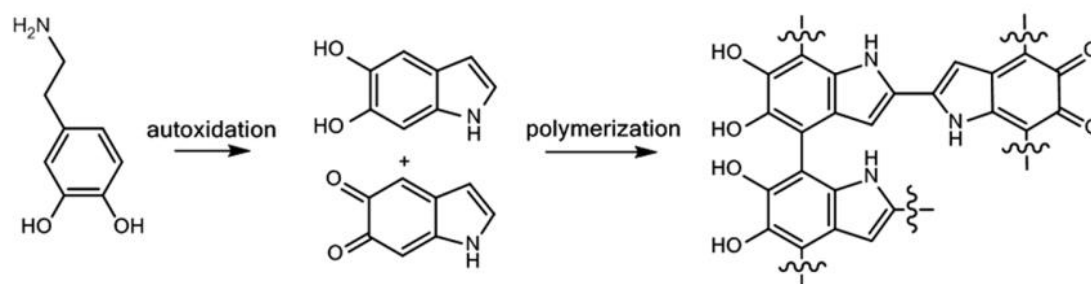
1.2.2. Surface-modification of PET

PET surfaces have been the target for many surface modification process, which might be divided into two main categories including wet chemical treatments and physical treatments.

1.2.2.1. Wet chemical treatments

a) Polydopamine as coating support

Inspired by interaction of mussel protein with surface, anchoring properties of catechol derivatives has been widely used as a coating method [73-78]. Among those, dopamine with its fast autoxidation and rapid self-polymerization properties (Scheme 2) presents to be the most used pathway for functionalization of many different substrates [79-86]. In general, chemical polymerization of dopamine is done in basic condition (pH = 8.5) and the coating process is done by immersing substrate on that reaction medium. The use of this approach has been applied on PET for various applications. The coating of polydopamine (PDA) on PET fibers has been reported to be efficient for silver deposition, hence, enhancing the electrical conductivity of the thermal plastics [87]. The same method of PDA grafting then silver deposition to improve the antibacterial properties of PET fibers against *S. aureus* and *E. coli* has been reported [88].



Scheme 2. Autoxidation and self-polymerization of dopamine

The polymerization of dopamine can be induced rapidly by UV irradiation to form a thin layer of PDA on PET film, that can be subsequently used to nickel-plating coating of Ni-P alloy [89]. Nonetheless, the use of PDA as support is beneficial for the uniform hybridization of

reduced graphene oxide and PET substrate via drop-casting method [90]. In another example, PDA has been employed to functionalize the polyester films with multilayer of sorbents for the enrichment of organic pollutants from water samples [91]. However, even though this method allows creating rapidly a uniform layer of PDA on PET surface, the coating layer is non-covalent, hence the durability and the attachment is rather weak.

b) Aminolysis

Primary amino groups can be introduced onto PET surface *via* aminolysis as illustrated in Figure 7. The aminolysis is done based on the nucleophilic attack of primary amine at the carbonyl sites of PET, leading to the appearance of end-chain amino groups and carboxylic acid functional groups on PET surface. Aminolysis of PET can also be done with chemical compounds that possess only one primary groups like (3-Aminopropyl)triethoxysilane [92] or alkanolamine [93], and therefore, resulted in other types of functional groups rather than primary amines on the surface.

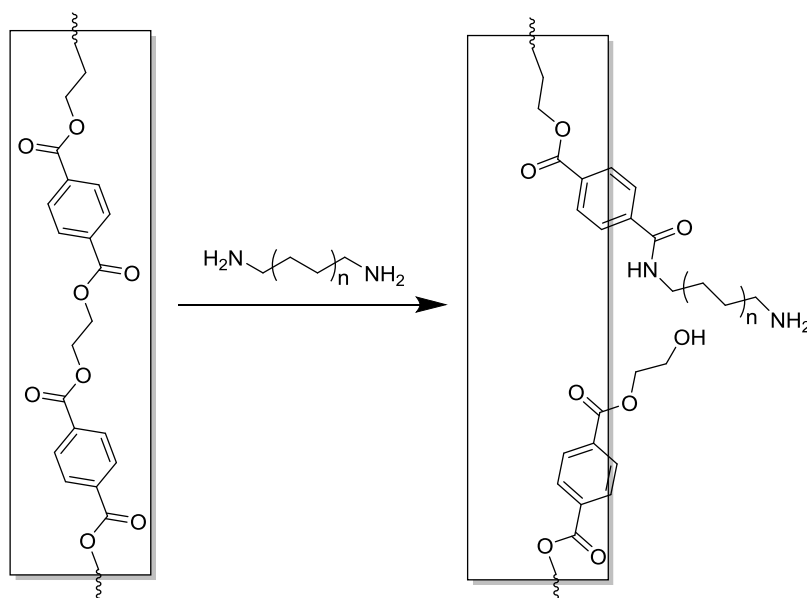


Figure 7. Surface modification of PET with diamines

In our lab, several studies have focused on this approach to further functionalize and carry out polymerization from PET films and fibers [68, 94, 95]. It is known that chemical modification by this approach is efficient and the grafting yield is time dependent. However, the aminolysis carried out by small diamine is a corrosive approach when reaction time is too long. In consequence, the bulk properties of PET substrate can be affected and a degradation of the surface can be observed [95, 96]. Other studies have been proposed to avoid this phenomenon. For example, the replacement of small diamine by polyethyleneimine (PEI), which is rich in primary amines, does not affect the structure of PET films proven by no observed damage under imaging microscopy and also no degradation events recorded by FTIR [94, 97]. Another study on the employment of polyvinylamine has confirmed to cause less damage to PET surface and almost no change in mechanical properties compared to

smaller diamines [98]. Compared to the use of PDA as mentioned above, aminolysis by polyamine presents to be a better candidate as the new reactive functional groups are attached stronger to the surface *via* covalent amide bonds.

c) **Other approaches**

As functionalization of PET surface has attracted much interest, other chemical modification approaches are available in literature. For example, the grafting of polyglycidol has been done by surface-initiated polymerization on pre-oxygen-plasma treated PET surface and proven to alter the adhesion of proteins compared to unmodified surface [99, 100]. Another study proposes the silanization of PET substrate that also allows further functionalization [101]. Moreover, treatment of PET substrate under strong acidic or basic conditions are well-known, for instance KMnO_4 [102, 103], NaOH [104, 105], LiAlH_4 [104], *tert*-butoxide [104], benzoyl peroxide [106]; however, such treatment shall eventually lead to serious damage on the surface, just as the case of short chain diamine, therefore leading to the loss in integrity and properties of PET.

1.2.2.2. Physical treatments

In contrast to wet chemical treatments, physical treatments enable the introduction of functional groups onto surface by using high energy stimuli like plasma, UV irradiation, ozone treatment, electron bombardment, and so on. The advantages of this technique include fast treatment, minor destruction and solvent free.

In physical treatment of PET, plasma exposure in accompany with radical sources is one of the most used approaches [107-120]. Plasma can be created in both atmospheric conditions or under vacuum and is considered the state where a matter exists in the form of hot ionized gas with approximately the same amount of positive and negative charge ions. Plasma treatment of the surface enables the introduction of functional group on a surface without losing chemical and mechanical properties of such materials. This technique is considered as a green method as it does not require the use of solvent and the treatment normally does not consume so much time. Plasma has been used to incorporate several different groups such as hydroxyl, carbonyl, peroxy, amide and amine onto surface. Depending on gas feeding, our group has been published several papers regarding the use of plasma to functionalize PET surface including the incorporation of primary amino groups by either ammonia or nitrogen/hydrogen mixture [121], the use of plasma as pretreatment to immobilize initiator for surface-initiated polymerization [67, 122]. Figure 8 presents an example where plasma treatment was used to pre-functionalized PET films in order to graft on supporting surface the polymer of thymyl methacrylate.

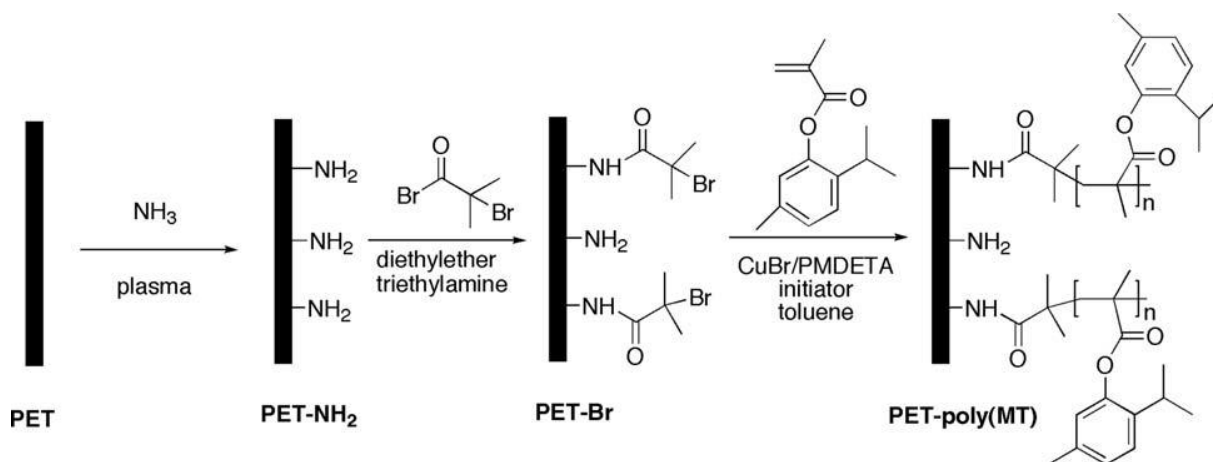


Figure 8. Plasma pretreatment to functionalize PET surface with initiator for surface-initiated polymerization of thymyl methacrylate [67]

On the other hand, UV irradiation is another approach that has been used (1) to modify the surface of PET either by introducing new functional group to the surface or (2) to induce polymerization grafting from PET surfaces [68, 118-120, 123-125]. Besides, electron beam also allows the modification of PET surface by exposing the target to electromagnetic short-wavelength light under air, inert gas or other chemicals to create active radicals or deposited onto such PET supporting surface a layer of inorganic compounds [126-133]. There are, of course, other studies on physical treatment of PET surface, yet these approaches are not under the goal of this dissertation, therefore, are less known to the author. However, the general disadvantage of physical treatment is that the modified surface is often affected by aging effect due to the presence of highly active radicals. Therefore, the functionalized surface tends to rapidly recover to its untreated state upon exposure to atmospheric condition, except for the case when new stable functions, another polymer or crosslinking layer are formed and covered the surface.

1.3. Reversible Deactivation Radical Polymerization and Surface-initiated Polymerization

Unlike ionic and living polymerization, where all polymer chains are formed and are growing homogeneously until all monomers are consumed, conventional radical polymerization is a process where propagating radicals have very short lifetime (up to few seconds) and would eventually undergo termination processes such as bimolecular termination, disproportionation or chain transfers. For such reasons, the control in structure and composition of radical polymerization had been considered an urge in polymer chemistry in the past. During the last two decades, the control of radical polymerization can be achieved by adding reagents that help minimize the event of bimolecular termination through reversible deactivation and extension of propagating radical's lifetime. The addition of such reagents may alter the coupling reaction of propagating radicals by either reversible termination or reversible transfer.

With the rapid development of advanced RDRP techniques, there is also the increasing interest in anchoring polymer chains to surface to enhance or create certain chemical and physical properties of interfaces. Polymer on surface, often called polymer brushes, has been studied for different applications including but not limited to bacterial and cell adhesion [67, 99, 135-139], bioelectronics system [140-146], conducting nanoparticles [145, 147-150], surface-supported catalysis and biocatalyst microreactors [151, 152], organic electronic devices [153-157], colloidal systems [158-163], and stimuli-responsive surfaces [164-170]. Two approaches are commonly employed to graft polymer chains to a surface so-called *grafting to* and *grafting from* approaches (Figure 10).

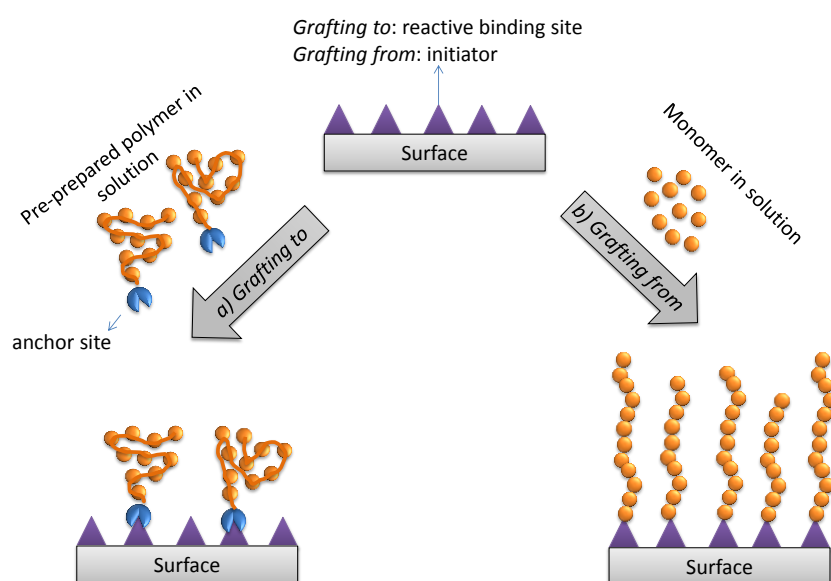


Figure 10. Surface functionalization with polymer brushes by *grafting to* and *grafting from* approaches.

In *grafting to* approach, synthesized polymers are modified at one end so that it can be linked to surface *via* one specific chemical reaction between the compatible polymer end and a functional group that pre-existed or grafted to supporting surface. The use of this technique is favored as the size of polymer is frequently well defined and characterized, leading to an expected film thickness. However, the coupling of polymer chain-end and surface suffers from steric hindrance between polymer chains, hence, resulting in difficulty to tether chain ends at short intermolecular distances. In contrast, the *grafting from* polymerization is regularly carried out by immobilizing initiator onto surface, and then polymers are obtained by surface-initiated polymerization. Unlike *grafting to*, this technique is not limited by steric hindrance, which makes it normally possessing higher grafting density.

The properties of grafted polymer might change in accordance with grafting density and the chain length. Figure 11 shows various conformations of polymer chains on surface.

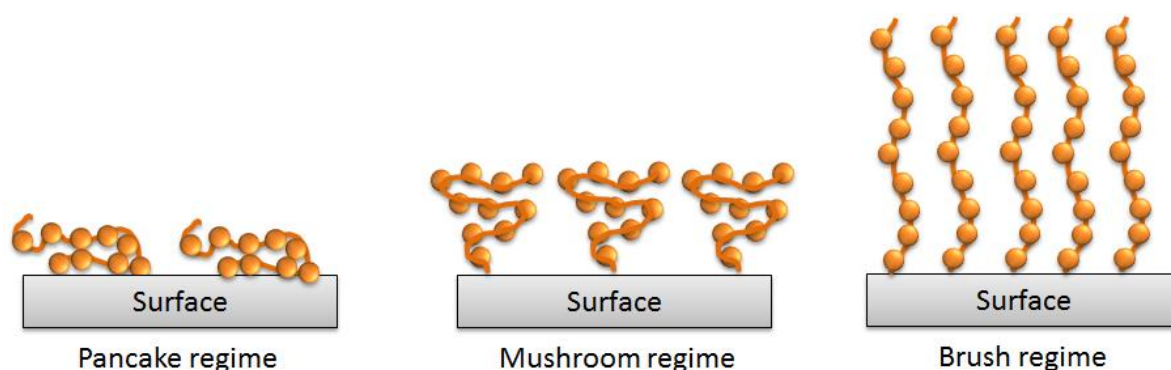
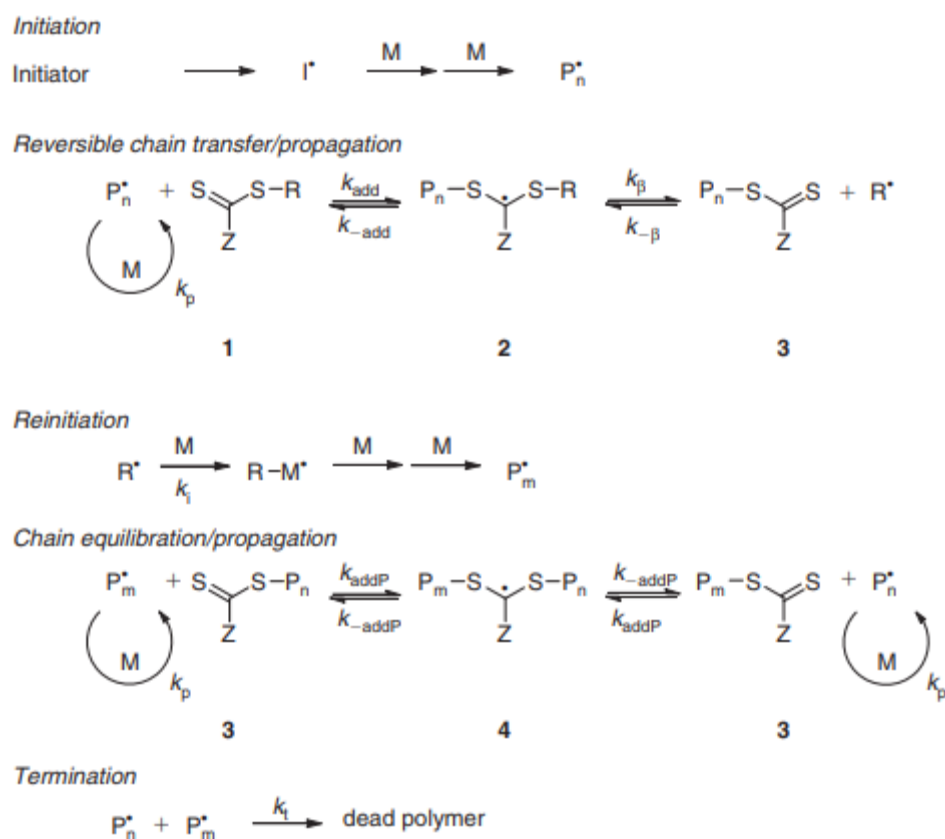


Figure 11. Conformations of polymers grafted on surface

Within RDRP, there are three main polymerization processes including Reversible Addition-Fragmentation chain Transfer (RAFT) polymerization, Stable Free Radical Polymerization (SFRP) including Nitroxide-mediated Polymerization (NMP), and Atom Transfer Radical Polymerization (ATRP). Though each of these three has their own advantages and disadvantages, which will be discussed later, they all possess a common feature which is the typical signatures of radical process including specific chemo-, regio- and stereo-selectivities, such as specific reactivity ratios, limited tacticity control, and unavoidable termination [171].

1.3.1. Reversible Addition–Fragmentation Chain Transfer Polymerization

Among the three most well-established RDRP techniques, reversible addition-fragmentation chain transfer (RAFT) polymerization is the sole based on the degenerative chain transfer process and chain equilibration to control the polymerization. This technique involves the use of a chain transfer agent (CTA) that reversibly transfers a labile end group to a propagating chain. A thiocarbonylthio compound is the most common and versatile CTA in RAFT polymerization. Scheme 4 presents the commonly accepted mechanism of RAFT polymerization using thiocarbonylthio CTA.



Scheme 4. Steps involved in RAFT polymerization and mechanism of chain transfer and equilibrium [172]

CTA serves as the factor that alters the suitability towards one monomer as well as the control of its polymerization by the control in chain transfer and chain equilibration. As seen in Scheme 4, the reactivity of CTA is determined by the nature of the Z and R end-groups. The Z-group influences the activity of thiocarbonyl group for radical addition and the stability of the resulting intermediate radical species, while the R-group initiates the growth of new polymeric chains.

To employ RAFT polymerization to introduce polymer chains to the substrate, there are three different strategies, which differ from the type of tethered points as illustrated in Figure 12.

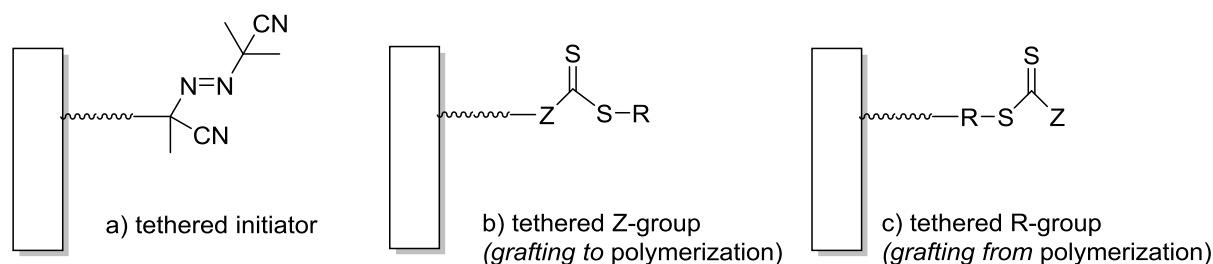


Figure 12. Strategies of RAFT polymerization from surface with (A) tethered initiator, (B) tethered Z-group, and (C) tethered R-group chain transfer agent.

The first approach is to attach initiators to the surface and then carry out the polymerization with RAFT agent in solution. Based on this approach, polymers of styrene, methacrylate and *N,N*-dimethylacrylamide were obtained from tethered azo-initiator on silicon substrate [173]. The drawback of this method is the formation of polymers both in solution and on surface, which can be minimized by grafting both initiator and RAFT agent to surface [174]. Due to this limitation, the fixation of free radical initiator to the surface is less common than the attachment of CTAs.

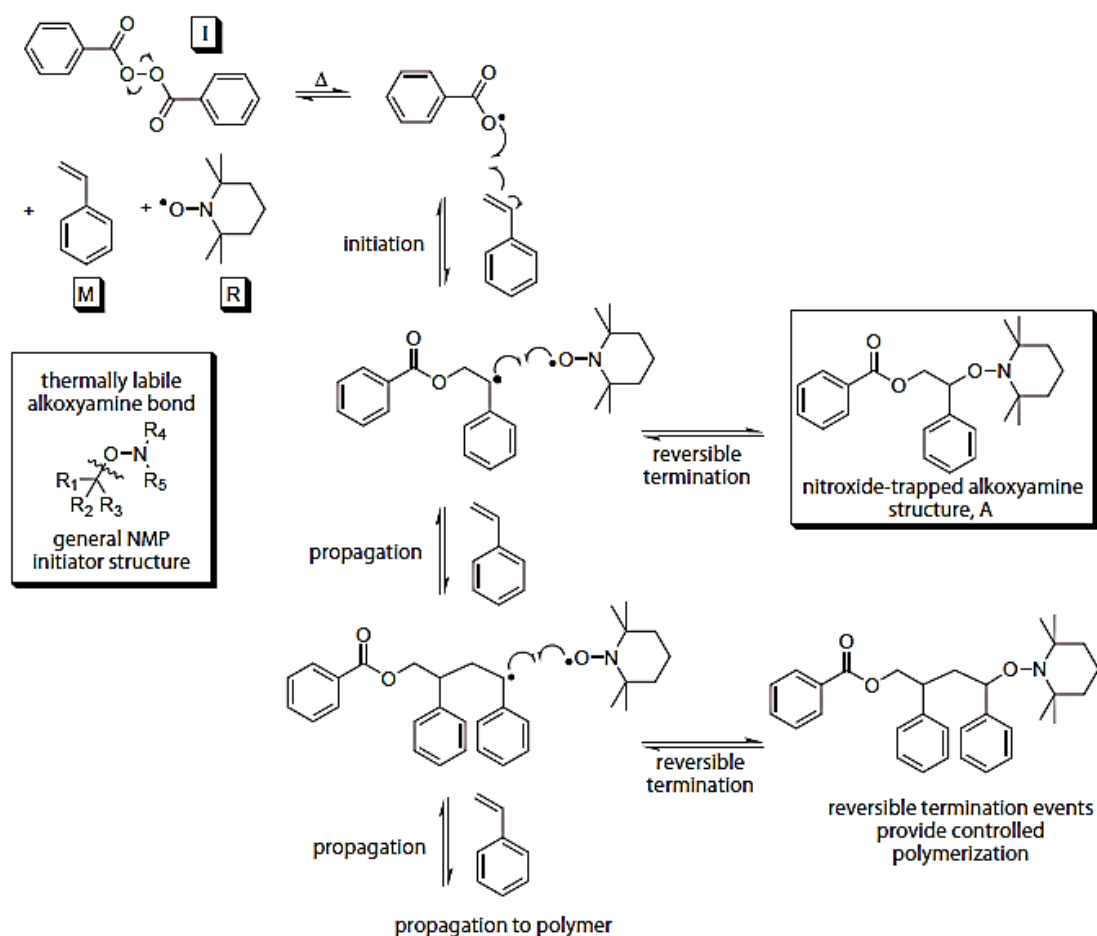
A CTA can be grafted to supporting surface *via* either tethered Z-group or immobilized R-group, upon which the grafting characteristics are significantly varied. As mentioned before, the R-group initiates the growth of polymer chains, hence, the method of tethering Z-group to the surface is considered to be closer to *grafting to* approach as the polymer chains grow in solution then diffuse to surface to undergo the degenerative chain transfer process. Several polymers have been obtained by this method including polymer of acrylate, methylmethacrylate, *N,N*-dimethylacrylamide [175-177], and glycopolymer [178]. In contrast, the use of R-group as tethering point is considered as *grafting from* approach because the propagating chains grow from surface rather than in solution. Therefore, the use of surface-immobilized R-group is widely adopted in RAFT polymerization from surface. However, the drawback of this approach is that at high CTA density, the tethered polymer chains would progress *via* uncontrolled radical polymerization, which is avoidable by keeping polymerization at low monomer conversion [179].

Overall, RAFT polymerization is a versatile, metal-free technique that shows good compatibilities towards various monomers. However, this technique generally cannot provide polymer brushes of thickness higher than 30 nm, and furthermore, the use of RAFT polymerization normally requires multi-step syntheses as CTAs are often either expensive or unavailable to purchase.

1.3.2. Nitroxide-Mediated Polymerization (NMP)

Stable Free-Radical Polymerization (SFRP) is one of the very first controlled radical polymerization techniques that had been developed. In SFRP, reversible termination is the core of the control over polymerization in which involved stable radicals are often nitroxides, triazolinyls, trinyls or dithiocarbamates; however, the use of nitroxide-mediated polymerization (NMP) is the most common in SFRP due to their higher efficiency.

In NMP, the polymerization is carried out either by the thermal decomposition of an aloyamine to form reactive radical and nitroxide stable radical or by mixing a free radical initiator with a nitroxide radical, which is stable at room temperature. Scheme 5 presents the mechanism of NMP of styrene (M) mediated with TEMPO (R) – a common-used nitroxide radical – and benzoyl peroxide (I) as initiator.



Scheme 5. Mechanism of NMP of styrene mediated with TEMPO nitroxide radicals and benzoyl peroxide as initiator [180]

Surface-initiated NMP is performed either from a conventional radical initiator attached at the substrate surface in the presence of free nitroxide radicals or from an alkoxyamine anchored to the support (Figure 13).

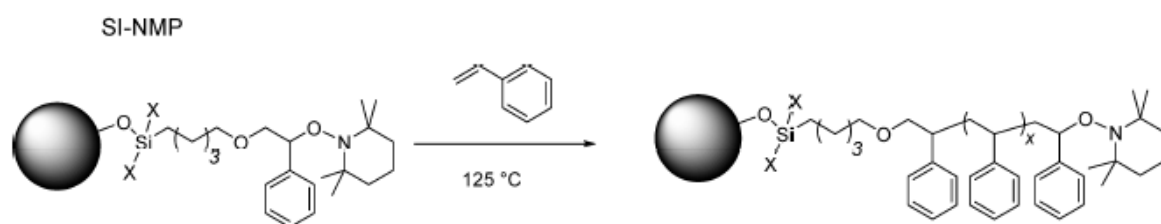


Figure 13. Illustration of surface-initiated NMP of styrene by grafted alkoxyamine [181].

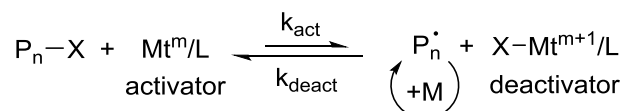
The advantage of SI-NMP is its unimolecular system that is free of catalyst and metal; therefore, it is suitable for the synthesis of polymer brushes for electronic or biological applications where the impurities are major concerns. However, this technique frequently suffers from various challenges that reduce its applications like slow polymerization kinetics accompanied with high temperatures and long duration, low compatibility with methacrylate monomers due to side reactions, unavailability of reagents and difficulty in synthesis of

nitroxide/alkoxyamine [182]. Even though these problematic issues have been addressed in recent years, NMP is still more complicated than RAFT and ATRP.

1.3.3. Atom Transfer Radical Polymerization (ATRP)

ATRP is another controlled polymerization technique based on reversible deactivation of dormant chain. This technique has been used for a countless number of monomer of different varieties like styrene, methacrylates, acrylates and dienes.

The reversible deactivation in ATRP is a catalytic process (Scheme 6) which is mediated by complexes of redox-active transition metals like Cu, Fe, Ru, Mo, Os, etc. The equilibrium between propagating radicals and dormant species is the driving force in control of ATRP. Indeed, the dormant species (P_n-X) reacts with metal complex at lower oxidation state (Mt^m/L) to form propagating radicals (P_n^*) and metal complex of higher oxidation state (Mt^{m+1}/L). Therefore, the Mt^m/L is so-called activator and the Mt^{m+1}/L is considered the deactivator. The activity of the activator complex must be high enough to create homolytic dissociation of the C-X bond in the alkyl halide initiator. This is called activation process, which is characterized by activation constant k_{act} . Similarly, the deactivator complex must quickly trap the propagating radicals to regenerate the dormant species P_n-X , this is called the deactivation process characterized by deactivation constant k_{deact} .



Scheme 6. Catalytic mechanism of ATRP equilibrium

SI-ATRP is also the most used polymerization technique [183] due to the ease in immobilization of various initiators onto substrates of different type, size and shape (Figure 14).

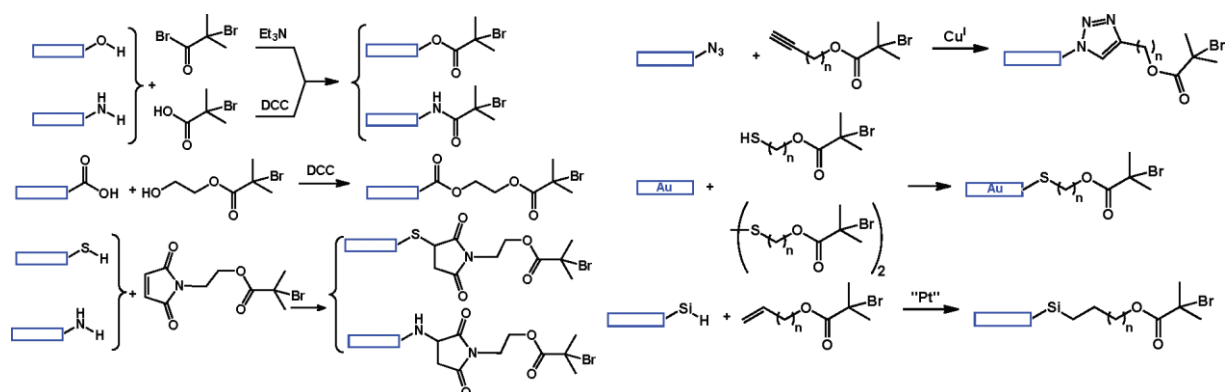


Figure 14. Some examples of chemical transformations used to attached ATRP initiator to supporting substrates

Most of ATRP reagents are commercially available; however, the involvement of redox reaction of metal complexes at different oxidation states makes ATRP a complex system. The control of ATRP is governed by various parameters, notably initiator, ligand, catalyst, and solvent. The influences of these parameters have been well explained in literature in term of ATRP equilibrium constant. ATRP equilibrium constant (K_{ATRP}) is the ratio between activation constant (k_{act}) and deactivation constant (k_{deact}). In order to maintain a low radical concentration and minimize termination events, the value of K_{ATRP} must be small ($\sim 10^{-9}$ to $\sim 10^{-4}$), and k_{deact} must be very large ($> 10^7 \text{ M}^{-1} \text{ s}^{-1}$). The following subsections summarize overall trend in influences of various factors on the control of polymerization by examining and comparing the change in reaction constants.

1.3.3.1. Influence of initiator

Several studies have shown that initiator structure plays a critical role in the control of ATRP [184-187] because it defines the nature of radical formed during initiation, which subsequently alter the activation constant, hence, kinetic equilibrium of polymerization.

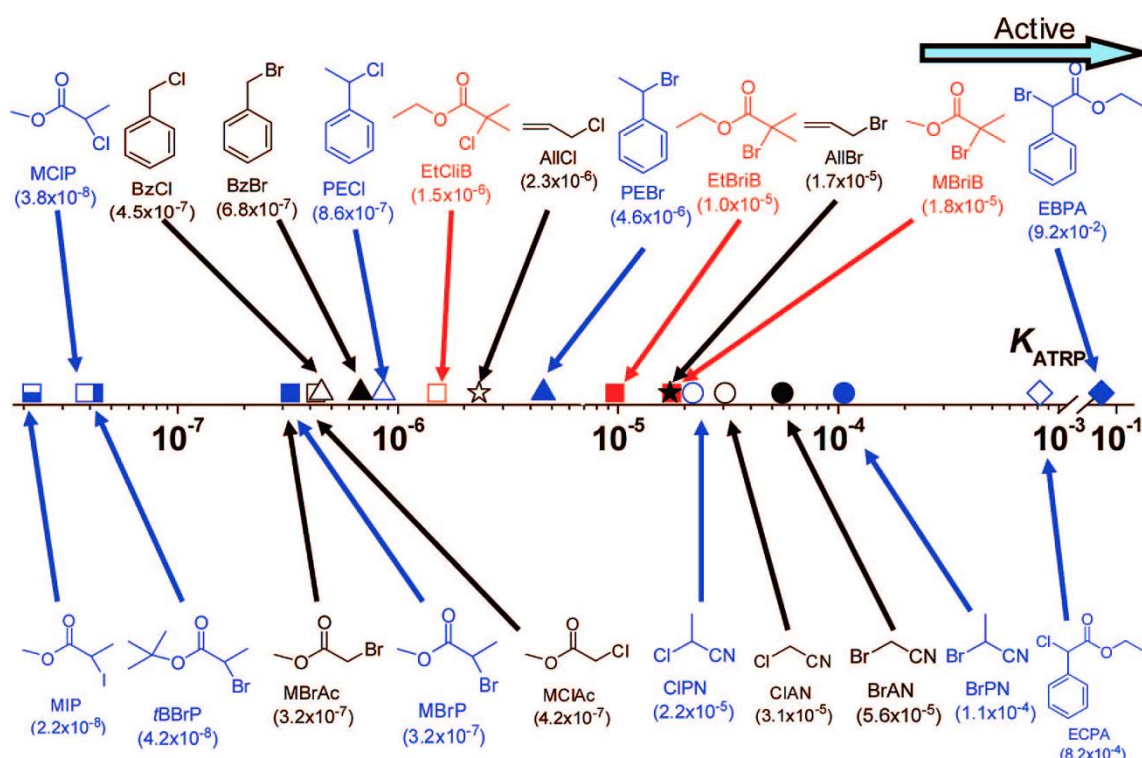


Figure 15. ATRP equilibrium constants of various initiators with CuX/TPMA in acetonitrile at 35 °C [186]

Figure 15 shows K_{ATRP} of various initiators with $\text{Cu}^{\text{I}}\text{X}/\text{TPMA}$ in acetonitrile at 35 °C. It is seen that the modification in structure of initiator shows moderate to enormous change in activation rate constants. The efficiency of initiator depends greatly on the nature of leaving atom/group, the substitution degree of initiator, and the activity of alkyl group. Generally, the activity of alkyl group for initiators follows (a) the order of substitution: $3^\circ > 2^\circ > 1^\circ$, (b) the

stabilization of (pseudo) radicals: phenyl ester > cyanide > ester > benzyl > amide. The activity of the leaving atom/group for the initiators decreases in the order of I > Br > Cl ≫ SCN ≈ NCS.

1.3.3.2. Influence of ligand and metal complexes

Ligands can tune the electronic, steric and solubility of ATRP catalysts, therefore, the use of ligand along with the choice of metal complexes may affect greatly the kinetics of polymerization by ATRP. As seen in Figure 16, ATRP equilibrium constant may vary within 7 orders of magnitude. In general, the activity of copper complex in classic ATRP follows the order of tetradentate (cyclic-bridged) > tetradentate (branched) > tetradentate (cyclic) > tridentate > tetradentate (linear) > bidentate.

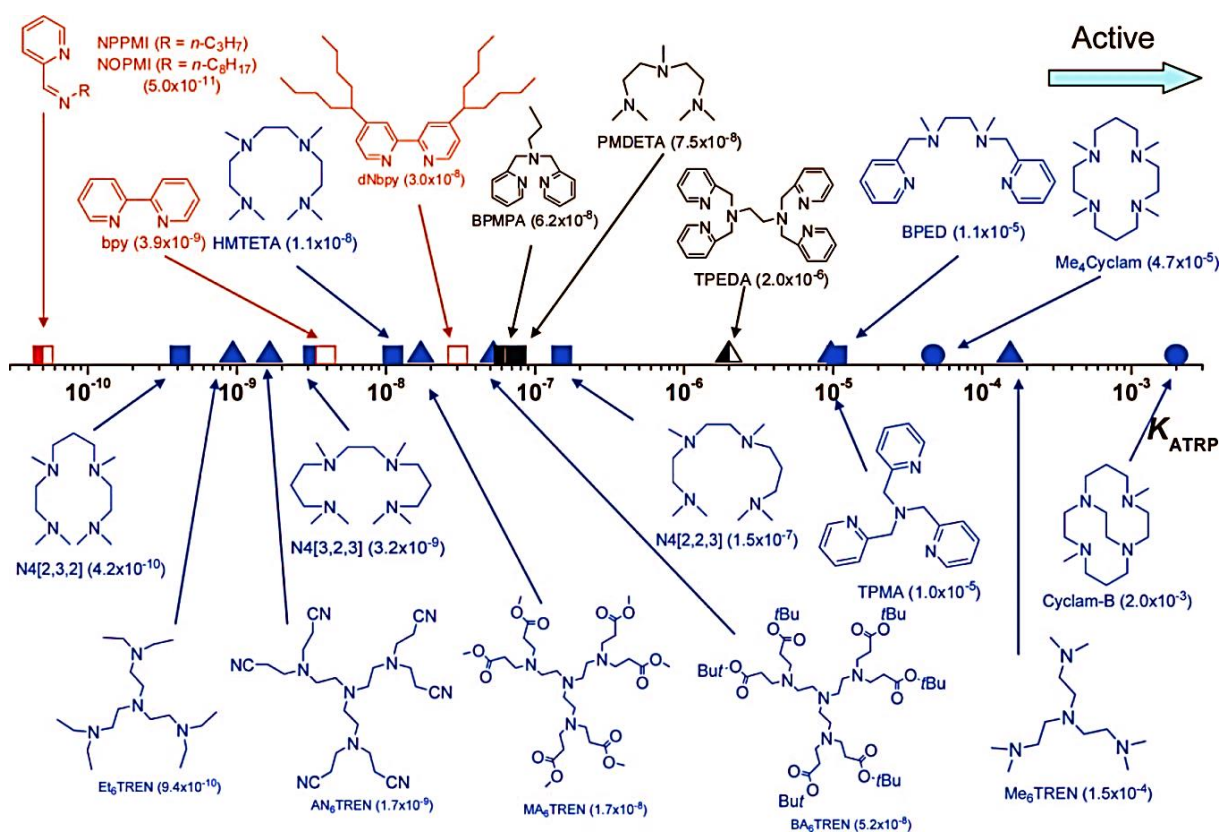


Figure 16. ATRP equilibrium constant of various ligands with eBiB as initiator, CuBr as catalyst, in acetonitrile at 35 °C [186]

Beside ligand's denticity, the nature of nitrogen atoms in ligands also contributes significantly to the activity of metal complexes. The order of activity in term of nature of nitrogen atoms is pyridine \approx aliphatic amine > imine < aromatic amines.

However, it is considered that the dynamic of exchange reaction may be even more important in ATRP than the overall K_{ATRP} [171]. The common rule in choosing catalyst for an ATRP is that for less reactive monomer or in diluted condition, a large K_{ATRP} and a very large k_{deact} are required so that radicals are rapidly deactivated. Figure 17 presents a summary of activation

rate constant k_{act} , deactivation rate constant k_{deact} and their ratio K_{ATRP} of various ligands and initiators in acetonitrile. On the other hand, while the rate of ATRP is strongly influenced by the value of K_{ATRP} , the control of polymerization in term of polydispersity index is determined by the deactivation rate constants. In term of ligand, those having stronger activating capacity is generally weaker deactivators.

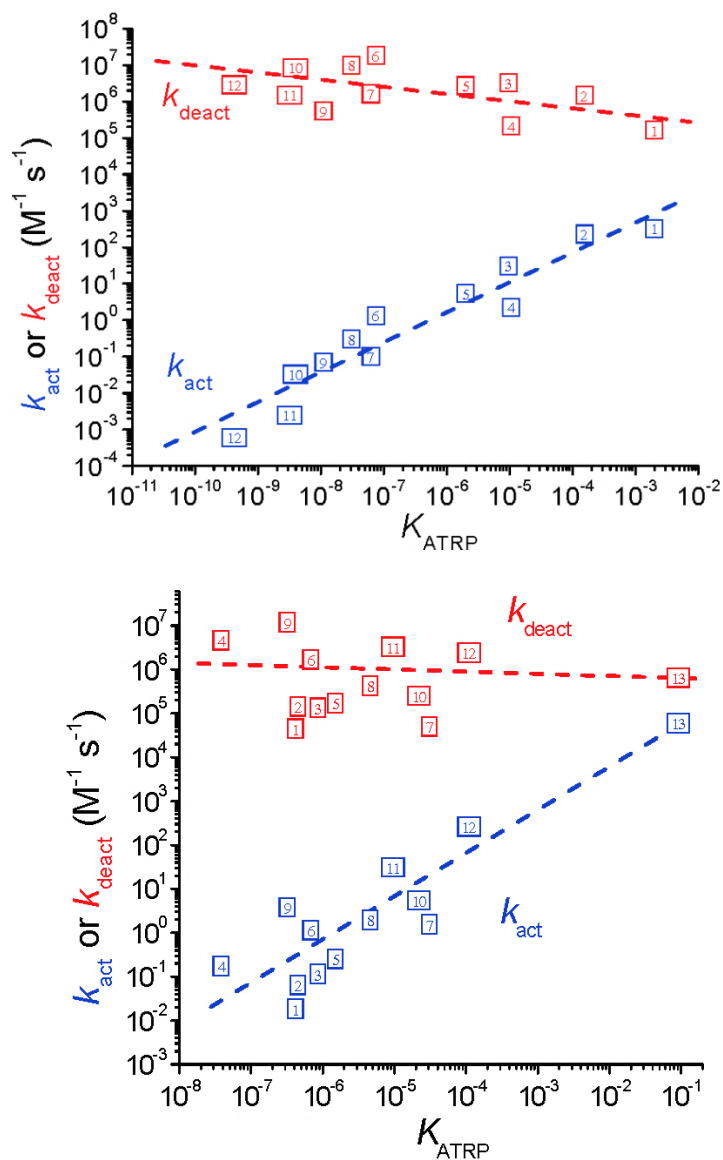


Figure 17. Relationship between activation rate constant (k_{act}), deactivation rate constant (k_{deact}) in function of K_{ATRP} of different ligands (top) and initiator (bottom) [188]. Ligands 1: Cyclam-B; 2: Me₆TREN; 3: TPMA; 4: BPED; 5: TPEDA; 6: PMDETA; 7: BPMPA; 8: dNbpy; 9: HMTETA; 10: bpy; 11: N4 [3,2,3]; 12: N4 [2,3,2]. Initiators 1: MClAc; 2: BzCl; 3: PECl; 4: MCIP; 5: ECiB; 6: BzBr; 7: CIAN; 8: PEBr; 9: MBrP; 10: CIPN; 11: EBiB; 12: BrPN; 13: EBPA.

1.3.3.1. Influence of solvent

Even though radical polymerization is normally less selective towards solvent than ionic polymerization, kinetics of ATRP still depends on the choice of solvent as the solvent polarity may exert remarkably the polymerization equilibrium and rate constant [189].

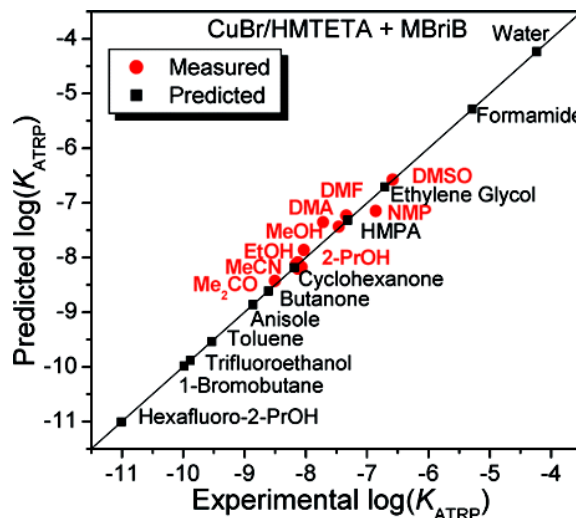


Figure 18. Experimental and predicted K_{ATRP} of ATRP in different solvents [190]

Figure 18 presents the effect of solvent on K_{ATRP} for CuBr/HMTETA with methyl α -bromoisobutyrate. It is to note that the effect of solvent is varied from the less polar character of Cu(I) complexes than the cationic Cu(II) complexes, which are strongly stabilized in more polar solvents [191]. Therefore, ATRP in polar solvent may lead to the accumulation of Cu(II) complex, hence, losing the balance between activation and deactivation processes.

Despite its enormous versatility, ATRP suffers from several disadvantages including (1) the use of air/oxygen tolerance Cu(I) halide which requires pre-treatment to remove the presence of air/oxygen, *i.e.* free-thaw-pump process, (2) the requirement of high catalyst concentration which is normally in equal equivalence with initiator, hence resulting in high concentration of copper residue at the end of reaction. In order to overcome these disadvantages, several approaches have been proposed where the direct use of Cu(I) halide is avoided by its *in situ* continuous (re)generation using either electrochemical mediated polymerization (*e*ATRP) [192], photoreduction (photoinduced ATRP) [193], chemical reductants (Activator Regenerated by Electron Transfer (ARGET) ATRP) [194], or the employment of Cu(II) halide and solid Cu(0) [195, 196]. Among these alternatives, the latest has attracted many interests due to the use of Cu(0), which is low cost, easy to remove and recyclable.

1.3.4. Cu(0)-mediated RDRP

The introduction of zero valent copper metal in RDRP system (so-called Cu(0)-mediated RDRP) had been proposed for the first time in the middle of 1990s. Since then, the interest in this polymerization technique has gradually increased due to its facile nature. Figure 19

provides an overview on the trend in research employing Cu(0)-mediated RDRP since its first appearance.

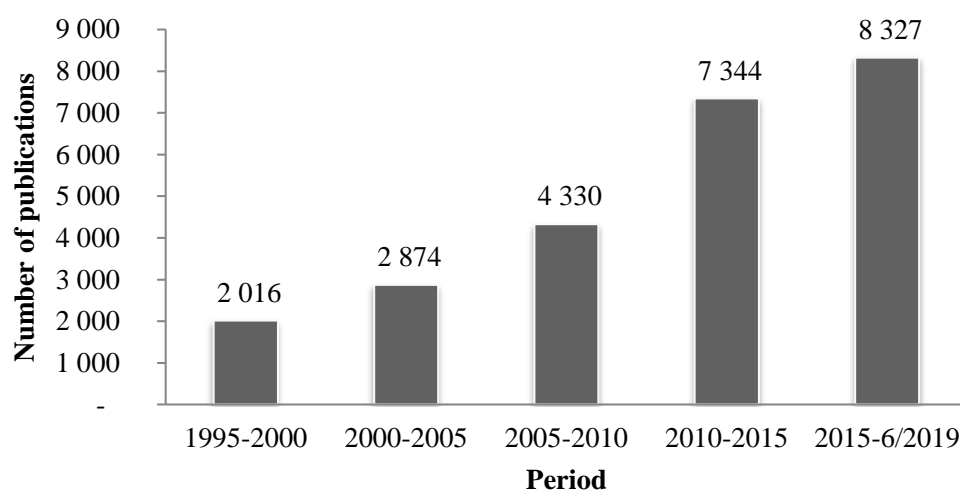


Figure 19. The increasing trend in research involving Cu(0)-mediated RDRP as of June 2019, data retrieved from Google Scholar.

The rapid rise in research using this technique lies in the use of Cu(0) and Cu(II) halide – which are much more stable compared to Cu(I) species. Therefore the polymerization is more tolerant to air/oxygen, hence reducing the labor work to avoid the influence of external factor on the polymerization process. Additionally, the activator in Cu(0)-mediated RDRP is produced *in situ*, thus, the amount of catalyst needed is significantly reduced compared to classic ATRP, which in consequence, resulting in polymer with ppm amount of copper residue.

As presented, several thousand studies have been done over the past two decades to gain in-depth knowledge on the mechanism, properties and characteristics of this technique. Figure 20 summarizes milestones in the development and understanding of Cu(0)-mediated RDRP since its birth till 2013. Despite its simple chemical requirements, the catalytic mechanism of this technique has created vigorous debate between Single Electron Transfer Living Radical Polymerization (SET-LRP) and Supplemental Activation and Reducing Agent Atom Transfer Radical Polymerization (SARA ATRP) [197-203].

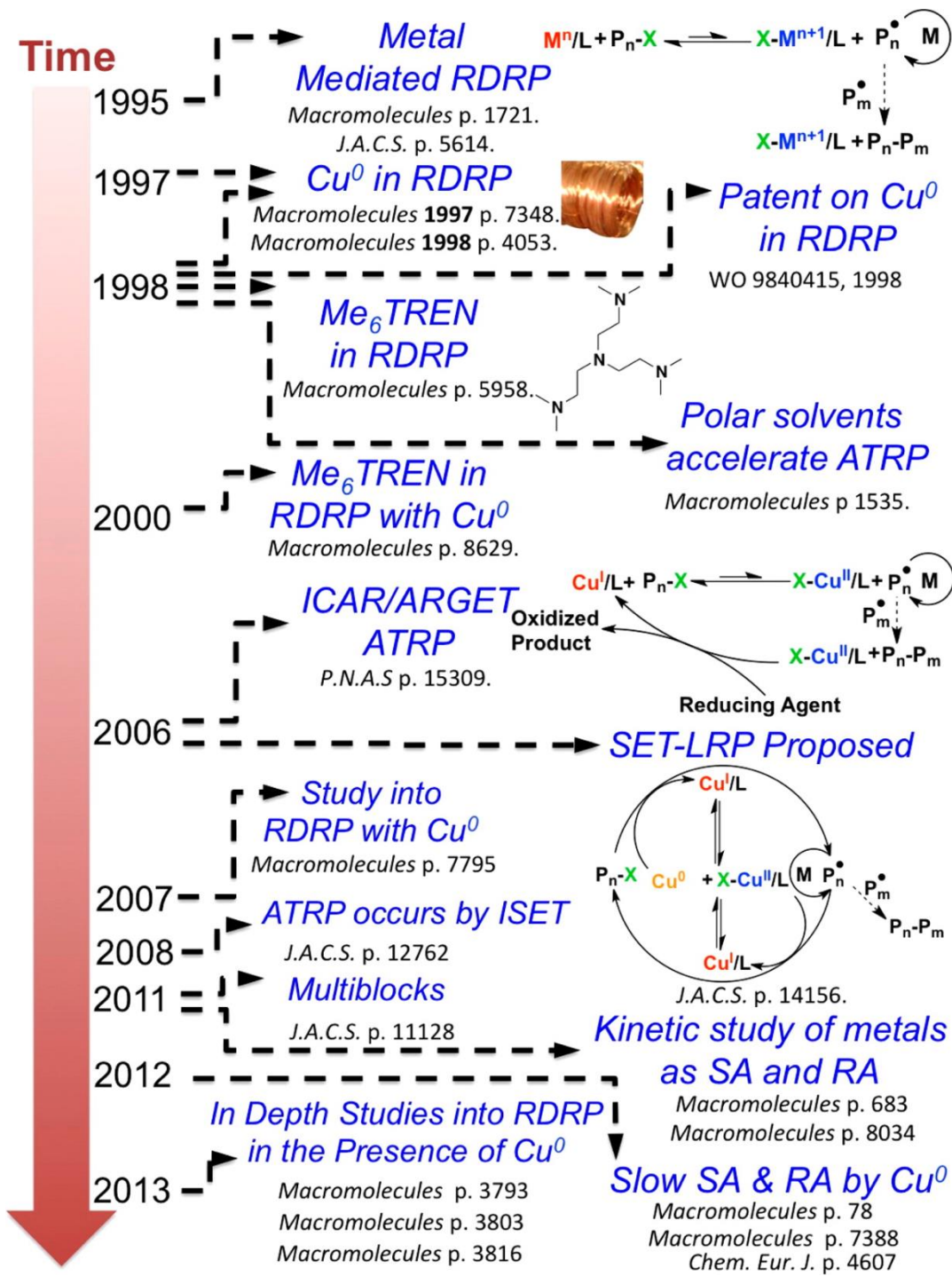


Figure 20. Milestones in development of Cu(0)-mediated RDRP [197]

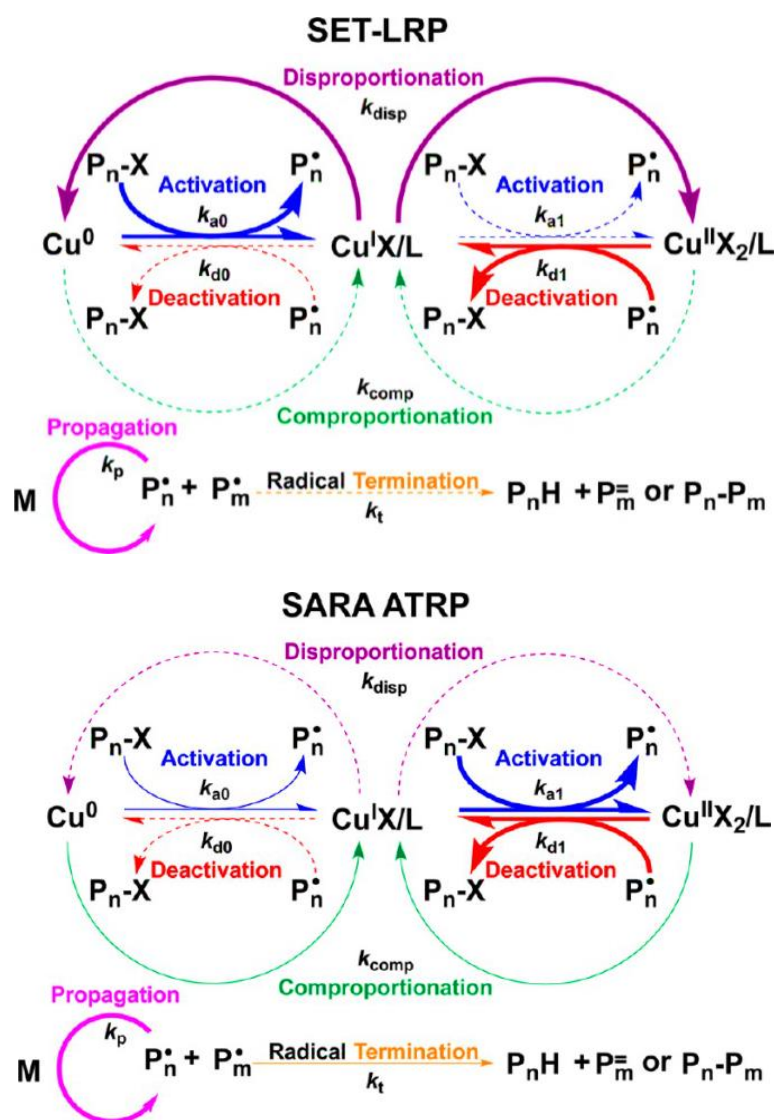


Figure 21. Mechanism of SET-LRP (top) and SARA ATRP (bottom) [197]

Figure 21 presents the mechanism of SET-LRP and SARA ATRP. The two proposed mechanisms of SET-LRP and SARA ATRP are to explain the rapid polymerization of different monomers in polar environment in presence of metallic copper, ligand and soluble copper complexes [197, 198, 200-209]. Though the chemical requirement, consideration on Cu(II) role, the control over polymerization are the same, there are significant differences between the two mechanisms. First of all, in term of alkyl halide activation, “nascent” Cu(0) nanoparticles are considered major activator in SET-LRP while SARA ATRP proposes that Cu(I) species play the role of main activator (as in classic ATRP) and Cu(0) is the supplemental activator and reducing agent. Secondly, SET-LRP considers inner sphere electron transfer as the core of activation while this process is considered to follow outer sphere electron transfer by SARA ATRP. Moreover, SET-LRP and SARA ATRP are debating on the equilibrium of disproportionation and comproportionation where SET-LRP suggests the instantaneous disproportionation of Cu(I) is the dominant event while SARA ATRP assumes the comproportionation of Cu(0) and Cu(II) to generate the activator Cu(I) to

be the main process. In term of termination, SARA ATRP is against SET-LRP on its consideration of no termination at 100% chain end functionality because that violates the principles of halogen conservation and microscopic reversibility. Additionally, the two proposed mechanisms also have different point of view on the effect of solvent. SET-LRP shows that disproportionating solvents like DMSO is better while there is no difference between disproportionating and non-disproportionating solvents and ligands from SARA ATRP point of view. As the goal of this research is not to participate into the debate but to focus on the use of SET-LRP/SARA ATRP to synthesize functional polymers and copolymers at ease, therefore, with our appreciation for in-depth research from both SET-LRP and SARA ATRP parties, we would like to refer this approach as Cu(0)-mediated RDRP hereinafter as recommended by IUPAC [210].

Regardless of that debate, polymerization mediated by Cu(0) has successfully used for a wide variety of monomers including but not limited to styrene [211], methyl (meth)acrylate [212], *n*-butyl acrylate [213], acrylamide monomers [214], glycidyl methacrylate [215], (3-acrylamidopropyl)-trimethylammonium chloride [216], polyether acrylate [217]. The utilization of Cu(0)-mediated RDRP has allowed the preparation of not only homopolymers but also hexablock polymer [219] to even decablock polymers [218]. Additionally, surface-initiated polymerization Cu(0)-mediated RDRP with its exceptional advantageous characteristics have recently been proven to function well for several different substrates including silicon substrates [220-230], graphene oxide [231, 232], cellulose nanocrystals/sheet [233-236], synthetic polymer substrates [97, 237-241], paper [242], TiO₂ [243], or even chicken feather [244]. Additionally, due to the robustness and versatility of this technique, the preparation of polymer brush array with several different polymers and block copolymers have also been reported [224] as illustrated in Figure 22.

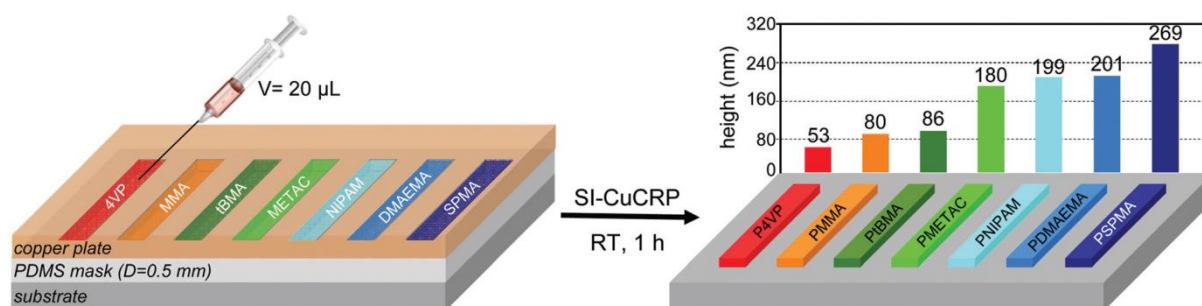


Figure 22. Fabrication of polymer brush array by SI-Cu(0)-mediated RDRP using a crosslinked PDMS layer as a mask and spacer between substrate and copper plate with various monomers [224]

1.4. Polymer Post-modification

1.4.1.1. Introduction on Polymer Post-modification

Polymer post-modification has been done in parallel with the history of polymer science. Post-modification of polymeric materials allows alternating partially or modifying completely

certain characteristics of the materials without losing macromolecular features like degree of polymerization, polydispersity, tacticity of the precursor polymers. During the 19th century, many post-modification has been done, for example, the treatment of natural rubber with sulfur in enhancement of toughness and elasticity of the material [245], or the exposure of cellulose to nitric acid in preparation of the explosive nitrocellulose [246]. However, the variety of chemical reactions involving in this process was limited until the early of 20th century where Hermann Staudinger placed the most important stone on the understanding of modification reactions of polymeric materials, giving birth to the term “polymer analogous reaction” which has been studied extensively to fabricate functional materials ever since [247].

The explosive growth in polymer post-modification has been striking since 1990s thanks to the blossom in controlled polymerization techniques, and the discovery and revive of several click reactions such as copper(I)-catalyzed azide alkyne cycloaddition and thiol-ene addition. The combination of efficient chemical transformation with functional macromolecules has been generously provided access in preparation of a plethora of materials with appealing characteristics, complex functionality as well as convoluted architectures. Figure 23 presents a summary of the main classes of reactions that can be used to prepare functional polymers *via* post-polymerization modification [247].

An ideal polymerization functionalization reaction should be fast, straightforward, orthogonal, amenable to large-scale purification, and efficient under equimolar conditions [248]. Among all of the reactions presented in Figure 23, the substitution of polymer of active esters with amino groups is one of the approaches that satisfy the concept of ideal post-polymerization modification. In addition, various methacrylate and methacrylamide monomers cannot be directly polymerized due to the reactivity of α,β -unsaturated carbonyl with many nucleophilic functional groups, in such cases, the use of post-modification of activated polyester can be beneficial. Until now, an incredible number of activated esters have been exploited [247], however, *N*-hydroxysuccinimide esters and the family of pentafluorophenyl esters are the most popular ones.

1.4.1. *N*-hydroxysuccinimide esters

N-hydroxysuccinimide (NHS) esters are the most used activated monomer for functionalization of macromolecules. Polymers of NHS esters are resistant to hydrolysis, and furthermore, the modification of their polymers with primary and secondary amines is innocuous and can be performed under mild condition. An example to show the enormous impact of post-polymerization modification is the possibility to prepare poly(*N*-allyl acrylamide). Due to the double presence of allyl group, direct polymerization to obtain poly(*N*-allyl acrylamide) is not possible. However, in 1972, the post-modification of poly(*N*-acryloxysuccinimide) and poly(*N*-methacryloxysuccinimide) with allylamine have made the impossible possible [249].

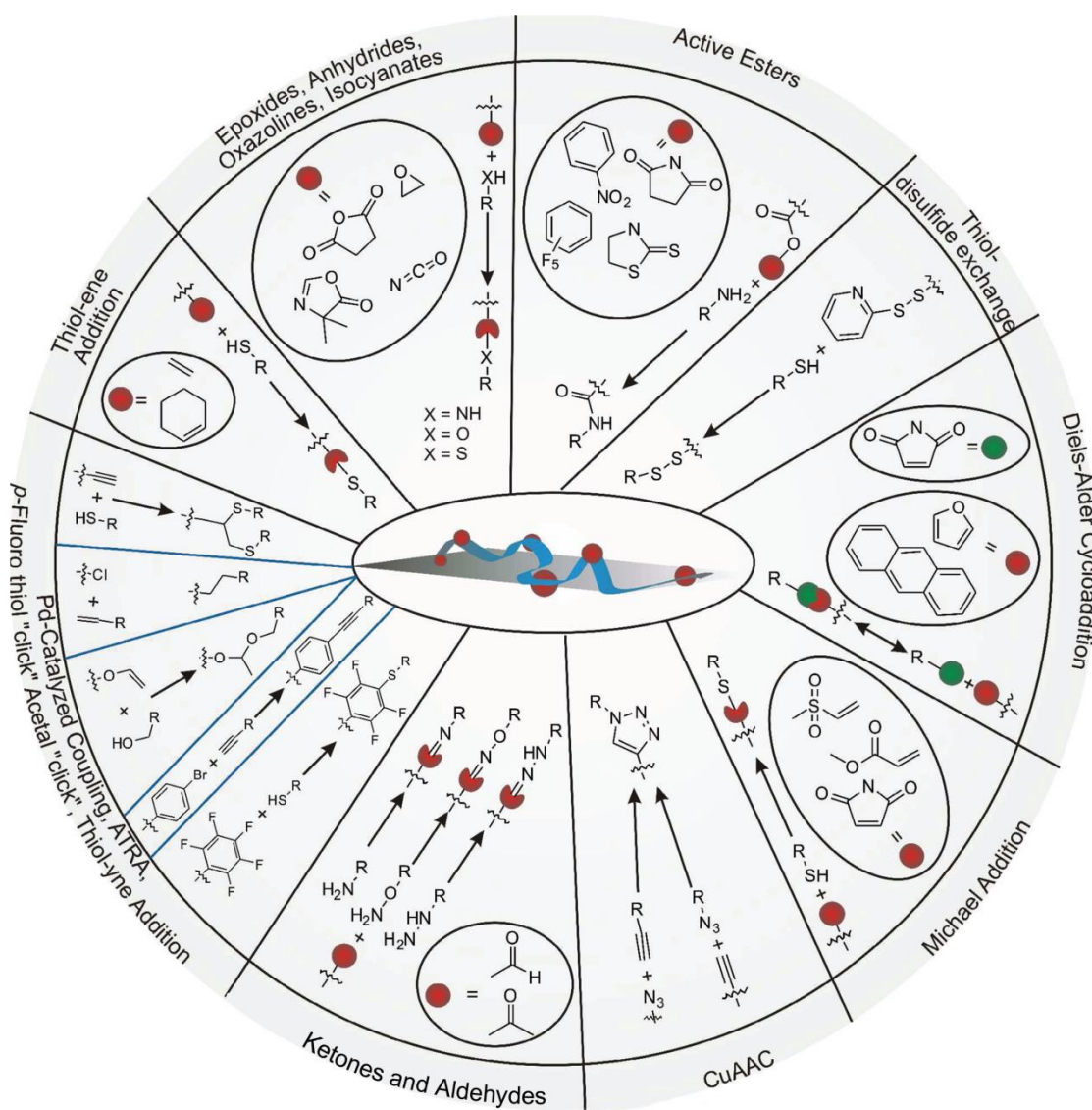
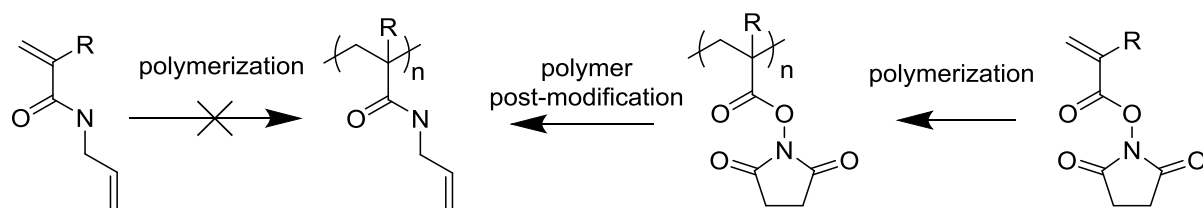


Figure 23. Summary of the main functional groups and class of reactions involved in polymer post-modification [247]



R = H or CH₃

Scheme 7. Pathways to obtain poly(*N*-allyl acrylamide) [249]

Furthermore, as the oldest class of activated polymer, NHS polymers present to be the first macromolecular precursor toolbox to prepare pharmacologically active polymers. Earliest of such studies involve functionalization of poly(NHSA-*co*-*N*-vinylpyrrolidone) with oligonucleotides [250], NHS-polynorbornene with sugars [251], and the preparation of

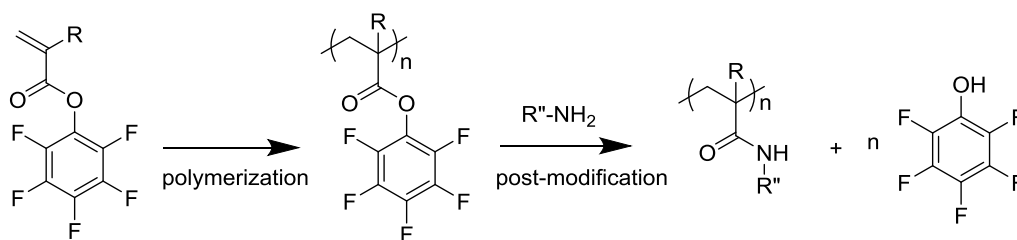
copolymer bearing sialic acid moieties from PNHSA for inhibition of influenza infection [252].

The advent of RDRP led to the revolution of activated esters because the combination of RDRP and post-polymerization modification allows the preparation of homo- and copolymers in a controlled manner, *i.e.* predetermined size, narrow molecular weight distributions, defined end-group and high compositional homogeneity. Then, many studies have been working on this powerful combination to prepare well controlled polymers with various applications. For instance, PNHSMA has been synthesized by ATRP as precursor to advanced therapeutics based on poly(*N*-2-hydroxypropyl methacrylamide) (PHPMA). This approach was especially intriguing as the infamous propensity of HPMA monomer towards autopolymerization [253]. Later on, other studies have been dedicated to improve the initiator efficiency using NHS monomer [254] and then to optimize polymerization conditions for PNHSMA where monomer conversion reached 70% [255]. Grafting of polymers onto substrate have been studied for NHSMA and 4-vinylbenzoate NHS monomers *via* SI-ATRP with high grafting density achieved [256, 257]. Unlike ATRP, RAFT polymerization of NHS-based monomer is much less efficient as the polymerization by this degenerative chain transfer polymerization often results in broad molecular weight distributions. However, RAFT copolymerization with other acrylamide monomers have been successfully achieved with acceptable control over molecular weight and polydispersity [258-261].

Although NHS polymers have been the most exploited activated polymer, some limitations in its utilization have been realized. For examples, the solubility of polyNHSA or polyNHSMA is restricted to DMSO and DMF. Secondly and more importantly, the post-modification of NHS polymers might be spoiled by side reactions such as ring opening of the succinimide part and/or the formation of *N*-substituted glutarimides by attack of amides on neighboring activated esters [262]. Although another study has proved that these side reactions could be mitigated by increasing the reaction time, temperature and equivalents of amine conjugates [263], these inefficiencies of NHS-based polymers have encouraged the adaptation of another class of activated esters: pentafluorophenyl-containing esters.

1.4.2. Pentafluorophenyl (meth)acrylates

It is known from 1973 that polymers of pentafluorophenyl esters are more reactive than NHS ester and less bulky compared to pentachloro ones [264]. However, the blossom of this class of reactive monomers had not been as well exploited as NHS esters before the first set of poly(pentafluorophenyl acrylate) (PPFPA) and poly(pentafluorophenyl methacrylate) (PPFPMA) was introduced by the group of Patrick Theato [265, 266].



Scheme 8. Polymerization of PFP(M)A and post-modification of PPFP(M)A

Compared to NHS esters, the use of PFP-esters possesses several advantages. First of all, unlike the low solubility of NHS-esters, PFPA and PFPMA are soluble in a wide range of solvent, including solvent for polymerization and modification. Furthermore, PPFP(M)A is more reactive in nucleophilic substitution than the NHS counterparts, *i.e.* PPFP(M)A can be substituted by aromatic amines and alkoxides, though the degree of substitution is lower than that with aliphatic amines. Nonetheless, the beauty in using PFP(M)A is also coming from its possession of pentafluorophenyl groups which makes it easier and more precisely in following monomer conversion as well as evaluating and understanding post-polymerization modification process (Scheme 8 and Figure 24). It is seen from Scheme 8 and Figure 24 that the nucleophilic substitution of PFP(M)A leads to the liberation of pentafluorophenol - whose signals are between -185 ppm and -168 ppm in ^{19}F -NMR spectra that are well distinctive from that of pentafluorophenyl monomer and polymers.

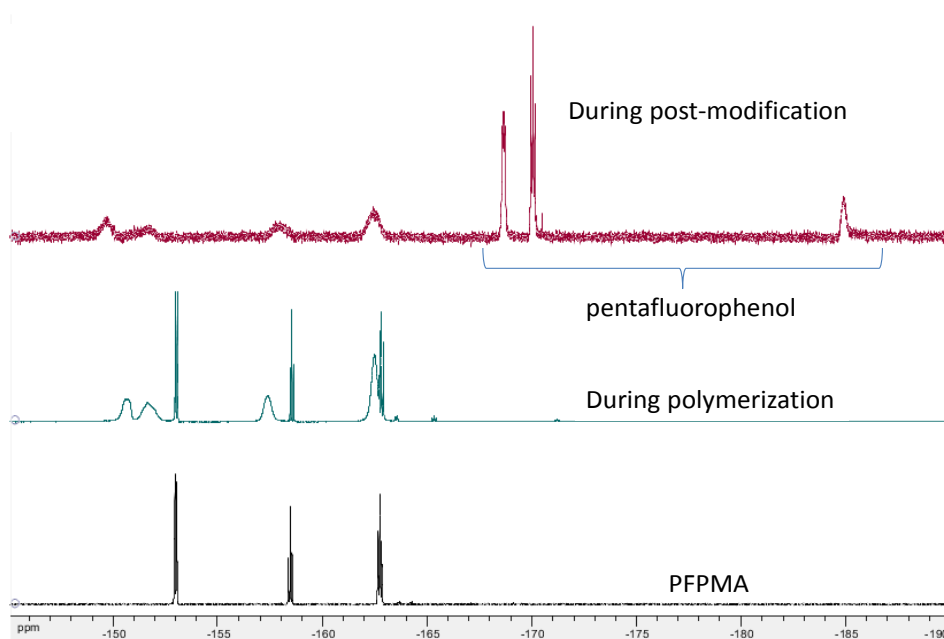


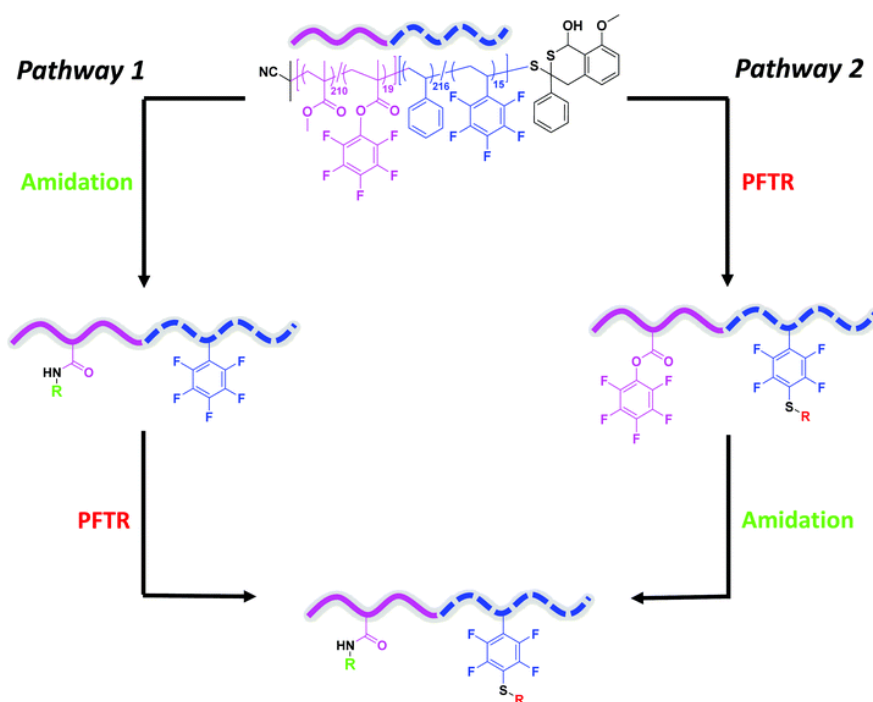
Figure 24. ^{19}F NMR spectra of PFPMA (bottom), during polymerization (middle) and during post-modification with release of pentafluorophenol (top)

Since their first introduction in the early of 20th century, hundreds of research have been involving the use of PPFP(M)A as precursor for the synthesis of polymers from simple to complicated, single to multifunctional chemical structure with various morphologies and

applications. Scheme 9 shows a representative example of sequential post-polymerization modification of PFPMA with primary amines to prepare highly functional hybrid polymer glycopeptide conjugates for tumor immunotherapy [267]. In this study, polymer of PFPMA has been obtained by RAFT polymerization in dioxane at 80 °C with AIBN as initiator and 4-cyano-4-(phenylthiocarbonylthio)pentanoic acid as CTA. The obtained homopolymer was subjected to either sequential aminolysis or chain extension with lauryl methacrylate then to sequential aminolysis. It is to remark that the liberation of thiocarbonylthio group at the end chain of polymer must be done before carrying out aminolysis to obtain precursor 10 or 20 as presented in Scheme 9. Finally, authors of this paper have been able to synthesize the first examples of well-controlled nanosized polymer-linked vaccines. This study is one of the phenomenal examples to present the beauty in using polymer of pentafluorophenyl esters as template for preparation of pharmacological macromolecules.

The reactivity of different pentafluorophenyl-containing esters has been investigated. Firstly, it has been reported that acrylate backbone show better reactivity compared to methacrylate analogue [266], *i.e.* the substitution with primary amine of PFPMA reached 100% conversion while the value achieved by PFPMA was 65%. Moreover, the pentafluorophenyl 4-vinyl benzoate (PFP4VB) has been reported to be even more reactive compared to PFPMA proven by its quantitative reaction with less nucleophilic aromatic or secondary amines such as aniline and morpholine or *N*-propylpiperazine [269]. Later on, due to such difference in reactivity, block and statistic copolymers of PFPMA and PFP4VB have been synthesized and demonstrated to be selective in sequential post-modification with aniline (targeted to PFP4VB) and isopropylamine (targeted to PFPMA) [270]. Furthermore, another study has proposed the synthesis of poly(methyl methacrylate-*stat*-pentafluorophenyl methacrylate)-*b*-poly(styrene-*stat*-pentafluorostyrene) as template for synthesis a series of bifunctional block copolymers [268] as presented in Scheme 10. That idea is based on acknowledging the amidation of PFPMA by primary amine, while the fluorine atom at para position of pentafluorostyrene is able to react with a thiol group, therefore, one can synthesize dual functional polymer from a single block copolymers.

While the activity in nucleophilic substitution can be enhanced in PFP4VB compared to PFPMA, another study has proven that polymer of pentafluorobenzyl methacrylate (PFPBMA) also has different reactivity compared to PFPMA. Not only that PFPBMA is reactive in para-fluoro thiol substitution, the substitution of PFPBMA also happens at para-fluoro position when subjected to amidation by primary amines, yet its selectivity is lost due to di-substitution of one primary amine with two neighbor repeating units. In contrast, the substitution with secondary amine is straightforward without presence of side reactions [271].



Scheme 10. General scheme representing the ideal orthogonal amidation and *para*-fluoro thiol reaction between two different functional PFP-based groups on the same block copolymer [268]

Although the post-polymerization functionalization of PFP(M)A has been mostly focused on the nucleophilic substitution with amines, transesterification with alcohol has been proven to be possible [272, 273]. From PFP(M)A precursor, various functional polyacrylates have been obtained by the reaction under mild condition (DMF as solvent and *N,N*-dimethylaminopyridine as catalyst) of the precursor with no more than 1.5 equivalent of alcohols containing aliphatic, benzylic, allylic, propargylic, acrylic, amino, and carboxylic functionalities [272]. Even though certain alcohols only showed near quantitative conversion, this achievement is of great significance because alcohol functionality is one of the most ubiquitous functional groups in organic chemistry and it is compatible with a large variety of other functionalities.

While post-polymerization modification of pentafluororo-containing polymers is of its plethora, controlled polymerization techniques to obtain this type of polymer is quite restricted. Unlike NHS-based monomer where ATRP is the mainstream technique, the first RDRP technique to synthesize PFP(M)A has been reported by RAFT polymerization [265] using either cumyldithiobenzoate or 4-cyano-4-((thiobenzoyl)-sulfanyl)pentanoic acid as CTA. After this publication, many other studies have been done following the same technique, which makes RAFT polymerization the most used controlled technique to synthesize polymer of pentafluorophenyl-containing esters [272-284]. However, this technique involves chain transfer agent that generally consists thiocarbonylthio groups, which should be retained during and after polymerization for the control purpose. Yet, this type of functional group is quite reactive and might be involving in many types of reactions including

nucleophilic substitution or alkene coupling [270]; hence, the conservation of these reactive groups may interfere with the post-modification of reactive polymers as in the case of pentafluorophenyl esters. As consequence, PFP(M)A obtained by RAFT polymerization normally requires an extra step to transform the thiocarbonylthio groups into another inert counterpart to ensure the straightforward point of view of post-polymerization modification, as presented by the example given in Scheme 9. On the other hand, SI-RAFT polymerization suffers from many disadvantages like the extra need to synthesize, tailor and graft CTA onto surface or the formation of free polymer in solution, as discussed before in section 1.3.1. Due to these restrictions, the possibility to polymerize pentafluorophenyl-containing monomers by ATRP is of interest.

Even though ATRP of PFP(M)A was considered impossible due to the interaction between Cu(I) and pentafluorophenyl moieties [285], a few studies using this technique has been reported to be successful both in solution and grafting from substrates [139, 286-289] or for a similar monomer yet less reactive tetrafluorophenyl methacrylate [290]. Yet, there exist some remaining disadvantages which either come from the polymerization technique itself or arise from the use for PFP(M)A. As mentioned in section 1.3.3, classic ATRP often requires an equivalent dose of copper catalyst, hence, it is needed to purify final product to eliminate remaining soluble copper. Furthermore, the low tolerance to air/oxygen of classic ATRP holds it back from large scale polymerization as well as applications to prepare a large number of individual samples for the case of SI-ATRP, not to mention the labor effort needed to avoid the presence of air/oxygen in reaction system. Therefore, there is a need of an alternative approach to polymerize pentafluorophenyl esters that consumes less catalyst with lower residue of copper, shows better air/oxygen tolerance, and is easy to perform yet robust in its outcome.

1.4.2.1. *p*-nitrophenyl (meth)acrylates

p-nitrophenyl containing esters are much less studied in literature compared to NHS-based and pentafluorophenyl-based esters; however, the employment of *p*-nitrophenyl polymer as precursor has been dated since 1970s [291]. In that research, a series of *p*-nitrophenyl esters of *N*-methacryloylamino acids was obtained and then subjected to aminolysis with various amine groups to investigate substitution rate constant as well as to evaluate the steric effect. Later on, free radical copolymerization of NP(M)A with other monomers like MMA [292, 293], *n*-butyl MA [294], Sty [295, 296], HPMA [292], glycidyl methacrylate [297], divinylbenzene [298-300] have also been done. It seems that controlled radical polymerization of NP(M)A is rare, where there are only a few examples to be named. First of all, it was found that homopolymerization of NPMA by ATRP could not be controlled due to the complexation of nitrophenyl pendant groups with Cu(II) halide, leading to accumulation of deactivator, hence, polymerization proceeded at low polymerization rate, poor monomer conversion and resulted in broad molecular weight distribution [301]. In the same work, the use of polystyrene macro-initiator was proposed to be able to circumvent such issue; hence, block PS-*b*-PNPMA was

obtained in a controlled manner. Nonetheless, controlled homopolymerization of NPMA was also achieved with RAFT polymerization [302] [303].

Polymers of *p*-nitrophenyl esters have been investigated for its reactivity in post-polymerization modification. It was found that this type of activated polymer can participate into aminolysis reaction; however, the efficiency of substitution seems to be lower than that with NHS-based and PFP-based ester. Indeed, though (presumable) high conversion was obtained when PSt-*b*-PNPMA was subjected to aminolysis by *n*-butylamine [301], substitution of PNPMA with a less reactive amine compound glycidine results in on 86% side group transformation [303].

1.5. Conclusion

In conclusion, the use of precursor polymer like PFPMA, PNPMA or their copolymers is an outstanding approach to obtain highly functional polymeric materials. These precursors can undergo post-polymerization modification with many other compounds bearing amino or hydroxyl ends, hence, allowing the graft of several different functional groups onto one polymer backbone. This approach is expected to be easier than studying the polymerization of each compound individually. It is also of our interest to study new polymerization technique like Cu(0)-mediated RDRP to obtain well-controlled polymer of activated ester owing to its facile yet robust manner. On the other hand, due to the urge for new antibacterial surface, the possibility to enhance antibacterial properties of surfaces like PET is getting attention because this polyester has been being used for various industrial applications thanks to its outstanding mechanical properties. Therefore, a part of this dissertation aims at modification without destruction the outer-most surface of PET films by wet chemistry in order to graft from the substrate a precursor reactive polymer, which will subsequently be used to immobilize prospective antimicrobial functional groups to seek antiadhesion properties. With these goals in mind, the (co)polymerization of activated esters including PFPMA and NPMA by Cu(0)-mediated RDRP will be discussed firstly in Chapter 2.

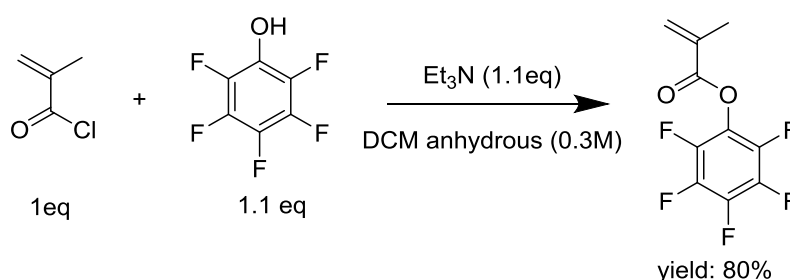
Chapter 2. Polymerization of active esters in solution

As mentioned previously in section 1.4, controlled radical polymerization of PFPMA and NPMA by either RAFT polymerization or classic ATRP has been reported, however, Cu(0)-mediated RDRP of these monomer is currently unavailable. Therefore, this technique has been studied in this dissertation to investigate its adaptability in polymerization and copolymer of PFPMA and NPMA whose results are presented and discussed in the current chapter.

2.1. Cu(0)-mediated Reversible Deactivation Radical Polymerization of PFPMA

2.1.1. A note on synthesis of PFPMA

Synthesis of PFPMA has been synthesized with modification of published procedure (**Scheme 11**) [266] where pentafluorophenol was employed in 1.1 equivalent compared to 1.0 equivalent of methacryloyl chloride. The excess of pentafluorophenol is to facilitate the purification process because if the volatile methacryloyl chloride is not totally consumed, it can be collected during distillation under pressure to obtain dry PFPMA.



Scheme 11. Synthesis of PFPMA by esterification of methacryloyl chloride and pentafluorophenol

It is necessary to mention that there was presence of at least one byproduct formed during the esterification to synthesize PFPMA. Indeed, these byproducts were originated from impurities in the announced-to-be at least 97% purity commercial methacryloyl chloride, from where they have been isolated and identified to be dimer of methacryloyl chloride and the product of HCl addition onto alkene of methacryloyl chloride as described in literature and presented in Figure 25 [304]. It is confirmed that the methacryloyl chloride used during the course of this dissertation also had these impurities, furthermore, once the bottle has been used and more or less exposed to air, the amount of methacryloyl chloride dimer increased.

Nonetheless, by using the spoiled methacryloyl chloride to synthesize PFPMA, esterification was also effective towards the dimer to form an undesired pentafluorophenyl-containing product. This undesired product was isolated from crude PFPMA solution by liquid chromatography and has been confirmed by ¹H NMR and ¹⁹F NMR (Figure 26). This byproduct is located very close to PFPMA in thin film chromatography.

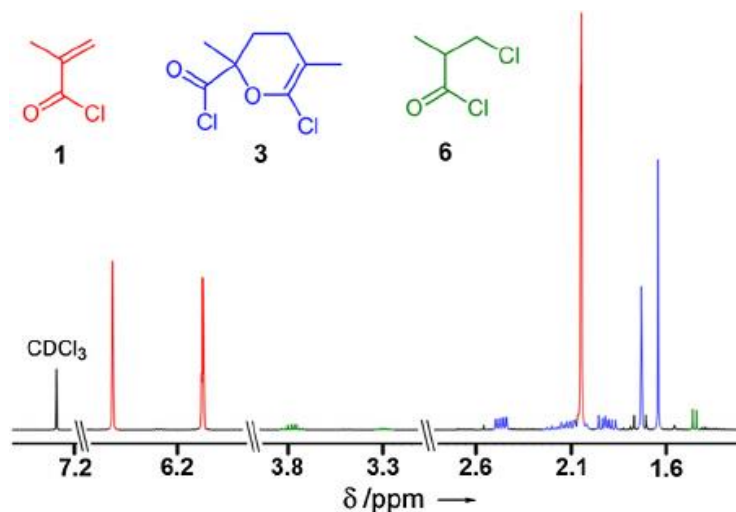


Figure 25. ^1H NMR spectrum of methacryloyl chloride (1), its dimer (3) and compound (6) resulted from HCl addition to methacryloyl chloride [304].

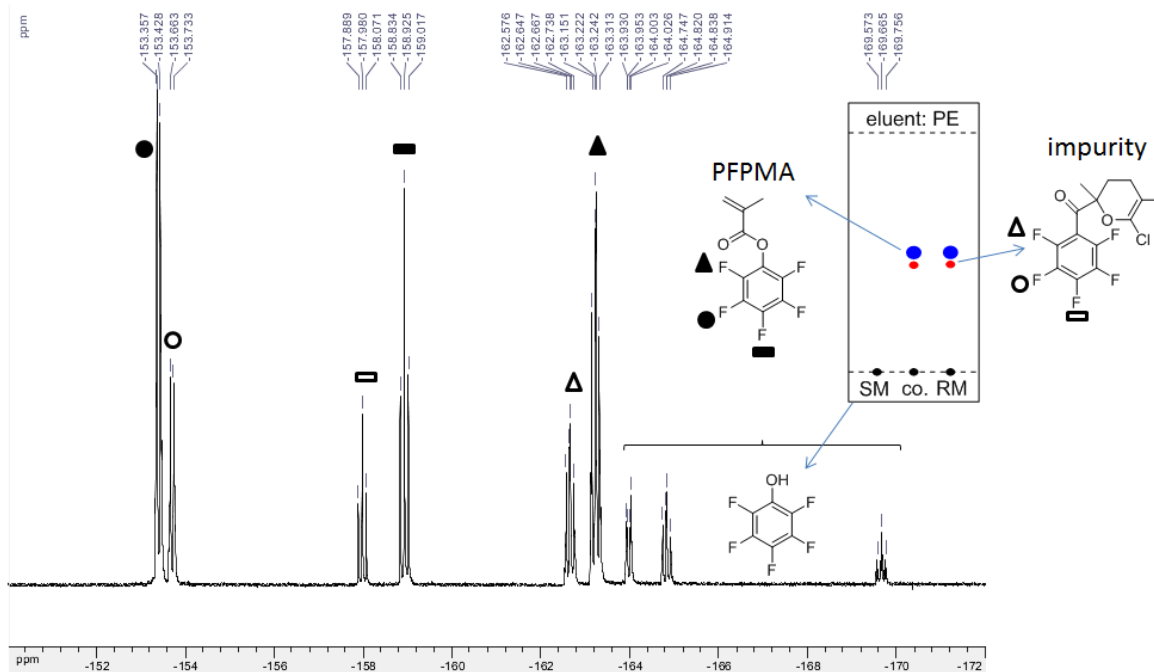
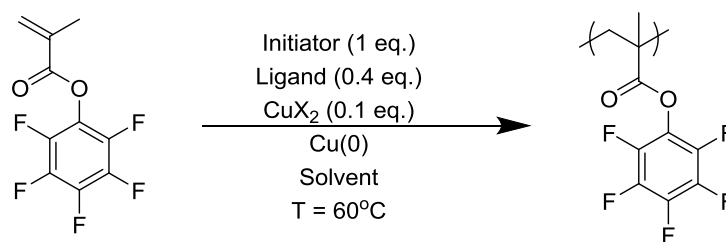


Figure 26. Example of ^{19}F NMR spectrum (250 MHz, CDCl_3) of reaction mixture to obtain PFPMA before column and vacuum distillation. SM: starting material, RM: reaction mixture, co.: SM + RM

$\text{Cu}(0)$ -mediated RDRP of PFPMA (Scheme 12) has been carried out under various conditions to achieve well-controlled PFPMA as final product.



Scheme 12. Different reagents involving in Cu(0)-mediated RDRP of PFPMA

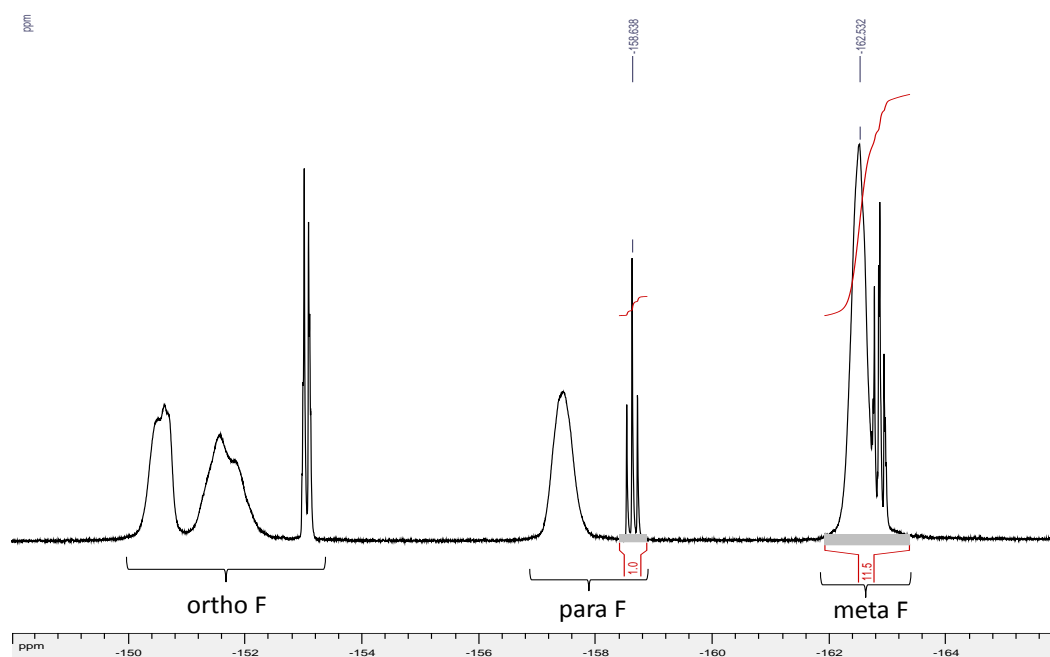


Figure 27. Demonstration of calculation of PFPMA conversion after polymerization

PFPMA conversion was calculated from ^{19}F NMR as demonstrated in Figure 27. Firstly, the peak corresponding to fluorine atoms at para position of monomer was taken as reference for 1 fluoro atom. Monomer conversion of a polymerization of PFPMA was then determined from meta peak area that ranges between -161.9 ppm to -163.3 ppm, which includes 2 fluoro atoms originated from monomer and the rest from polymer. Thus, PFPMA conversion is calculated as following:

$$\text{PFPMA conversion (\%)} = \frac{A_{-161.9 \text{ to } -163.3 \text{ ppm}} - 2}{A_{-161.9 \text{ to } -163.3 \text{ ppm}}} \times 100$$

In general, the optimization for Cu(0)-mediated RDRP of PFPMA was very challenging. Many factors including solvent, ligand, initiator or the length of Cu(0) were proven to play crucial contribution, hence, to achieve optimal condition, a synergic combination of these factors is needed.

2.1.2. Determination of refractive index increment for SEC analysis

SEC results of all PPFPMAs have been determined and are reported herein as “absolute” molar mass obtained using signals of multi-angle light scattering (MALS) detector and refractive index (RI) detector. The absolute molar mass of polymer determined by MALS coupled with RI as concentration detector is highly dependent on its specific refractive index increment (dn/dC) as described by the following equations:

$$Signal_{MALS} = K_{MALS} \times M_w \times \left(\frac{dn}{dC}\right)^2 \times c \times V_{injected}$$

$$Signal_{RI} = \frac{K_{RI}}{n_{solvent}} \times \frac{dn}{dC} \times c \times V_{injected}$$

where $K_{RI} = 10\,135\,990$, $n_{solvent} = 1.405$ (THF)

Therefore, to develop a trustworthy calculation using MALS system, dn/dC determination of PPFPMA in THF at 254 nm has been done using maximum RI intensities recorded with 3 injection volumes of PPFPMA stock solution of $4\text{ mg}\cdot\text{mL}^{-1}$ as presented in **Figure 28**.

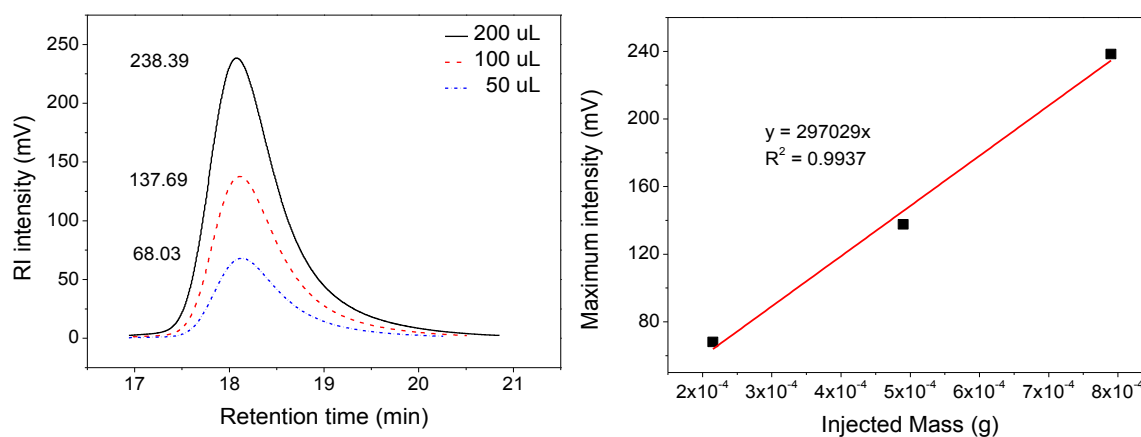


Figure 28. Left: RI signals of PPFPMA measured by different injection volumes, Right: maximum RI intensity in function of injected mass

From these results, dn/dC of homopolymer PPFPMA was determined to be $0.042\text{ mL}\cdot\text{g}^{-1}$ and had been used for all set of data. In addition, this value is much smaller than that of PS which is $0.185\text{ mL}\cdot\text{g}^{-1}$; thus, results obtained using conventional PS calibration could not reflect the true value of PPFPMA. However, the small dn/dC value of $0.042\text{ mL}\cdot\text{g}^{-1}$ suggests that the polymer might response poorly at low molar mass.

2.1.3. Influence of solvent

Solvent plays a significant role in polymerization in general and in ATRP-like techniques particularly as discussed in section 1.3.3.1. Herein, various solvent systems have been studied as summarized in Table 1.

Table 1. Summary of qualitative observations about influence of solvent on homogeneity of reaction mixture

Entry	Solvent system	Pros	Cons
1	bulk (no solvent)	-	<5% monomer conversion
2	toluene	-	<5% monomer conversion
3	anisole	-	<5% monomer conversion
4	acetonitrile	-	<5% monomer conversion
5	DMSO	1-phase mixture	Moderate conversion (TPMA: 50%)
6	THF	1-phase mixture	Low to moderate conversion TPMA: 40%; dnNbpy: 66%
7	sulfolane	High conversion (86%) with TPMA/eBiB	2-phase mixture, low conversion (23%) with dnNbpy/MBPA
8	50:50 % v/v (DMSO/Sulfolane)	1-phase mixture Moderate conversion	Evident of hydrolysis
9	20:80 % v/v (DMSO/Sulfolane)	Moderate conversion	Fairly homogeneous reaction
10	10:90 % v/v (DMSO/Sulfolane)	Moderate conversion	2-phase mixture
11	5:95 % v/v (DMSO/Sulfolane)	Moderate conversion	2-phase mixture
12	50:50 % v/v (THF/Sulfolane)	Moderate conversion for both TPMA and dnNbpy	2-phase mixture at conversion > 30%
13	67:33 % v/v (THF/Sulfolane)	Moderate conversion for both TPMA and dnNbpy	2-phase mixture at conversion > 50%
14	75:25 % v/v (THF/Sulfolane)	Homogenous mixture Moderate conversion with TPMA High conversion with dnNbpy	-

Firstly, other research on classic ATRP of PFPMA has been done in various solvent, including bulk condition, toluene or anisole. Therefore, preliminary experiments were also

carried out using these solvents, unfortunately, polymerization proceeded poorly after 24 hours with monomer conversions $< 5\%$ for these three solvents. These results are of great accordance with literature as classic ATRP and Cu(0)-mediated RDRP which often requires different medium. As discussed in section 1.3.3.1, classic ATRP in polar solvent may lead to the accumulation of Cu(II) complex, hence, apolar solvents are often used in this technique. In contrast, Cu(0)-mediated RDRP with the use of cationic Cu(II) halide, which is strongly stabilized in more polar solvents [191], generally requires the use of more polar system. Therefore, in this context, aprotic solvents like acetonitrile, DMSO, THF and sulfolane are proper choices, and furthermore, they have also been reported to mediate successfully Cu(0)-mediated RDRP of other monomers [200, 204, 207-209, 212, 255, 305-307]. Besides acetonitrile in which no polymer formation was observed, polymerization of PFPMA with the use of DMSO, sulfolane and THF had achieved to certain levels, yet each of them raised certain concerns in efficacy of polymerization, which are presented as observation in Table 1.

As presented, the use of DMSO and THF resulted in moderate monomer conversion (around 50-60%) while the value with sulfolane varied with the use of ligand (entries 5-7). It is acknowledged that to conserve good balance in redox reactions between copper complexes at different oxidation states, the reaction medium must be homogenous in ATRP-like polymerization. Under the scope of this dissertation, while the reaction mixture visually appeared to be homogenous in DMSO and THF, the use of sulfolane led to distinguished phase separation between polymer formed and solution mixture. Cu(0)-mediated RDRP of PFPMA in pure sulfolane was achieved with the use of either TPMA or dnNbpy as ligand. It is remarkable that with TPMA as ligand and eBiB as initiator, polymerization proceeded to much higher monomer conversion (86%, entry 7) than with dnNbpy as ligand and MBPA as initiator (23%). This result could be explained by the huge difference in solubility of copper (II) complexes with these two ligands in sulfolane. While the complexation of CuBr₂ and TPMA can be easily obtained at ambient temperature, higher temperature or sonication is required to prepare the complex of CuBr₂ and dnNbpy even with 4 equivalent of ligand. As several studies using Cu(0)-mediated RDRP have proposed the advantage of solvent mixture in polymerization, like sulfolane/water mixture in synthesis of various model monomers [207] or DMF/toluene in polymerization of glycidyl methacrylate [215], effort to seek the compromise in conversion and reaction homogeneity was made by mixing sulfolane with either DMSO or THF.

Table 2 summarized experimental results obtained by Cu(0)-mediated RDRP of PFPMA using DMSO:sulfolane mixture as solvent. As presented, though all mixture resulted in high monomer conversion, the monomer conversion and dispersity of final polymer varied and is dependent on the volume fraction of sulfolane, *i.e.* higher the sulfolane content, larger the dispersity (Table 2). When sulfolane was the sole solvent, the dispersity of PFPMA was very large ($D = 3.09$), which might be explained by the appearance of phase separation. As the content of sulfolane decreases, monomer conversion slightly reduces accordingly and dispersity also becomes narrower.

Table 2. Results of Cu(0)-mediated RDRP using DMSO:Sulfolane mixture as solvent. Polymerization conditions: [PPFMA]₀: [eBiB]₀: [TPMA]₀: [CuBr₂]₀ = 100:1:0.4:0.1, T = 60 °C, Cu(0) length = 1 cm per 3.4 mmol PPFMA, [Monomer]₀ = 2 M, t = 20 hours.

Entry	DMSO:Sulfolane (%v/v)	Conv. (%)	Mn _{theo} (g mol ⁻¹)	Mn _{SEC} (g mol ⁻¹)	Mw _{SEC} (g mol ⁻¹)	<i>D</i>
1	50:50	73	18 591	34 800	58 900	1.69
2	20:80	79	20 103	45 100	88 000	1.95
3	10:90	89	22 623	41 100	92 100	2.24
4	5:95	97	24 639	42 500	104 900	2.47
5	0:100	86	21 867	32 700	100 900	3.09

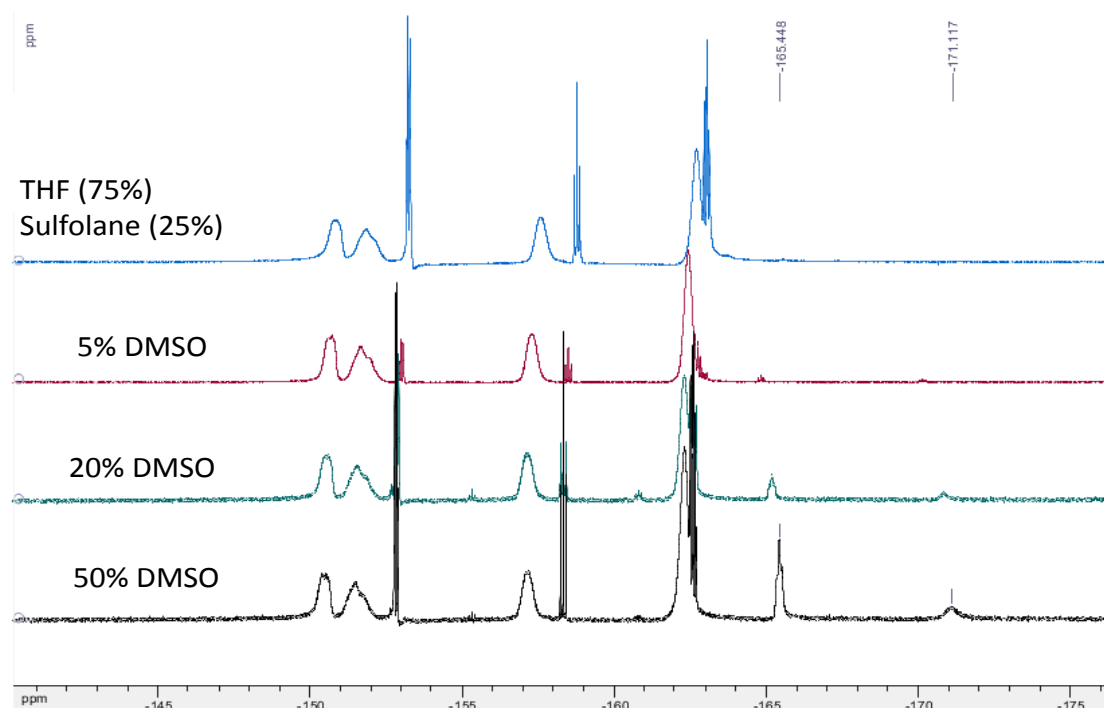


Figure 29. ¹⁹F NMR spectra obtained at the end of polymerization with different DMSO:sulfolane mixture compared to that with THF:sulfolane 75:25 %v/v

From these values, it seems that the mixture of 50:50 %v/v of DMSO:Sulfolane was the best condition with comparative monomer conversion and lowest dispersity. However, ¹⁹F NMR at the end of polymerization indicates the presence of two fluorines at -165.4 ppm and -171.1 ppm as presented in Figure 29. Interestingly, the relative ratio of these peaks compared to that of polymer increases with the augment of DMSO content in reaction mixture. This phenomenon is caused by the very hygroscopic trace of water contained in DMSO. It was described in literature that PPFMA underwent hydrolysis in ATRP with PMDETA as ligand [287] where the same type of ¹⁹F signals has been observed and assigned as of pentafluorophenol resulted by hydrolysis. In contrast, these two signals were absent when

THF, sulfolane or the mixture of the two was used to synthesize PPFMA by Cu(0)-mediated RDRP. Therefore, DMSO volume proportion of higher than 20% was not examined in further study.

Table 3. Results of Cu(0)-mediated RDRP using THF:Sulfolane mixture as solvent. Polymerization conditions: [PPFMA]₀: [initiator]₀: [ligand]₀: [CuBr₂]₀ = 100:1:0.4:0.1, T = 60 °C, Cu(0) length = 1 cm per 3.4 mmol PPFMA, [Monomer]₀ = 2 M, t = 18 hours.

Entry	Initiator/Ligand	THF: Sul. (%v/v)	Conv. (%)	Mn _{theo} (g mol ⁻¹)	Mn _{SEC} (g mol ⁻¹)	Mw _{SEC} (g mol ⁻¹)	<i>D</i>
1	eBiB/TPMA	0:100	86	21 867	32 700	100 900	3.09
2	eBiB/TPMA	50:50	65	16 575	24 600	29 500	1.99
3	eBiB/TPMA	75:25	69	17 617	45 700	89 400	1.95
4	eBiB/TPMA	100:0	40	10 275	18 400	25 900	1.41
5	MBPA/ dnNbpy	0:100	23	6 025	11 100	12 100	1.05
6	MBPA/ dnNbpy	50:50	77	19 633	36 300	57 300	1.58
7	MBPA/ dnNbpy	75:25	90	22 909	35 500	37 400	1.05
8	MBPA/ dnNbpy	100:0	66	16 861	27 000	37 400	1.48

As mentioned above, depending on complexation between CuBr₂ and ligand, the use of sulfolane as the sole solvent behaved differently with eBiB/TPMA (Table 3, entry 1) and MBPA/dnNbpy (Table 3, entry 5), *i.e.* higher monomer conversion and larger dispersity were acquired in the former case where the copper complex was easily obtained. In contrast, the two ligands can be complexed effortlessly with CuBr₂ in THF and resulted in the same range of dispersity while monomer conversion varied less significantly (Table 3, entries 4, 8). Moreover, THF is a good solvent for PPFMA, therefore, polymerization using only this solvent was always remained homogenous. Because both sulfolane and the polymer have high solubility in THF [308], sulfolane was added into THF-based reaction medium to seek the compromise between conversion and dispersity. It is to note that lower than 50% proportion of THF was not examined due to the very low solubility of PPFMA in sulfolane. Even though the addition of 50% volume sulfolane showed good monomer conversion (65% and 77%, entries 2, 6), a visible phase separation was still noticed after 19 hours of polymerization, leading to a less controlled polymerization respectively of *D* = 1.99 and 1.58. When the volume ratio between THF and sulfolane is 75:25 %v/v, a homogenous mixture was obtained after 19 hours of polymerization and a single, narrow and unimodal peak was recorded in SEC analysis with conversion. Therefore, this THF:sulfolane mixture of 75:25 %v/v was retained for further study to optimize polymerization condition so that Cu(0)-mediated RDRP of PPFMA can behave in a better controlled manner.

2.1.4. Synergic influence of ligand and initiator

Ligand and initiator are the two factors that can pronouncedly affect the polymerization system control. As mention in section 1.3.3, overall kinetic of ATRP can be altered hundreds to thousands times just by changing one ligand to another, the same way is applicable between initiators. In this dissertation, several ligands (Figure 30) and a few initiators (Figure 31) have been studied to find optimal conditions for Cu(0)-mediated RDRP of PFPMA.

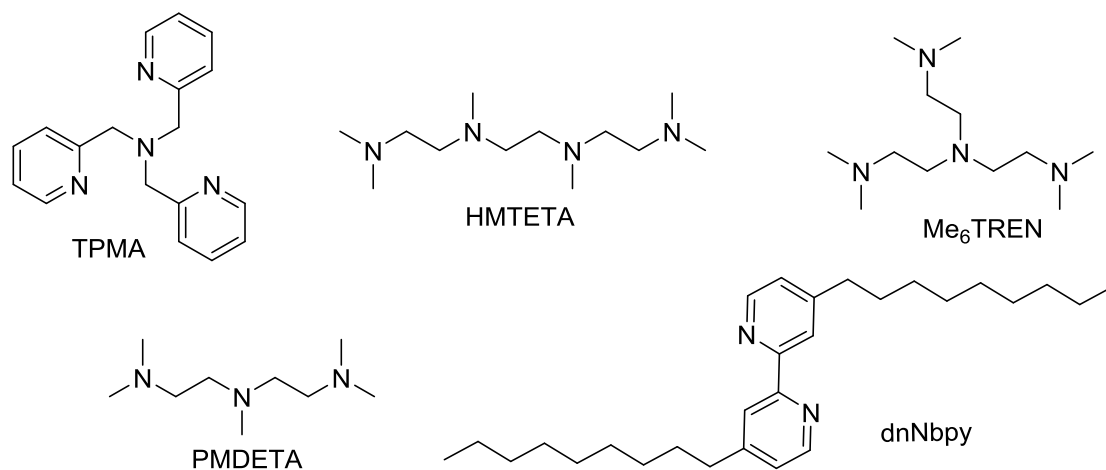


Figure 30. Different ligands studied in Cu(0)-mediated RDRP of PFPMA

First of all, PMDETA has been used for bulk ATRP of PFPMA [286], however, this ligand has been criticized to generate hydrolysis of the active monomer [287]. Herein, polymerization with PMDETA as ligand and eBiB as initiator has failed (<5% monomer conversion). On the other hand, polymerization where TPMA, Me₆TREN, HMTETA, or dnNbpy was used has proceeded from moderate to very high monomer conversion as presented in Table 4. It has been proven that TPMA and Me₆TREN share the same polymerization profile in Cu(0)-mediated RDRP of MA [309], herein, the same observation was recorded as shown in Table 4, entries 1, 2, 3, 6 and 7. Moreover, because the availability of TPMA is favored, TPMA was preferred rather than Me₆TREN. Moreover, PFPMA is known to be able to react with primary and secondary amine as discussed before in section 1.4.2, hence, the use of aromatic ligands like TPMA or dnNbpy is considered to be less risky choice.

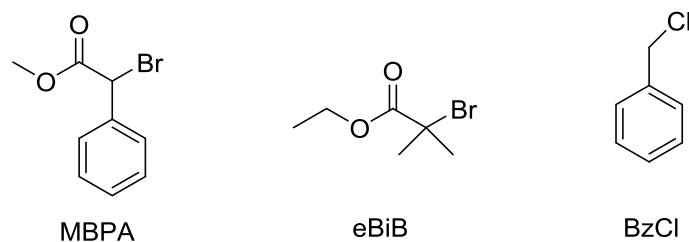


Figure 31. Initiators studied in optimization of Cu(0)-mediated RDRP of PFPMA

While ligand and their complexes play the role of catalytic process mediator in ATRP-like system, initiator choice is critical because it defines the nature of radical formed during initiation, thus, controls the activation constant and kinetic equilibrium of polymerization. During the course of this research, three ligands have been investigated including benzyl chloride (BzCl), ethyl α -bromoisobutyrylbromide (eBiB) and methyl α -bromophenylacetate (MBPA) as shown in Figure 31.

As resumed in Table 4, eBiB and MBPA show scattered control profiles but in accordance with the use of ligand. HMTETA was described to provide a good control in conventional ATRP of 2,3,5,6-tetrafluorophenyl methacrylate with CuBr₂ added as deactivator [290], herein, HMTETA gives an impressive monomer conversion (>88%, Table 4, entries 4 and 8), however, the dispersities of resulted polymers are broad regardless of initiator used ($\bar{D} = 2.24$ for eBiB and $\bar{D} = 1.94$ for MBPA) indicating a low control over polymerization. On the other hand, despite of its extensive usage in Cu(0)-mediated RDRP, TPMA affords lower monomer conversion compared to HMTETA with a slight improvement in dispersity ($\bar{D} = 1.95$ for eBiB and $\bar{D} = 1.78$ for MBPA) (Table 4, entries 3 and 7). Compared to those two ligands, the use of dnNbpy is plausible as it is demonstrated to provide well-control PFPMA by ATRP [310]. Herein, this ligand retains its effectiveness where it not only shows high monomer conversion (>80%) in Cu(0)-mediated RDRP of PFPMA, but more importantly a remarkable narrower dispersity compared to HMTETA and TPMA (Figure 32 and Table 4, entries 5, 9-11).

Table 4. Results on Cu(0)-mediated RDRP of PFPMA at different polymerization conditions. Polymerization conditions: [PFPMA]₀: [initiator]₀: [ligand]₀: [CuBr₂]₀ = 100:1:0.4:0.1, T = 60 °C, t = 18h, Cu(0) length = 1 cm per 3.4 mmol PFPMA, [Monomer]₀ = 2 M.

Entry	Initiator	Ligand	[M] ₀ /[I] ₀	Conv. (%)	Mn _{theo}	Mn _{SEC}	Mw _{SEC}	\bar{D}
					g mol ⁻¹			
1	eBiB	Me ₆ TREN	100	31	8 007	49 300	94 300	1.91
2	eBiB	Me ₆ TREN	50	76	19 247	30 400	59 100	1.94
3	eBiB	TPMA	100	69	17 617	45 700	89 400	1.95
4	eBiB	HMTETA	100	88	22 405	33 400	74 900	2.24
5	eBiB	dnNbpy	100	84	20 859	37 000	61 000	1.65
6	MBPA	Me ₆ TREN	100	70	17 869	20 800	64 300	1.71
7	MBPA	TPMA	100	78	19 885	36 500	69 100	1.78
8	MBPA	HMTETA	100	90	22 909	38 200	75 200	1.94
9	MBPA	dnNbpy	100	90	22 909	35 500	37 400	1.05
10	MBPA	dnNbpy	200	93	47 101	73 500	97 700	1.33
11	MBPA	dnNbpy	400	84	84 901	129 900	159 900	1.23

BzCl has been demonstrated to be a good initiator toward SARA-ATRP of 4-vinyl pyridine [226], however, only a very poor monomer conversion was achieved with PFPMA. In contrast, the other two initiators provided polymers with a wide spectrum of control. In general, the initiation of BzCl is slow due to the stronger C-Cl bond compared to C-Br, therefore it requires more energy to create radicals, and thus, activation constant of BzCl is much smaller than that of eBiB or MBPA regardless of ligands as summarized in Table 5.

Table 5. Summary of ATRP constants of corresponding ligands and initiators used in Cu(0)-mediated RDRP of PFPMA [186]

Ligand	Initiator	k_{act}	k_{deact}	K_{ATRP}
HMTETA	BzCl	2.60×10^4	2.60×10^5	9.90×10^{-10}
	eBiB	7.00×10^2	6.40×10^6	1.10×10^{-8}
	EBPA	1.40×10^2	1.30×10^6	1.10×10^{-4}
TPMA	BzCl	1.2×10^{-1}	1.30×10^5	8.60×10^{-7}
	eBiB	3.12	3.30×10^6	9.60×10^{-6}
	EBPA	6.10×10^4	6.60×10^5	9.20×10^{-2}
dnNbpy	BzCl	1.10×10^{-3}	4.10×10^5	2.70×10^{-9}
	eBiB	3.00×10^{-1}	1.10×10^7	3.00×10^{-8}
	EBPA	5.90×10^2	2.00×10^6	2.90×10^{-4}

ATRP constants of these ligands alongside three initiators were determined experimentally or by extrapolating [186] as summarized in Table 5. From these values, it is seen that the deactivation constants of the three ligands stay in quite the same range, however, their activation constants change sharply between one initiator to another, indicating synergic contribution of ligand and initiator to equilibrium constant of polymerization. As mentioned above, the use of MBPA resulted in narrower dispersity of obtained PFPMA in all experiments. This difference can be explained by the overall higher activation rate constants and larger equilibrium constants of MBPA compared to eBiB, assumed that the reactivity of MBPA is very close to that of EBPA. Thus, MBPA is more reactive than eBiB in creating propagating radicals, which is in accordance with chemical structure point of view because radical formed by MBPA is more stable than that of eBiB. Nonetheless, this achievement is in great agreement with a published research on the comparison in activity of the two initiators in Cu(0)-mediated RDRP of methyl methacrylate [212].

In conclusion, Cu(0)-mediated RDRP of PFPMA can only be controlled ($\mathcal{D} < 1.5$) with the combination of dnNbpy as ligand and MBPA as initiator. Nonetheless, the Cu(0)-mediated RDRP of PFPMA operated under such conditions was remained controlled with high monomer conversion even when higher chain lengths were expected ($DP_n = 200$ and 400) proved by $\mathcal{D} < 1.5$ (Table 4, entries 10, 11). The obtained values of $M_{n,theo} = 84\,900 \text{ g mol}^{-1}$, $M_{n,SEC} = 129\,900 \text{ g mol}^{-1}$ and $M_{w,SEC} = 159\,900 \text{ g mol}^{-1}$ are the highest molecular weights of PFPMA that have been reported so far.

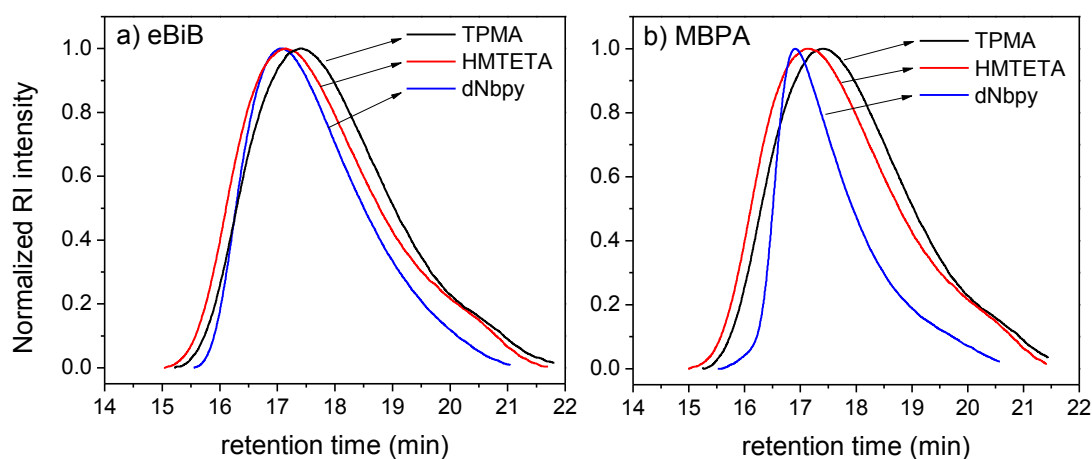


Figure 32. Chromatograms of PFPMAs obtained *via* Cu(0)-mediated RDRP with the use of different ligands and initiator. Polymerization conditions: $[PFPMA]_0 / [ligand]_0 / [initiator]_0 / [CuBr_2]_0 = 100/1/0.4/0.1$, $T = 60\text{ }^\circ\text{C}$, $t = 19$ hours.

On the other hand, the control of polymerization is strongly dependent on the use of ligand, and the solubility of ligand also plays a pivotal role in polymerization process as discussed before. Further investigation by UV-NIR study (Figure 33) shows that the addition of sulfolane produces a significant change in coordination and geometry of copper (II) complex with dnN bpy.

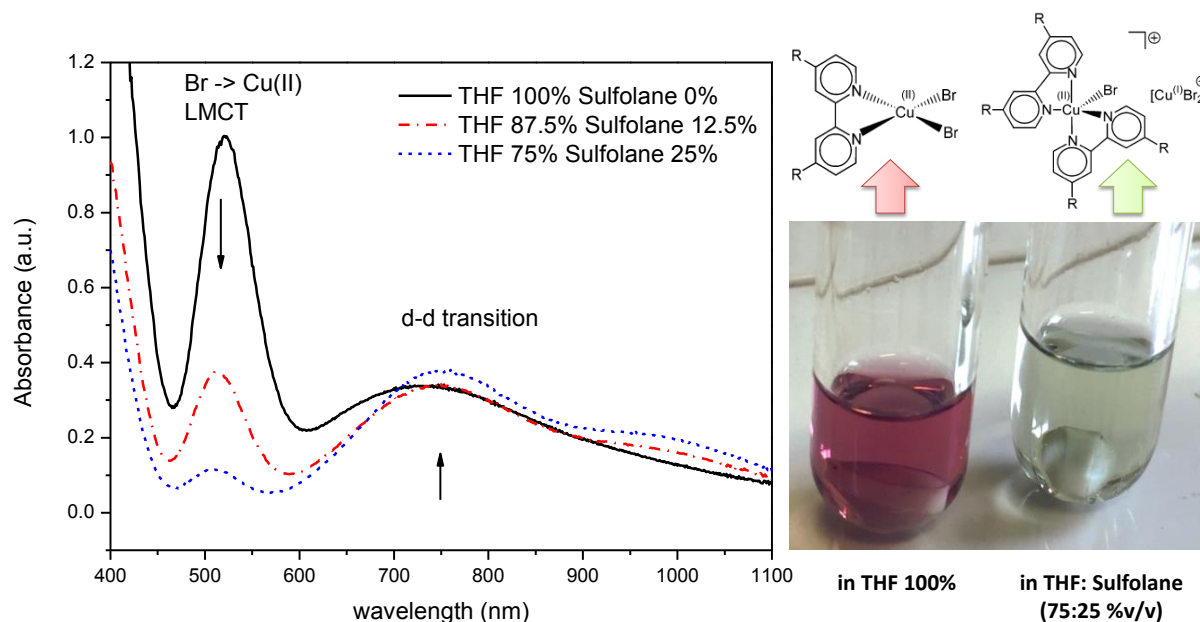


Figure 33. UV-NIR absorbance of Cu(II)/dnN bpy complex in THF with addition of sulfolane. $[CuBr_2]_0 = 6.7\text{ mM}$, $[dnN bpy] = 25.8\text{ mM}$

The first indication is the rapid change in color of copper complexes, from dark purple in pure THF to green upon addition of sulfolane. Depicted in Figure 33, the absorption spectrum of the complexes shows an intense band at $\lambda_{max} \approx 510\text{ nm}$ in THF 100%, which represents the

ligand to metal charge transfer (LMCT) between bromine atoms and Cu(II) centers [311]. The addition of sulfolane leads to a decrease of such absorption band, indicating the geometrical transformation from square planar of $\text{Cu}^{\text{II}}(\text{dnNbpy})\text{Br}_2$ into distorted trigonal bipyramidal $[\text{Cu}^{\text{II}}(\text{dnNbpy})_2\text{Br}]^+\text{Br}^-$ as reported for branched dinonyl bipyridine [311]. The distorted trigonal bipyramidal geometry is considered to be the coordination involved in deactivation process to form Cu(I) activator complex while it was isolated directly from polymerization reaction together with the ATRP activator tetrahedral $[\text{Cu}^{\text{I}}(\text{dnNbpy})_2]^+$ [312]. Thus, this observation confirms the lower performance of this complex due to the lack of ionic $[\text{Cu}^{\text{II}}(\text{dnNbpy})_2\text{Br}]^+\text{Br}^-$ when polymerization is carried out in THF 100%.

2.1.5. Influence of zero valent copper

The amount of zero valent copper also contributes in polymerization kinetics of zero valent-mediated RDRP [196, 201, 216, 306, 309, 313]. Figure 34 shows the dependence of polymerization on Cu(0) wire length, *i.e.* surface area. Kinetics of polymerization were investigated by varying Cu(0) wire length between 1 cm, 2 cm and 4 cm per 3.4 mmol of PFPMA (Figure 34).

Under the same reaction conditions, the variation of Cu(0) wire length affects kinetics of polymerization to a certain level. In terms of reaction rate, the increase in length leads to the increase of appearance kinetic rate (k_{app}), where k_{app} is 0.20 h^{-1} with the use of 1 cm of Cu(0) wire, k_{app} increased to 0.34 h^{-1} for 2 cm of Cu(0) and reached 0.36 h^{-1} for 4 cm of Cu(0).

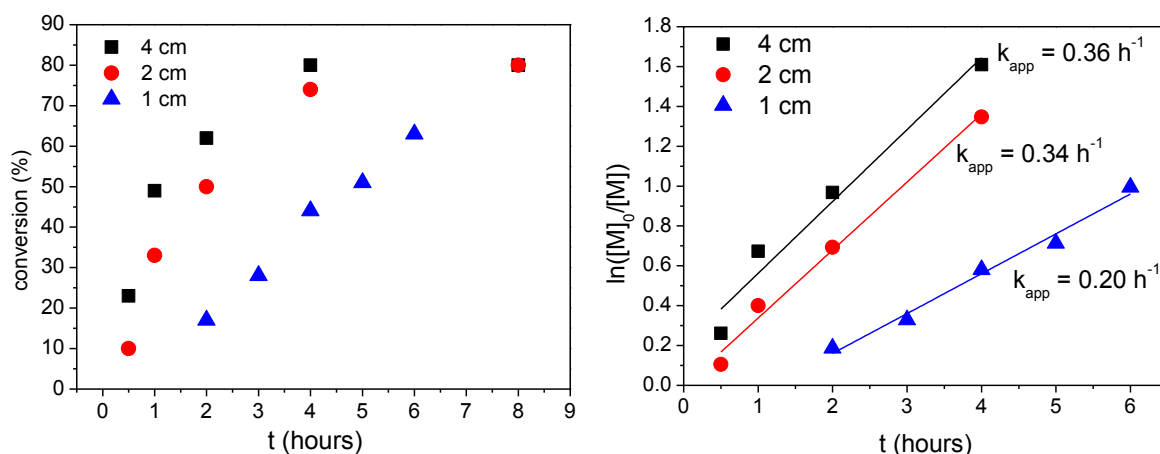


Figure 34. Kinetics of Cu(0)-mediated RDRP of PFPMA with varying Cu(0)-length. Polymerization conditions: $[\text{PFPMA}]_0/[\text{MBPA}]_0/[\text{dnNbpy}]_0/[\text{CuBr}_2]_0 = 100/1/0.4/0.1$, $T=60 \text{ }^\circ\text{C}$

Additionally, there are evidences showing that the length of Cu(0) also alters the induction period of Cu(0)-mediated RDRP of PFPMA. While the induction period is not obvious for Cu(0) length of 2 cm and 4 cm (*i.e.* conversion > 10% in the first 30 minutes of polymerization), it increases remarkably to 2 hours when only 1 cm of Cu(0) was used. This results is in an agreement with earlier study of Cu(0)-mediated RDRP of other monomers

[208, 306]. Furthermore, SEC analysis of polymer obtained from the end of kinetics experiment indicates that varying the length of Cu(0) wire also changes the dispersity, *i.e.* increasing the length of Cu(0) wire leads to increase in dispersity of polymers as in Table 6.

Table 6. Results obtained from Cu(0)-mediated RDRP of PFPMA with variation of Cu(0) wire length. Polymerization conditions: [PFPMA]₀/[ligand]₀/[initiator]₀/[CuBr₂]₀ = 100/1/0.4/0.1, T = 60 °C, Cu(0)-wire length is per 3.4 mmol of PFPMA, [M]₀ = 2 M, THF:Sulfolane = 75:25 % v/v.

Entry	Cu(0) length	ΣA (cm ²)	Conv. (%)	Mn _{theo}	Mn _{SEC} g mol ⁻¹	Mw _{SEC}	Đ
1	1 cm	0.330	63	16 105	31 100	35 600	1.14
2	2 cm	0.644	55	14 089	28 200	38 000	1.35
3	4 cm	1.272	63	16 105	26 000	41 500	1.60

This set of experiment demonstrates that the utilization of 2 cm of wire Cu(0) per 3.4 mmol of PFPMA provides good compromise between polymerization rate and good control over dispersity. Therefore, this length was taken for further experiment.

2.1.1. Kinetics of Cu(0)-mediated RDRP under optimal conditions

After examining the influences of several core factors as discussed above, it is found that the combination of optimized conditions for the Cu(0)-mediated RDRP of PFPMA includes THF:Sulfolane (72:25 %v/v) as solvent, dnNbpy as ligand, MBPA as initiator and 2 cm of Cu(0) wire for each 3.4 mmol of PFPMA and [PFPMA]₀/ [MBPA]₀/ [dnNbpy]₀/ [CuBr₂]₀ = 100/1/0.4/0.1, T=60 °C, volume ratio between monomer and solvent was maintained at 4:1,

The kinetics of Cu(0)-mediated RDRP of PFPMA under the aforementioned conditions are illustrated in Figure 35 and Table 7. As seen from Figure 35, no induction period was recorded under optimized condition, proven by a monomer conversion of 10% after 30 minutes, and PFPMA conversion reached around 80% after 8 hours of polymerization. Furthermore, a linear increase in molecular weight of polymer in function of conversions was achieved, indicating first-order kinetics of polymerization. Moreover, the linear fits of Mn_{theo} and Mn_{SEC} appears to be relatively parallel, indicating a good control of polymerization. Such constant difference between theoretical and experimental results might be attributed to a initiator efficiency of MBPA < 1. Additionally, SEC profiles of PFPMA remain unimodal and narrow as conversion of polymerization increases while the dispersity of obtained polymers shows small variation between low and high conversions and always remains in the range of Đ ≈ 1.05 – 1.29.

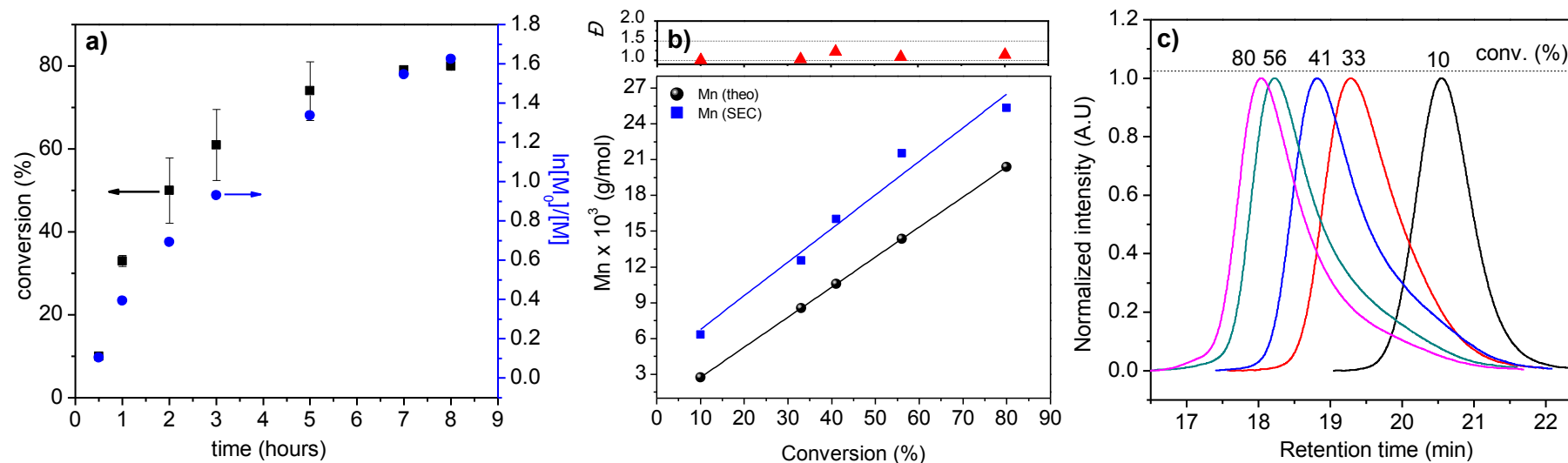


Figure 35. Kinetics of Cu(0)-mediated RDRP of PFPMA in terms of a) monomer conversion, b) average molecular weight and c) dispersity under optimized conditions and their corresponding SEC profiles of PFPMA. $[PFPMA]_0/[MBPA]_0/[dnNbpy]_0/[CuBr_2]_0 = 100/1/0.4/0.1$; 2 cm of Cu(0) wire ($d = 1$ mm) for each 3.4 mmol PFPMA, $T = 60$ °C

Table 7. Kinetics of Cu(0)-mediated RDRP under optimal conditions. $[PFPMA]_0/[MBPA]_0/[dnNbpy]_0/[CuBr_2]_0 = 100/1/0.4/0.1$; 2 cm of Cu(0) wire ($d = 1$ mm) for each 3.4 mmol PFPMA, $T = 60$ °C

Entry	Conv. (%)	Elution volume	Mn_{theo} $g\ mol^{-1}$	Mn_{SEC} $g\ mol^{-1}$	Mw_{SEC} $g\ mol^{-1}$	\mathcal{D}
1	10	20.547	2 749	6 000	6 300	1.05
2	33	19.285	8 545	11 300	12 500	1.11
3	41	18.819	10 561	16 300	20 900	1.21
4	56	18.225	14 341	18 900	24 300	1.29
5	80	18.042	20 389	25 700	30 600	1.15

2.2. End-chain analysis

Chain end fidelity is one important characteristic of controlled radical polymerization and makes it distinguished from free radical polymerization. Therefore, end-chain analysis has been done using one or combination of technique(s), including NMR, MALDI-ToF and chain extension experiment.

2.2.1.1. eBiB-based PFPMA

Figure 36 presents a representative ^1H NMR spectrum of PFPMA obtained by Cu(0)-mediated RDRP with eBiB as initiator. As the pendant group of the polymer contains only carbon and fluorine atoms, the ^1H NMR of PFPMA shows mainly protons originated from backbone and end-chain. Characteristic signals for methylene protons of eBiB appear at 4.1 ppm, methyl protons belonging to backbone appear between 1.0 ppm to 1.8 ppm while methylene protons are in the range of 1.8 ppm to 3.0 ppm. From these signals, the number average molecular weight of polymer was determined to be $17\,331\text{ g mol}^{-1}$, which is around twice that calculated from theoretical degree of polymerization and monomer conversion ($9\,519\text{ g mol}^{-1}$). This difference might come from either low initiator efficiency or termination by bi-molecular coupling.

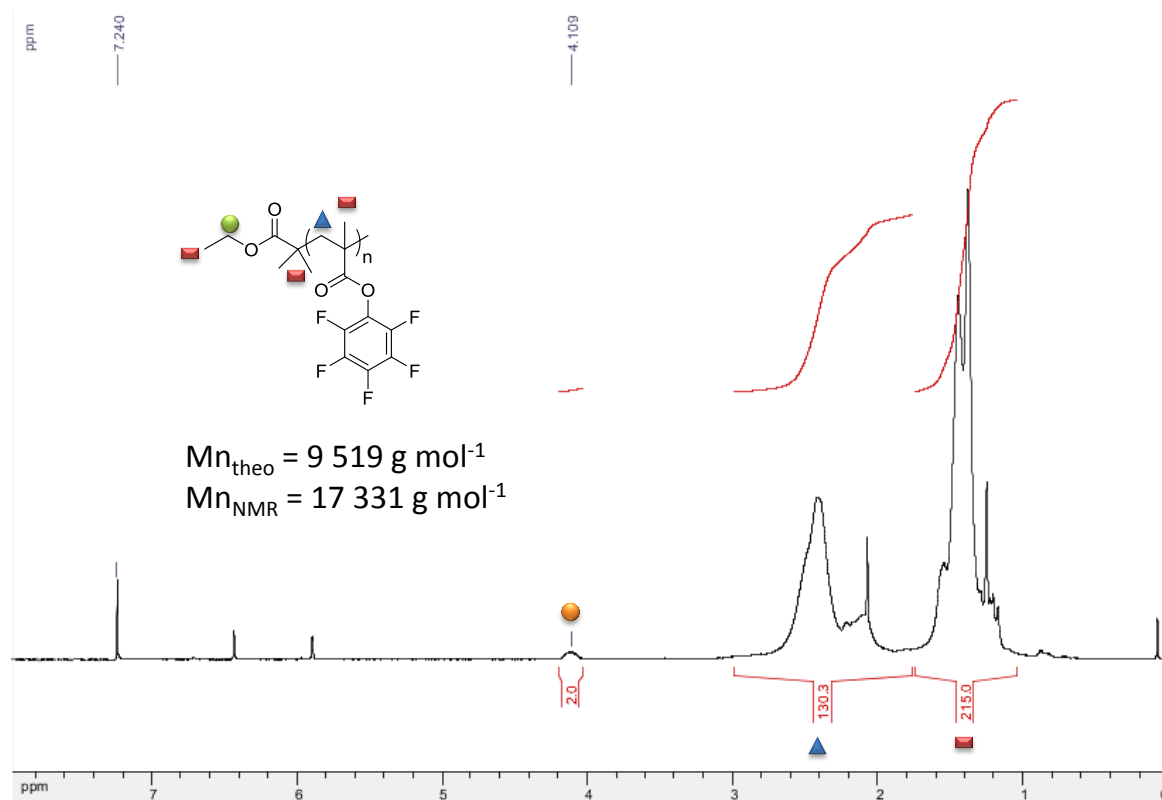
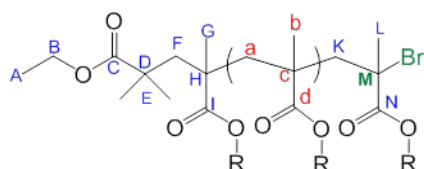


Figure 36. ^1H NMR of PFPMA obtained by eBiB, TPMA, THF:Sulfolane 75:25 %v/v, Solvent: CDCl_3 , 400 MHz.

In addition to ^1H NMR, HSQC experiment ($2\text{D } ^1\text{H}/^{13}\text{C}$ NMR) (Figure 37) was also carried out to study the end-chain as well to study livingness of PPFMA initiated by eBiB. The main correlations are listed in Table 8; all aliphatic C-H bond were observed between 0 to 4.2 ppm in ^1H NMR and between 0 to 62.0 ppm in ^{13}C -NMR. Other carbons were observed at higher intensity as presented in Figure 38 including carbonyl carbon at around 176.0 to 178.0 ppm and aromatic carbon between 120.0 to 140.0 ppm. Quaternary C-Br signal might be attributed to the peak at 41.8 ppm, which has no correlated proton.

Table 8. $2\text{D } ^1\text{H}/^{13}\text{C}$ NMR correlation data and their assignments

Label	^{13}C	^1H
A, L	13.92	1.24
A, L	14.09	0.86
b	17.61	1.37
b	19.02	1.44
G	20.60	1.55
D	29.75	1.25
E	29.05	1.20
G	23.77	1.17
B	60.90	4.12
a	52.63	2.38
F, K	49.64	2.43
c, H	45.41	2.52
a	52.80	2.07
a	50.69	2.21



In conclusion, NMR analysis of PPFMA obtained using eBiB as initiator indicates the integrity in chemical structure of the polymer. However, as the control of polymerization using this initiator was not achieved; thus, no further investigation was carried out.

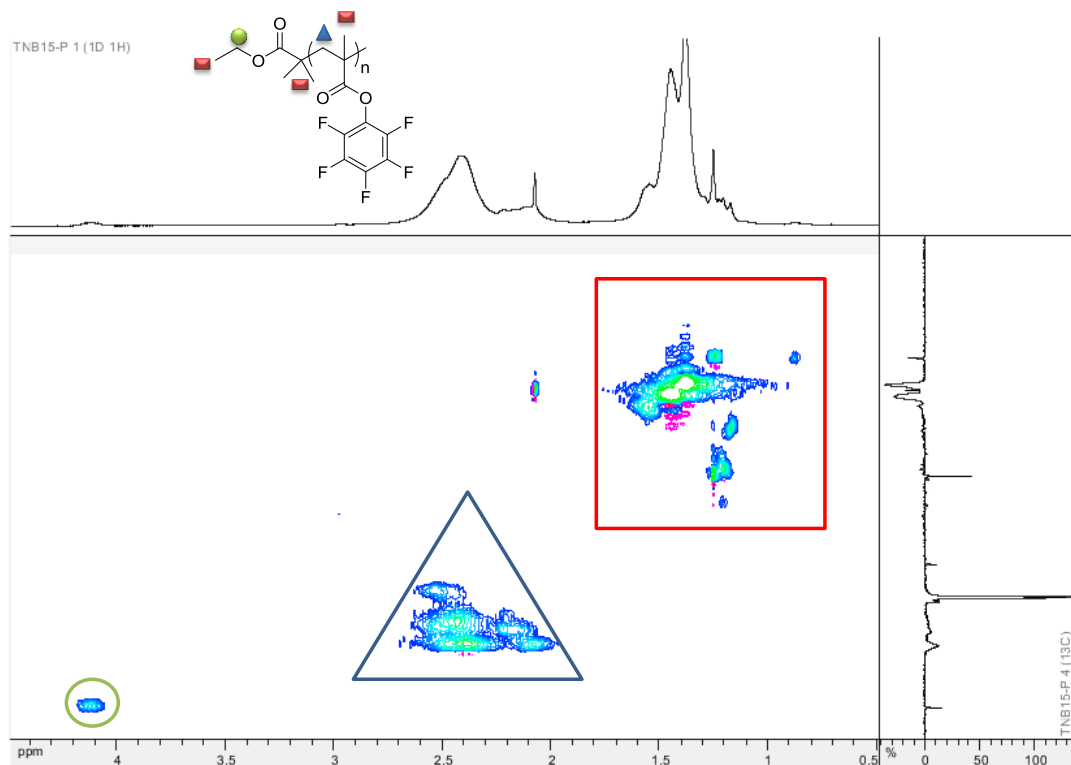


Figure 37. 2D $^1\text{H}/^{13}\text{C}$ NMR of PPFMA obtained by eBiB initiation system

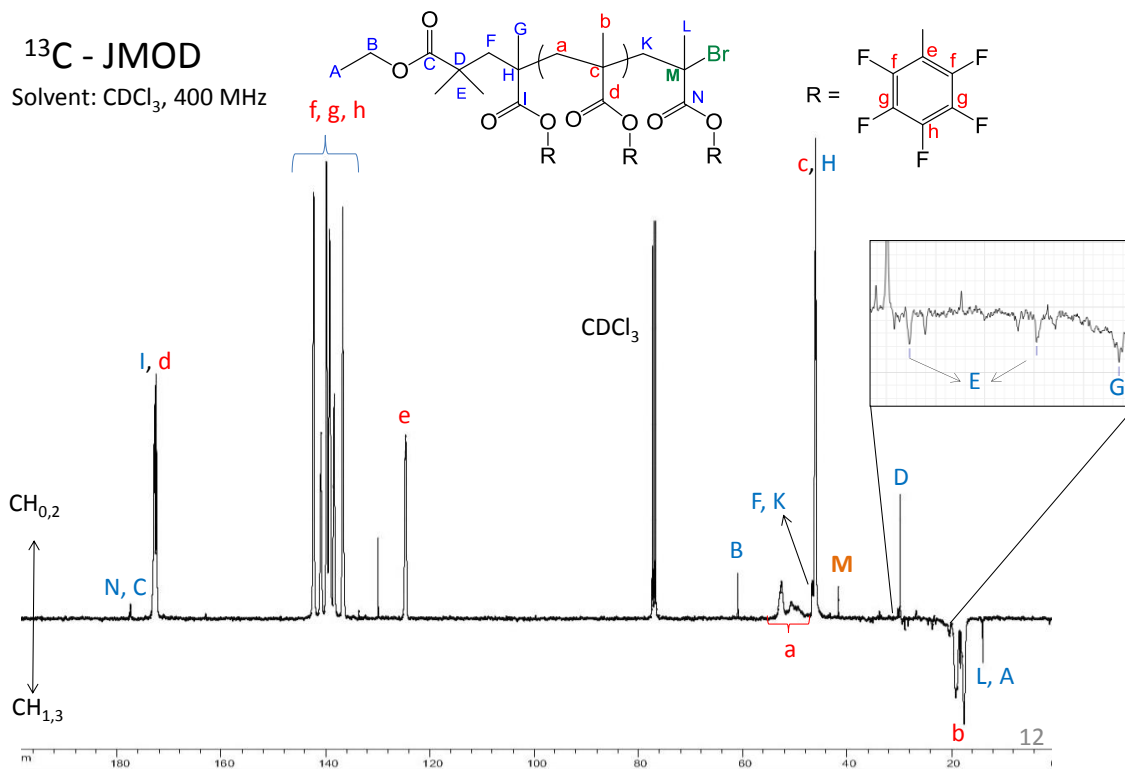


Figure 38. J-MOD ^{13}C -NMR of PPFMA obtained from eBiB initiation system

2.2.1.2. MBPA-based PPFMA

a) NMR

A typical ^1H NMR spectrum of PPFMA obtained by Cu(0)-mediated RDRP is as presented in Figure 39. The conservation of α -end is observed at around ≈ 3.6 ppm (4H) and ≈ 7.2 ppm (5H) at the same position as of CDCl_3 as indicated. The presence of α -end allows the calculation of M_n by NMR as well as initiator efficiency, which was determined to be 0.84.

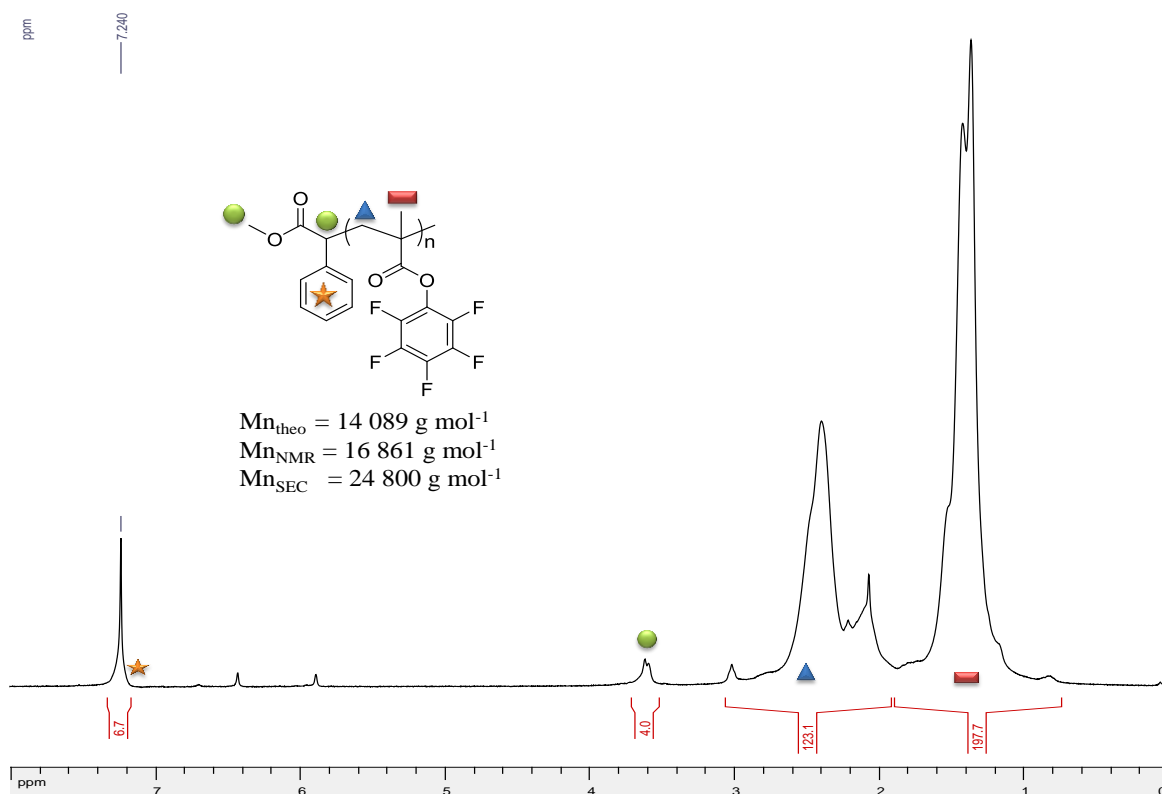


Figure 39. ^1H NMR of PPFMA obtained by Cu(0)-mediated RDRP of PPFMA under optimal conditions. Solvent: CDCl_3 , 360 MHz

In conclusion, ^1H NMR has confirmed the presence of α -extremity of PPFMA obtained by Cu(0)-RDRP, however, it is impossible to identify by NMR whether or not the ω -end is conserved. Therefore, further analysis is necessary to confirm the livingness of acquired PPFMA.

b) MALDI-ToF Mass Spectrometry

Matrix Assisted Laser Desorption/Ionization Time of Flight Mass Spectrometry (MALDI-ToF MS or simply MALDI-ToF) is a powerful technique to study intact mass of macromolecules, this technique has been widely used for end-chain analysis of polymers. In this study, a polymer obtained at low monomer conversion ($M_{n_{\text{theo}}} = 2749 \text{ g mol}^{-1}$, $M_{n_{\text{SEC}}} = 7000 \text{ g mol}^{-1}$, $D = 1.07$) of a typical Cu(0)-mediated RDRP was used to determine conservation of two extremities generated by initiator.

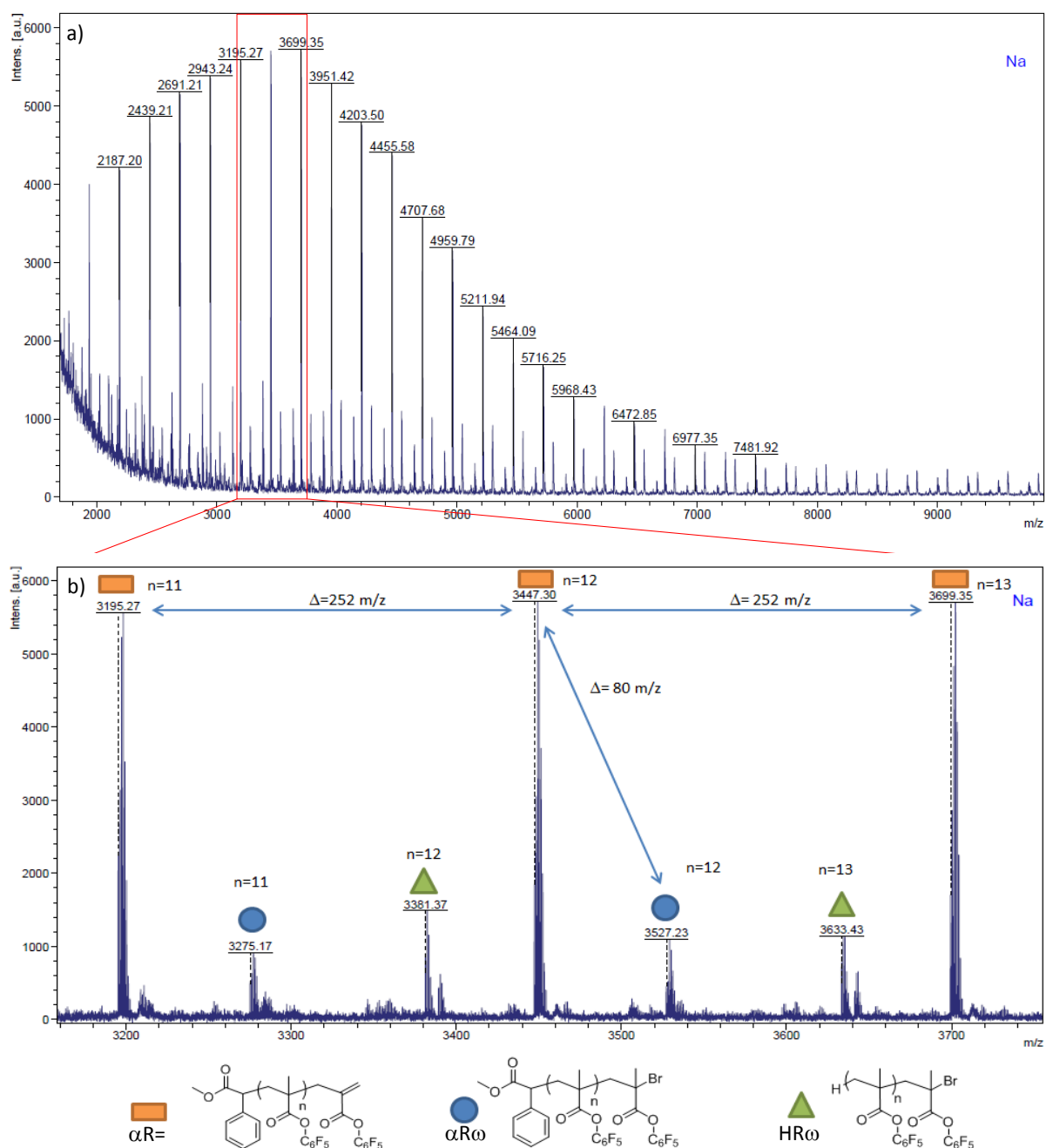


Figure 40. MALDI-ToF spectra of PFPMA obtained at 20% monomer conversion by typical Cu(0)-mediated RDRP: a) full spectrum, b) Section enlargement

Overall, MALDI-ToF spectrum presents a regular profile in which the change of 252 m/z was recorded throughout the decomposition of polymers. This change corresponds to the mass of one PFPMA unit, thus, indicating the chemical nature of the analyzed polymer. Furthermore, MALDI-ToF analysis of PFPMA shows 3 major species recorded (Figure 40) including: 1) polymers with only α -end and an ω -unsaturated end (indicated by \square), 2) polymers with a H-saturated α -extremity and C-Br ω -end (indicated by \triangle), and 3) expected polymers that conserved both α and ω -extremities generated by MBPA (indicated by \circ).

It is seen that the proportion of polymer that reserves both α and ω -extremities intact ($\alpha R\omega$) is lower than polymers with only α -end with an unsaturated extremity ($\alpha R=$), which is the most abundant species. On the one hand, the $\alpha R=$ species may be originated from halogen abstraction (Figure 41) of the $\alpha R\omega$ during MALDI handling and measurement, which has been reported for C-Br extremities of methacrylates [314].

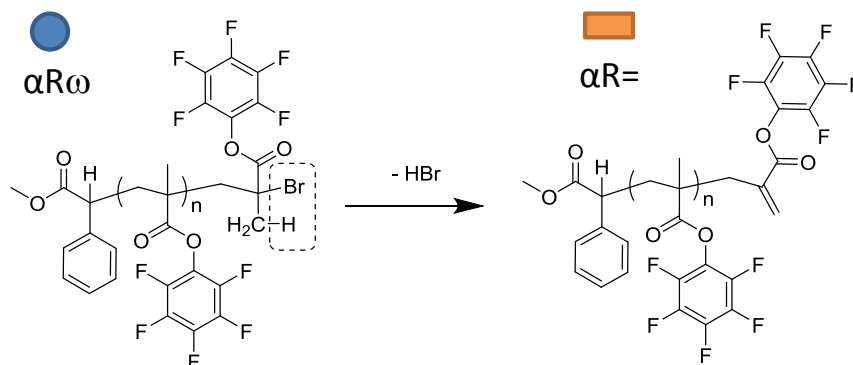


Figure 41. HBr abstraction of PPFPMMA-Br during MALDI-ToF handling or measurement

On the other hand, the appearance of $\alpha R=$ and $HR\omega$ species may also come from the termination by chain disproportion or depolymerization (Figure 42), hydrogen abstraction or from random chain scission [315, 316].

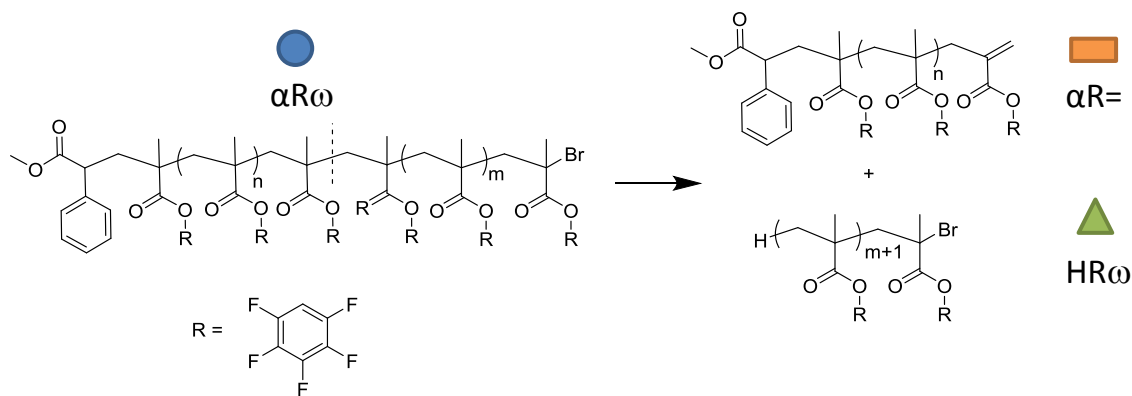


Figure 42. Proposed fragmentation pathway of initial PPFPMMA composed of both intact end-chains

In conclusion, MALDI-ToF results have indicated the conservation of end-chains, however, chain-end fidelity analysis has raised concerns as MALDI-ToF handling and measurement might have affected the integrity of in structure of obtained polymer. Thus, to confirm the livingness of synthesized PPFPMMA, chain extension of the polymer has been carried out.

2.2.2. Chain extension of PPFPMMA-Br as macro-initiator

When precipitated PPFPMMA was used as macro-initiator for chain extension, only a very limited monomer conversion after 18 hours is achieved. In accordance with MALDI-ToF, this

result indicates the loss of ω -end, *i.e.* livingness of polymer. However, the loss of the halogen-end can be originated from internal factor like termination or external factor like purification process. Therefore, an *in situ* chain extension was performed to evaluate the living characteristic of polymer before precipitation. The macro-initiator was prepared from an optimized polymerization of PFPMA with $DP_n = 20$. After 6 hours, the monomer conversion reached 87%, 200 μ L of reaction mixture was withdrawn and a degassed mixture of 1.5 mL of PFPMA, 1.5 mL THF and 0.5 mL sulfolane was introduced *via* an Ar-washed syringe and the reaction was prolonged for 18 hours, the total conversion was 69% ($DP_{theo} = 76$).

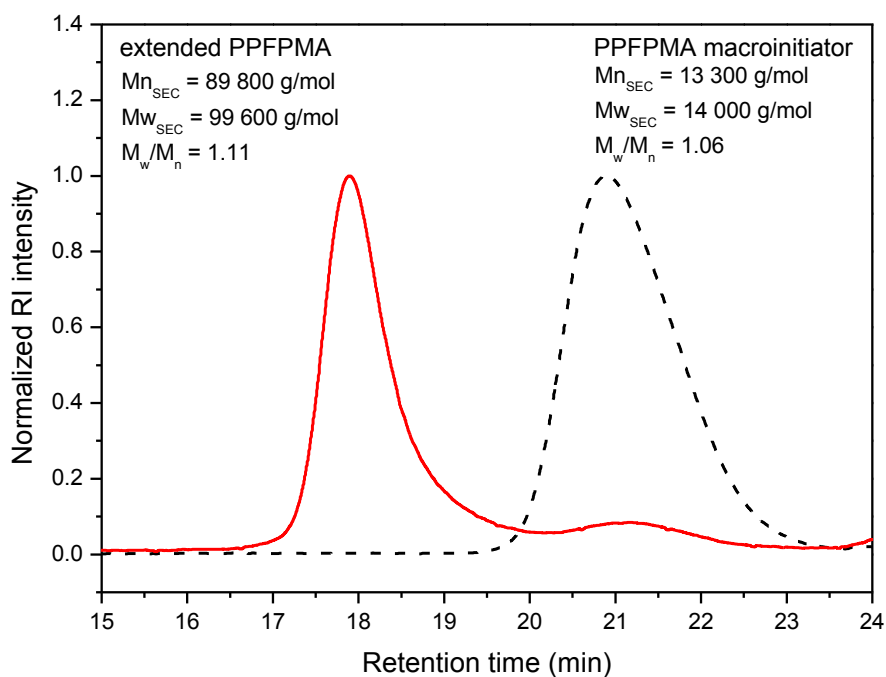


Figure 43. SEC profiles of macro-initiator PFPMA-Br (dashed line) and extended-PFPMA obtained by *in situ* chain extension (solid line)

SEC profiles of macro-initiator (PPFPMA-Br) and chain extended PFPMA demonstrate that PFPMA-Br formed *in situ* successfully reinitiated polymerization of PFPMA (Figure 43). Both macro-initiator and extended PFPMA has narrow dispersity, meaning that the ω -end was remained intact with polymer chain during polymerization process. However, the chain-extended polymer shows a small fraction of lower molecular weight polymer at the same retention time as macro-initiator, indicating a partial loss in functionality of macro-initiator. These results suggest that the dominant appearance of the $\alpha R=$ species in MALDI-ToF spectra was majorly resulted from sample preparation process rather than termination event during polymerization.

2.2.3. Termination or immortality: “In the long run we are all dead”

Despite a report on immortality of SET-LRP [317], many other research have proven that termination is inevitable [208, 318], or “in the long run we are all dead” – John Maynard Keynes. In an attempt to investigate the livingness properties of PFPMA macro-initiator, it

was found that termination does exist in Cu(0)-mediated RDRP of PFPMA. In this experiment, PFPMA macro-initiator (DP = 20) was obtained by polymerization at optimal conditions for 18 hours to achieve 96% monomer conversion. Chain-extension was carried out by addition of a fresh degassed solution of 1.5 mL of PFPMA, extra THF and sulfolane *via* Ar-wash airtight syringe. The polymerization was then again left to proceed for another 24 hours. SEC profiles of macro-initiator and extended PFPMA are presented as in Figure 44.

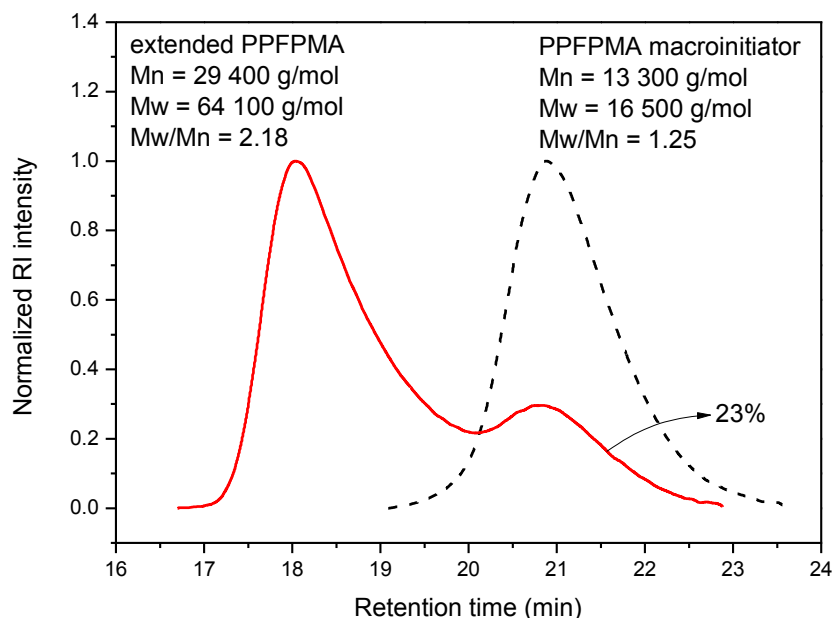


Figure 44. SEC profiles of macro-initiator PFPMA-Br (dashed line) and extended-PFPMA obtained by *in situ* chain extension (solid line)

As shown previously PFPMA macro-initiator can re-initiate polymerization *in situ*. However, when the macro-initiator was left at 96% monomer conversion overnight, termination event was recognized. Termination is visualized as the presence of a shoulder on the right of the main peak, which contributes around 23% total area in SEC profile of extended PFPMA. By comparing this shoulder and the position of macro initiator, it is seen that they came out of the column at the same position, hence possessing roughly the same molecular weight. The same range in molecular weight of macro-initiator and dead-end polymer suggests termination by other mechanisms like disproportionation rather than bimolecular coupling.

2.2.4. Characterization of PFPMA by other analyses

As PFPMA will be used for further post-modification either in bulk or after being grown from surface, hence, the characterization of the polymer by other analysis is necessary to evaluate the change before and after modification.

Figure 45 presents ATR FTIR spectrum of PFPMA obtained from Cu(0)-mediated RDRP. Four major stretching vibration bands emerged from the spectrum: C=O at 1778 cm^{-1} ,

aromatic C=C at 1517 cm^{-1} , C-O at 1056 cm^{-1} , and notably C-F at 993 cm^{-1} as reported in literature [319, 320].

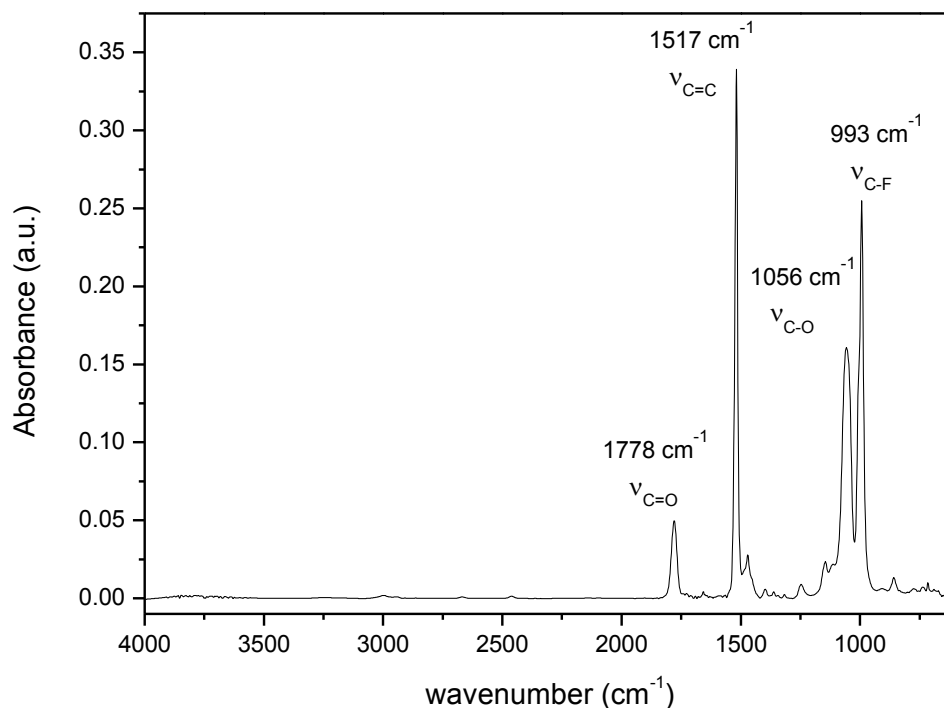


Figure 45. ATR FTIR spectrum of PPFMA and major bands' assignments of PPFMA

X-ray photon spectroscopy (XPS) was also employed to investigate chemical structure and bonding properties of PPFMA. Survey and core levels spectra obtained from this technique are presented in Figure 46. The survey scan shows three elements involved in structure of PPFMA, they appear at 284 eV (C1s), 533 eV (O1s) and 688 eV (F1s). By taking ratio between areas of these peaks, atomic percentage of each element could be calculated as 27.8% for F1s (theoretical: 29.4%), 10.8% for O1s (theoretical: 11.8%) and 61.4 for C1s (theoretical: 58.8%). From the survey spectrum, it should be noted that no copper species was found in PPFMA obtained by Cu(0)-mediated RDRP, meaning that this polymerization technique retains almost no copper residues.

As presented in Figure 46b, C1s deconvolution of PPFMA contains 6 different components including hydrocarbon (C-C, C-H) at 285 eV, quaternary aliphatic carbon (C*-CH₃) at 285.8 eV, ether carbon (C-O) at 286.5 eV, halogenated carbon C-F at 288.3 eV and carbonyl carbon (O-C*=O) at 289.7 eV. As the pendant group contains a substituted phenyl ring, π - π^* transition (satellite shake up) is also observed at 295.2 eV. A list of fitting parameters for deconvolution of C1s, O1s and F1s is given in Table 9. These data present a good correlation with results obtained for the same polymer by RAFT polymerization [319] and plasma polymerization [321]. Regarding O1s core level, it is seen from Figure 46b and fitting parameters in Table 9 that there is only carbonyl oxygen consisted in O1s core level apart of shake up presented at 540.0 eV. However, despite the good correlation with literature in the case of C1s, binding energies of C=O and C-O in O1s core level obtained herein show a

derivation compared to literature. In details, both of these two bonds in this study are 1.2 eV higher in binding energy than that reported for PPFMA prepared by surface-initiated RAFT polymerization [319]. In case of F1s, it is seen that this core level can be fitted using only one C-F signal at 687.4 eV along with 4.3% of shake up satellite at 694.4 eV. Overall, XPS analysis indicates no deflection in chemical structure of PPFMA synthesized by Cu(0)-mediated RDRP, and more importantly, no sign of copper residues is recorded confirming the achievement in using this technique to synthesize precursor for biological application.

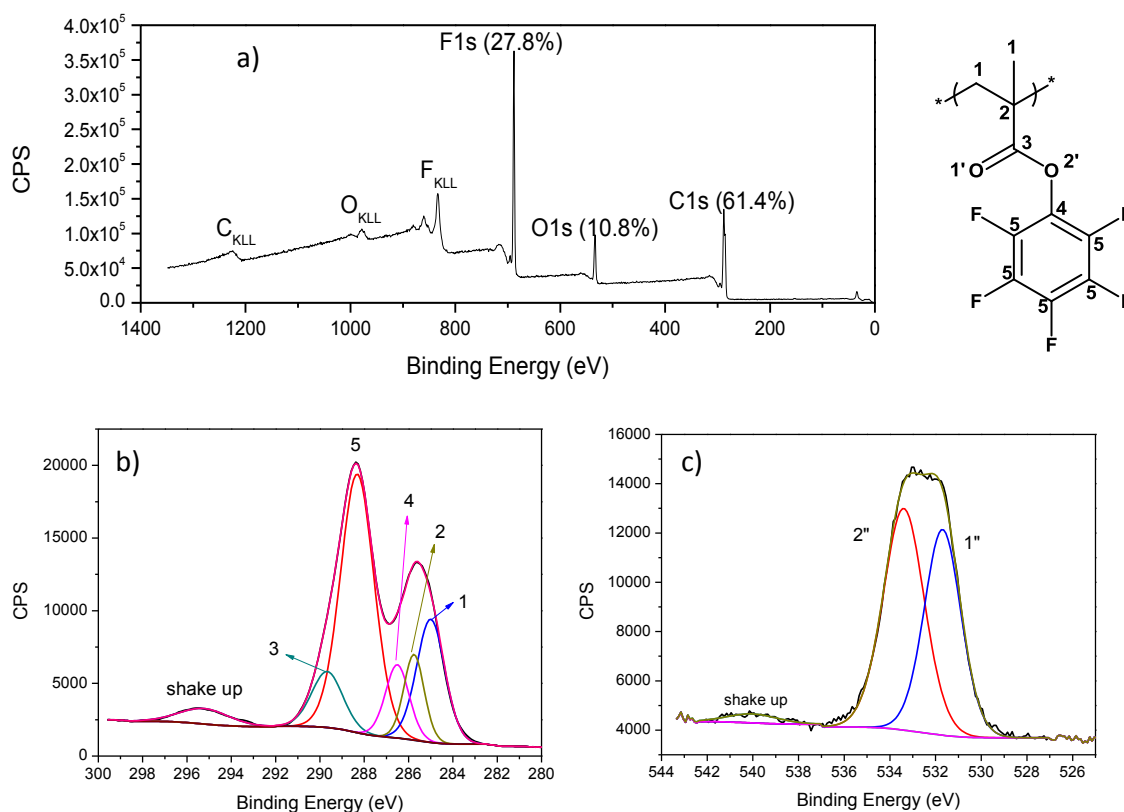


Figure 46. XPS results of bulk PPFMA: a) survey scan and assignment of major elements, b) C1s core level and its deconvolution, c) O1s core level and its deconvolution

Table 9. Details on fitting parameters of XPS core levels of PFPMA.

	Bond assignment	BE (eV)	FWHM	%
C1s	C-C, C-H	285.0	1.50	19.2
	C*-CH3	285.8	1.08	9.5
	C-O	286.5	1.26	9.6
	C-F	288.3	1.79	47.9
	C=O	289.7	1.65	9.5
	Shake up	295.2	2.65	4.3
O1s	C=O	531.7	1.90	44.3
	C-O	533.4	2.11	53.1
	Shake up	540.0	2.59	2.6
F1s	C-F	687.4	1.96	95.7
	Shake up	694.4	2.17	4.3

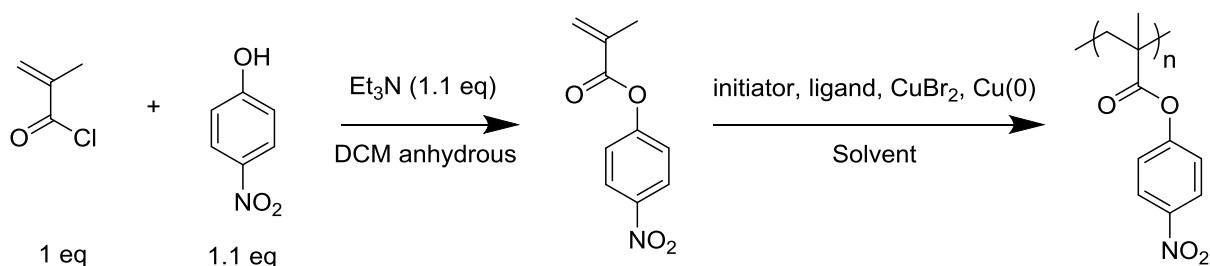
2.2.5. Conclusion

Optimization of PFPMA polymerization by Cu(0)-mediated RDRP has been demonstrated to be challenging. As the control of polymerization shows a synergic dependence on several core factors including solvent, ligand, initiator as well as length of Cu(0). In terms of solvent, better results were afforded with a mixture of 75:25 %v/v of THF and sulfolane where a balance of monomer conversion and control over dispersity is achieved in contrast to the use of a sole solvent. Indeed, the addition of 25% sulfolane as co-solvent led to the change in coordination and geometry of Cu(II) complexes with dnNbpy, *i.e.* the transformation into trigonal bipyramidal ionic complex $[\text{Cu}^{\text{II}}(\text{dnNbpy})_2\text{Br}^+]\text{Br}^-$. Furthermore, different pairs of ligand and initiator were compared and the combination of dnNbpy and MBPA was determined to be the standout condition to prepare narrow dispersity of PFPMA ($D = 1.05 - 1.33$). Moreover, polymerization rate and dispersity were shown to be dependent of Cu(0) wire length used in the system, *i.e.* the longer the length, the faster the polymerization, yet a certain loss in dispersity control was observed. By combining optimal conditions, a linear first order kinetic plot of the gain in molecular weight against time was observed, and the control over dispersity remained narrow regardless of conversion. Moreover, the optimal condition proves to be robust as it allowed the preparation of long chain polymer with molecular weight up to $M_{\text{SEC}} = 129\,900 \text{ g mol}^{-1}$, which have never been reported so far. Additionally, NMR and MALDI-ToF spectroscopies was proven the chain-end fidelity of obtained polymer. The intact conservation of C-Br extremity was demonstrated by the *in situ* extension of short chain ($M_{\text{SEC}} = 13\,300 \text{ g mol}^{-1}$) to much longer polymer chain ($M_{\text{SEC}} = 89\,900 \text{ g mol}^{-1}$) without losing control over polymerization process indicated by $D \approx 1.10$ for both macro-initiator and extended polymer chain.

2.3. Cu(0)-mediated Reversible Deactivation Radical Polymerization of NPMA

Cu(0)-mediated RDRP of NPMA was roughly investigated as the monomer shares the possession of good leaving groups with PFPMA.

Similar to PFPMA, NPMA was synthesized by esterification of methacryloyl chloride and *p*-nitrophenyl phenol as shown in Scheme 13. The monomer was obtained by recrystallization in cold MeOH at a yield of 40% to get white to pale yellow crystals.



Scheme 13. Synthesis of NPMA and its polymerization by Cu(0)-mediated RDRP

As briefly discussed in section 1.4.2.1, controlled homopolymerization of NPMA was achieved by RAFT polymerization rather than ATRP. In this dissertation, Cu(0)-mediated RDRP of NPMA was examined by using different reagents as generalized in Scheme 13.

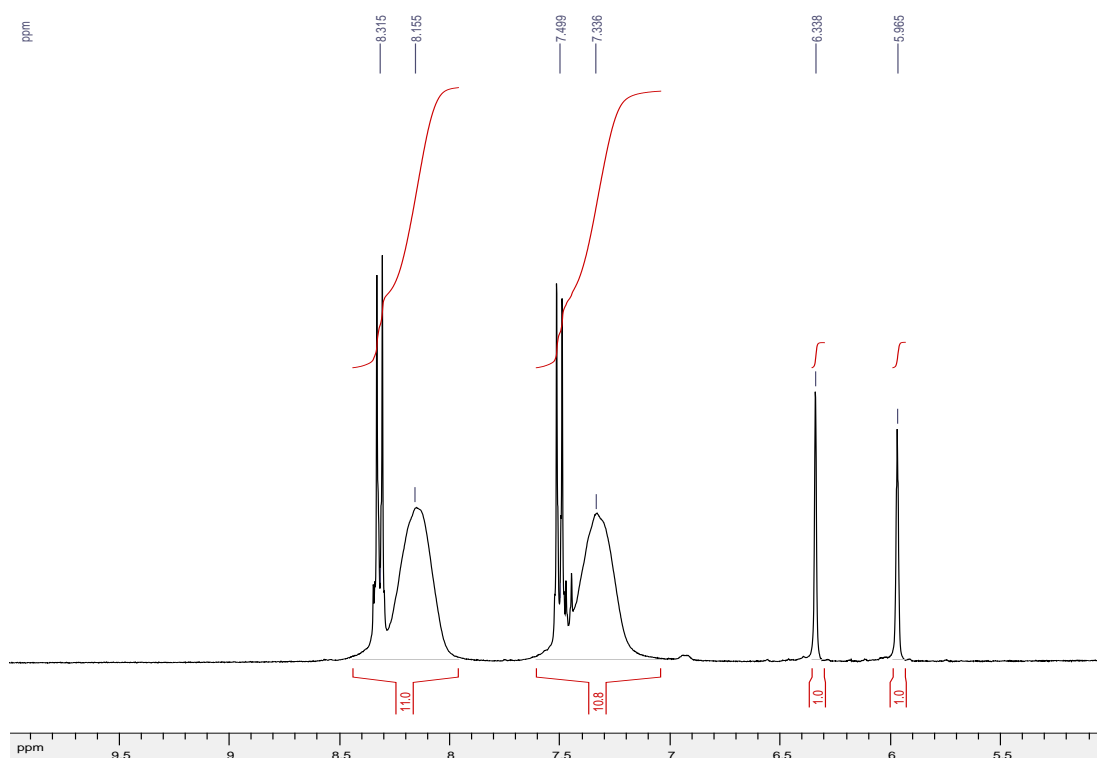


Figure 47. Demonstration on calculation of NPMA conversion after polymerization

Results on Cu(0)-mediated RDRP of NPMA at different polymerization conditions are given in Table 10. Monomer conversion was calculated from ^1H NMR spectrum of reaction mixture

in DMSO-d₅ by taking area of peaks corresponding to methylene proton at 5.96 ppm or 6.34 ppm as reference then comparing ratio of phenyl protons originated from monomer to that of polymer as demonstrated in Figure 47 and the following equation:

$$NPMA\ conversion(\%) = \frac{A_{6.99-7.6\ ppm} - 2}{A_{6.99-7.6\ ppm}} \times 100$$

Table 10. Results on Cu(0)-mediated RDRP of NPMA at different polymerization conditions. Polymerization conditions: [NPMA]₀: [initiator]₀: [ligand]₀: [CuBr₂]₀ = 100:1:0.4:0.1, t = 18 hours. [Monomer]₀ = 2M, Cu(0) wire: 2 cm for each 3.4 mmol monomer, *CuCl₂ was used instead of CuBr₂, **DP = 50

Entry	Solvent	Initiator	Ligand	T (°C)	Conv. (%)	Mn _{theo}	Mn _{SEC}	Mw _{SEC}	Đ
						g mol ⁻¹			
1	Sulfolane	eBiB	TPMA	60	82	17 183	-	-	-
2	DMSO	eBiB	TPMA	60	83	17 390	-	-	-
3	DMSO	BzCl*	TPMA	60	46	9 657	-	-	-
4	DMSO	eBiB**	TPMA	60	84	8 896	20 000	38 600	1.93
5	DMSO:Sul (1:1 v/v)	eBiB	dnNbpy	60	74	15 523	15 800	35 300	2.25
6	DMSO	eBiB	dnNbpy	60	96	19 872	21 100	43 100	2.04
7	DMSO	eBiB	dnNbpy	40	91	19 000	16 200	31 800	1.97
8	DMSO	MBPA	dnNbpy	60	98	20 532	13 500	24 300	1.80

In terms of initiators, eBiB and MBPA resulted in much higher monomer conversion (>80%) than BzCl (46%). As discussed for PFPMA, this might be explained by the common knowledge that BzCl has lower activation rate of 1.2×10^{-1} compared to 3.12 of eBiB and 6.10×10^4 of EBPA with TPMA as ligand as given in Table 5. On the other hand, PNPMA is soluble in both DMSO and sulfolane; hence, high monomer conversion was achieved in both cases. Unfortunately, the control in Cu(0)-mediated RDRP in polymerization of NPMA has not been achieved after all efforts to narrow down dispersity. On the other hand, in the same tendency as with PFPMA, the use of MBPA as initiator and dnNbpy as ligands has helped reduce value of dispersity due to formation of more stable propagating radicals. However, SEC characterization of NPMA was not adaptable to our lab's condition due to the low solubility of PNPMA in THF; therefore, further investigation to optimize polymerization of NPMA is remained subject for future study.

Chemical structure of PNPMA has been investigated by NMR (Figure 48) and ATR FTIR (Figure 49).

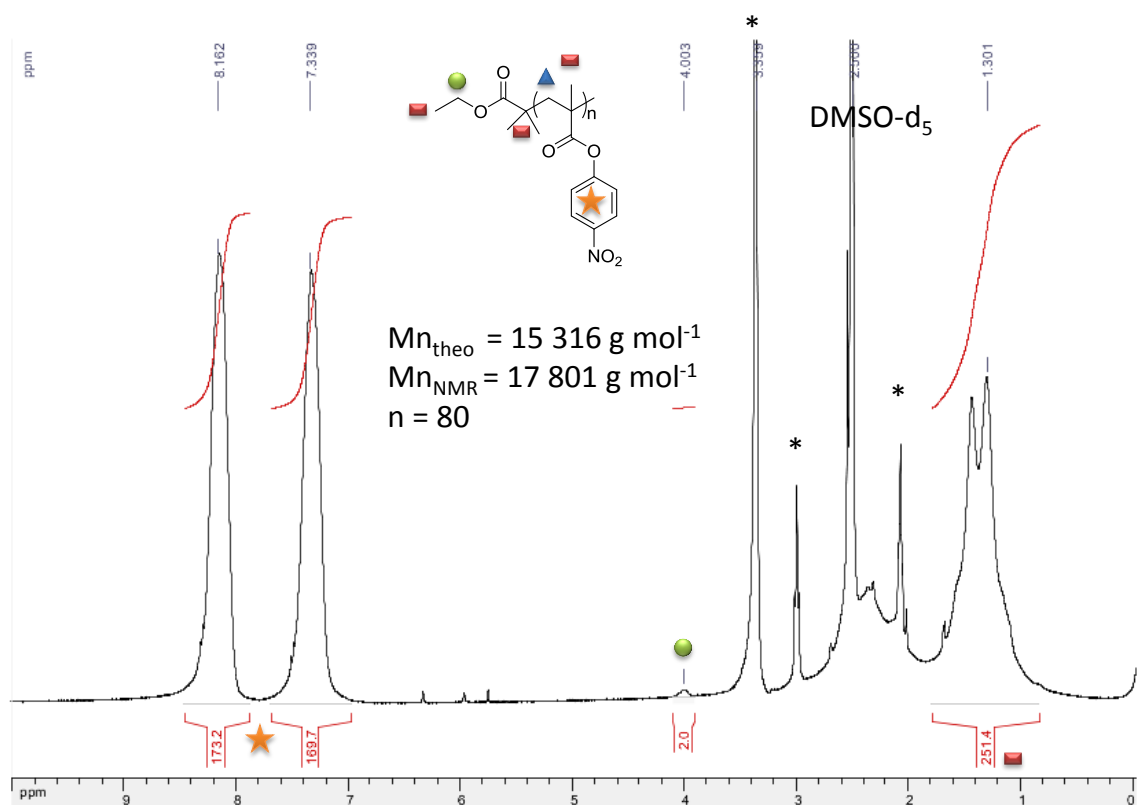


Figure 48. ^1H NMR of PNPMA and in DMSO-d_6 (360 MHz) and assignment of its end-chain and major peaks

^1H NMR of PNPMA indicates the presence of proton at 4.0 ppm corresponding to α -end of initiator eBiB. Methyl protons of polymer main chain ranges between 0.8 to 1.80 ppm while methylene protons ranges between 1.8 to around 3.0 ppm in the same range as signal of NMR solvent as well as other solvent residues as indicated in Figure 48. Protons of nitrophenyl pendant groups appear as two separated peaks at 7.39 ppm (ortho position) and 8.16 ppm (meta position). These distinguished signals from end-chain and pendant group allow calculation of degree of polymerization and number average molecular weight, which was determined to be 80 and 17 801 g mol^{-1} respectively in this example. Thus, initiator (eBiB) efficiency during preparation of this polymer is 0.86. From these proton assignment, chemical structure of PNPMA obtained by $\text{Cu}(0)$ -mediated RDRP was confirmed to match with that from theoretical expectation.

The chemical skeleton of PNPMA was also confirmed by ATR FTIR as shown in Figure 49; signals between 1820 cm^{-1} and 2900 cm^{-1} were omitted for clarification. It is obvious that all representative functional groups present in PNPMA structure are observed. The first proof is the stretching vibration of nitro groups at 1350 cm^{-1} (N-O) and 1205 cm^{-1} (C-N). Furthermore, the appearance of band characterized for aromatic C=C at 1523 cm^{-1} accompanying by stretching and scissoring signals of aromatic C-H at 3249 cm^{-1} and $862\text{-}746\text{ cm}^{-1}$ were also

observed respectively. In addition, carbonyl groups were distinguished by their absorbance at 1089 cm^{-1} (C-O stretching) and 1752 cm^{-1} (C=O stretching).

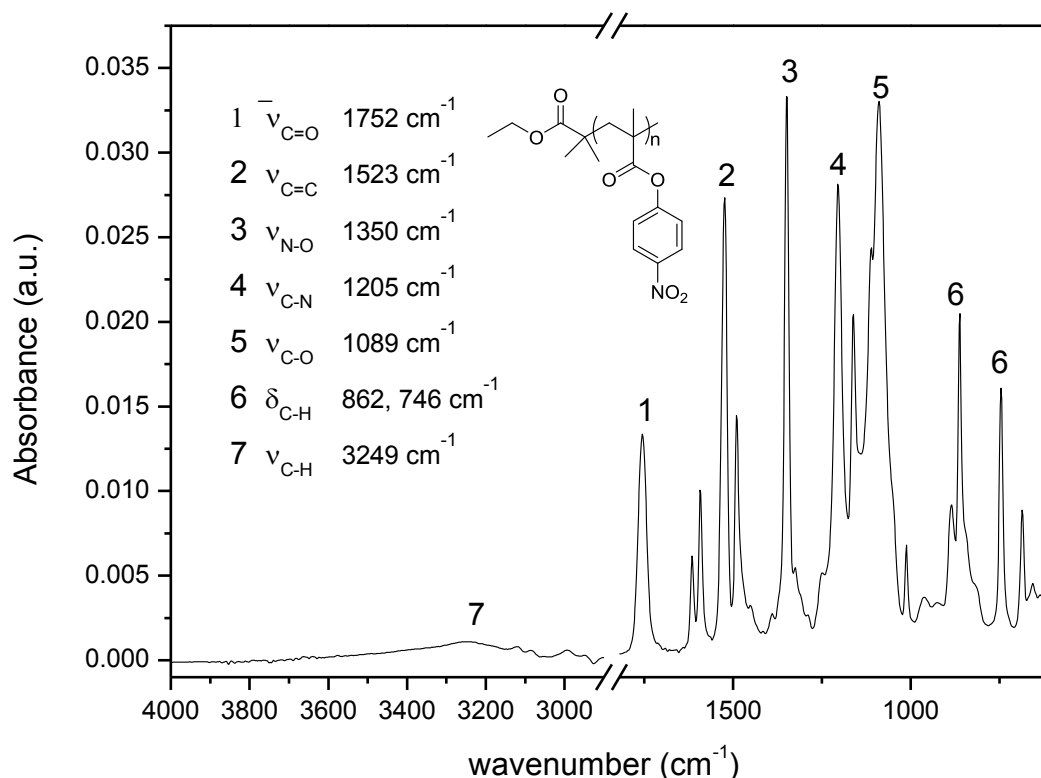


Figure 49. ATR FTIR spectrum of PNPMA obtained by Cu(0)-mediated RDRP.

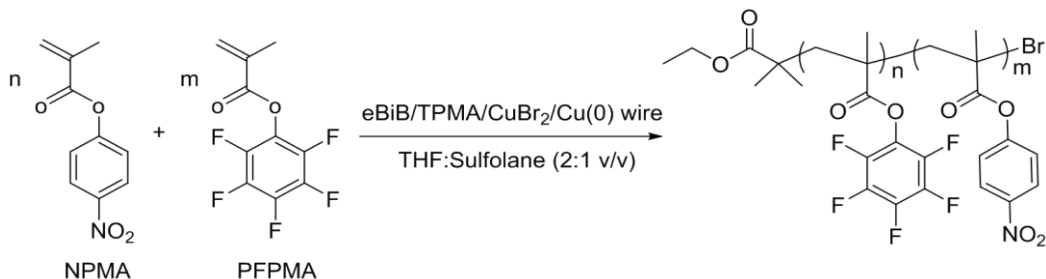
In conclusion, Cu(0)-mediated RDRP presents to be a promising technique in polymerization of NPMA where high monomer conversion was achieved and acquired polymer has been confirm to match with expected chemical structure. However, this approach should be examined in a deeper manner to obtain controlled condition to synthesize the reactive polymer.

2.4. Cu(0)-mediated Reversible Deactivation Radical Copolymerization

From the studies in Cu(0)-mediated RDRP of PFPMA and NPMA, it is highlighted that both homopolymers can be obtained in similar polymerization conditions at high monomer conversion. Moreover, as discussed in 1.4.2.1, post-polymerization modification of these two polymers suggests that PNPMA is less reactive than PFPMA in substitution with alcohols, *i.e.* lower conversion was recorded for PNPMA than PFPMA. Therefore, random copolymerization of NPMA and PFPMA by Cu(0)-mediated RDRP has been studied at different comonomer ratios in order to synthesize a prospective selective dual-responsive template for further modification.

From individual studies on Cu(0)-mediated RDRP of NPMA and PFPMA, conditions for copolymerization of PFPMA and NPMA were selected as following:

- Solvent: THF:sulfolane 2:1 v/v
- Initiator: eBiB
- Ligand: TPMA
- Catalyst: CuBr₂/Cu(0)
- Temperature: 60 °C



Scheme 14. Copolymerization of PFPMA and NPMA via Cu(0)-mediated RDRP

Three different comonomer ratios have been chosen where molar proportion of PFPMA varied from 33%, 50% to 67% and expected degree of polymerization was retained 100 in all experiment (Scheme 14).

2.4.1. NMR analysis: total conversion, solubility and composition

Conversions of NPMA and PFPMA were calculated by ¹H NMR and ¹⁹F NMR, respectively. It is to note that double bonds signals of two monomers are well separated in ¹H NMR, *i.e.* methylene protons of NPMA are at 5.8 ppm and 6.2 ppm and PFPMA's ones are at 5.8 ppm and 6.3 ppm as illustrated in Figure 50. Thus, the determination of NPMA conversion was independent from PFPMA. Theoretical number average molecular weight of copolymers can be determined from comonomer conversion as following:

$$M_n \left(\frac{g}{mol} \right) = p_{NPMA} \times DP_{theo, NPMA} \times 207.183 \frac{g}{mol} + p_{PFPMA} \times DP_{theo, PFPMA} \times 252.14 \frac{g}{mol} + 195 \frac{g}{mol}$$

where *p* is fractional monomer conversion, *DP* is expected degree of polymerization of corresponding monomer, and 195 g mol⁻¹ is molecular weight of eBiB.

Error! Reference source not found. presents a summary of results obtained from copolymerization of the two active esters by Cu(0)-mediated RDRP. After 19 hours of reaction, copolymerization at any composition reached at least 55% for NPMA and more than 60% for PFPMA. As polymerization was prolonged until 68 hours, near-complete monomer conversions were achieved, especially for equimolar composition.

Table 11. Summary of results on Cu(0)-mediated RDRP of NPMA and PFPMA at different polymerization conditions.

Entry	% PFPMA in feed	Initiator	Ligand	Time (h)	Conversion (%)		% PFPMA obtained	$M_{n,theo}$ (g mol ⁻¹)	$M_{n,NMR}$ (g mol ⁻¹)	SEC measured in THF (PS)			SEC measured in DMF (PMMA)			
					PFPMA	NPMA				$M_{n,SEC}$	$M_{w,SEC}$	\bar{D}	$M_{n,SEC}$	$M_{w,SEC}$	\bar{D}	
																g mol ⁻¹
1	Copo1N2F-19	67	eBiB	TPMA	19	69	71	66	16 921	-	25 500	57 300	2.25	38 900	58 000	1.49
2	Copo1N1F-19	50	eBiB	TPMA	19	65	55	54	14 087	-	18 500	29 900	1.61	28 900	38 300	1.33
3	Copo2N1F-19	33	eBiB	TPMA	19	64	68	32	14 796	-	32 400	64 400	1.98	42 100	62 700	1.49
4	Copo1N2F-68	67	eBiB	TPMA	68	89	78	70	21 065	26 759	28 800	51 300	1.78	33 900	42 300	1.43
5	Copo1N1F-68	50	eBiB	TPMA	68	98	98	50	22 702	26 420	37 200	75 800	2.03	35 900	61 300	1.71
6	Copo2N1F-68	33	eBiB	TPMA	68	92	96	32	20 911	26 843	32 500	79 800	2.46	42 300	62 600	1.48
7	Copo1N1F-M	50	MBPA	dnNbpy	20	80	76	51	20 245	-	17 100	44 300	2.59	-	-	-

Solubility of obtained copolymers is an interesting aspect to discuss. Firstly, homopolymers of PFPMA and NPMA have opposite solubility, *i.e.* PFPMA is soluble in chloroform, dichloromethane, THF and acetone while PNPMA is only soluble in more aprotic solvents like DMSO, sulfolane and DMF. Incorporation of both pendant groups into copolymers has improved significantly their solubility; thus, copolymers obtained in this project are visually soluble in all of the solvents mentioned above. One example is the possibility to visualize signals coming from *p*-nitrophenyl groups in THF- d_8 as presented in **Figure 51**.

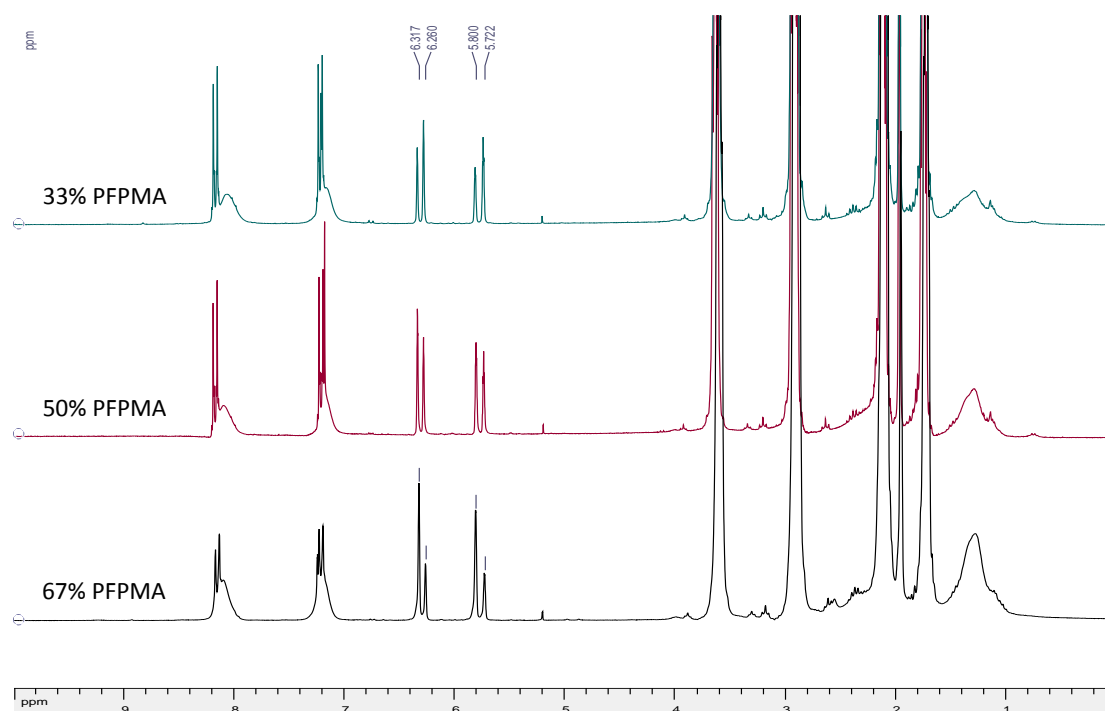


Figure 50. ^1H NMR spectra of copolymerization of PFPMA and NPMA by Cu(0)-mediated RDRP after 19 hours (CDCl_3 , 250 MHz)

In Figure 51 common protons of backbone appear at 0.8-1.9 ppm (methyl protons) and 1.9-3.0 ppm (methylene protons) while protons from *p*-nitrophenyl pendant group response between 7.2 ppm and 8.5 ppm. In addition, signals coming from methylene group of α -extremity at 4.1 ppm were also recorded, indicating the conservation of end-chain generated by initiator. These distinguished signals of end-chain, nitrophenyl groups as well as backbone enable:

- Calculation of number of repeating units of NPMA: $n_{\text{NPMA}} = \frac{A_{7.44\text{ppm}}}{A_{4.13\text{ppm}}}$
- Calculation of number of repeating units of PFPMA: $m_{\text{PFPMA}} = \frac{A_{2.5\text{ppm}}}{A_{4.13\text{ppm}}} - n_{\text{NPMA}}$
- Calculation of number average molecular weight of copolymers:

$$Mn_{\text{NMR}} \left(\frac{\text{g}}{\text{mol}} \right) = n_{\text{NPMA}} \times 207.183 \frac{\text{g}}{\text{mol}} + m_{\text{PFPMA}} \times 252.14 \frac{\text{g}}{\text{mol}} + 195 \frac{\text{g}}{\text{mol}}$$

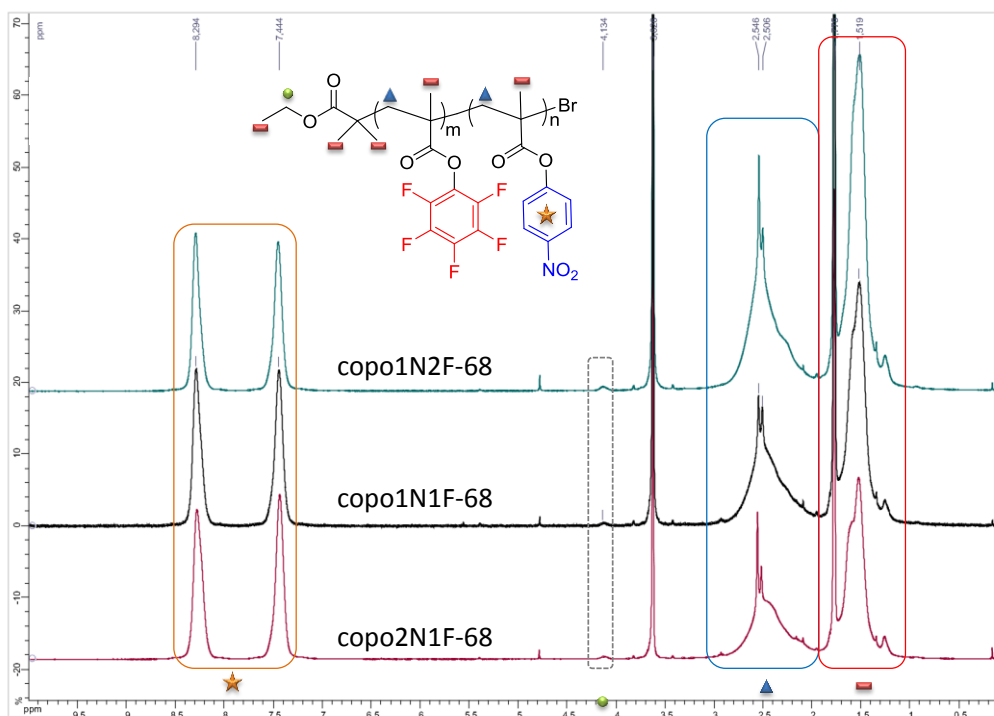


Figure 51. ^1H NMR spectra of copolymers of NPMA and PFPMA obtained by Cu(0)-mediated RDRP after 68 hours of reaction (THF- d_8 , 360 MHz).

From these formulas, $M_{n\text{NMR}}$ of copolymers were calculated as given in **Error! Reference source not found.**. This also allows the calculation of initiator efficiency by taking ratio of theoretical M_n and $M_{n\text{NMR}}$. For the three 68-hour samples of, initiator efficiency ranges between 0.78-0.89.

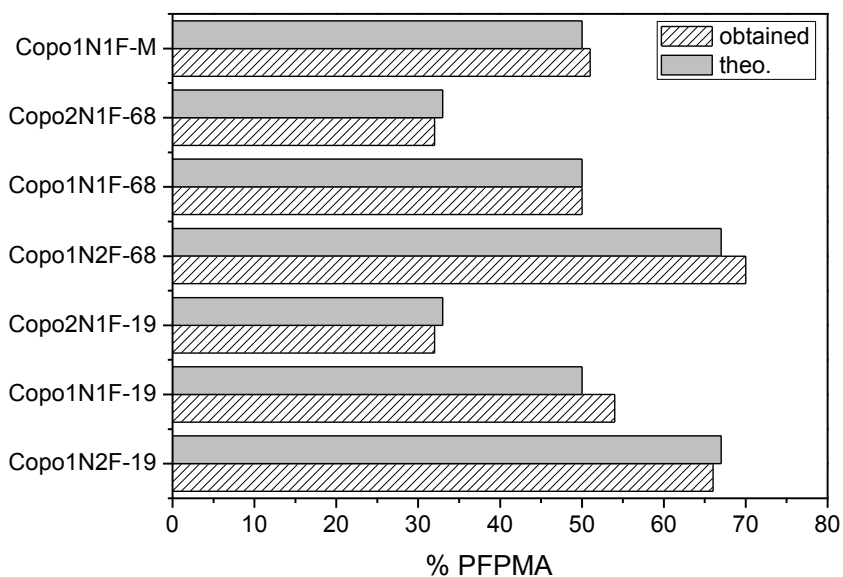


Figure 52. Comparison of PFPMA proportions in feed and in final copolymers

Nonetheless, regardless of feeding composition, conversion of NPMA and PFPMA are of the same range with at most 10% difference. In addition, because the conversion of NPMA and PFPMA was calculated independently, one is able to calculate more precisely the proportion of each monomer unit in final products and to compare these values to expected composition. Figure 52 presents a comparison between molar proportion of PFPMA in feed and in obtained copolymers; corresponding values are given in **Error! Reference source not found.** It is seen that the value expected and one acquired are always of a great agreement. This indicates that the two active esters are highly compatible in copolymerization by Cu(0)-mediated RDRP. However, further study needs to be considered in the future to determine reactivity ratios of two comonomers. SEC analysis: homogeneity and dispersity

As aforementioned, solubility pattern of obtained copolymers seems to be synergic effect of the two homopolymers PFPMA and PNPMA. To confirm this, SEC analyses were performed in two solvent systems including THF/TEA (95:5) at 30 °C, flow rate 1 mL/min calibrated with narrow PS standards and DMF/LiBr at 60 °C, flow rate 0.8 mL/min calibrated with narrow PMMA standards.

Results from SEC analysis prove that all obtained products are copolymers rather than mixture of two homopolymers due to the presence of single monomodal profiles regardless of composition as shown in Figure 53 and Figure 54.

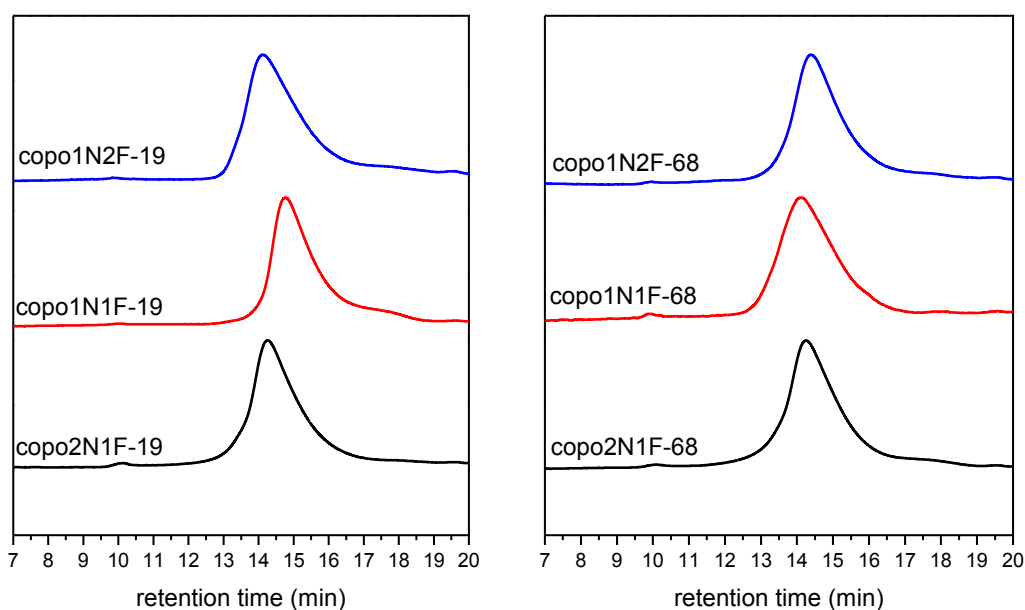


Figure 53. RI responses obtained by SEC in THF/TEA with PS as standards

It is seen from Table 101, Figure 53 and Figure 54 that results obtained by SEC in THF and DMF systems are distinguishable one from another, especially in terms of dispersity index. The discrimination between two sets of data may be due to several reasons, for example: the dissimilarity in column characteristics, the distinction behavior of copolymers regarding to solvents, and difference in standards used for conventional calibration. Comparing ratios

between M_n obtained in THF to that obtained in DMF ranges between 0.6 - 0.8, suggesting the difference in hydrodynamic volume of copolymer in the two solvents. For the sake of comparison between homopolymerization and copolymerization results, further discussion will be made based on SEC results using THF/TEA system.

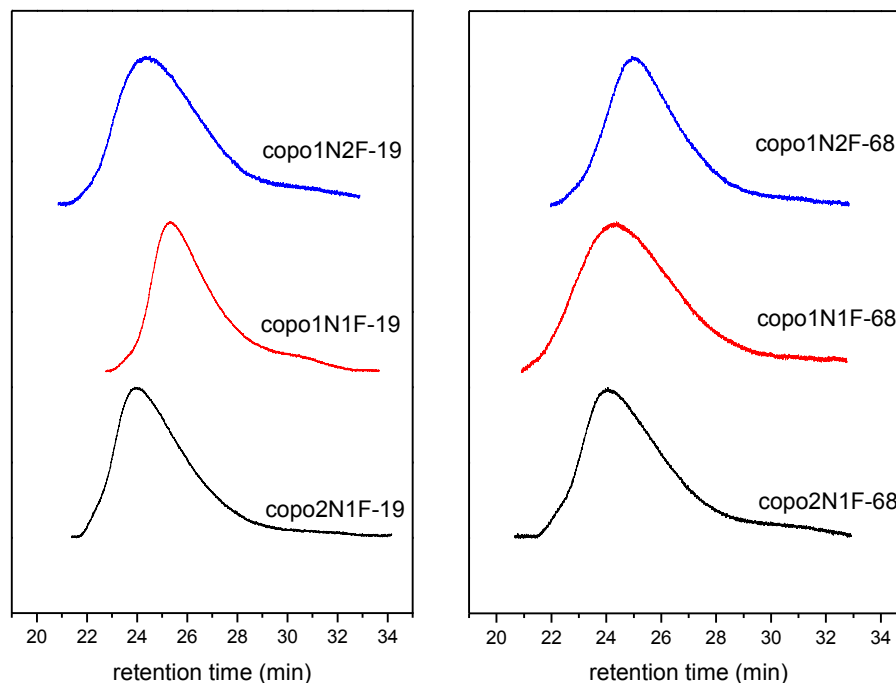


Figure 54. RI responses obtained by SEC in DMF/LiBr with PMMA as standards

As discussed in homopolymerization of PFPMA and NPMA by Cu(0)-mediated RDRP, the use of TPMA as ligand and eBiB as initiator were not the controlled conditions for both monomers, as consequence, copolymerization of the two monomers under such conditions resulted in copolymer with wide dispersity, even though high total conversion was achieved. On the other hand, the use of MBPA and dnNbpy was a good combination that provided well-controlled PFPMA and narrow down dispersity of PNPMA. However, the adaption of this condition for copolymerization is not promising with a very broad dispersity of 2.59 as seen in **Error! Reference source not found.**, entry 7. Thus, copolymerization of NPMA and PFPMA *via* Cu(0)-mediated RDRP remained uncontrolled and further studies are needed to find out optimal conditions.

Besides mechanism of polymerization, compositions and characterizations of obtained copolymers were also investigated by different techniques including ATR FTIR, XPS, NMR and elemental analysis.

2.4.2. FTIR analysis: chemical environment analysis

ATR FTIR has been used to rapidly validate chemical environment in acquired copolymers. Table 12 summarizes bond assignment of major peaks observed in spectrum presented in Figure 55a of two homopolymers and three examples of copolymers studied in this

dissertation. It is obvious that copolymers composed of PFPMA and NPMA possess bands that characterize for the two components including bands corresponding to nitro groups (C-N at 1205 cm^{-1} and N-O at 1350 cm^{-1}), bending signals of aromatic C-H (862 cm^{-1}) of NPMA as well as stretching of C-F bond (993 cm^{-1}) in PFPMA. Interestingly, vibration bands of C=O and C-O of PFPMA and PNPMA are not identical where C-O band of PFPMA is located at lower wavenumber, meaning that this bond has lower energy in PFPMA than in PNPMA presumably due to higher conjugation effect caused by pentafluorophenyl compared to that of *p*-nitrophenyl group. Consequently, C=O and C-O bands of copolymers are shifted compared to that of homopolymers due to the incorporation of both NPMA and PFPMA. Figure 55b presents enlargement section of peaks corresponding to vibration of carbonyl bonds and Figure 55c shows the correlation between peak maxima with molar proportion of PFPMA in copolymers. It is seen from these two figures that C=O band shifts to higher wavenumber as the quantity of pentafluorophenyl increases while the opposite trend is observed for C-O bands.

Furthermore, Figure 55d shows ratios between area of bands characterized for C-F of PFPMA and C-H of NPMA in function of theoretical molar percentage of PFPMA. As expected, as the amount of PFPMA in copolymer increases, the ratio of peak between C-F/C-H bonds increases linearly. Nonetheless, comparison between peak areas of C-F and N-O bonds as in Figure 55e also presents the same trend with the same linearity. These results confirm in a qualitative manner that the composition of obtained copolymers is close to the values expected.

Table 12. Summary of absorption peaks of PFPMA, PNPMA and their copolymers

Entry		PFPMA	Copo1N2F	Copo1N1F	Copo2N1F	PNPMA
1	$\nu_{\text{C=O}}$	1778 cm^{-1}	1772 cm^{-1}	1766 cm^{-1}	1757 cm^{-1}	1752 cm^{-1}
2	$\nu_{\text{C=C}}$	1517 cm^{-1}	1519 cm^{-1}	1519 cm^{-1}	1519 cm^{-1}	1523 cm^{-1}
3	$\nu_{\text{N-O}}$	-	1350 cm^{-1}	1350 cm^{-1}	1350 cm^{-1}	1350 cm^{-1}
4	$\nu_{\text{C-N}}$	-	1205 cm^{-1}	1205 cm^{-1}	1205 cm^{-1}	1205 cm^{-1}
5	$\nu_{\text{C-O}}$	1056 cm^{-1}	1058 cm^{-1}	1076 cm^{-1}	1083 cm^{-1}	1089 cm^{-1}
6	$\nu_{\text{C-F}}$	993 cm^{-1}	993 cm^{-1}	993 cm^{-1}	993 cm^{-1}	-
7	$\delta_{\text{C-H}}$	-	862 cm^{-1}	862 cm^{-1}	862 cm^{-1}	862 cm^{-1}

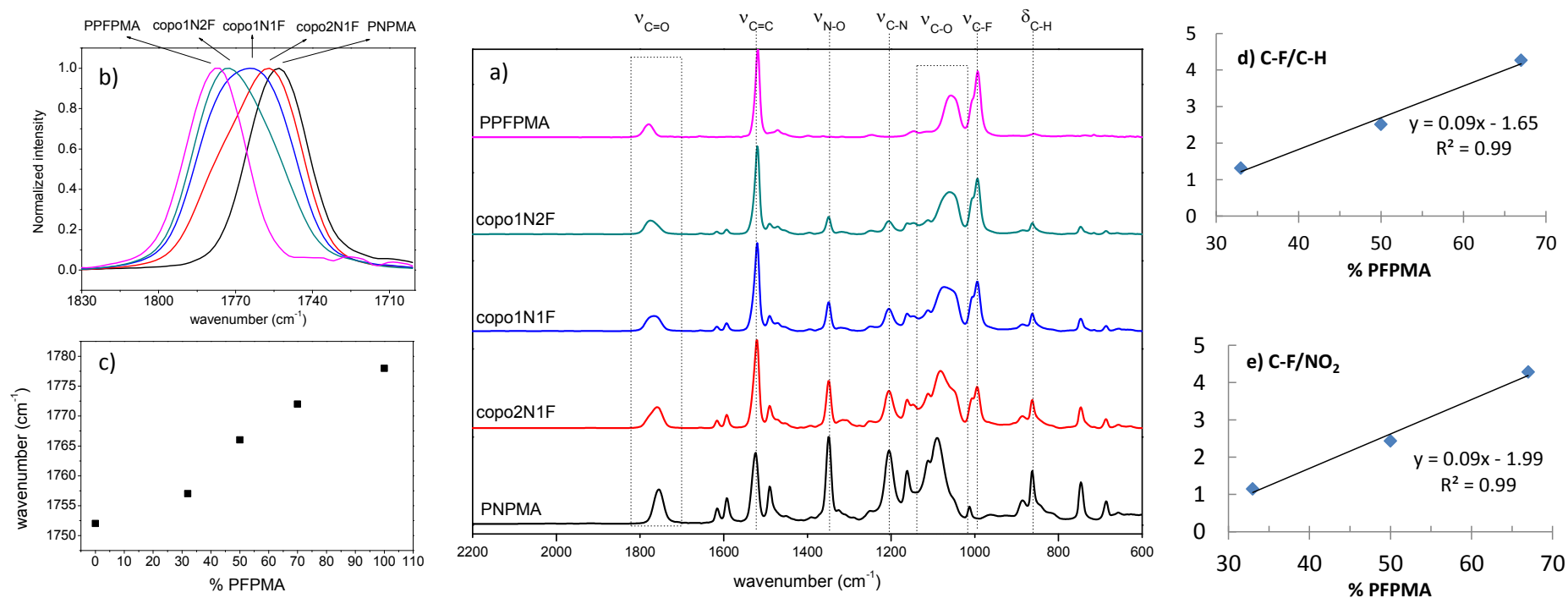


Figure 55. a) ATR FTIR spectra of copolymer at different compositions, b) enlargement of peaks characterized for C=O vibration, e) maxima of C=O peaks in function of molar percentage of PPFMA d) area ratio of C-F and C-H peak areas, e) area ratio of C-F and NO₂ peak areas

2.4.3. X-ray Photon Spectroscopy: details on composition of copolymers

X-ray Photon Spectroscopy (XPS) is a powerful technique to measure elemental composition of substrate. As all NMRs done in this dissertation is liquid-based technique, thus, dependent greatly on solubility of a compound in a solvent, XPS is able to process with material in bulk. Therefore, XPS analysis of three copolymers (copo1N2F-68, copo1N1F-68 and copo2N1F-68) was investigated for their composition in comparison with other techniques like NMR or elemental analysis. Furthermore, as the copolymers will be later used as substrate for sequential post-modification, knowledge on its chemical environment is necessary.

The very first information that can be acquired from XPS is the atomic number percentage of elements composing copolymers calculated from survey spectra of copolymer as shown in Figure 57a. It is seen that survey scans indicate the presence of C1s (284 eV), N1s (406 eV), O1s (533 eV) and F1s (688 eV) for all three copolymers and the proportions between these atoms also vary visually. Table 13 summarizes atomic number/mass percentage of carbon, nitrogen, oxygen and fluorine obtained by XPS in comparison to NMR and elemental analysis results. The contribution of hydrogen atoms was considered to be negligible. Atomic number percentage by NMR was calculated based on ratio between NPMA and PFPMA signals present on NMR spectra of copolymer in THF-d₈. In case of elemental analysis, the amount of oxygen was not taken in charge due to the presence of fluorine atoms which could generate the interference HF during mineralization process. As seen from Table 13, the difference in atomic number percentage obtained by NMR and XPS are very similar, yet the ratios between elements are slightly uneven. However, in general overview, there is a consistency between atomic weight percentages obtained by three alternative analyses. More importantly, the atomic weight ratios of C/N, C/O and F/N as presented in Figure 56 prove that the composition of examined copolymers are of great harmony between experimental and theoretical data.

Table 13. Atomic number percentage and atomic mass percentage of 3 random copolymers of PFPMA and NPMA calculated from NMR, XPS and elemental analysis results.

	Atomic Number Percentage (%)						Atomic Weight Percentage (%)								
	NMR			XPS			XPS			NMR			Elemental Analysis		
	2N1F	1N1F	1N2F	2N1F	1N1F	1N2F	2N1F	1N1F	1N2F	2N1F	1N1F	1N2F	2N1F	1N1F	1N2F
%C	64	62	61	65	62	62	57.82	53.14	52.73	52.94	51.47	50.14	53.96	52.29	50.88
%N	4	3	2	4	3	2	4.15	3.00	1.98	3.97	2.9	1.94	4.25	3.02	1.97
%O	22	18	16	20	17	15	22.54	19.43	17.01	23.29	20.45	17.91	-	-	-
%F	10	17	21	11	18	21	15.49	24.43	28.28	14.41	20.53	26.34	-	-	-
C/N	15.99	20.67	30.50	16.25	20.67	31.00	13.93	17.71	26.57	13.34	17.75	25.85	12.70	17.31	25.83
C/O	2.91	3.44	3.81	3.42	3.65	4.13	2.57	2.74	3.10	2.27	2.52	2.80	-	-	-
N/F	0.40	0.18	0.10	0.36	0.17	0.10	0.27	0.12	0.07	0.28	0.14	0.07	-	-	-

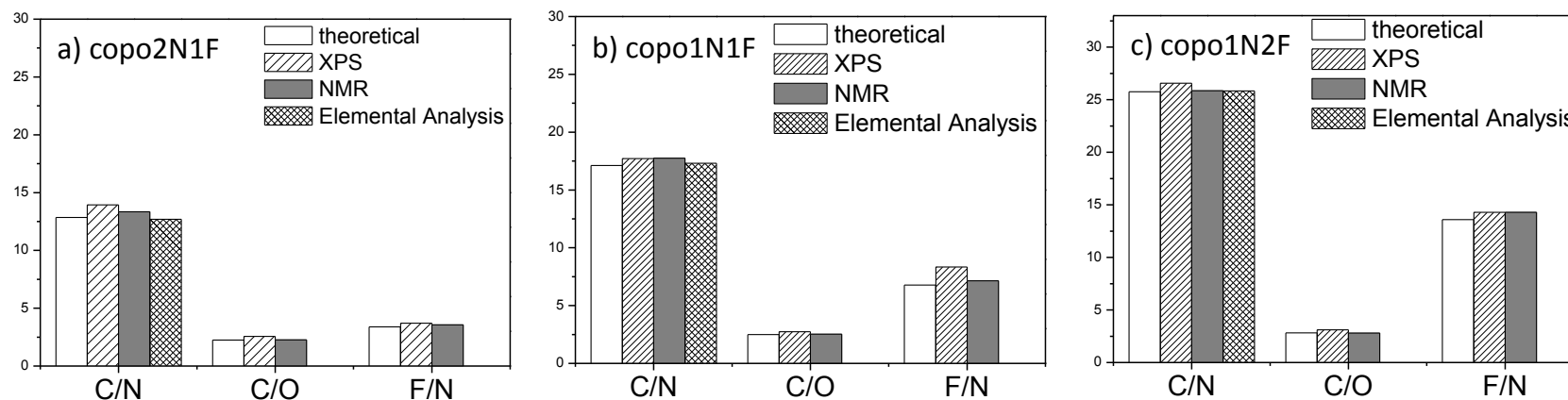


Figure 56. Comparison of atomic weight ratios obtained by different analyses

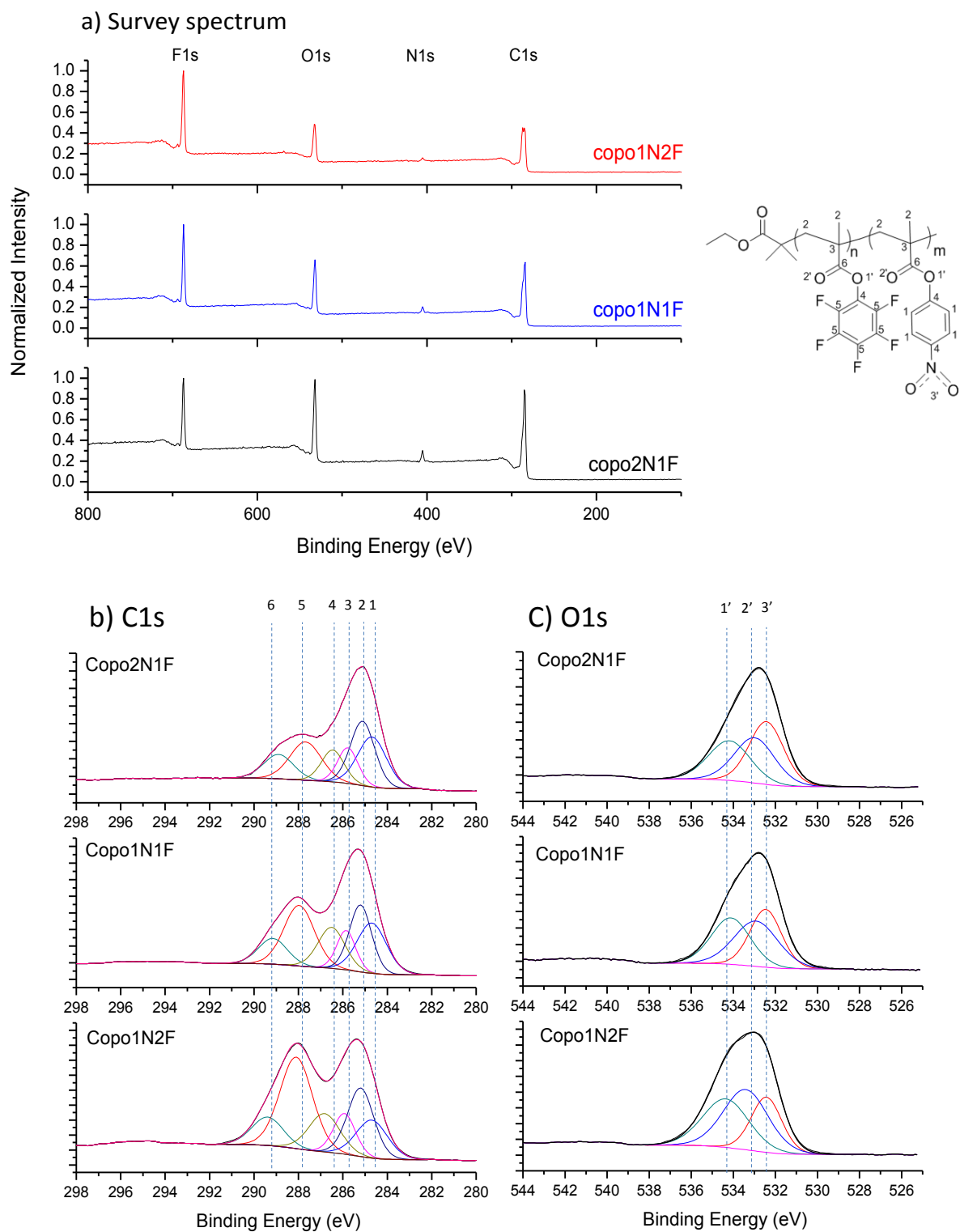


Figure 57. XPS results of PPFMA-*co*-PNPMA at different compositions. a) atomic survey spectrum and atoms' assignments, b) C1s core level spectra and its deconvolutions, c) O1s core level spectra and its deconvolutions

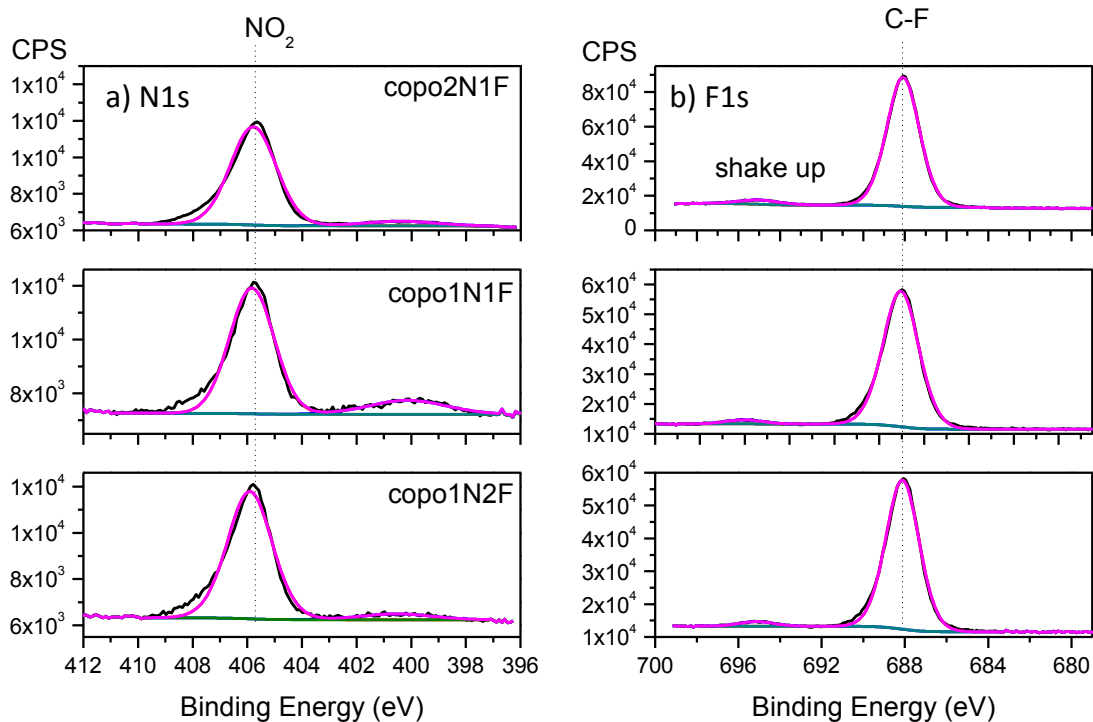


Figure 58. Deconvolution of a) N1s core level scans and b) F1s core level scans of copolymers at different composition.

Table 14. Details on fitting parameters for deconvolution of different atomic core levels,

Core level	Bond assignment	Copolymer								
		Copo1N2F			Copo1N1F			Copo2N1F		
		BE	FWHM	%	BE	FWHM	%	BE	FWHM	%
C1s	C=C	284.5	1.60	13.3	284.6	1.70	21.1	284.6	1.54	22.6
	C-C	285.0	1.34	20.0	285.0	1.27	21.1	285.0	1.29	24.5
	C*-CH ₃	285.8	1.20	13.3	285.6	1.01	10.5	285.7	1.07	11.3
	C-O, C-N	286.8	1.40	10.0	286.3	1.22	10.5	286.4	1.21	11.3
	C-F	287.9	1.69	33.4	287.7	1.65	26.3	287.6	1.67	18.9
	COO	289.2	1.65	10.0	288.9	1.56	10.5	288.8	1.58	11.3
O1s	NO ₂	532.3	1.72	25.4	532.4	1.75	32.3	532.3	1.87	38.24
	C=O	533.2	2.50	40.7	532.9	2.47	35.5	533.1	2.00	32.35
	C-O	534.2	2.52	33.9	534.1	2.18	32.2	534.3	2.25	29.41
N1s	NO ₂	405.9	2.14	100	405.8	1.90	100	405.8	1.92	100
F1s	C-F	688.2	2.02	96.7	688.1	1.85	96.1	688.1	1.88	96.9
	Shake up	695.3	2.02	3.3	695.0	2.27	3.9	695.1	1.91	3.1

High resolution core level scans during XPS measurement and their deconvolution into various contributions allows further confirmation on chemical structure of copolymers. Figure 57b and Figure 57c present C1s and O1s core level scans in accompanied with results of their deconvolution based on expected chemical structures. Table 14 summarizes details on fitting parameters employed for deconvolution of different atomic core levels obtained from XPS measurements.

For all three copolymers, their C1s core level experimental data can be decomposed into minimum six components. The first component is the C=C aromatic present in pendant groups, whose binding energy lies around 284.5-284.6 eV. On the other hand, aliphatic C-C bonds are characterized by their binding energy at 285.0 eV which has been taken as reference for calibrating the whole fitting process. The quaternary carbon of the methacrylate copolymers has higher binding energy (285.8 eV) than that of aliphatic carbon but lower than that of C-O and/or C-N bond, whose peak maximum is around 286.3 eV to 286.8 eV. More importantly, the presence of PFPMA in copolymer leads to an intense signal of C-F bond at around 287.6 eV to 287.9 eV. The last component taking part in C1s core level deconvolution is carbonyl COO which has the highest binding among all components, which is of 288.8 eV to 289.2 eV. Because the three copolymers differ by their composition between contributing comonomers, therefore, as presented in Table 14, percentages of components found in C1s core level scan also vary. In overall, it is seen that as the amount of NPMA increases, the contribution weights of carbon-to-carbon and C-O/C-N also raise accordingly but the percentage of C-F bonds decreases. The same trend is retained when O1s core level is taking into consideration where the amount of N-O contributor rises in copolymers with higher proportion of NPMA. O1s core level can be deconvoluted into three major components including the shared C=O, C-O of carbonyl groups and N-O specified for NPMA. It is to note that the FWHM of C=O and C-O here is quite large due to the fact that the carbonyl of PFPMA and that of NPMA have a slight difference in bonding as observed by FTIR, *i.e.* absorbance band of C=O and C-O in PFPMA and PNPMA do not show up at the same position. However, such derivations were neglected to simplify the fitting procedure for XPS data. Figure 58 presents N1s and F1s core level scans of three copolymers and their deconvolution. Each core level of all copolymers can be deconvoluted into only one species that characterize for nitro groups (around 405.8 eV) in case of N1s and C-F bond (around 688.2 eV) in case of F1s.

From XPS results, it is evident that chemical structure of each copolymer is well corresponding to that expected from other analyses.

2.4.4. Thermal properties of copolymers

Thermal properties of copolymers, especially random copolymers, are one type of indicators representing synergic contribution of its components. Except for its interest in polymer post-modification, PFPMA has been copolymerized with other comonomer specifically to improve thermal properties of the counterpart homopolymer. For example, addition of PFPMA as comonomer during free radical polymerization of PMMA can not only enhance glass transition temperature [322] but also help increase decomposition temperature and induce the transmittance properties of PMMA [323].

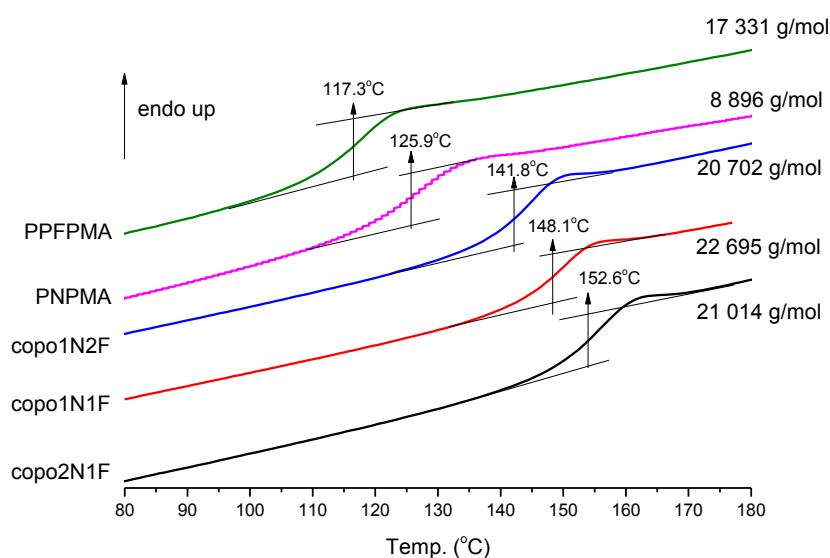


Figure 59. T_g determination of PFPMA, PNPMA and copolymers at different composition

Figure 59 presents DSC graphs of PFPMA, PNPMA and three copolymers obtained after 68 hours of polymerization. All polymers were synthesized using eBiB as initiator with reaction temperature of 60 °C. First of all, it is seen that regardless of composition, each polymer possesses only one glass transition temperature (T_g) in the studied temperature range, indicating that the microstructure of copolymers are relatively even along the backbone.

PNPMA ($DP_{theo} = 50$, $M_n \approx 8\,900\text{ g mol}^{-1}$) was determined to be 126 °C which is lower than 195 °C - T_g of PNPMA synthesized by free radical polymerization with $DP_{theo} = 200$ ($M_n \approx 41\,500\text{ g mol}^{-1}$) [324]. This deviation may be attributed to the difference in molecular weight of polymer due to the dependence of glass transition temperature on molecular weight according to Fox-Flory equation [325]. On the other hand, the value of T_g of PFPMA obtained herein is less deviated from that reported by free radical polymerization, which ranges between 90 °C [323] and around 125 °C [322].

The Fox equation is a mathematic equation that can be used to predict the glass transition temperature of mixture of polymer as a blend or as copolymers. The Fox equation states that:

$$\frac{1}{T_g} = \frac{w_1}{T_{g,1}} + \frac{w_2}{T_{g,2}} = \frac{n_1 \times M_1 \times T_{g,2} + n_2 \times M_2 \times T_{g,1}}{(n_1 \times M_1 + n_2 \times M_2) \times T_{g,1} \times T_{g,2}}$$

where T_g and $T_{g,i}$ are the glass transition temperature of the copolymer and of the component i , and w_i is the mass fraction of component i .

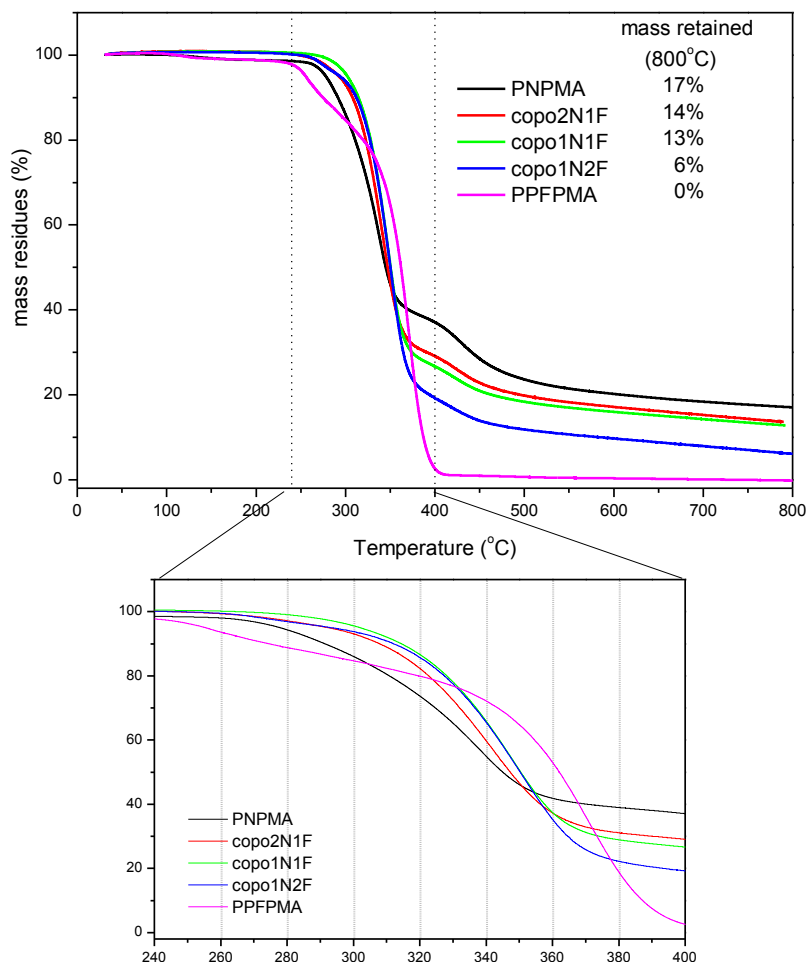


Figure 60. TGA profiles of PPFPMA, PNPMA and copolymers at different composition and their mass residues retained at 800 °C with a zoom-in section specified the change in thermal properties of different polymers.

If the Fox equation is applicable to copolymer of NPMA and PFPMA, glass transition temperatures of three obtained copolymers should be 119 °C, 121 °C and 122 °C for copo1N2F, copo1N1F and copo2N1F, respectively. Unfortunately, experiment data presented herein does not follow this prediction. Copolymer of NPMA and PFPMA shows much higher T_g compared to its homopolymer counterparts, *i.e.* T_g of copo1N2F is 142 °C, that of copo1N1F is 148 °C and copo2N1F has the highest T_g of 153 °C. This out-of-expectation phenomenon can be explained by the fact that PNPMA herein has low molecular weight and lower T_g compared to PNPMA of higher molecular weight. Thus, the studied homopolymer may have not reached the critical value in size above which T_g is no longer molecular weight

dependent [326]. However, further in-deep study focusing on thermal properties of PNPMA is needed to confirm this hypothesis.

Thermal stability of homopolymers and copolymers has been examined by TGA under argon as presented in Figure 60. Firstly, it is seen that the two homopolymers exhibit different thermal stability. For the case of PNPMA, the polymer possesses two major degradation temperatures at $T_{d, \max} = 336 \text{ }^\circ\text{C}$ (~60% loss in mass) and at $T_{d, \max} = 431 \text{ }^\circ\text{C}$ (~80% loss in mass). On the other hand, PFPMA has its first degradation zone at $T_{d, \max} = 257 \text{ }^\circ\text{C}$ (~20% loss in mass) and the second degradation is around $T_{d, \max} = 368 \text{ }^\circ\text{C}$ (complete degradation – 100% loss in mass). It is noteworthy that at $800 \text{ }^\circ\text{C}$, while PFPMA was completely decomposed, PNPMA retained 17% of initial mass.

Owing to the presence of both PFPMA and NPMA monomer units, degradation temperature of copolymers varied according to composition. It is seen that the higher the content of PFPMA, the higher the degradation temperature as expected. Indeed, copo2N1F has $T_{d, \max}$ of $343 \text{ }^\circ\text{C}$, copo1N1F has $T_{d, \max}$ of $348 \text{ }^\circ\text{C}$ and copo1N2F has the highest $T_{d, \max}$ of $350 \text{ }^\circ\text{C}$. In contrast, as the content of PFPMA increases, the mass retained at $800 \text{ }^\circ\text{C}$ decreases. These observations can be explained by the different thermal characteristics of two homopolymers as discussed before. It is noted that the PNPMA studied by TGA has $DP_{\text{theo}} = 100$, which is higher than that studied by TGA. The change in thermal stability when copolymer has higher composition of PFPMA is possibly due to the increase in amount of C-F bond, which has higher dissociation energy compared to C-H, C-N or C-O bonds.

2.4.5. Conclusion

In conclusion, copolymerization of NPMA and PFPMA *via* Cu(0)-mediated RDRP was successfully with high to very high comonomer conversion. Chemical composition and characteristics of each copolymer has been analyzed using several techniques including NMR, FTIR, SEC, elemental analysis, XPS, TGA and DSC. All of obtained results provide a great agreement on chemical composition where it is found that molar ratio between comonomers in final product is very close to that in feed, indicating good compatibility between NPMA and PFPMA. In addition, three copolymers obtained after 68 hours of reaction exhibited high glass transition temperature ($T_g > 140 \text{ }^\circ\text{C}$) and relatively good thermal stability. However, the control over polymerization process is remained questionable as SEC results obtained from two different solvent systems (THF/TEA *vs* DMF/LiBr) indicated two extreme phenomena.

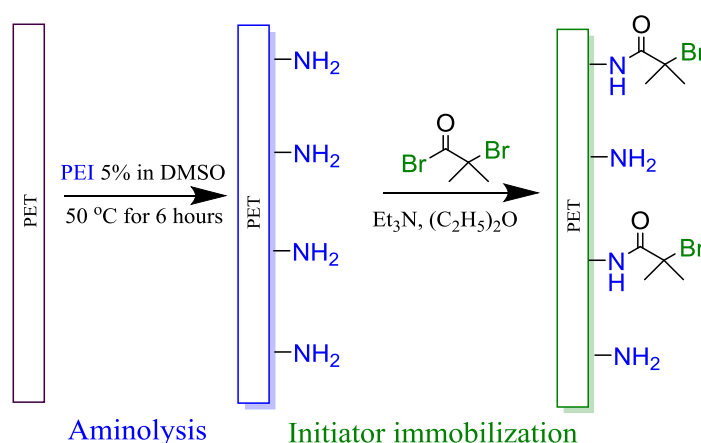
2.5. Conclusion

From three individual studies discussed in this chapter, Cu(0)-mediated RDRP presents to be a good candidate for synthesis of polymers containing reactive pendant groups like PFPMA or NPMA. Both homopolymerization and copolymerization process of these two active esters resulted in high monomer conversions, yet it seems that Cu(0)-mediated RDRP requires careful selection and case-study to achieve control properties of a RDRP process. Among three polymerization studies, only PFPMA has been investigated in depth to finally acquire optimal controlled conditions with final PFPMA of narrow dispersity. Despite of its pickiness, once selection of polymerization catalyst is optimal, Cu(0)-mediated RDRP proceeds in a sturdy manner even at high expected degree of polymerization. Nonetheless, this technique is a promising to apply for grafting from polymerization process due to the ease to handle, its robustness and versatility, its low catalyst requirement and its high tolerance against air/oxygen. Therefore, surface-initiated Cu(0)-mediated RDRP of PFPMA, NPMA and copolymerization of two have been studied and will be discussed in the next chapter.

Chapter 3. Surface-initiated polymerization of active esters

3.1. Immobilization of initiator onto PET films

In order to anchor initiator on PET substrate for later step of grafting polymer, activation of PET is needed to introduce reactive groups like hydroxyls or amines. Among various choices as discussed in section 1.2.2, PEI presents to be the most practical one because it allows immobilizing significant amount of amino groups onto surface without either the need of heavy instruments as for physical treatment or degradation as with the use of smaller diamines. Furthermore, in our lab, the application of PEI has led to successful studies on PET-initiated polymerization of LAMA [94] and 4VP [97]. Thus, aminolysis of PET by PEI was chosen for this dissertation. Among the two studies aforementioned, the use of DMSO was demonstrated to provide a denser network of amines compared to methanol, which in turn would result in a higher density of initiator, suggesting the probability to grow brush-like polymer from surface. The process of PET aminolysis and initiator immobilization is as given in Scheme 15.



Scheme 15. Procedure to immobilize initiator on PET films

Herein, aminolysis was carried out by immersing PET film of 1 cm x 2 cm in solution of 5% w/w of PEI in DMSO at 50 °C during 6 hours.

The immobilization of initiator was done with the initiator precursor α -bromoisobutyryl bromide that resembles eBiB. It is to recall that eBiB was proven in previous chapter to result in less controlled (co)polymerization of PFPMA and NPMA. However, the better initiator MBPA was not chosen to study herein because its corresponding chloride precursor (α -Bromophenylacetyl chloride) is only available with technical grade of purity (80%) while the acetic acid derivative (α -bromophenylacetic acid) has lower performance in nucleophilic substitution with amines. Initiator was anchored to PET surface by reaction between free primary amines of grafted PEI and α -bromoisobutyryl bromide as illustrated in Scheme 15.

To ensure the success of surface modification, after each treatment, several surface analyses have been performed to determine qualitatively and quantitatively the characteristics of modified-PET.

Surface modification results in an enormous change in chemical properties of extreme outer layer of materials, hence, the static water contact angle (WCA) has been used as the first and fastest method to ensure the success of a modification. As seen in Figure 61, pristine PET film became more hydrophilic after PEI treatment due to the appearance of amino groups on the surface, which subsequently led to the drop in WCA from $82^\circ \pm 2$ to $55^\circ \pm 5$. After amidation of amines and initiator precursors, the WCA of PET-Br films enhances to $67^\circ \pm 3$, suggesting the presence of methyl groups and bromine atoms, which are less polar compared to amino groups.

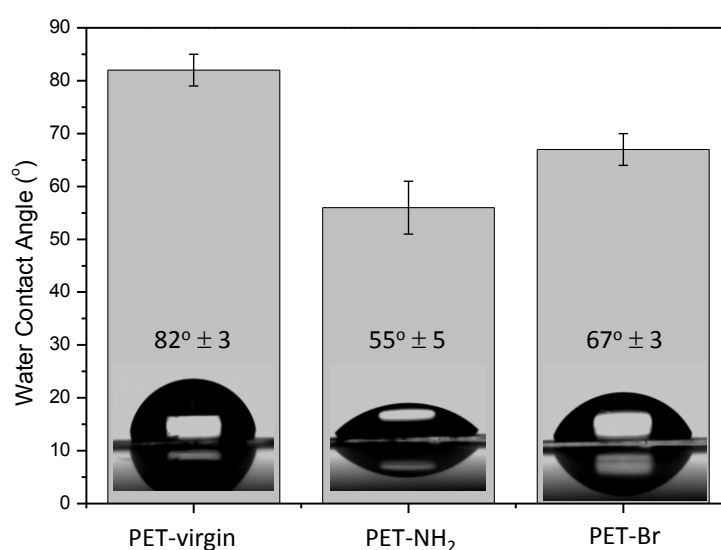


Figure 61. WCA of static water deposition on PET-virgin, PET-NH₂ and PET-Br

The amount of grafted initiator on a surface plays an important role in surface-initiated polymerization as it can determine the nature and morphology of polymer chain in later step. Unfortunately, direct and rapid method to quantify bromine atoms is not available in literature. However, because certain amino groups of PET-NH₂ will react with initiator precursor, indirect quantification of grafted initiator could be estimated by taking the difference between amount of amino groups before and after initiator immobilization. Efficient quantification of amino groups on aminolyzed PET surface by colorimetric titration with Orange II dye has been studied in literature [327] and is adapted herein.

As shown in Figure 62, titration of amino functional group on pristine PET surface shows the absence of amino groups as a non-significant number of amino groups was recorded. After aminolysis, the amount of amino groups on PET-NH₂ surface was corresponding to 0.61 ± 0.04 NH₂ per nm², in good agreement with results reported previously by our group [97]. With anchoring initiator, the number of amino groups on surface was determined to be $0.32 \pm$

0.07 NH_2 per nm^2 , corresponding to a yield of 50%, thus 0.3 bromine functions per nm^2 . It is expected that the PET-Br generates the same amount of polymer chains on PET surface, *i.e.* density of tethered polymer is expected to be 0.3 chains per nm^2 . This grafting density corresponds to chains in moderate to high density brush regime as reported in literature [328, 329] suggesting a complete coverage of the active polymer.

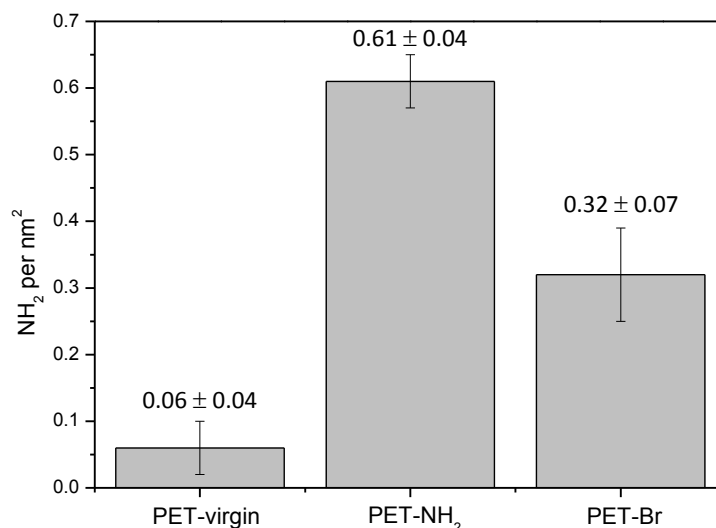


Figure 62. Quantification of amino groups on PET-virgin, PET- NH_2 and PET-Br

ATR FTIR spectra of PET- NH_2 and PET-Br surfaces did not show any difference to that of untreated PET films. It is to note that ATR FTIR intensity depends greatly on the penetration depth of evanescent wave into sample surface, which is about one micron for Ge crystal used in this project. The impossibility to “see” grafted PEI and BiB may be attributed to the very thin layer of deposited PEI and the “monolayer” of initiator.

In contrast to ATR FTIR, XPS is a technique that provides meaningful information of extreme surface with a penetration depth of around 10 nm. Figure 63 and Table 15 show XPS survey spectra and atomic percentage of different atoms present on each surface, respectively. Firstly, survey spectra presented Figure 63 shows that pristine PET surface presents basic peaks of C1s (284 eV) and O1s (531 eV), while surface after PEI aminolysis shows additional signal of N1s at 399 eV with atomic percentage contribution of 7%. The success of aminolysis of PET surface PEI is also confirmed by the appearance of a new contribution which corresponds to an amide N-C=O bond at 287.9 eV in C1s core level and at 530.7 eV in O1s core level of PET- NH_2 film, indicating the strong covalent attachment of the PEI to the support. Fitting results of core level of N1s region of PET- NH_2 surface suggests the dominance of C-N bonds, corresponding to 69% of total recorded signals, while the charge built up from amines (NH^+) takes 31 %. Initiator grafting was confirmed as the Br3d and Br3p signals appeared concomitantly with a slight decrease of N1s signal intensity (Figure 63c).

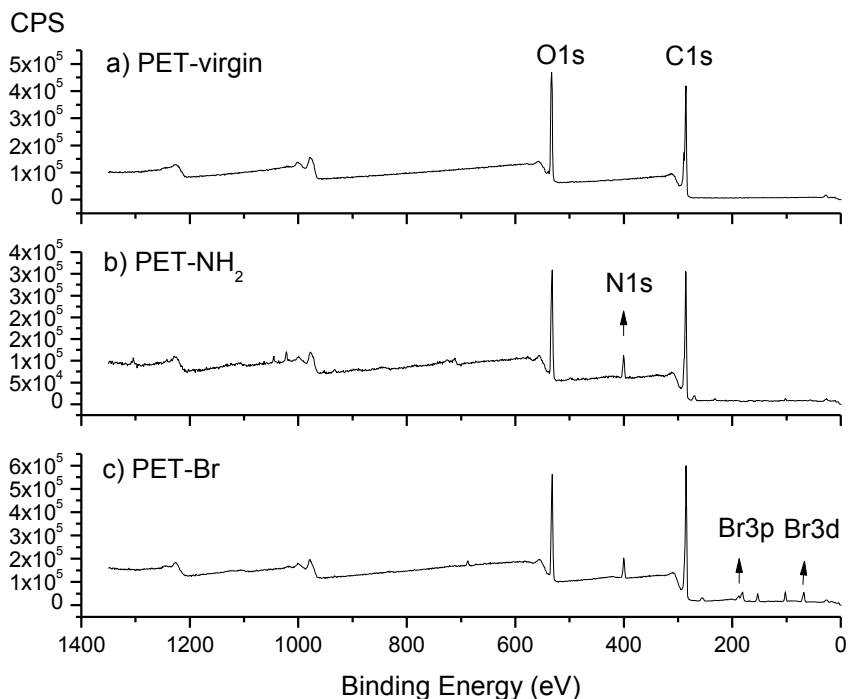


Figure 63. XPS survey spectra of a) PET-virgin, b) PET-NH₂ and c) PET-Br

Table 15. Atomic percentage of different atoms present on PET-virgin, PET-NH₂ and PET-Br films

Entry	Sample type	%C1s	%O1s	%N1s	%Br3d
1	PET-virgin	77	23		
2	PET-NH ₂	68	25	7	
3	PET-Br	70	21	6	3

Figure 64, Figure 65 and Table 16 present core level scans, their deconvolutions as well as fitting parameters. Additionally, for N1s core level of PET-Br film (Figure 65c), the fitting results showed a modification in the ratio between C-N/NH⁺ due to the reaction between amines and initiator precursor. The use of PEI to graft amino groups on PET surface resulted in a higher percentage of initiator on surface, proved by a higher amount of Br3d recorded by XPS, which was 2.5% in this research compared to 1% in a previous report [94]. Figure 64c presents the fitting results of high resolution Br3d core level with 4 major contributors of neutral and charge bromine atoms. It is seen in Figure 64d that the covalently bonded initiator is stable on the surface, but a partial amount of bromine is getting charged during measurement indicated by the increase in intensity of shoulder peak at 67 eV. On the other hand, the analysis of N1s and Br3d ratios with regard to C1s and O1s indicated a very thin layer of PEI and initiator grafted onto surface. This observation was in correspondence with ATR FTIR data where almost no difference among PET-virgin, PET-NH₂ and PET-Br films spectra was observed.

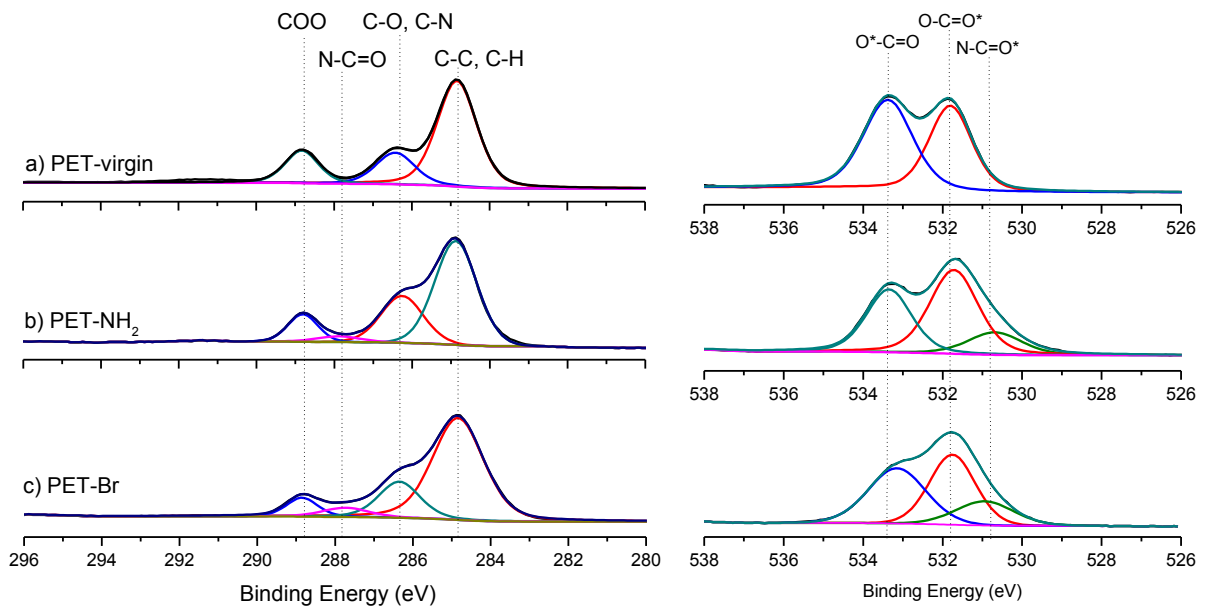


Figure 64. C1s and O1s deconvolutions of a) PET-virgin, b) PET-NH₂ and c) PET-Br

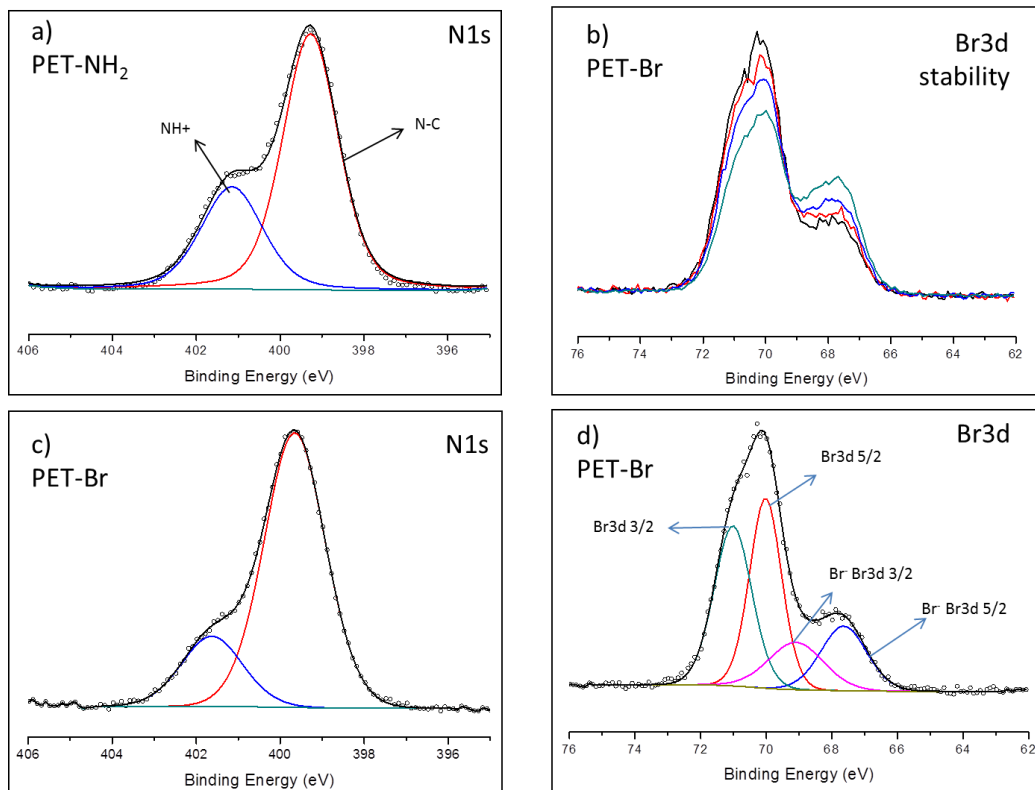


Figure 65. N1s and Br3d core level fitting results for PET-NH₂ and PET-Br surfaces.

Table 16. Fitting parameters for deconvolution of different core levels of PET-virgin, PET-NH₂ and PET-Br

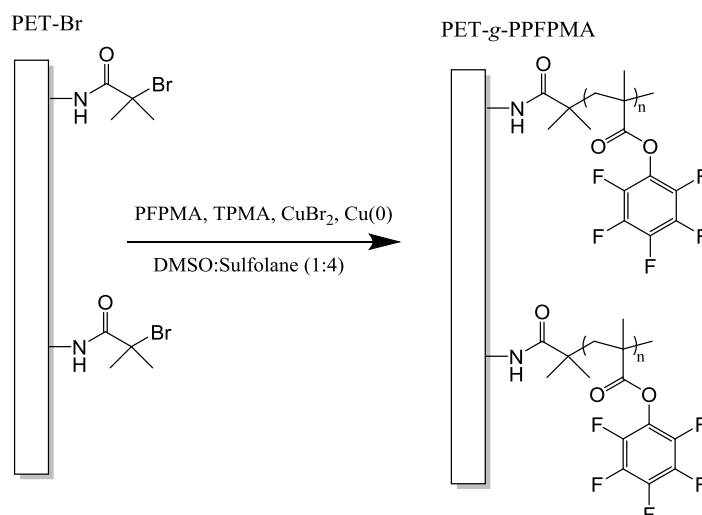
Core level and Bonding type		Surface								
		PET-virgin			PET-NH ₂			PET-Br		
		BE	FWHM	%	BE	FWHM	%	BE	FWHM	%
C1s	C-C	284.9	1.19	64.5	284.9	1.27	59.1	284.8	1.55	67.5
	C-O, C-N	286.5	1.17	18.7	286.3	1.26	26.4	286.4	1.25	19.2
	COO	288.9	1.01	16.8	288.8	0.89	10.7	288.9	0.94	7.7
	N-C=O	0	0	0	287.9	1.45	2.8	287.7	1.42	5.6
O1s	C=O	532.0	1.27	50	531.7	1.44	50.1	531.8	1.35	41.2
	C-O	533.6	1.46	50	533.3	1.30	35.0	533.2	1.70	40.8
	N-C=O	0	0	0	530.7	1.60	14.9	531.0	1.72	18.0
N1s	N-C	0	0	0	399.3	1.56	69.0	399.7	1.72	79.6
	NH ⁺	0	0	0	401.2	1.74	31.0	401.6	1.72	20.4
Br3d	Br3d 3/2	0	0	0	0	0	0	71.0	1.35	34.1
	Br3d 5/2	0	0	0	0	0	0	70.0	1.15	34.40
	Br-3d 3/2	0	0	0	0	0	0	69.1	1.97	14.7
	Br-3d 5/2	0	0	0	0	0	0	67.6	1.65	17.8

Overall, these above analyses and characterizations confirm that the aminolysis of PET film by PEI and the immobilization of eBiB-like initiator have been successfully achieved. The density of initiator on surface was determined to be 0.3 bromine functions per nm², which should be sufficient to carry out polymerization on such surface with expectation of dense polymer brushes.

3.2. PET-initiated Cu(0)-mediated RDRP of PFPMA

Surface-initiated Cu(0)-mediated radical polymerization of PFPMA from PET-Br surface was performed in DMSO:sulfolane (1:4 in volume) mixture with molar feed ratio among reactants of [PFPMA]₀/ [TPMA]₀/ [CuBr₂]₀ = 612/4/1 for large batch (12 films in a flask as illustrated in Figure 66) and [PFPMA]₀/ [TPMA]₀/ [CuBr₂]₀ = 944/4/1 for small batch (2 films). Initial monomer concentration was 0.75 mol.L⁻¹ and 5-cm Cu(0) wire was used for each 2 films in both setups.

It is important to address that this surface-initiated polymerization was done as a stand-alone project and studied in parallel with Cu(0)-mediated RDRP of PFPMA in solution. However, the major results presented herein were obtained before the success of control optimization; hence it is of our awareness that the catalysts and solvent mixture used were not the optimal conditions. Nonetheless, the amount of grafted initiator (0.3 groups per nm²) is very small compared to the amount of monomer, thus, one might not expect a good control in this surface-initiated polymerization system.



Scheme 16. Surface-initiated Cu(0)-mediated RDRP of PFPMA from PET-Br films

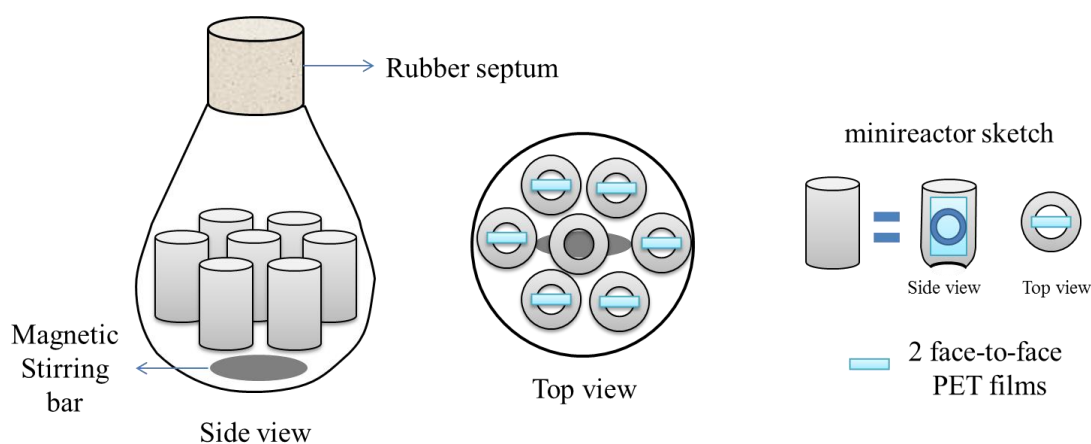


Figure 66. Illustration of large batch polymerization tools and setup

3.2.1. Water contact angle

As predicted, the presence of nonpolar moieties on extreme surface of PET after polymerization has led to an increase in water contact angle from $67^\circ \pm 3$ of PET-Br surface to $110^\circ \pm 1$ (1-day polymerization), reaching $127^\circ \pm 1$ (3-day polymerization), higher than those observed in literature from SI-RAFT polymerization [319]. When a lower degree of polymerization is expected (in the case of large batch condition), the contact angle still reaches $90^\circ \pm 1$ after 24 hours, which is the minimum threshold between hydrophilic and hydrophobic surface classification.

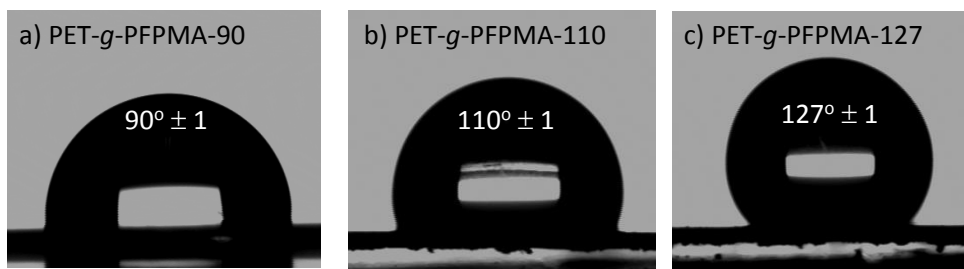


Figure 67. WCA of PET-g-PPFMA at different polymerization conditions

As the large batch polymerization allows the preparation of 12 films at the same time, surface film homogeneity has to be investigated.

First of all, the average WCA of 12 films in a large batch is $92^\circ \pm 3$, indicating a quite homogeneous result among all samples. Furthermore, a study on water contact angle of PET-*virgin* and PET-*g*-PPFMA-90 films by micro-goniometer was achieved by depositing 231 water droplets of 300-picoliter on the 1 cm x 2 cm film (Figure 68).

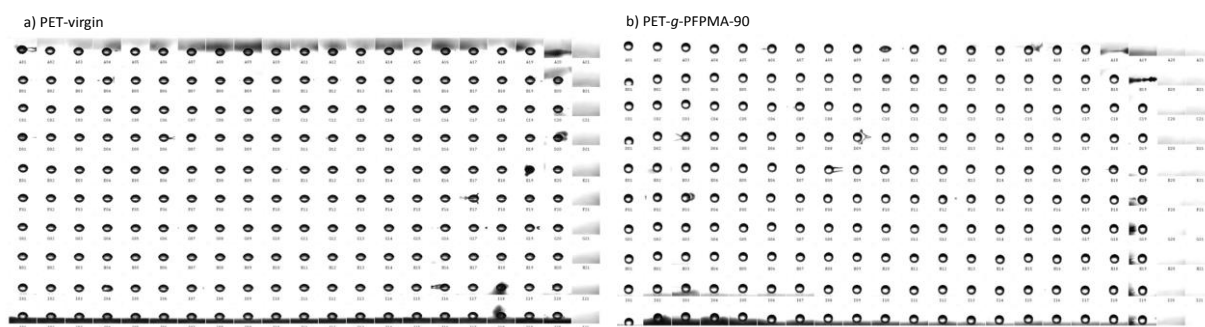


Figure 68. Photos of 231 drops deposited on a) PET-*virgin* and b) PET-*g*-PPFMA-90

The few degree difference in results between conventional contact angle and micro-goniometer is due to the huge difference not only in volume of droplet but also in the evaporation rate. Figure 69 presents the photos of 56 droplets deposited in the centre region of PET-*virgin* and PET-*g*-PPFMA-90 films. The PET-*g*-PPFMA-90 surface has a comparable homogeneity with the non-modified surface. Furthermore, water contact angles of all drops on surface presents to be similar with a difference of 2-3 degree in WCA. This result indicates that the surface-modification process as well as the surface-initiated polymerization has proceeded in a uniform manner and the polymer of PFPMA has completely covered the supporting surface.

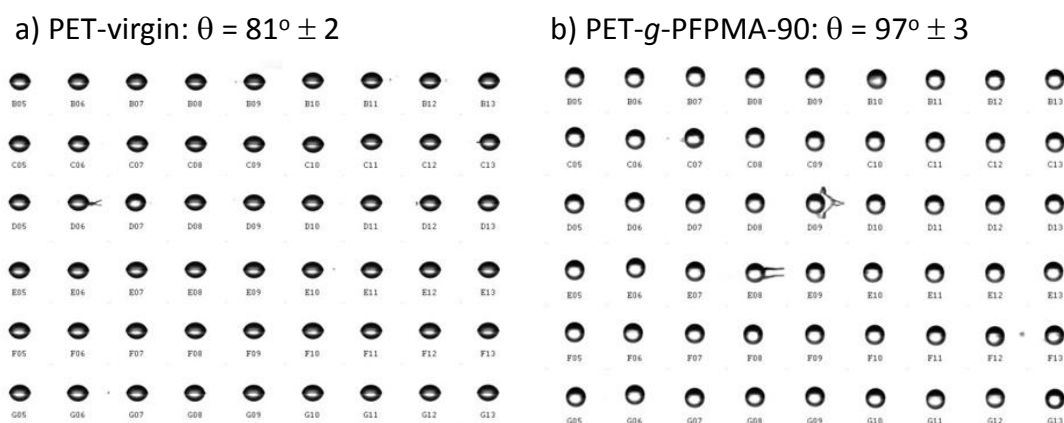


Figure 69. Images of 54 water drops deposited on the middle region of a) PET-virgin and b) PET-*g*-PPFMA-90

3.2.2. ATR FTIR

The graft of PPFMA from PET supporting surface resulted in a huge obvious change in ATR FTIR spectrum (Figure 70) shown by the distinguished appearance of the peak at 995 cm^{-1} , correlates to the C-F bond.

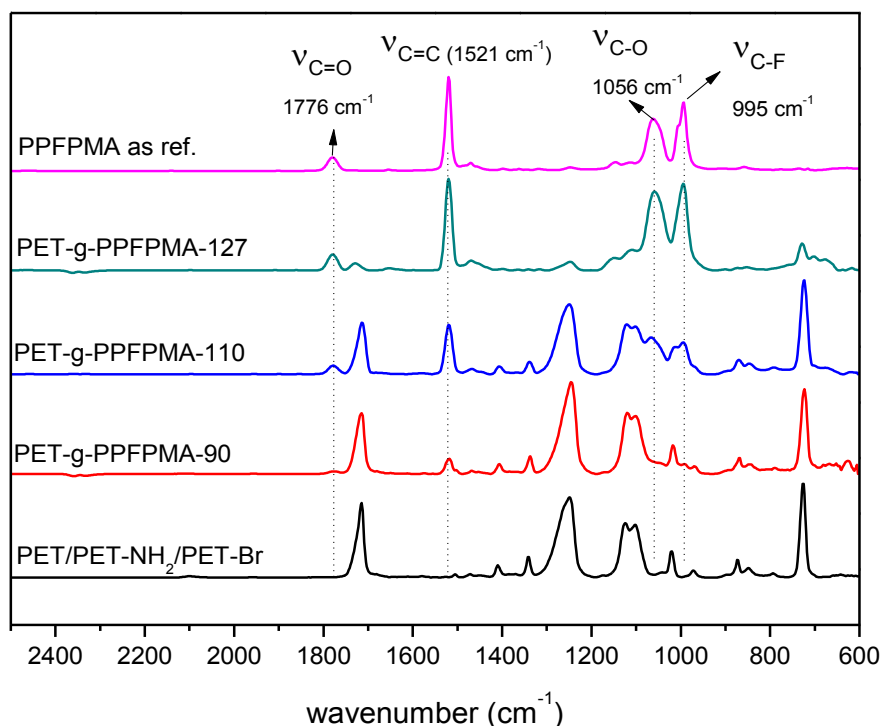


Figure 70. ATR FTIR spectra of PET-*g*-PPFPMA obtained by different polymerization conditions

Furthermore, the high conjugation of PPFMA was observed with peaks corresponding to C-O, C=C and C=O of PPFMA shifted to higher wavenumbers (at 1056 cm^{-1} , 1521 cm^{-1} and

1776 cm⁻¹, respectively) compared to that originated from PET and were close to those reported previously [319, 321].

It is seen that the induction in hydrophobicity is associated with the increase in intensity of PFPMA recorded by FTIR. While at lower contact angle, the intensity from PET is more intense than that of active polymers, FTIR spectrum shows the dominance in signals originated from PFPMA at contact angle of 127° suggesting that within the penetration depth of infrared light, which ranges between several hundred nanometres, the quantity of active polymer is much greater than that of supporting surface. Last but not least, 12 films obtained in the same large batch presents to have identical ATR FTIR spectra; hence, the conditions and setup for large batch polymerization enable the preparation of several films at the same time. This possibility is important to obtain the same functional surfaces for other analyses and biological tests.

3.2.3. XPS analysis

As the result of surface-initiated Cu(0)-mediated radical polymerization of PFPMA from PET-Br films, XPS survey spectra of all PET-*g*-PPFPMA surface show an intense signal of F1s (Figure 71), albeit WCA of PET-*g*-PPFPMA varies, three surfaces show close values in atomic percentage of C1s, O1s and F1s compared to corresponding values by XPS of PFPMA in powder (Table 17). This indicates that even at low contact angle (PET-*g*-PPFPMA-90 films), the thickness of PFPMA grafted layer is at least of the same magnitude as the penetration depth of X-ray used in this technique, *i.e.* around 10 nm.

These results in number atomic percentage confirmed that the vast majority of signals recorded originated from grafted PFPMA moieties. Therefore, the negligible amounts of PET signals were not considered during the deconvolution of core level scans for PET-*g*-PPFPMA surfaces as shown in Figure 72.

Table 17. Atomic percentages of atoms present on PET surface at different modification

Entry	Sample type	%C1s	%O1s	%N1s	%Br3d	%F1s
1	PET- <i>g</i> -PPFPMA-90	61	12	1	0	26
2	PET- <i>g</i> -PPFPMA-110	59	12	1	0	28
3	PET- <i>g</i> -PPFPMA-127	60	12	0	0	28
4	PPFPMA _{bulk}	58.8	11.8	0	0	29.4

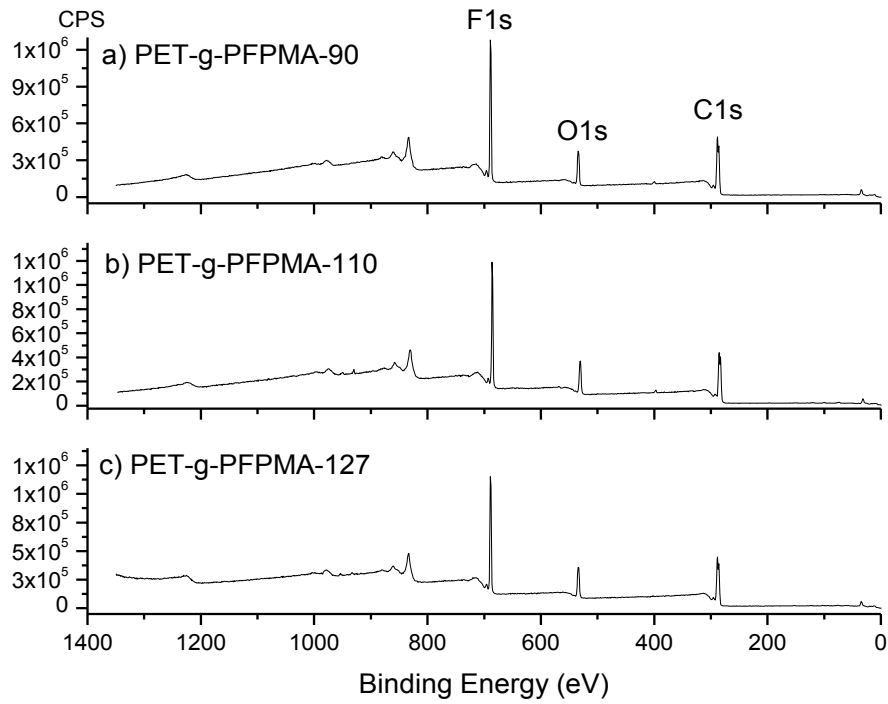


Figure 71. Survey spectra of PET grafted with PPFMA at different polymerization conditions

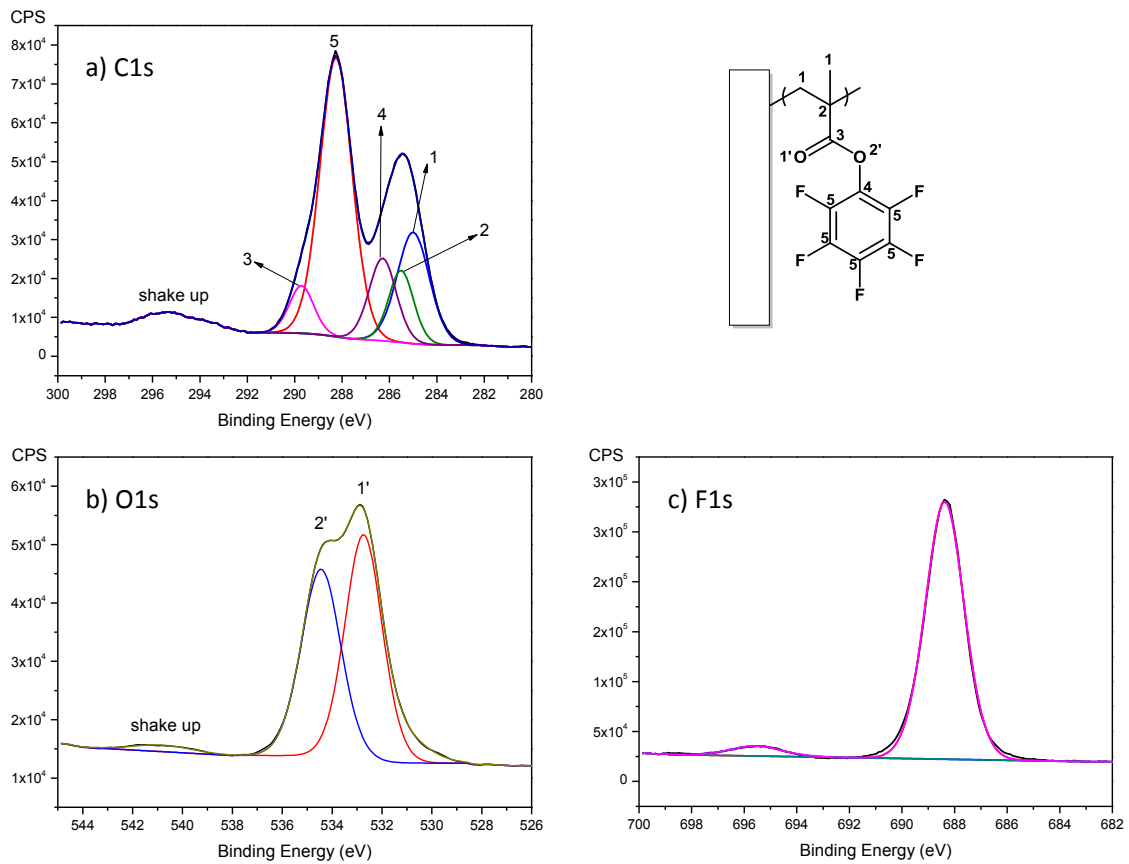


Figure 72. Deconvolution of a) C1s, b) O1s and c) F1s of PET-g-PPFMA

Table 18. Fitting parameters for deconvolution of PET-g-PPFPMA

Core level	Bonding	PET-g-PPFPMA-90			PET-g-PPFPMA-110			PET-g-PPFPMA-127		
		BE	FWHM	%	BE	FWHM	%	BE	FWHM	%
C1s	C-C	285.0	1.60	19.7	285.0	1.59	19.5	285.0	1.60	19.3
	C-O, C-N	286.2	1.23	12.3	286.2	1.24	12.2	286.3	1.35	12.1
	COO	289.7	1.05	4.6	289.7	1.17	4.9	289.7	1.21	6.2
	C*-CH ₃	285.4	1.20	9.9	285.4	1.22	9.8	285.5	1.23	9.6
	C-F	288.2	1.64	49.3	288.2	1.66	48.7	288.3	1.60	48.2
	Shake up	294.8	2.70	4.15	295.26	3.18	5.0	294.9	2.83	4.6
O1s	C=O	532.7	1.71	50.2	532.7	1.80	51.8	532.6	1.70	52.4
	C-O	534.4	1.91	49.8	534.4	1.83	40.3	534.3	1.84	47.6
F1s	C-F	688.3	1.71	96.2	688.4	1.76	93.6	688.2	1.73	95.1
	Shake up	695.2	1.95	3.8	695.7	3.03	6.4	695.6	2.27	4.9

As seen in Figure 72 and Table 18, the core level scan of C1s can be deconvoluted according to the chemical structure of PFPMA, which includes carbon atoms of: aliphatic carbons (285 eV), quaternary C*-CH₃ (285.4 eV), conjugated COO (289.7 eV), C=C-O (286.2 eV), C-F (288.1 eV) and π - π^* shake-up (295.5 eV). These assignments present a good agreement to those reported in literature [319, 321]. O1s core level profile could be deconvoluted into 2 major contributions of C=O at 532.6 eV and C-O at 534.3 eV. These values are approximately 1eV higher compared to carbonyl oxygen of PET, this is reasonable because ATR FTIR spectra (Figure 70) of PET-g-PPFPMA surfaces show that the carbonyl C-O and C=O of PFPMA are also shifted to higher wavenumber compared to that of PET, indicating the difference in chemical environment between carbonyl groups bonds of the supporting surface and the active ester polymer.

3.2.4. Surface topology by AFM and SEM

Surface topology and root-mean-square surface roughness (RMS) of PET-Virgin, PET-Br and PET-g-PPFPMA were then observed with AFM and SEM (Figure 73). The change in topology of PET films before and after surface initiated polymerization was remarkable. PET-Br surface appeared to be smooth as observed in SEM image (Figure 73A); besides, AFM (Figure 73a) indicated a RMS value of 6.4 nm. The surface roughness increased visually after polymerization, AFM and SEM images (Figure 73b and Figure 73B) show obvious topology changes of PET-g-PPFPMA-90 films compared to PET-Br films in particular with higher roughness (RMS of 6.4 nm and 33.9 nm before and after polymerization, respectively). With regard to surface topology, while AFM exhibited the appearance of islands on the surface, SEM provided a wider image, demonstrating a structural development. The change in topology was more pronounced in the case of PET-g-PPFPMA-110 and PET-g-PPFPMA-127 with RMS increased to 203 nm and 323 nm, respectively. On these surfaces, well-oriented chains of islands were also recognized from both AFM and SEM images.

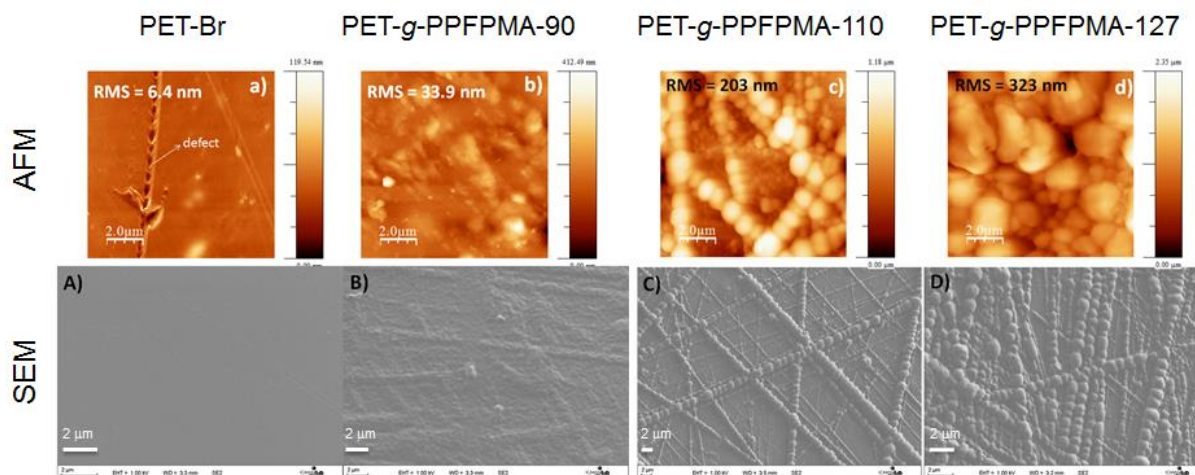


Figure 73. AFM and SEM of PET-g-PPFPMA at different polymerization conditions

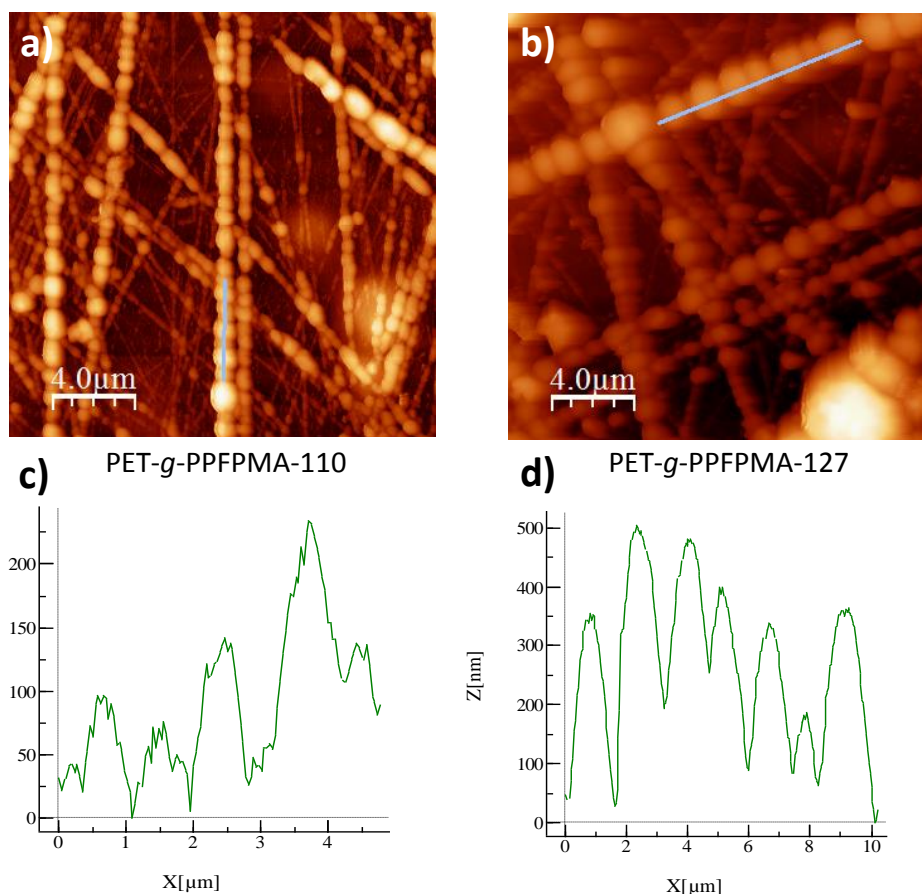


Figure 74. AFM images (top) and profiling of representative chain of islands (bottom) of a, c) PET-g-PPFPMA-110 surface; b, d) PET-g-PPFPMA-127 surface

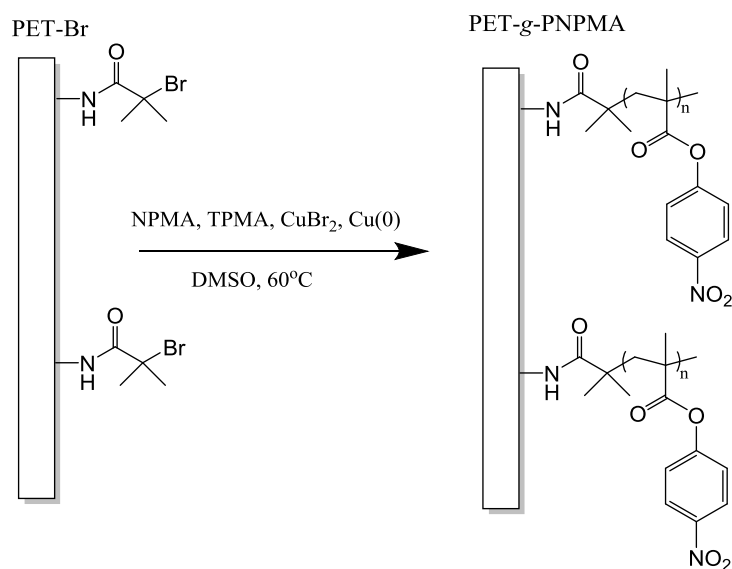
Profiling these chains (Figure 74) indicated that, on the same film, each island along the chain was of approximately the same size which increase with prolonged polymerization time; PET-g-PPFPMA-110 and PET-g-PPFPMA-127 surface had islands of approximately 1 micron and 1.8 micron in width respectively. On the other hand, XPS analyses attest the same chemical composition for the extreme surfaces of all three types of PET-g-PPFPMA, while the

wettability of the three surfaces varied. This phenomenon could be explained by the increase in surface roughness, which reinforces the hydrophobicity or hydrophilicity of a surface [330]. It is necessary to note that after 24 hours of Soxhlet extraction in THF, the same contact angle and identical AFM images were recorded, indicating the strong attachment of the polymer of PFPMA onto PET surface.

3.2.5. Conclusion

A sequential chemical modification process of PET surface has been proposed and proved to be effective. The process includes aminolysis of PET virgin surface, followed by initiator immobilisation and finally the surface-initiated Cu(0)-mediated polymerization of PFPMA. Each modification step was evaluated qualitatively and quantitatively by several analysis methods including water contact angle, titration with orange II dye, ATR FTIR and XPS. Firstly, the amount of tethered initiator on PET surface was determined indirectly to be 0.3 groups per nm², which is sufficient for growing brush polymer chains via “grafting from” polymerization. Cu(0)-mediated RDRP conditions could provide PFPMA polymerization from PET surface tethering eBiB-like initiator. By varying polymerization conditions and scales, PET-*g*-PPFPMA surfaces showed the change in surface roughness and topology as observed by AFM and SEM, which, in consequence, led to the change of surface wettability. Therefore, surface-initiated Cu(0)-mediated radical polymerization has been shown to be a good alternative for easy grafting of PFPMA polymer from PET surface.

3.3. PET-initiated Cu(0)-mediated RDRP of NPMA



Scheme 17. PET-Br initiated Cu(0)-mediated RDRP of NPMA

Following the same process as above described for PFPMA, surface initiated polymerization of NPMA by Cu(0)-mediated RDRP from PET-Br surfaces has been investigated as depicted in Scheme 17.

After polymerization, modified PET-Br films were analyzed by WCA. It increase from $67^\circ \pm 2$ (PET-Br films) to around $80^\circ \pm 1$, indicating enhancement in hydrophobicity likely due to the presence of grafted *p*-nitrophenyl groups on the surface, which was confirmed later on by ATR FTIR. As presented in Figure 75, PET-*g*-PNPMA films show some distinguished peaks. Even though not all PNPMA peaks were found in PET-*g*-PNPMA spectrum, some characteristic stretching vibrations of the reactive polymer were recorded including the carbonyl C=O at 1762 cm^{-1} , the N-O stretching vibration at 1523 cm^{-1} and the C-N band at 1209 cm^{-1} . Furthermore, the peak characterized for C-H out-of-plane scissoring vibration of PET at 725 cm^{-1} has been slightly shifted to 727 cm^{-1} due to its fusion with that of NPMA. Additionally, the intensity of this C-H vibration also became the most intense one in PET-*g*-PNPMA, which is not the case of PET. All these observations confirmed the surface-initiated polymerization of NPMA from PET-Br.

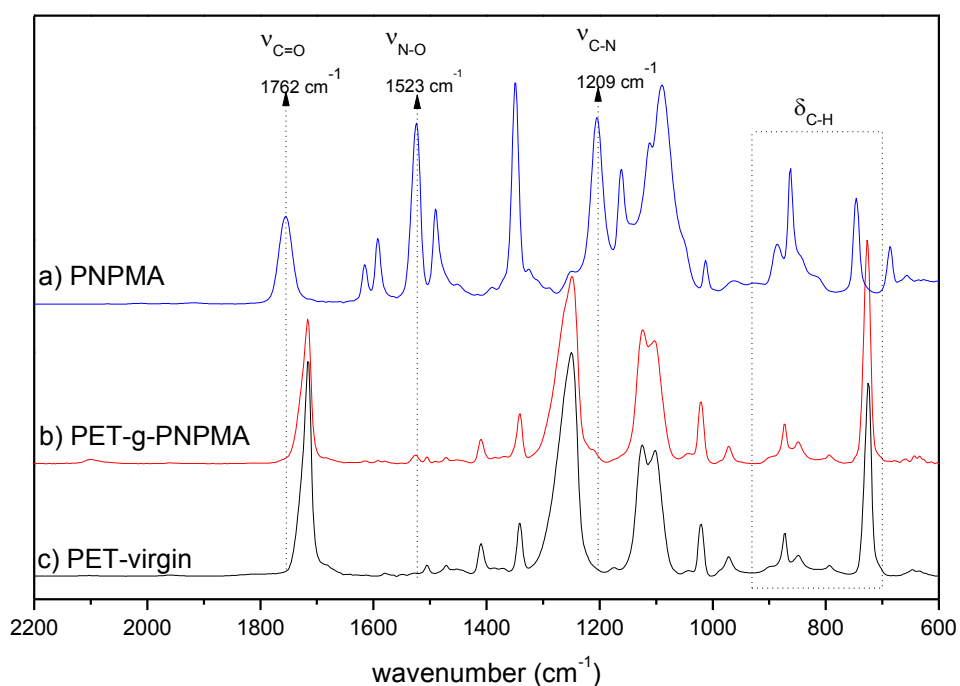


Figure 75. ATR FTIR of a) PNPMA, b) PET-*g*-PNPMA and c) PET-virgin

Furthermore, XPS analysis was carried out to investigate in details the chemical environment of PET-*g*-PNPMA films (Figure 76). As expected, survey spectrum of PET-*g*-PNPMA shows majority of signals coming from C1s with peak maximum at 286 eV (70.4%), N1s at around 400 eV (5.6%) and O1s at 534 eV (24%). These values are about 2-3% deviated from theoretical atomic percentages of each atom in NPMA: 67% for carbon, 27% for oxygen and 6% for nitrogen. Atomic ratios calculated from XPS results are O/N = 4.3 and C/N = 12.5, approaching those calculated from chemical structure of PNPMA: C/N = 11.2 and O/N = 4.5.

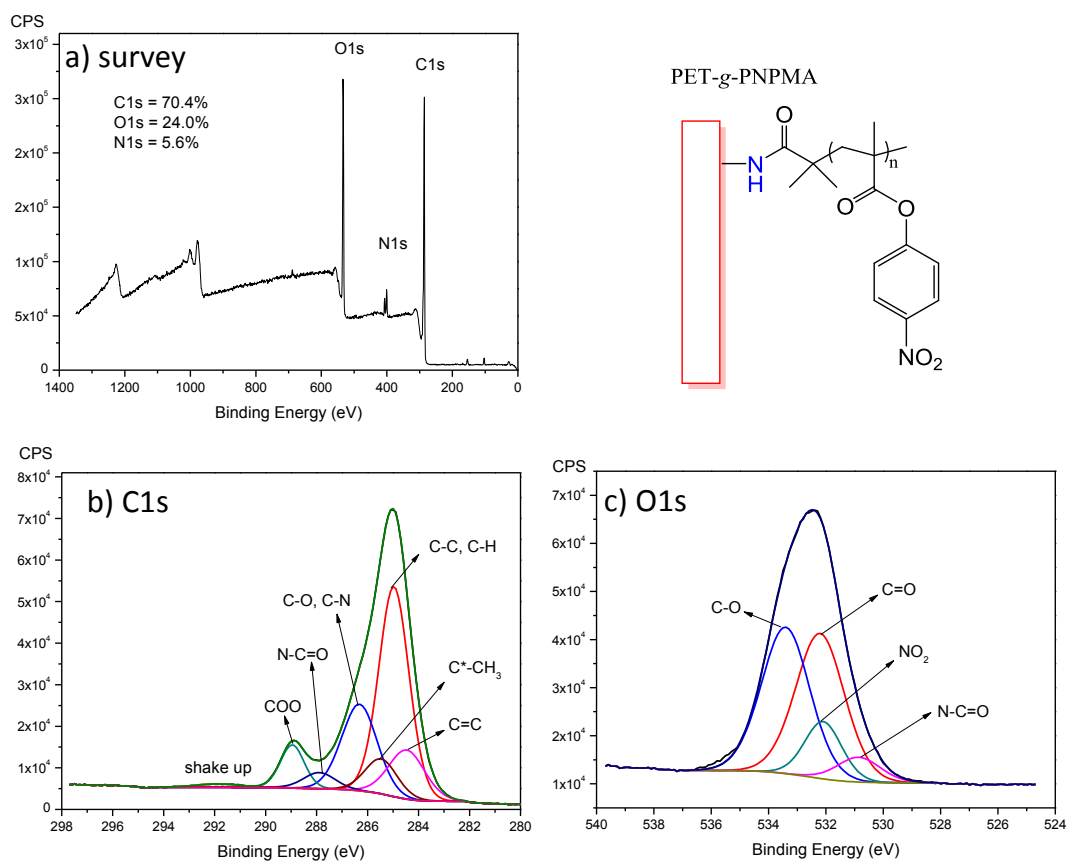


Figure 76. Chemical Structure XPS of PET-g-PPNPMA: a) survey scan, b) C1s scan and deconvolution, c) O1s scan and deconvolution

Two separated types of signals are recorded from N1s core level scan of PET-g-PPNPMA, at peak maxima of 399.8 eV and 405.9 eV attributed to binding energy of C-N bond and NO₂ (Figure 77). Taking the presence of C-N bonds into account, core level scans of C1s and O1s were deconvoluted as presented in Figure 76a and Figure 76b; summary of fitting parameters is listed in Table 18. Regarding C1s core level, the spectrum can be deconvoluted into six major contributions and a small fraction of π - π^* satellite (shake up) signals. All carbons involving in the chemical structure of PNPMA are present including aromatic carbon of pendant groups at around 284.5 eV, aliphatic C-C, C-H at around 285.0 eV of polymer backbone, the quaternary carbon C*-CH₃ at 285.5 eV, C-O/C-N at 286.3 eV while C=O present at 289.0 eV. Additionally, the contribution of carbon in N-C=O at 287.9 eV as discussed above helps getting the best fit during fitting process, indicating its appearance on the surface. On the other hand, O1s core level can be fractionated into four major contribution including oxygen of an amide (N-C=O) at 530.9 eV, oxygen of nitro groups at 532.1 eV and oxygen of carbonyl groups at 532.2 eV (C=O) and 533.4 eV (C-O). It is insisted that the contribution of amide oxygen is necessary to get the best fit at lower binding energy, which confirms the presence of such bond in the 10-12 nm depth of PET-g-PPNPMA surface. From results obtained herein, the first hypothesis seems to be more reasonable as the signal of C-N bond is much more intense (69.6%) than that of NO₂ (30.4%).

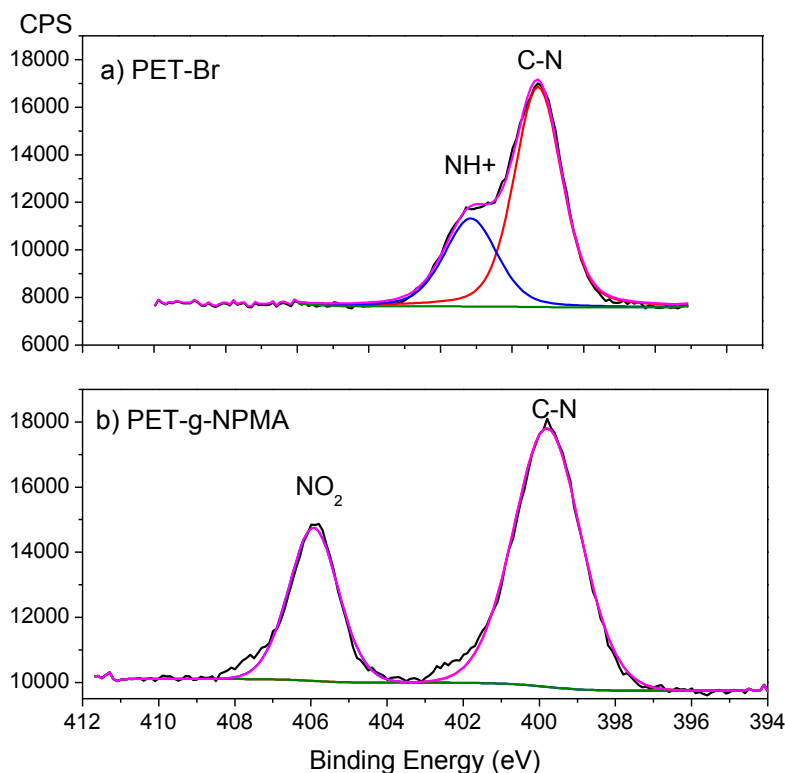


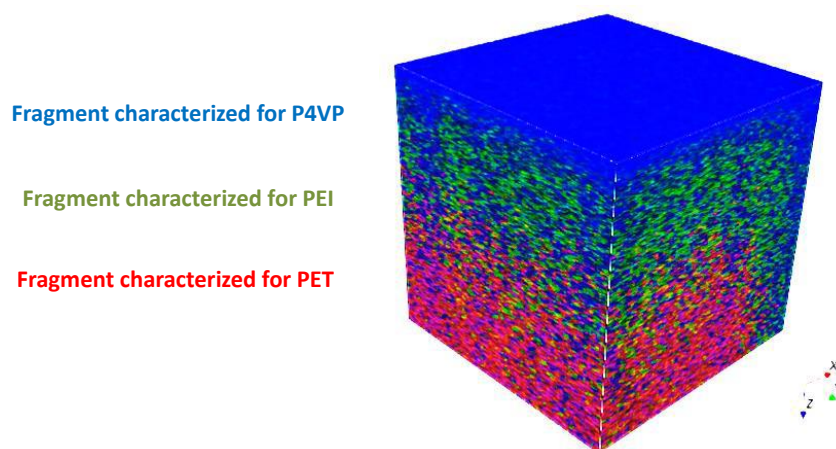
Figure 77. N1s core level scans of a) PET-Br and b) PET-g-PNPMA

In comparison to N1s core level of PET-Br film as presented in Figure 77, it is suggested that the binding energy at 399.8 eV might be originated from the intermediate layers of PEI and grafted initiator. This phenomenon can be explained as that 1) the polymerization proceeded at low conversion so that the “thickness” of PNPMA layer is smaller than penetration depth of X-ray during XPS measurement, or 2) the polymer did not cover PET-Br surface completely, thus a part of PET-Br layer was still exposed to X-ray beam.

In contrast, our lab’s previous work on Cu(0)-mediated RDRP of 4VP from PET surface had demonstrated that the use of PEI is responsible for the incorporating of intermediate layer and polymer layers as illustrated in Figure 78 [97]. In this study, depth profiling by ToF-SIMS shows that dense and uniform layer of P4VP was formed on PET substrate after 5-day polymerization, yet the grafted polymer were initiated from different sites that are geometrically localized at various depths due to the use of branched PEI. Consequently, interphases were observed rather than sharp interfaces between the consecutive components. From similar point of view, both low conversion and low coverage might be responsible for the exposure of C-N bond in PET-g-PNPMA surfaces.

Table 19. Fitting parameters of XPS core level scans of PET-g-PNPMA film

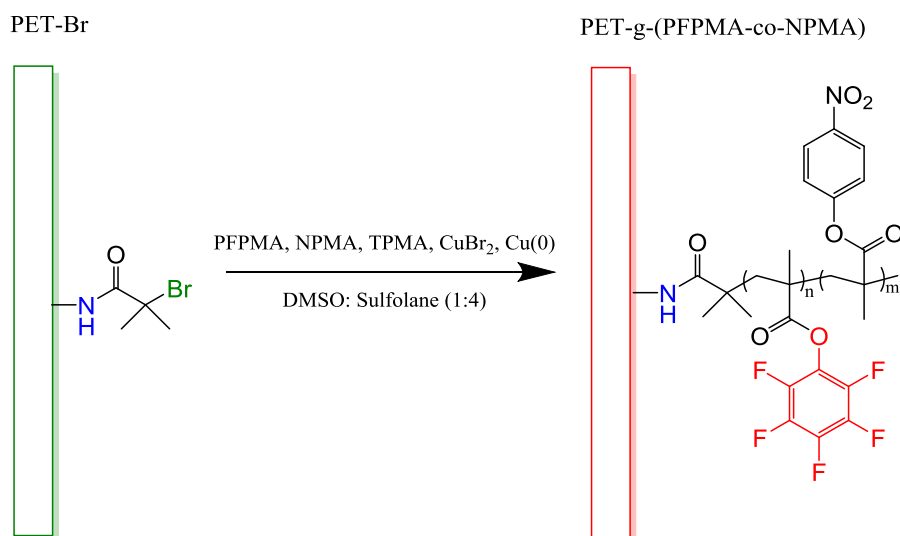
Core level	Bonding	PET-g-PNPMA		
		BE	FWHM	%
C1s (70.4%)	C=C	284.5	1.67	12.7
	C-C	285.0	1.39	45.3
	C-O, C-N	286.3	1.63	21.9
	COO	289.0	1.10	7.3
	C*-CH ₃	285.5	1.49	8.1
	N-C=O	287.9	1.47	3.7
	shake up	291.9	2.04	1.0
O1s (24.0%)	C=O	532.2	2.00	40.8
	C-O	533.4	1.98	40.8
	NO ₂	532.1	1.52	12.2
	N-C=O	530.9	1.77	6.2
N1s (5.6%)	C-N	399.8	2.08	69.6
	NO ₂	405.9	1.53	30.1

**Figure 78. 3D reconstruction of ToF-SIMS result of PET-P4VP [97]**

In conclusion, Cu(0)-mediated RDRP was proven to be able to grow PNPMA from initiator-grafted PET. The success of polymerization was confirmed by different surface analyses. However, XPS quantification for atomic percentages and deconvolution of core level scans suggest the existence of C-N bond within the penetration depth of X-ray beam during measurement, *i.e.* 10-12 nm. This observation can be explained by different hypotheses such as the low conversion of polymerization process or the interphase incorporation between polymer chains and branched PEI intermediate layer. Further studies like ToF-SIMS or mapping of chemical functions need to be done in order to validate which hypothesis is more reasonable.

3.4. PET-initiated Cu(0)-mediated RDRP of NPMA and PFPMA

As demonstrated in the above subsections, Cu(0)-mediated RDRP is applicable to surface-initiated polymerization of PFPMA and NPMA from initiator-grafted PET surface. In addition, we have demonstrated that copolymerization of NPMA and PFPMA in solution by the same technique provided copolymers with composition as envisaged. Therefore, an attempt to replicate copolymerization of PFPMA and NPMA by Cu(0)-mediated RDRP from PET-Br surface has been implemented with nearly equimolar ratio between the two comonomers. Polymerization condition is as given in Scheme 18. The polymerization condition was $[PFPMA]_0: [NPMA]_0: [TPMA]_0: [CuBr_2]_0 = 340:387:4:1$, and 3 cm of Cu(0)-wire was used for one PET-Br film.



Scheme 18. Surface initiated copolymerization of PFPMA and NPMA from PET-Br film

After polymerization, water contact angle of 3- μ L water drop on PET grafted with copolymers of NPMA and PFPMA was $84.3^\circ \pm 2$, giving an increase of 18° compared to PET-Br film used to initiate polymerization. This improvement in hydrophobicity suggests the change in chemical environment where less polar groups are present on surface of PET-Br after polymerization.

As in other parts of this dissertation, ATR FTIR was used to qualitatively study the chemical structure of PET-g-(PFPMA-co-NPMA), the spectrum is as presented in Figure 79. Vibration signals of PFPMA is obvious with the presence of bands characterized for stretching vibration of C-F at 993 cm^{-1} . In contrast, signals showing the contribution of NPMA itself are less apparent. The first indication is the moderate signal at 1209 cm^{-1} from C-N bond of NPMA. Secondly, the out-of-plane scissoring C-H of PET at 725 cm^{-1} is shifted to 727 cm^{-1} , as already mentioned with NPMA solely grafted on PET. In addition, like in the case of PET-g-PNPMA, out-of-plane scissoring vibration of C-H in PET grafted with copolymers is more intense than on non-treated PET, indicating the presence on surface of another phenylic compound. Additionally, as discussed in 2.4.2, the stretching vibration

signals of phenyl C=C in PFPMA at 1517 cm^{-1} and the band characterized for N-O at 1523 cm^{-1} of three copolymers are fused together to give a maximum peak at 1519 cm^{-1} which is independent of composition; the same distinguished maximum is seen also in PET-g-(PFPMA-*co*-PNPMA), which is totally absent in spectrum of PET-*virgin*, suggesting the appearance of copolymer structure on PET surface.

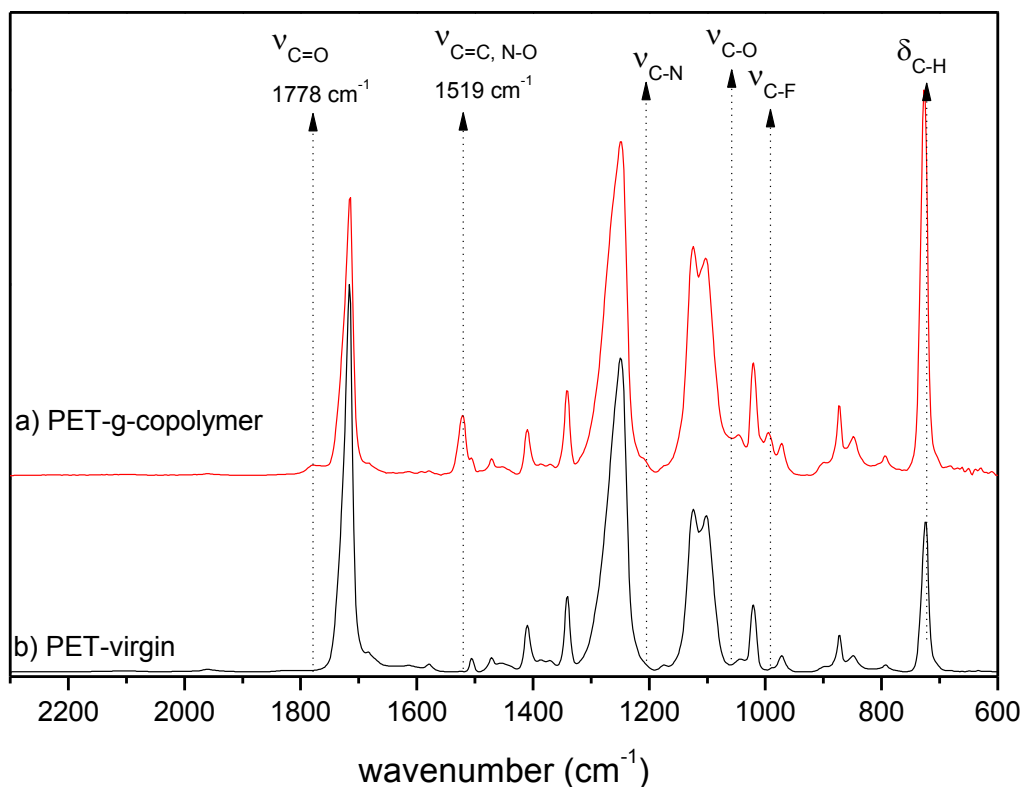


Figure 79. ATR FTIR of a) PET-*virgin* and b) PET-g-P(PFPMA-*co*-PNPMA)

In overall, ATR FTIR analysis of PET-g-(PFPMA-*co*-PNPMA) surface confirms the presence of copolymer on surface, yet it is not possible to determine the ratio between the two components. Therefore, XPS analysis to quantify atomic percentage as well as core level scans to investigate the chemical structure of 10-12 nm extreme surface of modified PET with copolymer is necessary.

Figure 80 and Figure 81 present respectively XPS survey spectrum and core level fitting results obtained after copolymerization of PFPMA and NPMA from PET-Br surface. From survey spectrum, atomic percentages of N1s and F1s were calculated to be 1.8% and 21.2% respectively. However, the enlargement of region characterized for N1s signals suggests the presence of two types of nitrogen. This hypothesis is confirmed by fitting results of N1s (Figure 81d) where within 1.8% detected N1s, there are 55.3% coming from nitro groups. Thus, the total amount of nitrogen that originated from NPMA in copolymer grafted from PET film is around 1.0%. Indeed, for each unit of PFPMA, there are 5 fluorine atoms while for each unit of NPMA, there is one nitrogen atom. Therefore, the ratio of PFPMA and NPMA in grafted polymer is calculated to be 4.3:1 which is largely deviated from the 1:1 ratio in feed. However, the reaction was done for only one film without replication and copolymerization from surface may follow different kinetics than polymerization in solution, which has been suggested in literature [331, 332].

Table 20. Fitting parameters of XPS core level scans of PET-g-(PPFPMA-co-PNPMA)

Core level	Bonding	PET-g-(PPFPMA-co-PNPMA)		
		BE	FWHM	%
C1s (62.5%)	C=C	284.3	1.50	9.5
	C-C, C-H	285.0	1.28	22.8
	C-O, C-N	286.2	1.10	9.9
	COO	289.3	1.31	8.2
	C*-CH ₃	285.6	1.00	5.8
	C-F	287.8	1.67	41.1
	Shake up	294.7	2.60	2.7
O1s (14.4%)	C=O	532.5	2.09	44.4
	C-O	534.1	2.09	40.3
	NO ₂	532.1	2.00	15.3
N1s (1.9%)	C-N	400.0	2.37	44.7
	NO ₂	405.9	1.68	55.3
F1s (21.2%)	C-F	688.2	1.79	96.3
	Shake up	695.0	2.15	3.7

On the other hand, the N1s core level scan shows another nitrogen intensity rather than NO₂. Similar to PET-g-PNPMA film, herein, the C-N bond can be attributed to binding energy at around 400 eV. As discussed for PET-g-PNPMA case, this may originate from the low

polymerization and/or the interpenetration of PEI with the short copolymer chains, making PEI visible within 10-12 nm extreme layer of the surface. Similarly, O1s core level scan can be fitted successfully considering that at least 3 major components including carbonyl C=O (532.5 eV), C-O (534.1 eV) and nitro group originated from *p*-nitrophenyl pendant group N-O (532.1 eV). In contrast, only one source of fluorine atom from C-F pentafluorophenyl pendant was observed at 688.2 eV as presented in Figure 81c.

Taking into account the fits of N1s, O1s and F1s, C1s core level of PET-*g*-(PPFPMA-*co*-PNPMA) was deconvoluted into 6 major contributors as given in Figure 81a with fitting parameters listed in Table 20. The contribution of NPMA is confirmed by the existence of binding energy characterized for C=C of nitrophenyl groups. On the other hand, the presence of PFPMA is given by C-F bond assigned to binding energy at 287.8 eV. Other common bonds includes aliphatic C-C at 285 eV, aliphatic quaternary C*-CH₃ at 285.6 eV, C-O/C-N at 286.2 eV and carbonyl COO at 289.3 eV.

Overall copolymerization of PFPMA and NPMA by Cu(0)-mediated RDRP from PET grafted with eBiB-like initiator has been achieved and proven by WCA, ATR FTIR and XPS to be successful to a certain level. Regarding composition of copolymer on surface, XPS suggests the amount PFPMA is 4-time higher than NPMA, which is largely deviated from 1.1:1 molar ratio between the two active esters in feed.

3.5. Conclusion

Results on surface-initiated polymerization of PFPMA and NPMA by Cu(0)-mediated RDRP have been presented; indirect quantification of amount initiator on surface was determined by colorimetric titration with orange acid to give a result of 0.3 functional groups per nm². Following the success of polymerization and copolymerization in solution of the two active esters, polymerization has also been confirmed to be applicable for PET film grafted with eBiB-like initiator. An in-detail study has been examined in the case of PFPMA where Cu(0)-mediated RDRP has worked well both in a small scale with 1-2 films and a large scale with 12 films at the same time. Characterization by different techniques including WCA, ATR FTIR and XPS confirmed the complete coverage of PFPMA on PET supporting surface while imaging techniques (AFM and SEM) demonstrate the development of nanometric to micrometric structures of PET-*g*-PPFPMA obtained at different polymerization conditions. As proof-of-concepts, results obtained from surface initiated polymerizations of NPMA and copolymerization of two active esters prove that Cu(0)-mediated RDRP is a good approach to graft these macromolecules from supporting surface. However, further studies as well as replication are needed to validate the reproducibility of the technique as well as to clarify whether the intermediate layer of PEI can penetrate onto “layer” of grafted polymers.

Chapter 4. Post-modification of reactive polyesters in solution

4.1. Post-modification of PFPMA

PPFPMA can be easily substituted *via* nucleophilic substitution with amines [266, 279] and alcohols [272]. As this dissertation focuses on the preparation of polymer containing essential oil derivatives, the post-modification was firstly tested with a highly reactive amine to briefly validate the possibility of polymer post-modification. Then, another preliminary was performed to identify the proper base to mediate efficiently the substitution during post-modification process.

4.1.1. Post-modification with amines

4.1.1.1. Post-modification of PFPMA with *n*-butylamine

Post-modification of PFPMA with *n*-butylamine was carried out in large excess (9 eq.) of the amine and without addition of base. Nucleophilic substitution of PFPMA was reported to occur at faster rate in polar solvents such as DMF and DMSO [280]. However, as the polymer has low solubility in DMSO and DMF, the substitution with *n*-butylamine was tested in THF, *i.e.* a good solvent for PFPMA, at 70 °C. After 24 hours of reaction, a complete conversion was validated by ^{19}F NMR of reaction mixture. Figure 82 presents ^{19}F NMR of reaction mixture before and after 24-hour reaction with *n*-butylamine. It is seen that no signals coming from polymer were recorded; instead, the signals coming from pentafluorophenol is visible.

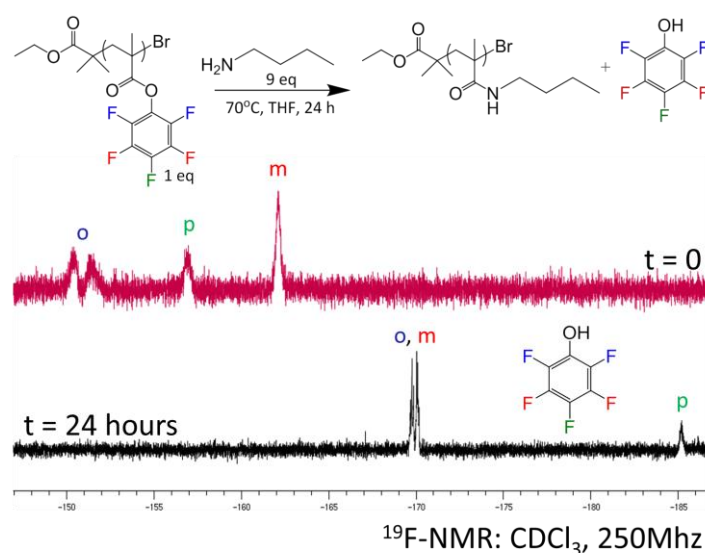


Figure 82. ^{19}F NMR spectra of post-modification of PFPMA with *n*-butylamine: reaction mixture at $t = 0$ and $t = 24$ hours

An attempt to perform the substitution at room temperature was also implemented and the total conversion was also successful.

Figure 83 presents ^1H NMR spectrum of poly(*n*-butyl methacrylamide) (PBMAm). Two significant peaks of the acrylamide polymer are observed at 5.93 ppm (1 proton of amide bond) and at 3.08 ppm (methylene $-\text{CH}_2-$ adjacent to amide bond). ^{19}F NMR spectrum of PBMAm obtained by post-modification of PPFMA shows the absence of the reactive polymer signals, confirming the complete substitution conversion.

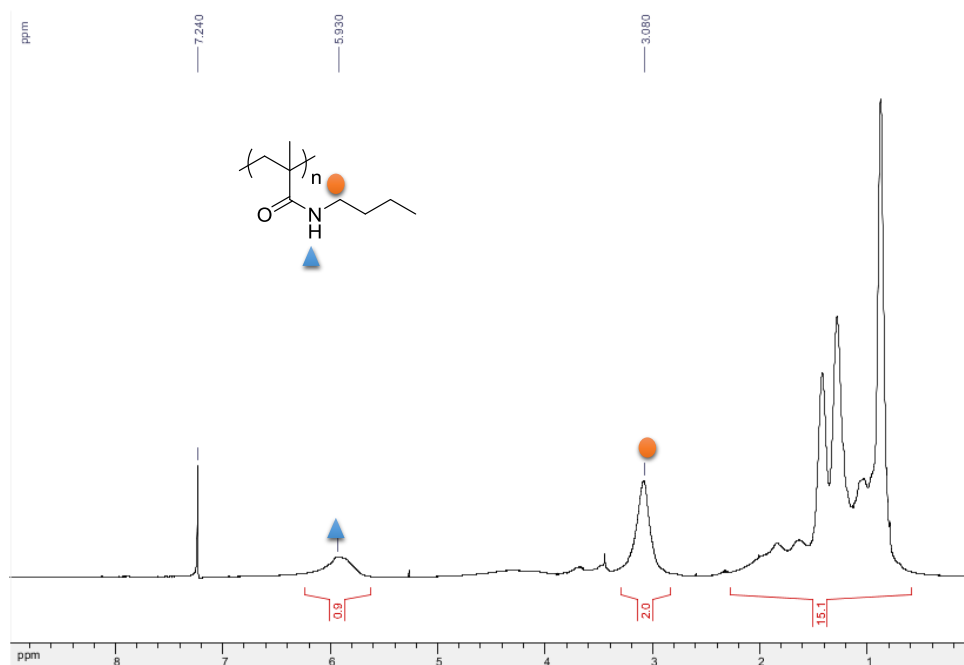


Figure 83. ^1H NMR of poly(*n*-butyl methacrylamide) (CDCl_3 , 360 MHz)

Kinetics of PPFMA post-modification with *n*-butylamine in THF at room temperature was also investigated as presented in Figure 84. The substitution proceeded rapidly with more than 40% substitution after 30 minutes and reached 100% conversion in 3 hours.

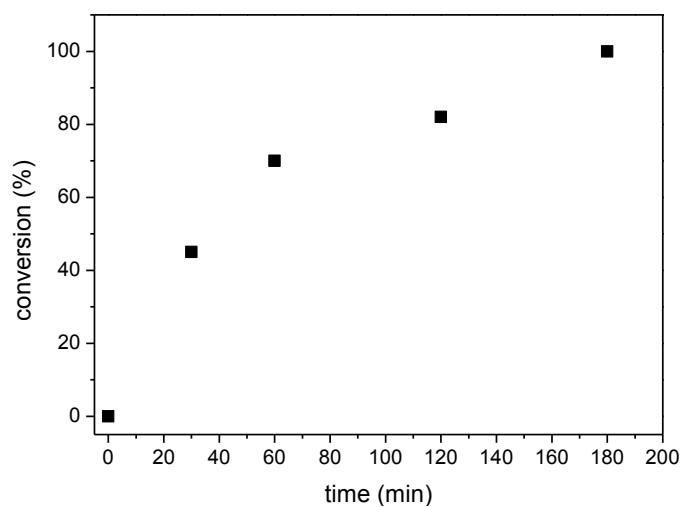


Figure 84. Kinetics of PPFMA substitution by *n*-butylamine

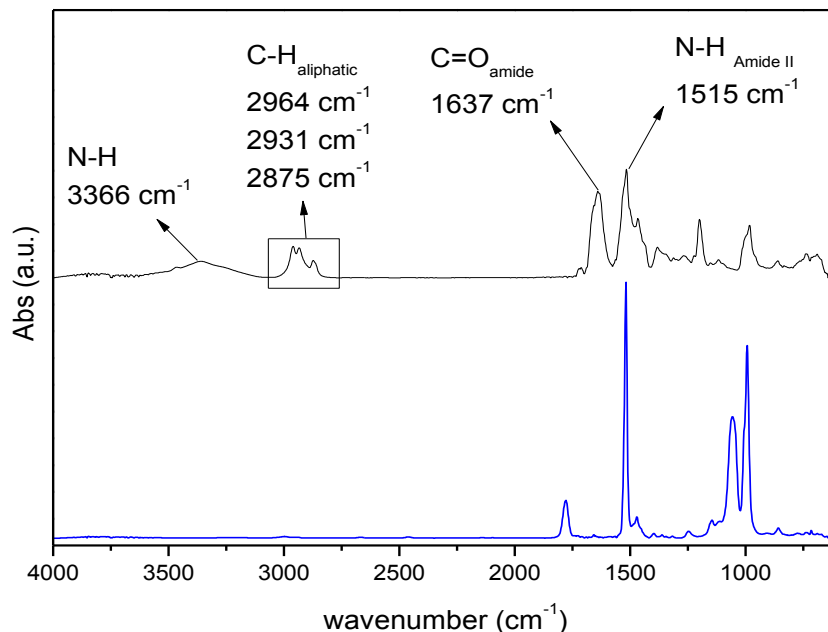
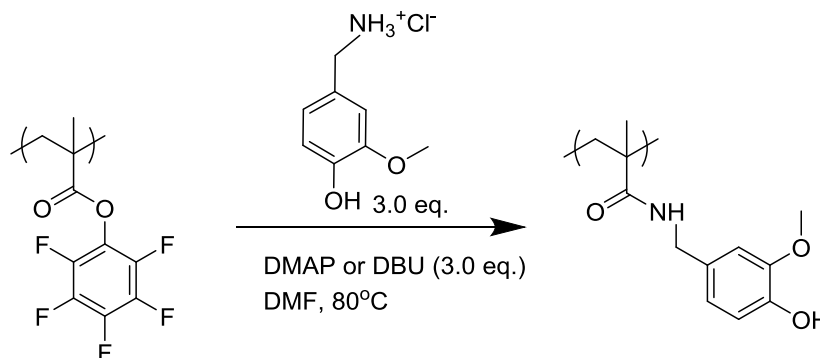


Figure 85. ATR FTIR of PPFpMA (bottom) and PBMAm (top)

Comparison of ATR FTIR spectra of PPFpMA and PBMAm (Figure 85) confirms the total conversion from a polyester structure into polyamide. Besides the total disappearance of characteristic PPFpMA bands, specific absorbance band characterized for amide groups are present, *e.g.* stretching vibration of C=O (amide) at 1637 cm^{-1} , broad stretching vibration at 3366 cm^{-1} accompanied with in-plane deformation at 1515 cm^{-1} of N-H bond, and asymmetric/symmetric stretching of aliphatic C-H between 2800 cm^{-1} and 3000 cm^{-1} .

4.1.1.2. Post-modification of PPFpMA with vanillylamine hydrochloride

A recent study on covalently grafted poly(vanillyl methacrylamide) (PVaMAm) has been reported by our group, this glass coated with polymer derived from vanillin can suppressed efficiently the biofilm formation of *B. subtilis* [333]. Therefore, preliminary experiment to prepare the same type of polymer from PPFpMA was performed as presented in Scheme 19.



Scheme 19. Post-modification of PPFpMA with vanillylamine hydrochloride

Firstly, the post-modification was tested with DMAP (3 eq.); however, the reaction proceeded at low conversion (17%) compared to the reaction carried out with DBU which resulted in 100% substitution of PPFMA into poly(vanillyl methacrylamide) (PVaMAm) after 24 hours (Figure 86). The difference between the use of DMAP and DBU may be attributed to their pKa values. DMAP has slightly smaller pKa (9.6) than DBU (pKa 13.5) compared to vanillylamine, which pKa should be between 9 and 11 – the range of primary amine pKa's value. Thus, DBU as base catalyst is more efficient in amine deprotonation than DMAP; hence, complete conversion was achieved.

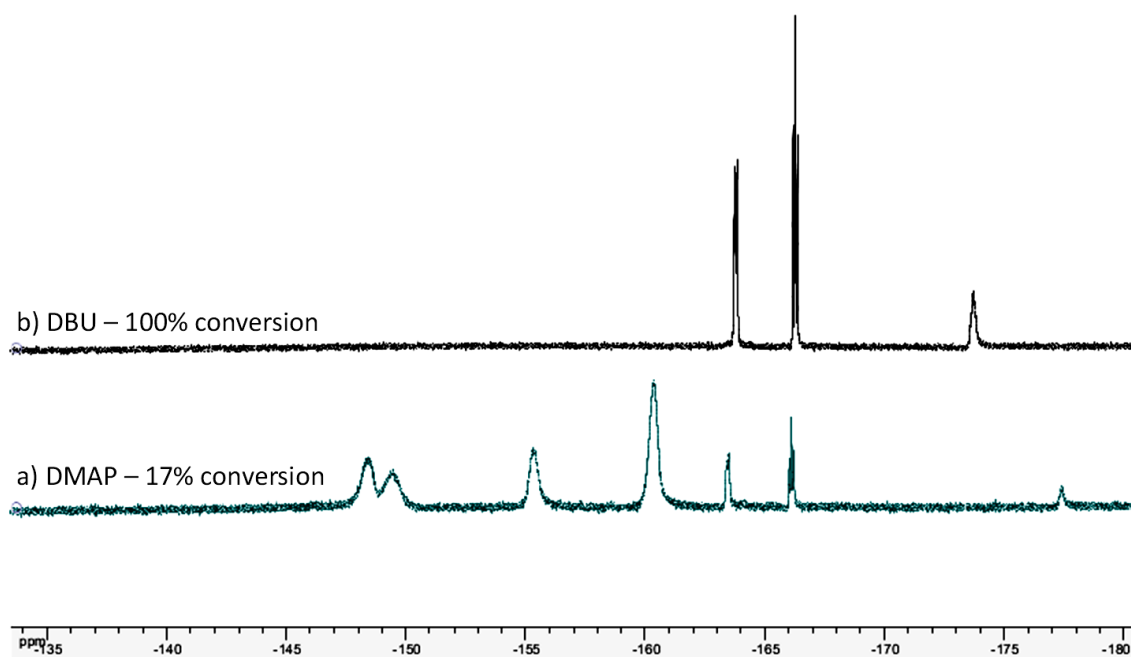


Figure 86. ^{19}F NMR of PPFMA post-modification with vanillylamine hydrochloride using 3 equivalents of a) DMAP and b) DBU, $T = 70\text{ }^\circ\text{C}$, $t = 24$ hours

Figure 87 presents ^1H NMR spectrum of PVaMAm obtained after PPFMA post-modification with vanillylamine hydrochloride at 100% conversion. From this spectrum, major peaks characterized for the vanillin derivative are visible, including the appearance of 3 aromatic protons at 6.4 – 6.9 ppm, the phenolic hydroxyl at 8.8 ppm, $-\text{CH}_2-$ next to amide group at around 4.1 ppm and the methoxyl proton at 3.7 ppm. This spectrum is also in good agreement with that has been obtained by free radical polymerization [333]. However, the reported PVaMAm obtained by traditional radical polymerization is limited in molecular weight. Herein, PPFMA can be obtained at DP as high as 400, hence, providing the possibility to obtain PVaMAm at longer chain and higher molecular weight.

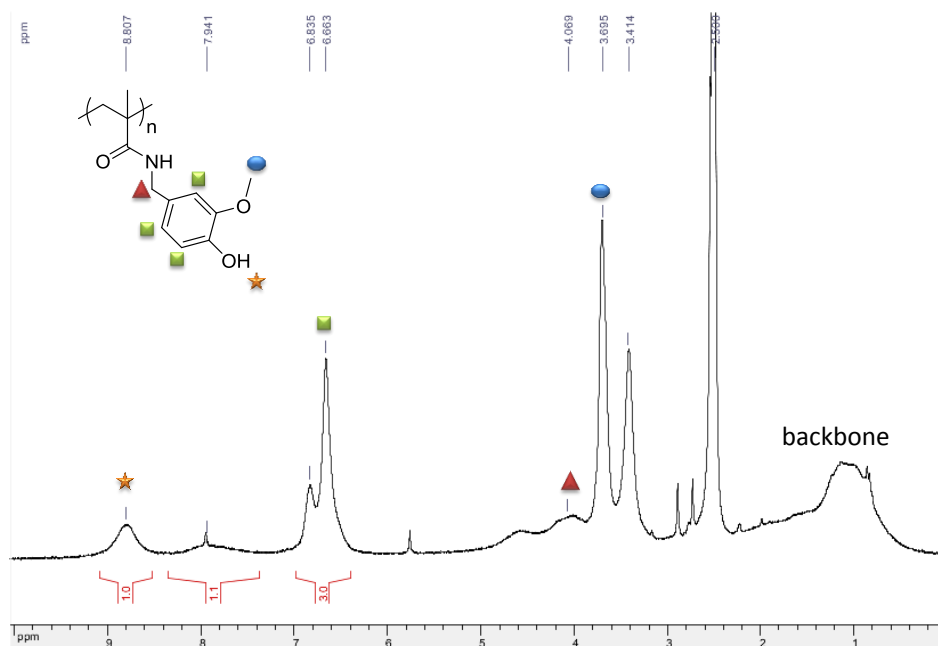


Figure 87. ^1H NMR spectrum of PVaMAM (DMSO- d_5 , 250 MHz)

Absorbance spectrum measured by ATR FTIR also confirms the structure of the obtained PVaMAM (Figure 88).

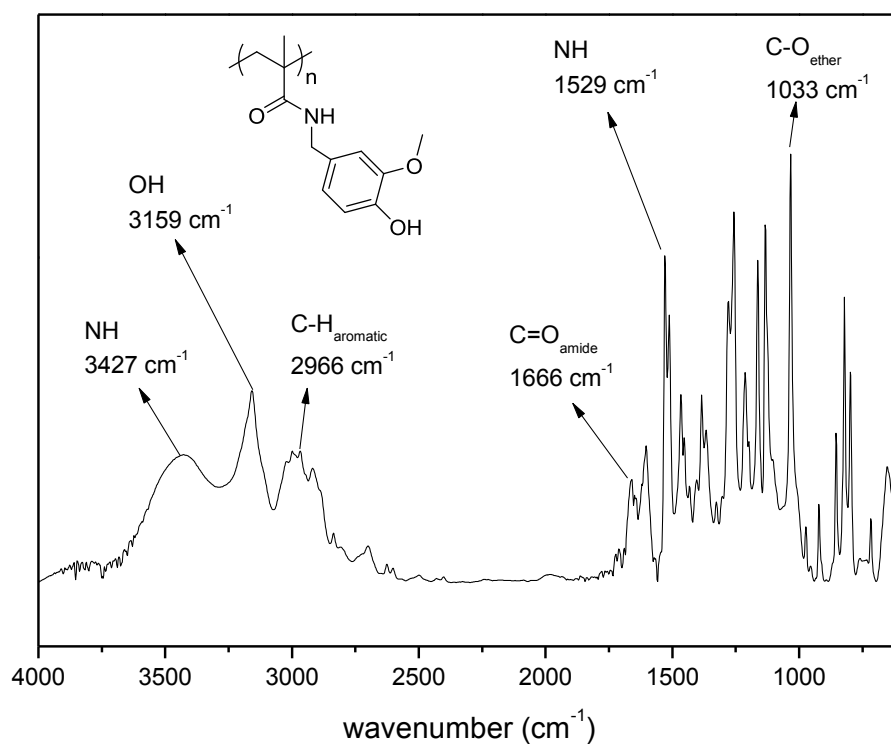


Figure 88. ATR FTIR spectrum of PVaMAM

First of all, the stretching of C=O in PFPMA at 1776 cm^{-1} has totally disappeared and the intensity at 1666 cm^{-1} characterized for the carbonyl of amide bond in PVaMAm is observed. The secondary amide is confirmed by the appearance of two bands characterized for vibration of NH at 3427 cm^{-1} and 1529 cm^{-1} . The phenolic hydroxyl group is visible given by the existence of absorbance band at 3159 cm^{-1} . An intense signal at 1033 cm^{-1} is also observed, which is corresponding to the vibration of ether C-O. Signals coming from aromatic protons are observed at wavenumber $< 1000\text{ cm}^{-1}$ and at 2966 cm^{-1} .

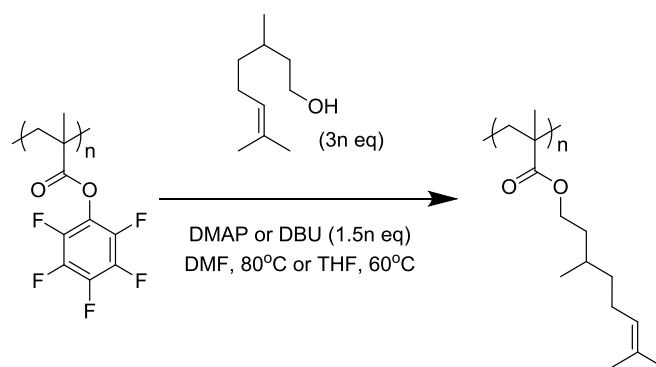
From these above analyses, the structure of PVaMAm obtained from post-modification of PFPMA with vanillylamine hydrochloride has been confirmed to match with its chemical structure.

4.1.2. Post-modification with essential oils

Transesterification of PFPMA has been studied for several different classes of alcohol [272]. This section provides discussion on the transesterification of PFPMA with different essential oils that possess hydroxyl group.

4.1.2.1. Citronellol

The substitution of PFPMA by citronellol was achieved following Scheme 20 to obtain poly(citronellyl methacrylate) (PCiMA). As the transesterification of PFPMA has been well described in literature [272], similar conditions to modify the PFPMA, *i.e.* 0.5 eq. of DMAP as catalyst and DMF as solvent has been employed. Even though the post-modification process worked, the conversion of pentafluorophenyl moieties into citronellyl moieties was low ($<20\%$). By increasing the amount of DMAP to 1.1 equivalents, a better conversion was achieved but limited to 31%. When DMAP was replaced by DBU, a huge improvement in conversion was observed ($>95\%$). As discussed previously, DBU is a stronger base compared to DMAP; therefore, it is more efficient when serving as a base catalyst. Furthermore, it was mentioned in literature that PFPMA has higher reactivity in nucleophilic substitution than PFPMA [266], which explains why the use of DMAP resulted in higher substitution conversion ($>95\%$) for the reactive acrylate than that of the methacrylate counterpart. DMF is a good solvent for substitution of PFPMA; however, relatively high temperature ($80\text{ }^{\circ}\text{C}$) is required because PFPMA is not soluble in DMF at room temperature. In contrast, THF is a good solvent for the active ester at room temperature. Herein, post-modification carried out in THF and excess of citronellol and DBU also resulted in $>90\%$ post-modification conversion and lower temperature ($60\text{ }^{\circ}\text{C}$) was needed.



Scheme 20. Post-modification of PPFMA with citronellol

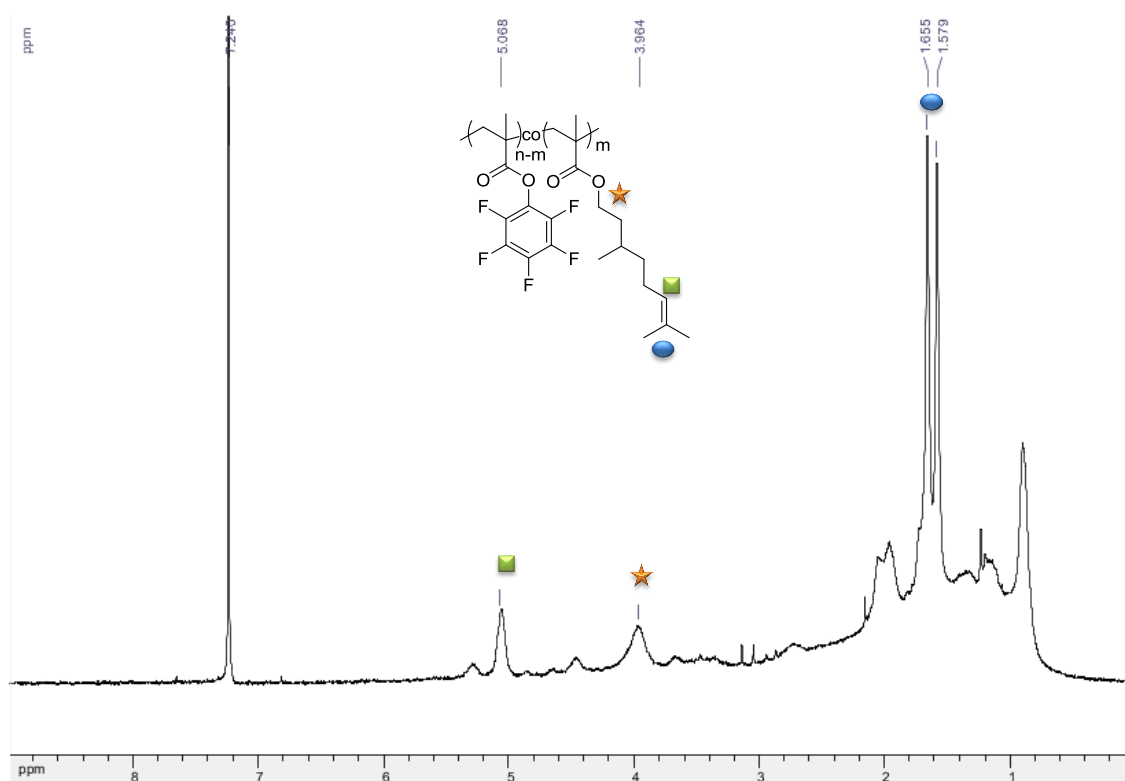


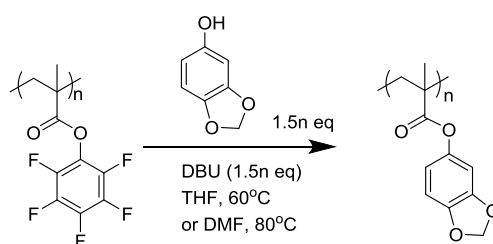
Figure 89. ^1H NMR spectrum of poly(citronellyl methacrylate) (PCiMA) (CDCl_3 , 250 MHz)

Figure 89 presents ^1H NMR of PCiMA obtained after dialysis of reaction mixture in water. Characteristics peaks of citronellyl pendant groups are observed including two methyl groups at around 1.5 and 1.6 ppm, methylene protons in adjacent to ester group at 3.9 ppm and ethylenic protons at 5.0 ppm. ^{19}F NMR spectrum of this product indicates that a small amount of PPFMA pendant groups has been retained. It is noteworthy that at high substitution yield, the PCiMA is obtained as a sticky viscous matter; thus, ATR FTIR was not carried out for such sample.

Experimental results in post-modification of PFPMA with citronellol indicate that for the reactive methacrylate, DBU as base results in higher conversion of pentafluorophenyl to citronellyl side chain than DMAP. Thus, further studies were carried out using only DBU as base catalyst for nucleophilic substitution of PFPMA.

4.1.2.2. Sesamol

Sesamol has been studied in many biological research purposes such as antioxidant property [334-336], antiaging agent [337], radioprotective effect [338], and chemopreventive effect [339]. Therefore, polymers with sesamyl sidechain may have interesting biological effects. Poly(sesamyl acrylate) was obtained in literature from post-modification of PFPMA [272]. Herein, the post-modification of PFPMA was done as presented in Scheme 21.



Scheme 21. Post-modification of PFPMA with sesamol

The substitution of sesamol to PFPMA was effective in either THF or DMF and both solvents present to mediate very well the substitution with 100% conversion achieved. However, the substitution in DMF turns out to be much faster than in THF. Indeed, 100% conversion was obtained after 30 minutes in DMF while during the same period, reaction proceeded to 33% in THF. The difference in rate of nucleophilic substitution of PFPMA in various solvents has been reported [280], where reaction rate in DMF was demonstrated to show a few times higher than THF. As the chemical modification herein is a nucleophilic substitution, it was expected and was confirmed that reaction rates in THF can be enhanced by double the amount of DBU used from 1.5 eq. to 3.0 eq. as presented in Figure 90.

Even though the reaction in DMF seems to be advantageous from kinetics point of view, the purification of poly(sesamyl methacrylate) (PSeMA) from such reaction medium was difficult. In contrast, the use of THF led to easy precipitation of PSeMA in cold methanol.

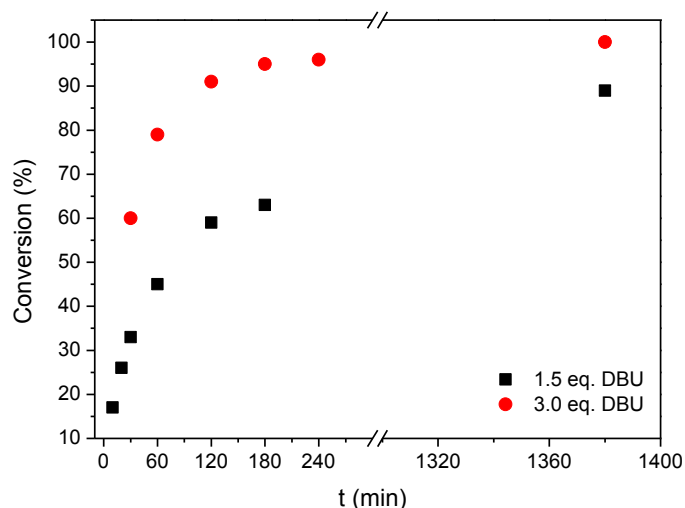


Figure 90. Kinetics of post-modification of PPFMA with sesamol in THF, conversions calculated from ^{19}F NMR spectra

Figure 91 presents ^1H NMR spectrum of PSeMA obtained from 100% substitution conversion of PPFMA post-modification. Protons for sesamol side chain are visible and characterized by the methylenedioxy at 5.9 ppm and phenylic protons between 6.4 ppm - 6.8 ppm. However, suspicious intense peaks are also present at ≈ 3.2 ppm to 3.6 ppm and lower, which also interferes with intensity coming from polymer backbone. These peaks can be attributed to the presence of DBU salts (DBUH^+) which have been reported before [340].

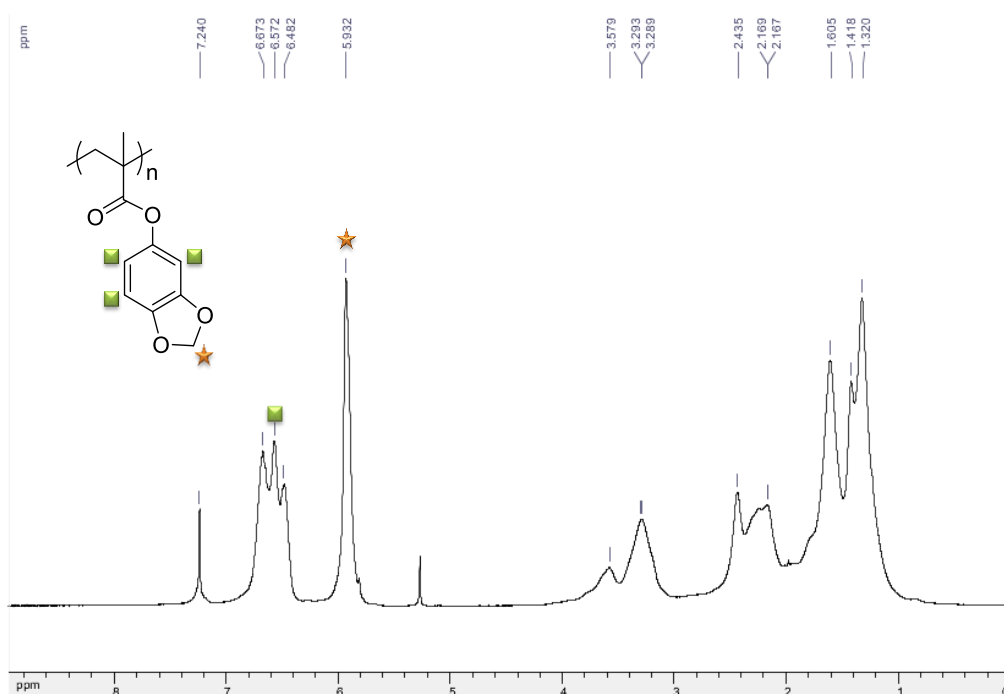


Figure 91. ^1H NMR of PSeMA (CDCl_3 , 360 MHz)

Further chemical characterization was done by ATR FTIR as illustrated in Figure 92. First of all, the total conversion was confirmed by disappearance of peaks corresponding to PPFPMMA. Secondly, peaks characterized for PSeMA structure are observed and present to match with that reported in literature [341]. Firstly, the stretching vibration of carbonyl C=O is present at 1747 cm^{-1} . The phenyl skeleton is visible at 1670 cm^{-1} and 1635 cm^{-1} which are accompanied with the C-H vibration at 2933 cm^{-1} . An intense absorption band at 1484 cm^{-1} is attributed to CH₂ bending vibration. The presence of ether bond is evident thanks to signal of C-O-C symmetric stretching at 1126 cm^{-1} . Furthermore, one of the most specific vibration signals of methylenedioxy absorbance band is also present at 923 cm^{-1} .

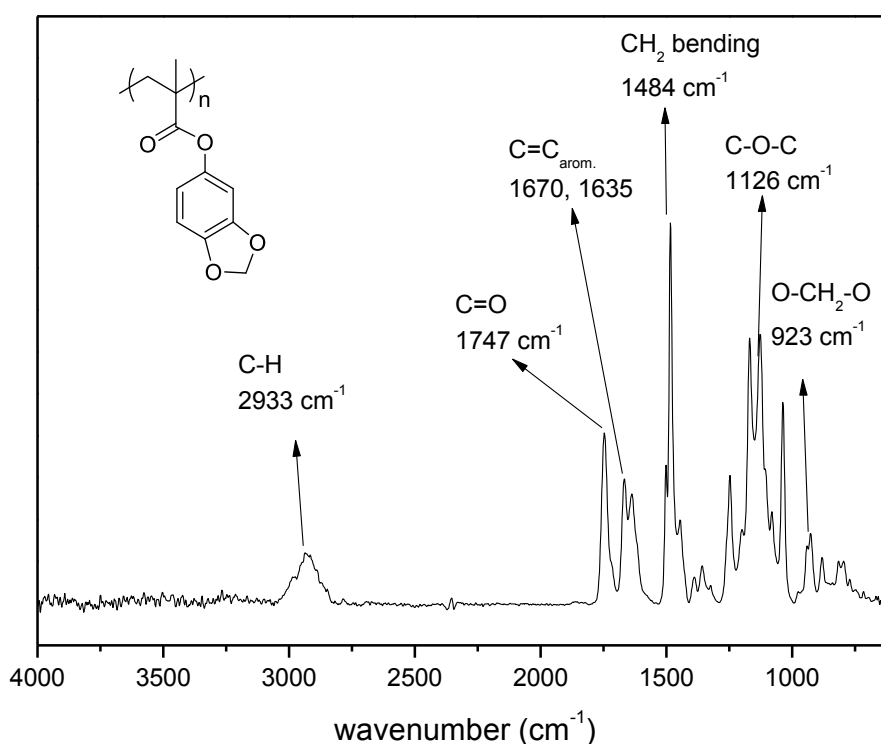


Figure 92. ATR FTIR spectrum of PSeMA obtained at 100% conversion of PPFPMMA post-modification.

XPS analysis was also performed on PSeMA obtained herein. Survey spectrum (Figure 93a) indicates the presence of C1s, N1s and O1s and the total disappearance of F1s, insisting the 100% conversion of PPFPMMA post-modification. However, the existence of N1s was unexpected and is attributed to the signal of DBUH⁺ remained after reaction as discussed in ¹H NMR before. From the structure of DBU, it is seen that N1s takes 18.2% in number atomic percentage and C1s takes 81.8%, giving a C/N ratio of 4.49. Taking into account the contribution of DBUH⁺ in the measurement of PSeMA, the amount of C1s originated from the salt is 16.2%. Thus, the amount of C1s originated from sesamyl polymer is 60.7% giving an atomic C/N ratio of 3.1, which is quite closed to theoretical value of 2.8.

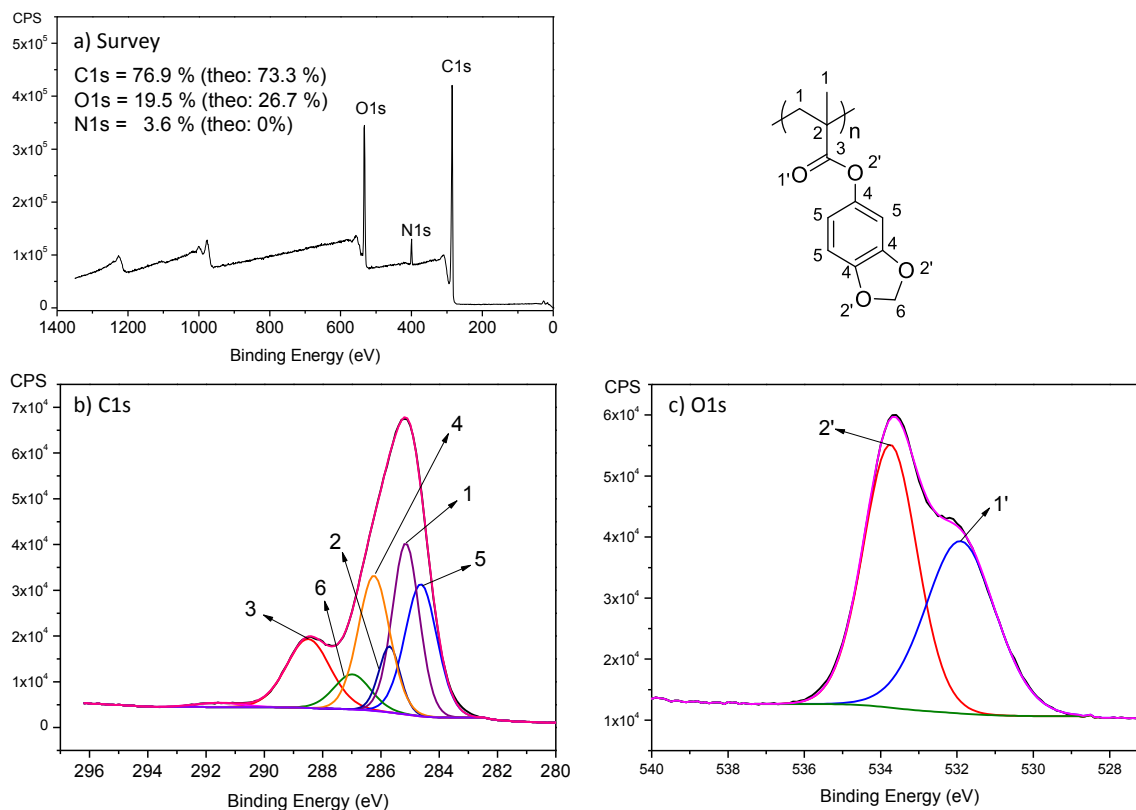


Figure 93. XPS results of PSeMA: a) survey spectrum, b) C1s fitting result and b) O1s fitting result

Despite the presence of DBU, C1s and O1s core level scans could be deconvoluted in accordance with the structure of PSeMA as given in Figure 93b, c. Fitting parameters of these two core level scans are summarized in Table 21.

Table 21. Fitting parameters of C1s and O1s core level scans obtained by XPS of PSeMA

Core level	Bonding	PSeMA		
		BE	FWHM	%
C1s	C=C	284.5	1.30	22.4
	C-C, C-H	285.0	1.08	24.2
	C*-CH ₃	285.6	0.86	7.5
	C-O, C-N	286.1	1.27	22.4
	O-CH ₂ -O	286.8	1.47	6.7
	COO	288.3	1.76	15.8
	Shake up	291.4	1.88	1.0
O1s	C=O	531.8	2.16	46.1
	C-O	533.6	1.66	53.9

As seen in Figure 93b, C1s core level of PSeMA can be deconvoluted into at least 6 major contributors including phenylic C=C at 284.5 eV, aliphatic C-C/C-H at 285.0 eV, C*-CH₃ at 285.6 eV, C-O/C-N at 286.1 eV and carbonyl COO at 288.3 eV. The observed carbon of methylenedioxy O-CH₂-O at 286.8 eV is the most specific intensity of PSeMA under C1s core level. On the other hand, O1s core level can be deconvoluted into two contributors including C=O at 531.8 eV and C-O at 533.6 eV. The deviation between the two peaks is 1.8 eV, which is larger than the deviation of C-O and C=O in ester. This difference is due to the presence of methylenedioxy functional groups of PSeMA, making the C-O shifted to higher binding energy.

Overall, NMR ATR FTIR and XPS analyses and characterizations confirm that the post-modification of PPFPMMA with sesamol was complete; yet, residues of DBU are remained. Dialysis or water washing could be useful to remove this salt.

On the other hand, the change in chemical structure from PPFPMMA to PSeMA also led to the modification in molecular weight of polymer due to the difference in mass of the two functional groups. Therefore, SEC analysis was performed with the PPFPMMA precursor and the obtained PSeMA as demonstrated in Figure 94. For total change from PPFPMMA to PSeMA, a loss in molecular weight is calculated theoretically to be $\approx 46 \text{ g mol}^{-1}$. It is seen from SEC profiles of the polymer before and after post-modification, PSeMA has higher retention time compared to PPFPMMA precursor, indicating a smaller molecular weight in overall. By conventional calibration against PS standards, the precursor PPFPMMA has Mn of 8300 g mol^{-1} ($D = 1.71$) and PSeMA has Mn of 7300 g mol^{-1} ($D = 1.85$), confirming the change in molecular weight after post-modification.

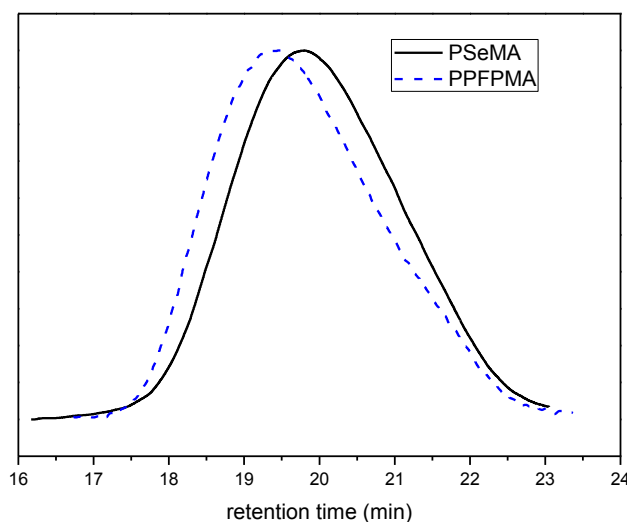
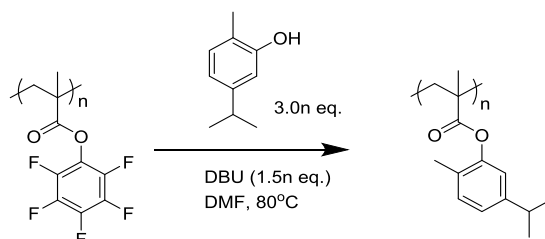


Figure 94. SEC profiles of precursor PPFPMMA (dashed line) and obtained PSeMA (solid line)

In conclusion, the post-modification of PPFPMMA with sesamol was successfully performed with complete conversion confirmed by various analyses.

4.1.2.3. Carvacrol

Our group has previously reported that poly(thymyl methacrylate) grafted to PET was proven to enhance the antiadhesion property of the substrate [67]. Carvacrol is an isomer of thymol and as thymol, it also exhibit antibacterial property [59, 342]. Furthermore, carvacrol ($pK_a = 10.4$) is assumed to be less reactive in nucleophilic substitution than sesamol ($pK_a = 9.8$). Therefore, PFPMA post-modification of carvacrol was tested. The reaction was carried out as presented in Scheme 22.



Scheme 22. Post-modification of PFPMA with carvacrol

After 24 hours, the conversion of pentafluorophenyl group into carvacryl group has proceeded to $\approx 65\%$. This result was expected because under the same condition, sesamol as the more reactive nucleophile has replaced $\approx 85\%$ of pentafluorophenyl moieties. Even though higher equivalent of DBU was not examined, but as described for the case of sesamol, a faster reaction with higher conversion can be obtained by increasing the quantity of base catalyst.

Final product of PFPMA post-modification with carvacrol at 65% conversion was obtained by precipitation in cold methanol and is considered as a random copolymer of PFPMA and CarMA, hence denoted as PFPMA_{35-co}-PCarMA₆₅.

Figure 95 represents ^1H NMR spectrum of PFPMA_{35-co}-PCarMA₆₅ where the peaks characterized for the presence of CarMA is well distinguished. The first indicator of CarMA is the presence of phenylic protons between 6.8 - 7.2 ppm. The proton of isopropyl substituent C-H is also observed at 2.7 ppm. The methyl substituent of phenyl ring is also seen at 2.1 ppm.

Further characterization by ATR FTIR was performed to investigate the chemical environment of the copolymer as seen in Figure 96. The incompleteness of substitution was confirmed by peaks corresponding to PFPMA. On the other hand, new vibration band originated from PCarMA is also visible with the presence of carbonyl C=O at 1749 cm^{-1} . In addition, the phenyl skeletal structure is seen with the vibration characterized for C=C at 1645 cm^{-1} and band at 2964 cm^{-1} .

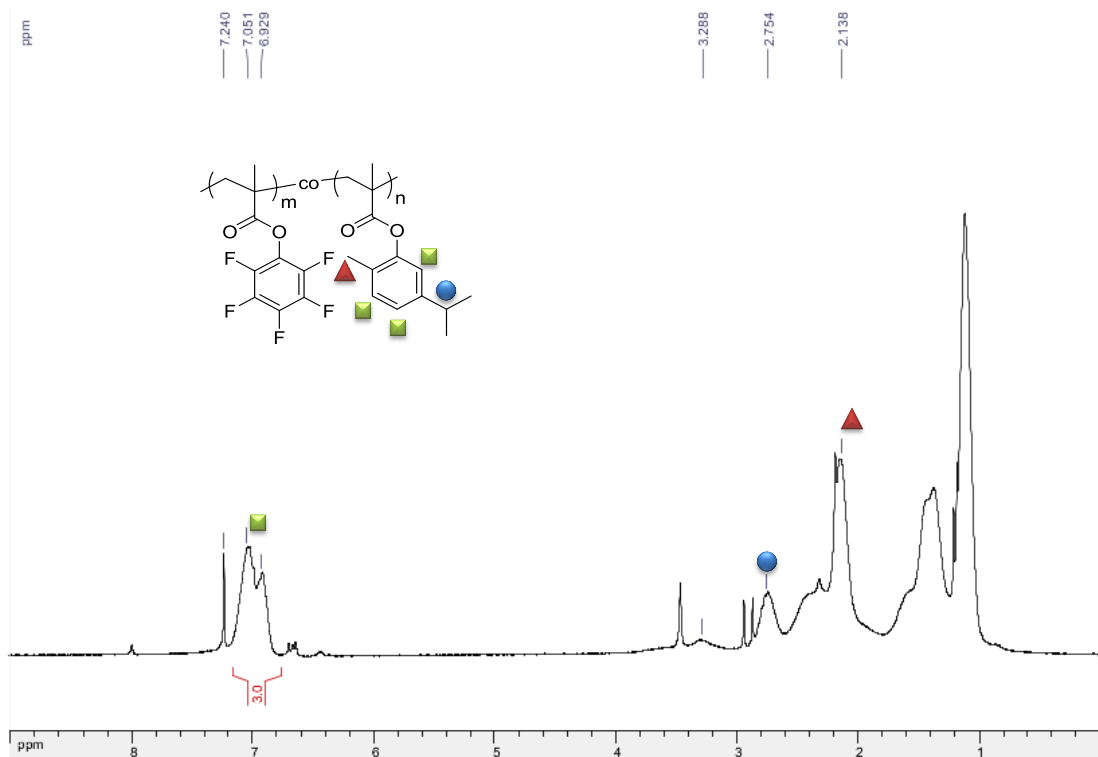


Figure 95. ^1H NMR of PPFMA₃₅-*co*-PCarMA₆₅ obtained from PPFMA post-modification with carvacrol (CDCl_3 , 360 MHz)

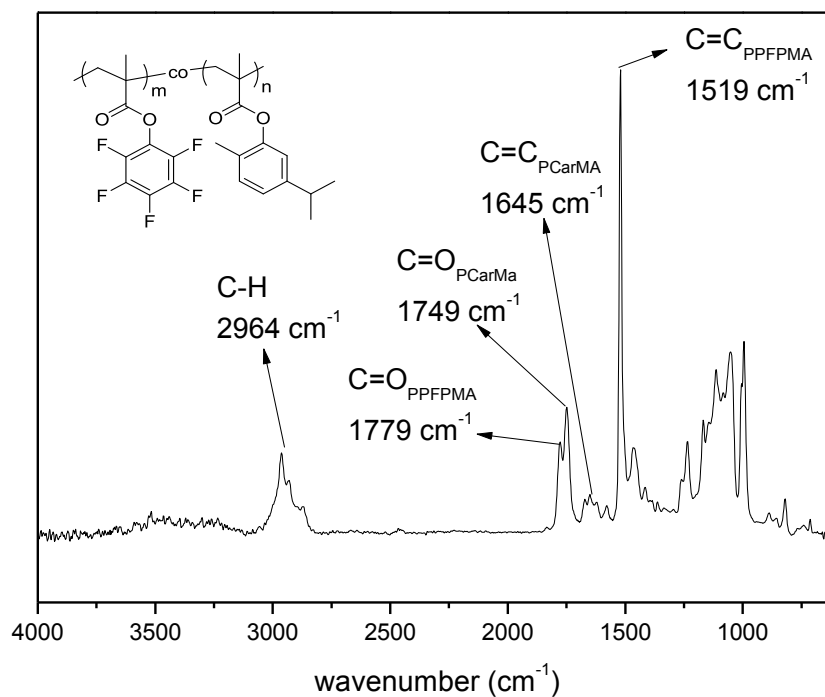


Figure 96. ATR FTIR of PPFMA₃₅-*co*-PCarMA₆₅

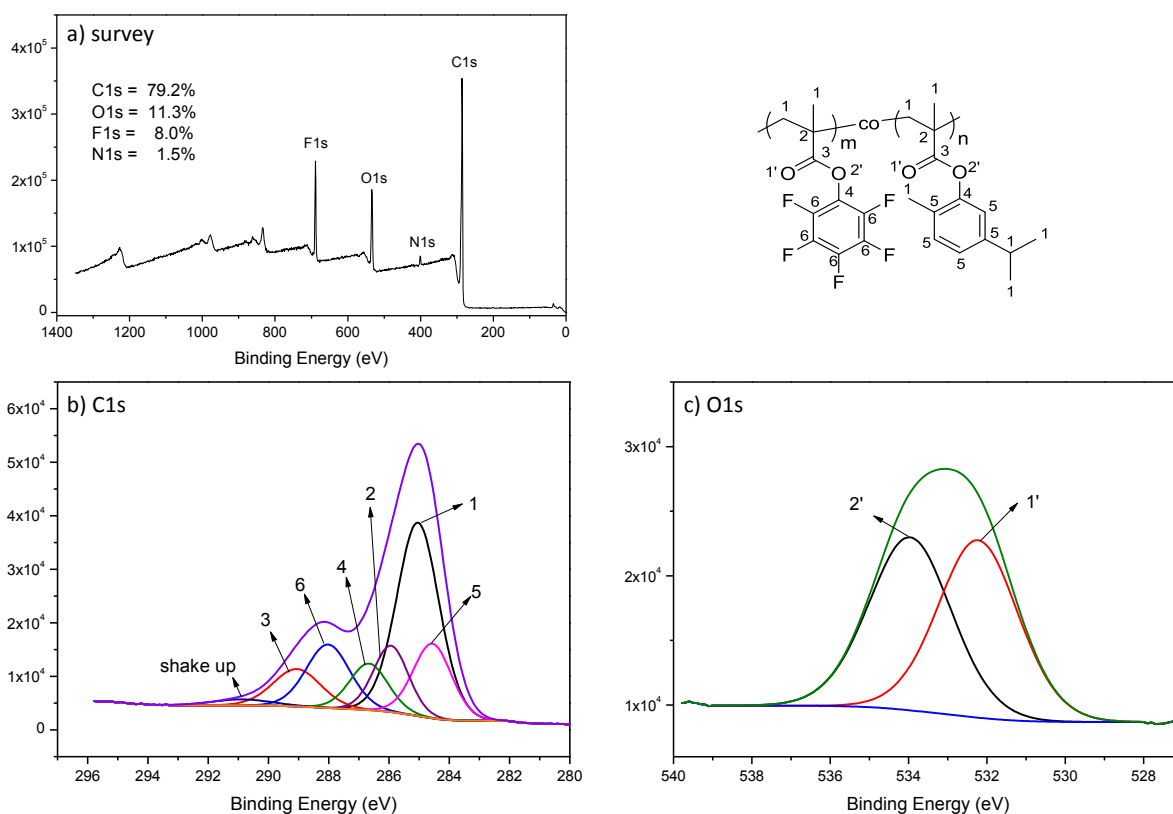


Figure 97. XPS results of PPFMA₃₅-co-PCarMA₆₅: a) survey spectrum, b) C1s core level scan and fitting, c) O1s core level scan and fitting

XPS analysis was carried out to understand deeply the structure of the polymer in powder, which might contribute greatly to the characterization of the polymer grafted to surface in future research. XPS results are presented in Figure 97 and parameters for fitting of C1s and O1s core levels are summarized in Table 22.

Quantification results of atomic percentage from the XPS survey spectrum indicate that the examined polymer is composed of 79.2% C1s, 11.3% O1s, 1.5% N1s, and 8.0% F1s. The presence of N1s is attributed to the residue of DBU remained after reaction. On the other hand, it is seen that the ratio of F/O in PFPMA is 5/2, thus, the amount of O1s originated from PFPMA can be determined to be 3.2%, meaning that the ratio of O1s coming from PFPMA and CarMA is 3.2/8.1 = 2/5, hence, the proportion of PFPMA and CarMA is 28.5% and 71.5% respectively. This value is deviated from 65% conversion in PFPMA substitution with carvacrol estimated by NMR.

C1s core level scan can be deconvoluted into at least 6 major contributors (Figure 97b). In contrast to C1s spectrum of PFPMA (Figure 46), herein, the signal assigned to C-F bond at 288.0 eV is much less intense in overall. In contrast, the amount of C=C (284.5 eV) and C-C/C-H (285.0 eV) are much more pronounced. These observations are in correspondence with the incomplete transition from PFPMA structure into PCarMA structure. Other bonds that have been assigned including C*-CH₃ of backbone at 285.9 eV, C-O at 286.7 eV and carbonyl

COO at 289.1 eV. In addition, deconvolution of O1s shows equal contribution between C=O and C-O bond which is in great agreement with the structure of obtained copolymer.

Table 22. Fitting parameters for deconvolution of C1s and O1s core level scans obtained by XPS of PFPMA_{35-co}-PCarMA₆₅

Core level	Bonding	PFPMA _{35-co} -PCarMA ₆₅		
		BE	FWHM	%
C1s	C=C	284.5	1.50	14.3
	C-C, C-H	285.0	1.65	40.8
	C*-CH ₃	285.9	1.36	11.6
	C-O	286.7	1.50	8.9
	C-F	288.0	1.70	13.8
	COO	289.1	1.86	8.9
	Shake up	290.9	2.27	1.6
O1s	C=O	532.2	2.41	50
	C-O	534.0	2.47	50

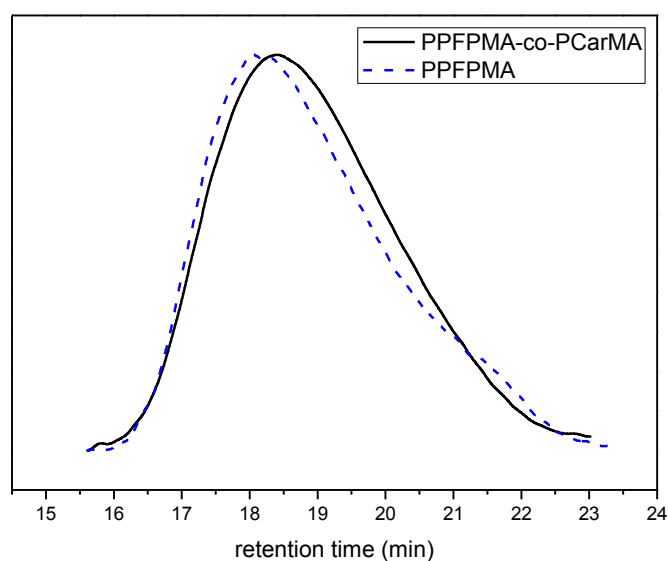


Figure 98. SEC profiles of PFPMA before (dashed line) and after (solid line) reacted with carvacrol, conversion = 65%

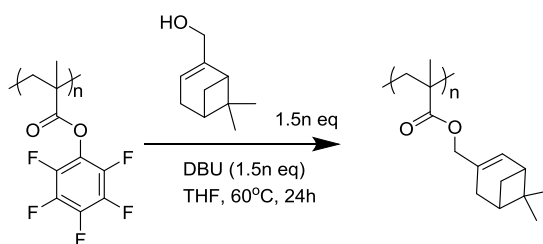
SEC analysis of the polymer before and after post-modification with carvacrol was performed; the profiles of the precursor and final product are shown in Figure 98. As in the case of sesamol, the change from pentafluorophenyl pendant groups into carvacryl pendant groups led to the decrease in molecular weight, even though the transformation was not complete. That decrease in molecular weight is evident as comparing the retention time of

PPFPMA (18.09 minutes) and PFPMA₃₅-co-PCarMA₆₅ (18.47 minutes). Comparing Mn obtained from conventional calibration, the value of PFPMA precursor is 12800 g mol⁻¹ (*D* = 2.48) while the value of the collected polymer after post-modification is 12500 g mol⁻¹ (*D* = 2.29). The decrease in Mn is expected because of the difference between molecular weight of two types of repeating units, *i.e.* PFPMA and PCarMA.

In overall, post-modification of PFPMA with carvacrol as presented and discussed herein was successful. Even though the transformation was incomplete, the structure and chemical environment of the product were confirmed to match with expectations.

4.1.2.4. Myrtenol

Polymer of myrtenyl methacrylate was obtained in literature by classic ATRP [66]. The same study also described that coating of this polymer on glass substrate can help reducing the adhesion of *B. subtilis*. Therefore, the preparation of polymer with similar structure is of our interest herein and has been prepared as shown in Scheme 23. After 24 hours of reaction, a total substitution was achieved and the polymer can be easily precipitated in cold methanol, which might be due to its bulkier structure compared to PCiMA.



Scheme 23. Post-modification of PFPMA with myrtenol

Figure 99 shows ¹H NMR spectrum of poly(myrtenyl methacrylate) (PMyMA) obtained from PFPMA precursor. The 100% modification of PFPMA side chain with myrtenol has resulted in the presence of new peaks in ¹H NMR spectrum. The appearance of these peaks confirms the structure of PMyMA, where two methyl groups of pendant group shown at 0.8 and 1.3 ppm, methylene protons adjacent to ester group appeared at 4.3 ppm, and the ethylenic CH of myrtenol presents at 5.5 ppm.

ATR FTIR of PMyMA is shown in Figure 100. As the conversion of PFPMA into PMyMA was complete, no signal characterized for PFPMA was recorded. Instead, new absorption bands are obtained including the stretching vibration of carbonyl C=O for a non-conjugated ester at 1727 cm⁻¹, the vibration band of C-O bond at 1166 cm⁻¹ and signals characterized for C-H vibration at 2935 cm⁻¹. The presence of these functional groups/bonds fit well with chemical bonds found in PMyMA, indicating the success of PFPMA post-modification with myrtenol.

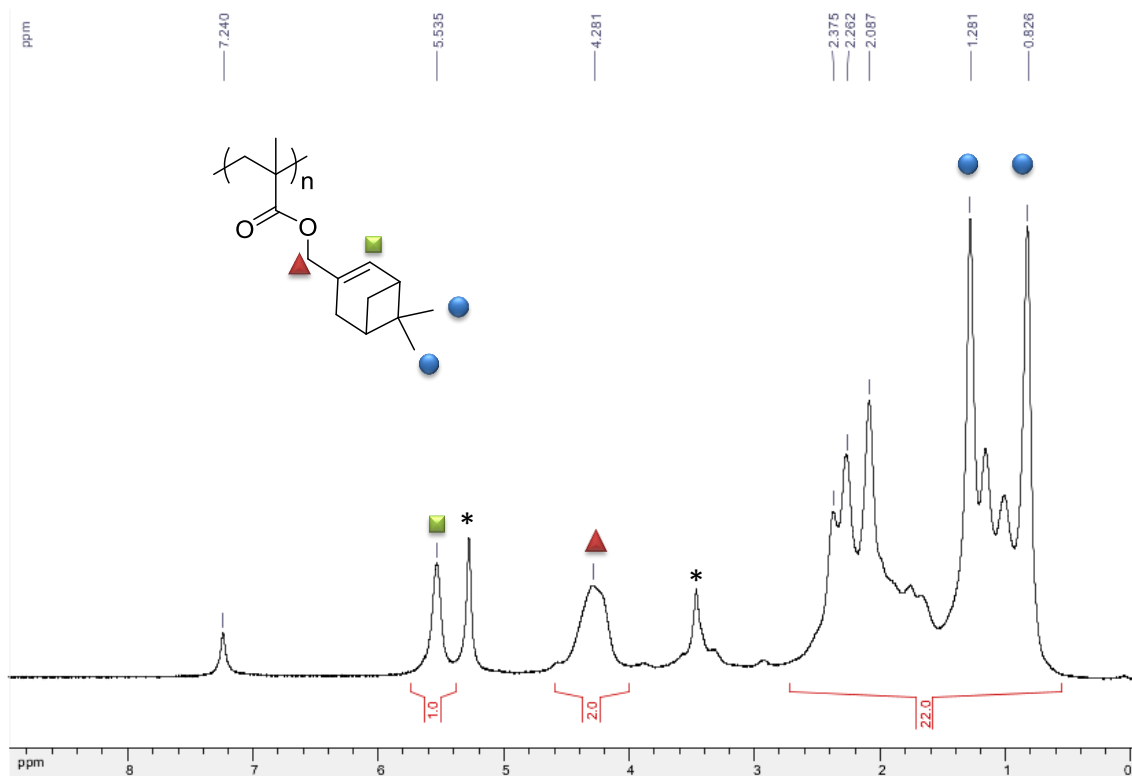


Figure 99. ^1H NMR of PMyMA obtained from post-modification of PPFMA with myrtenol (CDCl_3 , 360 MHz), * indicates solvent residues

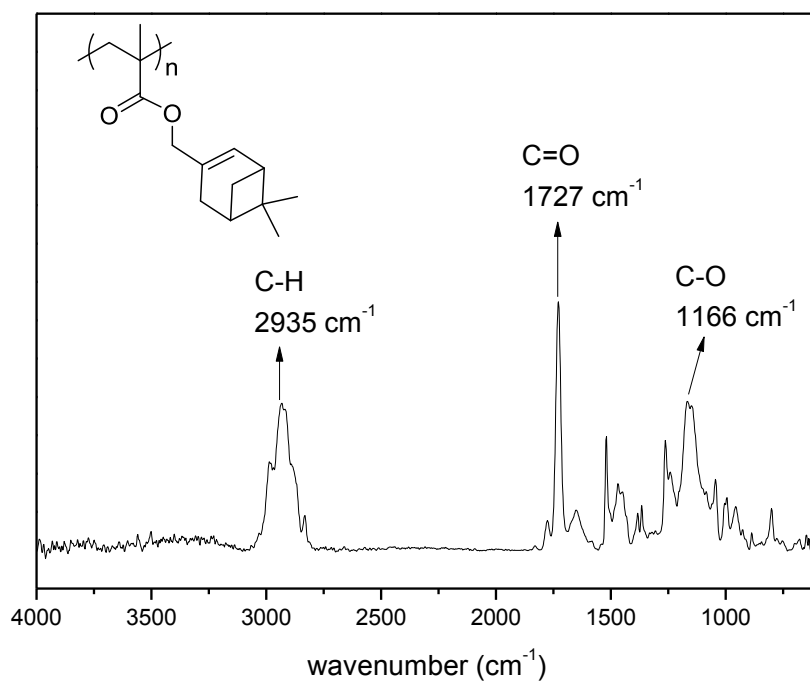


Figure 100. ATR FTIR spectrum of PMyMA

Figure 101 shows results obtained from survey scan and core level scans as well as deconvolution and quantification results of PMyMA. It is seen that a small amount of F1s and N1s is still remained after reaction. However, their residue is quite small (1.5% atomic percentages for each element), thus, the presence of these two elements can be neglected during fitting core level scans. The atomic percentage of C1s and O1s were calculated to be 85.9% and 11.2%, respectively. These values are deviated from theoretical value where atomic percentage of C1s and O1s are 87.5% and 12.5% respectively.

From the chemical structure of PMyMA, the deconvolution of C1s and O1s core level scans are as presented in Figure 101b, c and Table 23. The C1s core level scan can be deconvoluted into at least 5 components including C=C at 284.3 eV, C-C/C-H at 285.0 eV, C*-CH₃ at 285.9 eV, C-O at 287.1 eV and COO at 289.0 eV. In case of O1s core level, deconvolution was perfectly done with equal contributions from C=O at 532.2 eV and C-O at 533.7 eV. It is noteworthy that unlike the case of PSeMA and PCarMA, there is no π - π^* transition (characterized by shakeup intensity) at binding energy higher than 290 eV was recorded for PMyMA due to its possession of only one π -bond.

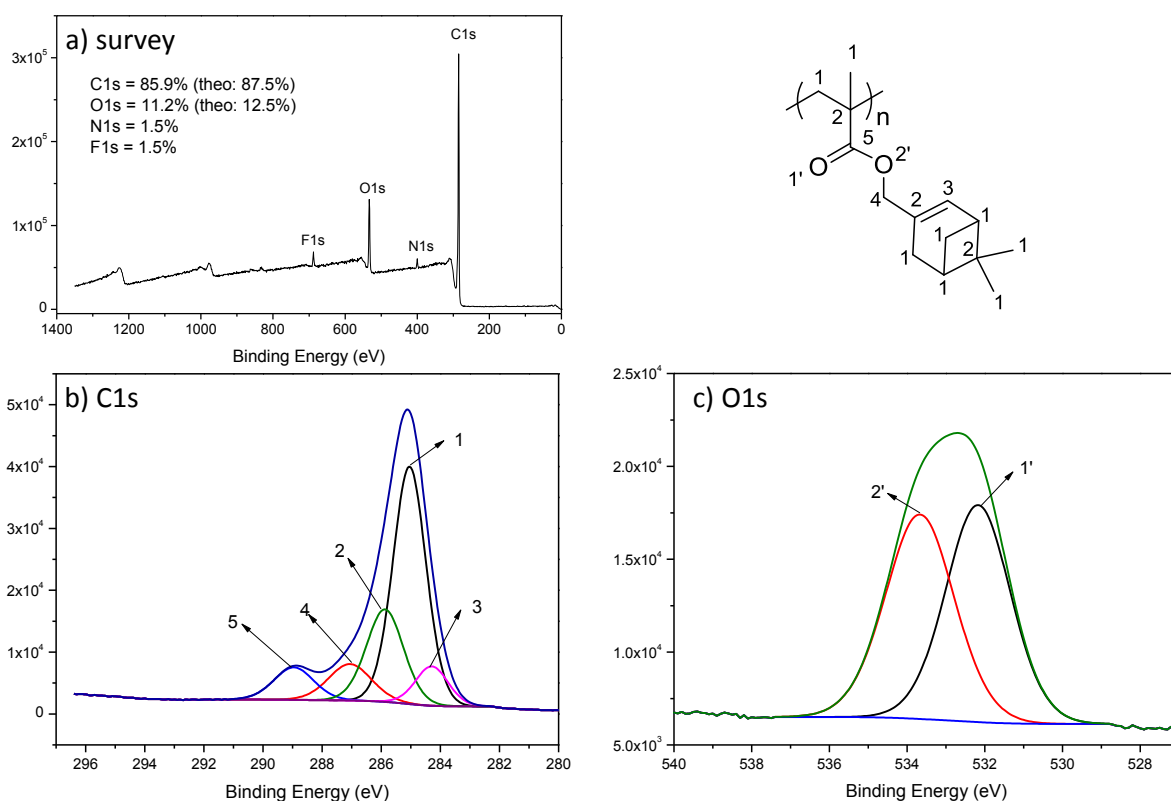


Figure 101. XPS results of PMyMA: a) survey spectrum, b) C1s core level and deconvolution, c) O1s core level and deconvolution

Table 23. Fitting parameters of C1s and O1s core level scans obtained by XPS measurement of PMyMA

Core level	Bonding	PMyMA		
		BE	FWHM	%
C1s	C=C	284.3	1.30	8.4
	C-C, C-H	285.0	1.31	50.9
	C*-CH ₃	285.9	1.47	22.2
	C-O	287.1	1.70	10.1
	COO	289.0	1.58	8.4
O1s	C=O	532.2	1.96	50
	C-O	533.7	2.08	50

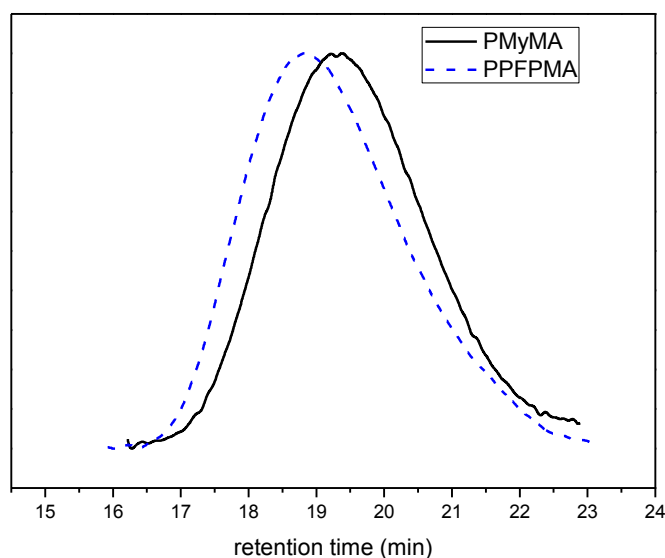


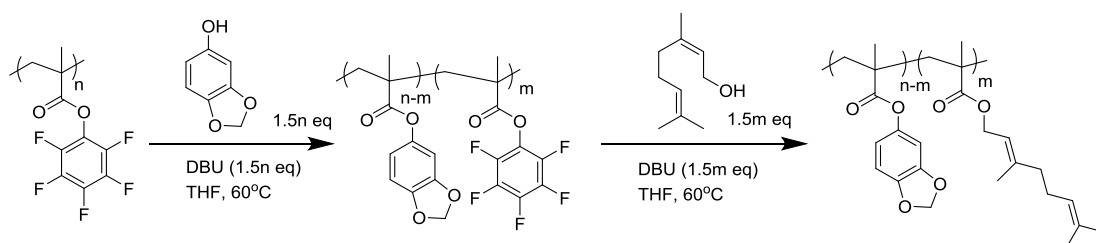
Figure 102. SEC profiles of PPFpMA precursor (dashed) and obtained PMyMA (solid)

SEC profiles of PPFpMA precursor and PMyMA are illustrated in Figure 102. The two profiles are alike in shape of contribution. Furthermore, due to the difference in molecular weight of repeating units in polymer before and after modification, *i.e.* loss in weight by transforming from PPFpMA to PMyMA, PMyMA has higher retention time (19.3 minutes) compared to the reactive polymer (18.8 minutes). In term of number average molecular weight obtained from conventional calibration of PS narrow standards, polymer derived from myrtenol was determined to have a M_n of 9700 g mol^{-1} ($D = 1.73$) while M_n of PPFpMA precursor was determined to be 11500 g mol^{-1} ($D = 1.92$). This change in molecular weight is conformed to expectations as discussed above while the overall dispersity was retained.

In conclusion, the nucleophilic substitution of myrtenol to PPFpMA precursor was successfully performed. All analyses and characterization confirms the modification in chemical structure and molecular weight of the polymers before and after modification.

4.1.2.5. Sequential post-modification with sesamol and geraniol

The final aim is to introduce at will different groups, especially essential oils' derivatives, into one polymer backbone so that one can benefit from their synergic or additive bacterial effects. This can be done by subsequently modification of PPFpMA template. Herein, sequential post-modification of PPFpMA with sesamol and geraniol was demonstrated to be possible and was performed as in Scheme 24.



Scheme 24. Sequential post-modification with sesamol and geraniol

The sequence was performed firstly with sesamol because polymer obtained from the reaction between PPFpMA and sesamol can be easily precipitated at any conversion. This first step was stopped at 50% conversion of transformation between pentafluorophenyl and sesamyl moieties. The obtained polymer (PPFPMA_{50-co}-PSeMA₅₀) was precipitated and later used as template for second step to introduce geranyl moieties. The second modification was successfully accomplished with complete conversion, thus the copolymer PSeMA_{50-co}-PGeMA₅₀ was obtained.

Figure 103 presents ¹H NMR of PPFpMA_{50-co}-PSeMA₅₀ (top) and PSeMA_{50-co}-PGeMA₅₀ (bottom). It is seen that all the peaks characterized for both PSeMA and PGeMA are shown. By comparing the ratio between protons of side chains originated from SeMA and GeMA, the proportion of the two can be estimated to be approximately 50:50.

This example of sequential post-modification presents the possibility to achieve our goal of introducing at will different functional groups to one single polymer chain.

On the other hand, as PPFpMA is highly reactive and its post-modification has been demonstrated to proceed up to 100% conversion for primary alcohols and sesamol, attempts to carry out the dual post-modification with sesamol and geraniol has been implemented.

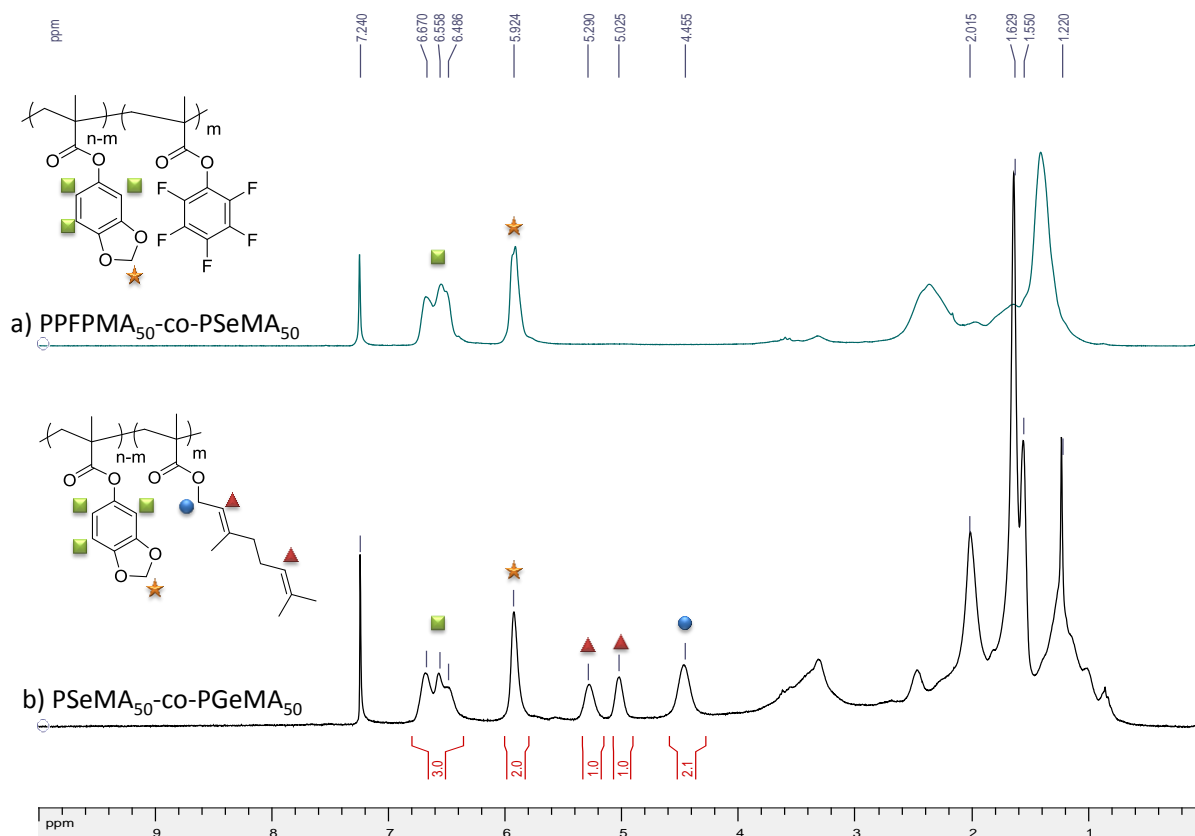
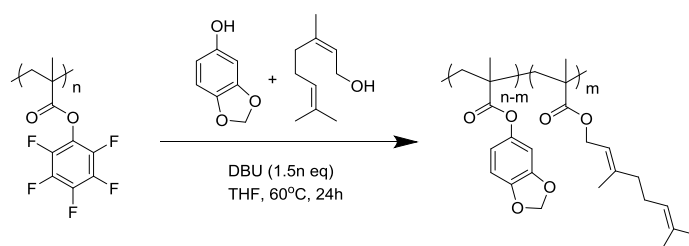


Figure 103. ^1H NMR of a) PPFMA₅₀-co-PSeMA₅₀ and b) PSeMA₅₀-co-PGeMA₅₀

4.1.2.6. Dual post-modification of sesamol and geraniol

Dual post-modification of PPFMA with sesamol and geraniol was firstly tested with equimolar of the two alcohols.



Scheme 25. Dual post-modification of PPFMA with sesamol and geraniol

After 24 hours of reaction, total conversion was achieved and the polymer was obtained by direct precipitation of reaction mixture in cold methanol. Figure 104a presents ^1H NMR spectrum of copolymer PSeMA-co-PGeMA obtained from dual PPFMA post-modification with initial equimolar of sesamol and geraniol. By comparing signals originated from sesamyl moieties at 5.9 ppm (2H) and \approx 6.5 ppm (3H) to geranyl moieties at 5.2 ppm (1H), 5.0 ppm (1H) and 4.4 ppm (2H), the ratio between two types of repeating units was estimated to be [Se]: [Ge] = 4:1.

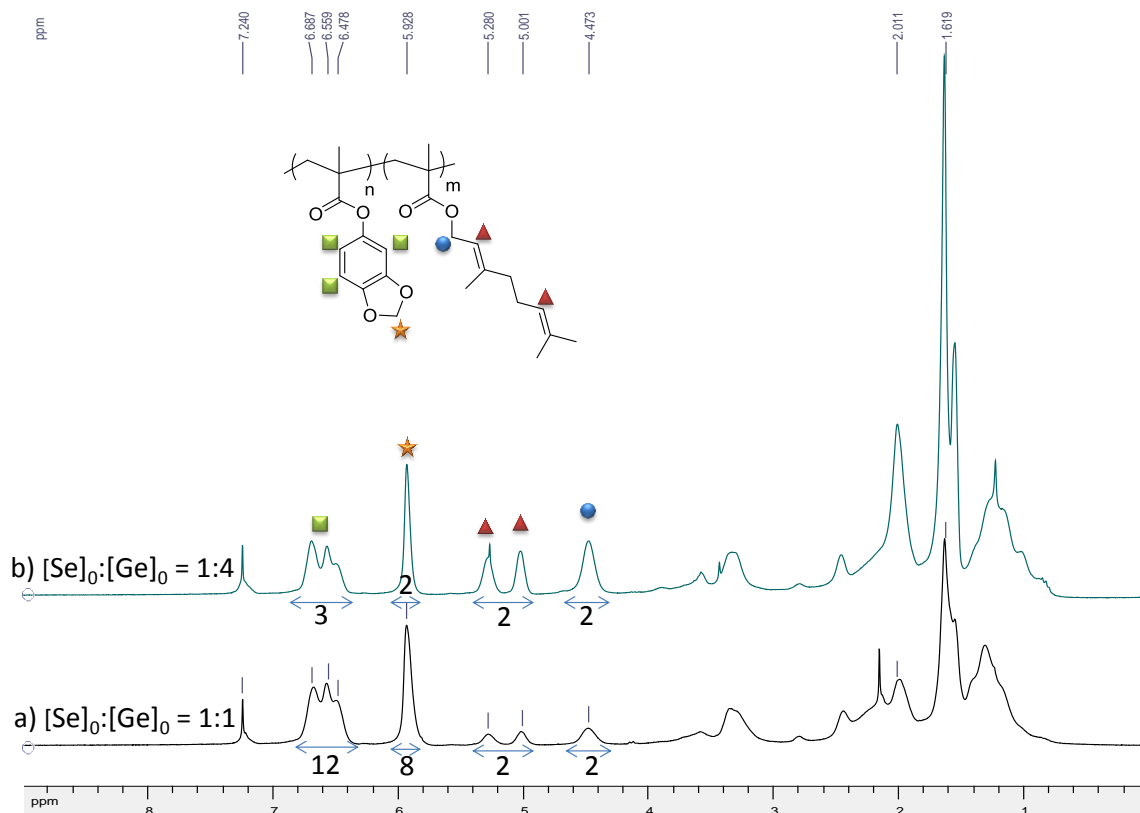


Figure 104. ^1H NMR spectra of polymer obtained from dual post-modification of PPFMA with a) $[\text{Sesamol}]_0:[\text{Geraniol}]_0 = 1:1$, and b) $[\text{Sesamol}]_0:[\text{Geraniol}]_0 = 4:1$

The deviation between ratio of sesamol and geraniol in feed and ratio in obtained polymer can be attributed to their different reactivity of the two alcohols in nucleophilic substitution reaction. Indeed, in DBU media, phenol sesamol hydroxyl ($\text{pK}_a \approx 9,8$) is deprotonated, leading in a phenolate ion more reactive while hydroxyl of geraniol with higher pK_a is more or less no deprotonated ($\text{pK}_a > 16$). The substitution kinetic is thus not comparable. This hypothesis was confirmed by a post-modification reaction where initial concentration of geraniol is 4 times higher than that of sesamol. Under that condition, the ratio between sesamyl and geranyl moieties in obtained copolymer was determined to be 1:1, as seen in Figure 104b.

In addition, the change in proportion between SeMA and GeMA in copolymer also led to the change in state of copolymer. When SeMA takes 80%, the copolymer is obtained in white solid powder; on the other hand, at equimolar ratio of SeMA and GeMA, the copolymer is obtained as a viscous fluid. This difference may be due to that the linear geranyl moieties are more flexible than the sesamyl moieties.

ATR FTIR spectrum of $\text{PSeMA}_{80}\text{-co-PGeMA}_{20}$ obtained from PPFMA dual post-modification is presented in Figure 105a. The whole spectrum resembles that of PSeMA (Figure 105b), yet the presence of 20% of PGeMA is recognized by the appearance of a shoulder at 1720 cm^{-1} .

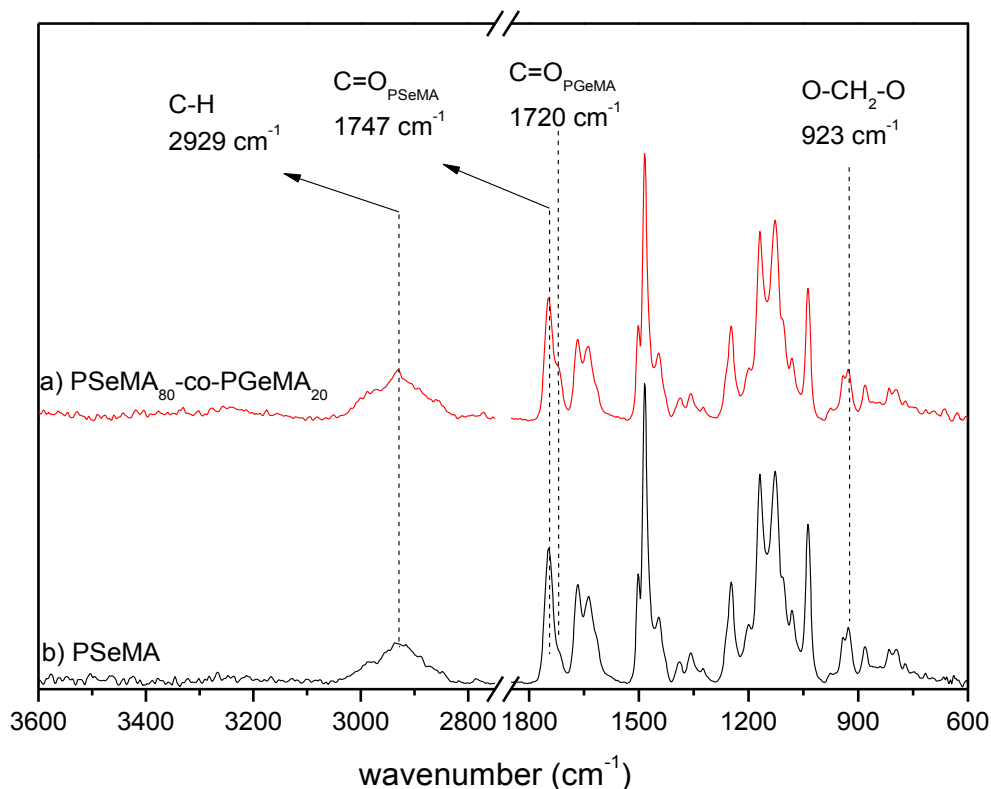


Figure 105. ATR FTIR spectra of a) PSeMA_{80-co}-PGeMA₂₀, and b) PSeMA as reference

XPS was also performed on PSeMA_{80-co}-PGeMA₂₀ and results are presented in Figure 106 and Table 24.

C1s and O1s atomic percentage calculated from XPS survey spectrum are 80.0% and 17.3% respectively, giving a ratio between C1s and O1s of 4.6. In comparison to the C/O ratio in PSeMA of ≈ 3.9 (76.9/19.5), the ratio of C/O in PSeMA_{80-co}-PGeMA₂₀ is higher, indicating larger proportion of C1s. This difference is reasonable as the PGeMA itself has higher C/O ratio than PSeMA with two extra oxygens. The deconvolutions of C1s and O1s core levels of PSeMA_{80-co}-PGeMA₂₀ are similar to PSeMA. However, in C1s core level deconvolution, it is seen that the proportion of C-C/C-H in the copolymer increases compared to the homopolymer of SeMA, owing to the presence of the carbon-rich GeMA moieties. The shakeup satellite is still visible because the copolymer is rich of SeMA moieties. XPS results confirms that the obtained copolymer PSeMA_{80-co}-PGeMA₂₀ comprises of all chemical functions as expected from NMR and ATR FTIR.

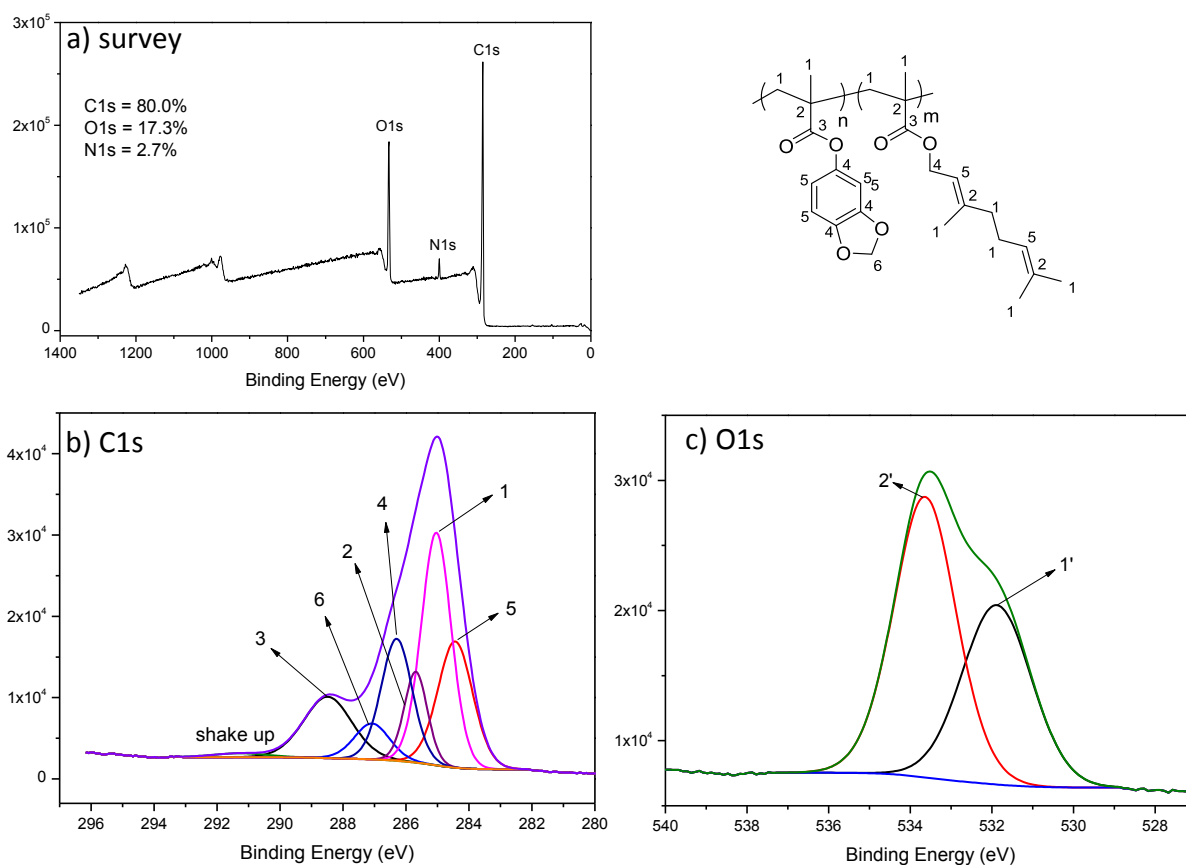


Figure 106. XPS results of PSeMA₈₀-co-PGeMA₂₀ : a) survey spectrum, b) C1s core level and deconvolution, c) O1s core level and deconvolution

Table 24. Fitting parameters of C1s and O1s core level scans obtained by XPS measurement of PSeMA₈₀-co-PGeMA₂₀

Core level	Bonding	PSeMA ₈₀ -co-PGeMA ₂₀		
		BE	FWHM	%
C1s	C=C	284.4	1.30	20.3
	C-C, C-H	285.0	1.12	32.2
	C*-CH ₃	285.7	0.86	9.7
	C-O	286.3	1.15	17.4
	O-CH ₂ -O	287.1	1.31	5.8
	COO	288.5	1.79	13.6
	Shake up	291.3	1.99	1.0
O1s	C=O	531.9	2.0	41.2
	C-O	533.6	1.80	58.8

4.1.2.7. Conclusions

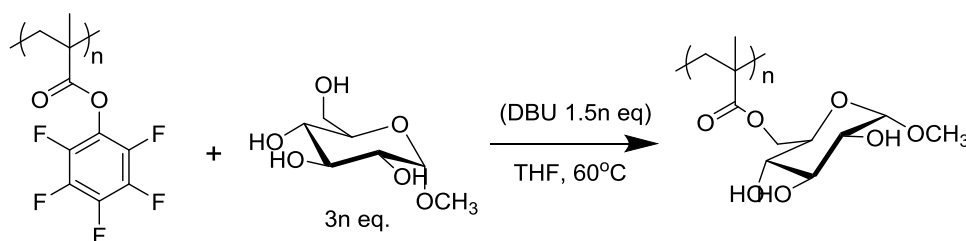
Several experiments of PFPMA post-modification with essential oils were successful and discussed in this section 4.1.2. In general, it is seen from these results that the post-modification of reactive template can be carried out with alcohol of different order and chemical structures. In most of the cases, PFPMA substitution with alcohol can proceed to complete conversion with the use of 1.5 to 3.0 equivalents of the alcohol, 1.5 equivalent of DBU as base catalyst in either DMF at 80 °C or THF at 60 °C. The post-modification process was demonstrated not only to allow single molecule substitution, thus, sequential post-modification but also to enable dual post-modification. From the example of dual post-modification with sesamol and geraniol, it is seen that, by tuning molar ratio between alcohols in dual post-modification based on their nucleophilic reactivity, one can alter the ratio between two components in final product.

4.1.3. Post-modification with sugars and their derivatives

As discussed before in section 1.1.2.2.a), hydrophilic polymers in general and glycopolymers in particular have been investigated widely in preparation of antimicrobial surfaces. On the other hand, due to the possibility to modified PFPMA with an alcohol – which is the chemical possession of saccharides, it is believed that the polymer derived from saccharides can be obtained via the post-modification of PFPMA with natural saccharides and also their derivatives.

4.1.3.1. Post-modification with methyl α -D-glucopyranoside

The post-modification of PFPMA with methyl α -D-glucopyranoside was performed as a model as described in Scheme 26. After 20 hours of reaction, 100% conversion was achieved. The poly(methyl α -D-glucopyranosyl methacrylate) (PMGluMA) was obtained from precipitation in Et₂O as white powder soluble in methanol.



Scheme 26. PFPMA post-modification with methyl α -D-glucopyranoside

Figure 107 compares ¹H NMR spectra between 3 – 5 ppm of methyl α -D-glucopyranoside (a) and PMGluMA (b) obtained from PFPMA post-modification.

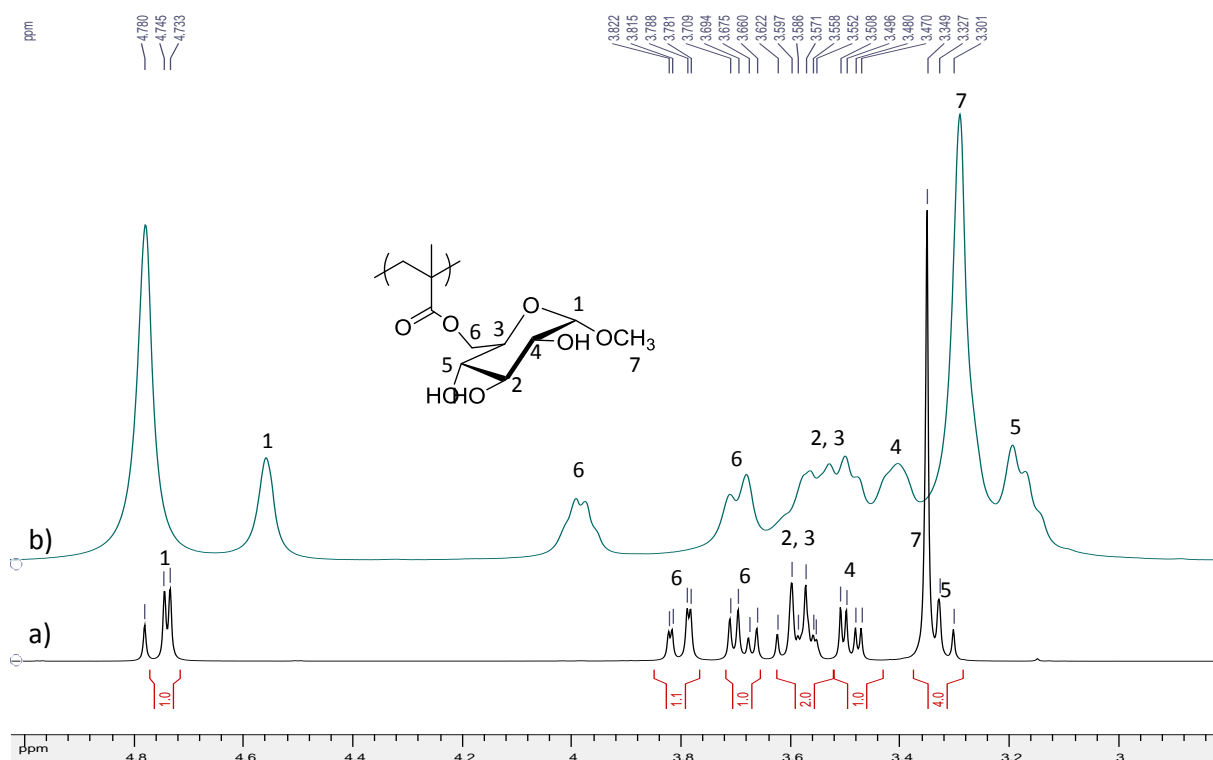


Figure 107. ^1H NMR spectra of a) methyl α -D-glucopyranoside (D_2O , 360 MHz) and b) PMGluMA (MeOD, 360 MHz)

All protons found in methyl α -D-glucopyranoside are also found in PMGluMA. However, there is a shift in position of protons at C1 to lower intensity. More importantly, the signal of 1 proton of C6 is shifted from ≈ 3.8 to ≈ 4.0 ppm, this shift is due to the change in chemical nature of that carbon (from linking to a hydroxyl group to an ester group). The shift of protons at C6 reassures that the replacement of pentafluorophenyl group with the glucose moieties was successful, and confirms that primary hydroxyl is the mainly reactive position as expected.

ATR FTIR measurement also confirmed the success of post-modification. As presented in Figure 108, ATR FTIR spectrum of obtained PMGluMA shows signals that are in great agreement with the chemical structure of the polymer. First of all the signals characterized for PFPMA are absent, especially the $\text{C}=\text{O}$ of ester of PFPMA at 1779 cm^{-1} is totally diminished and the $\text{C}=\text{O}$ in PMGluMA is present at 1724 cm^{-1} . The glycopolymer is rich with hydroxyl group represented by its broad stretching band at 3286 cm^{-1} . C-O stretching vibration of ester, ether/alcohol is also observed at 1141 cm^{-1} and 1033 cm^{-1} respectively.

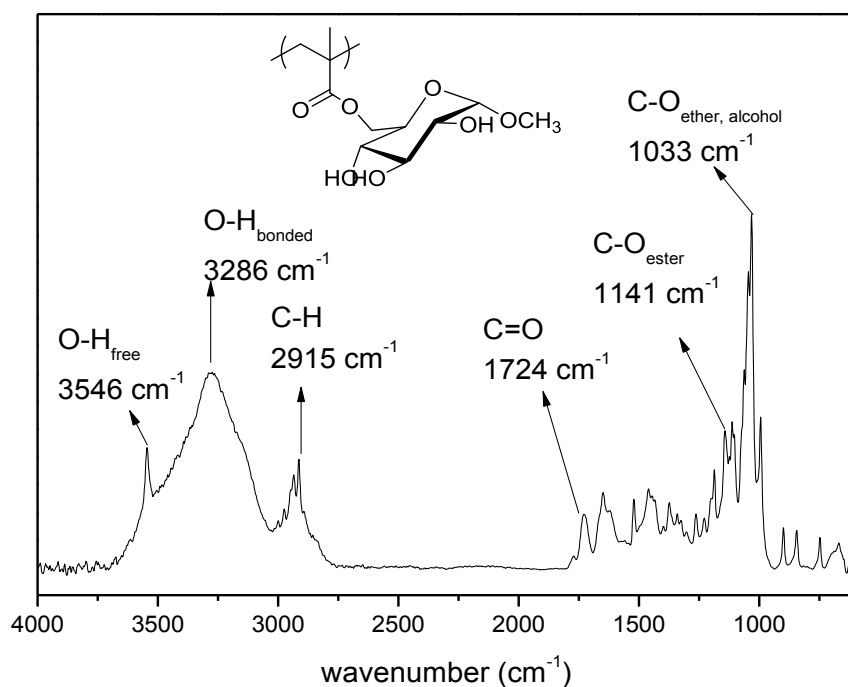


Figure 108. ATR FTIR spectrum of PMGluMA

XPS measurement was also performed to have another point of view on structure of PMGluMA. Figure 109 and Table 25 summarize results obtained XPS measurement as well as fitting parameters for C1s and O1s of PMGluMA.

It is seen from Figure 109a that the sample contains a small amount of retained N1s and F1s. These may be attributed to DBU and PFPMA residues either from pentafluorophenol or PFPMA itself. Due to the presence of these residues, the atomic percentage of C1s and O1s in obtained PMGluMA is slightly different compared to theoretical values which can be calculated from the structure to be 61.1% C1s and 38.8% O1s.

Additionally, as presented in Figure 109b, c, fitting results of C1s and O1s core levels can be done nearly perfectly by neglecting the presence of N1s and F1s and considering only the chemical structure of PMGluMA. C1s deconvolution was done by taking into account 3 mains type of carbons, including aliphatic C-C/C-H at 285.1 eV, ether C-O at 286.4 eV and carbonyl C=O at 288.1 eV. On the other hand, O1s core level scan can be deconvoluted into at least 3 different contributors including C=O at 531.2 eV, C-O at 533.2 eV and O-H at 532.5 eV.

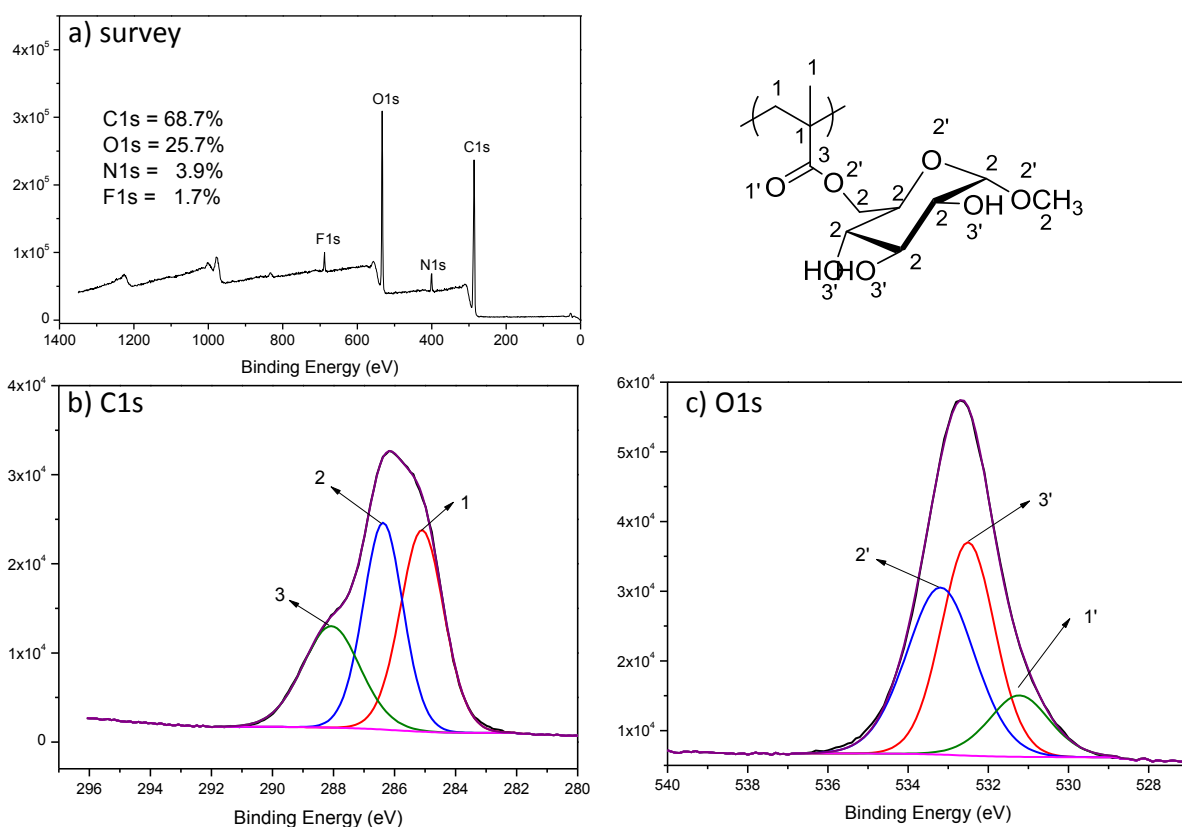


Figure 109. XPS results of PMGluMA : a) survey spectrum, b) C1s core level and deconvolution, c) O1s core level and deconvolution

Table 25. Fitting parameter of C1s and O1s core level scans in XPS measurements

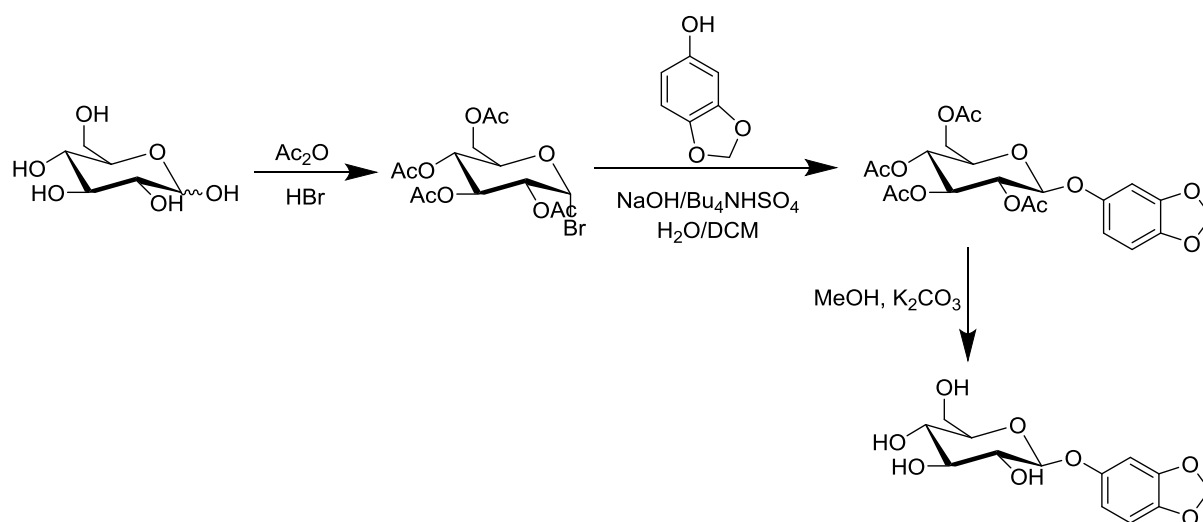
Core level	Bonding	PMGluMA		
		BE	FWHM	%
C1s	C-C, C-H	285.1	1.68	38.6
	C-O	286.4	1.53	35.9
	COO	288.1	2.21	25.5
O1s	C=O	531.2	1.77	14.2
	C-O	533.2	2.00	42.9
	O-H	532.5	1.57	42.9

Results from NMR, ATR FTIR and XPS confirm that even though there is a small quantity of impurity, in general, the chemical structure of PMGluMA prepared by PPFMA post-modification with methyl α -D-glucopyranoside is in great agreement with expected chemical structure.

4.1.3.2. Post-modification with sesamyl β -D-glucopyranoside

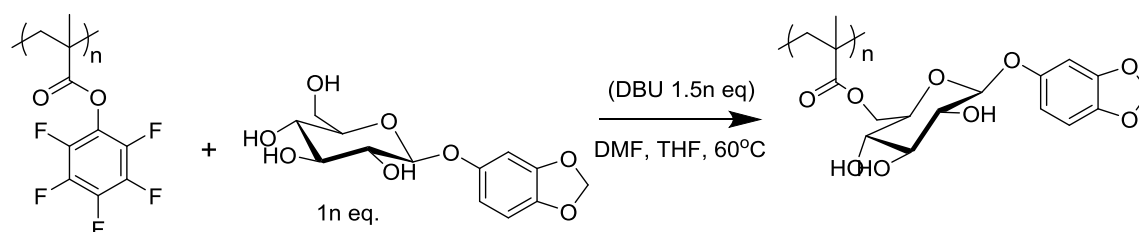
Taking advantage of our team's expertise in chemistry of saccharides, a compound derived from sesamol and β -D-glucopyranoside was prepared as given in Scheme 27.

The sesamyl β -D-glucopyranoside was prepared in three steps from D-glucopyranose. First, α -D-bromoglucopyranoside was afforded by acetylation in hydrobromic acid media, then treated with the phenolate ion promoted by sesamol in presence of sodium hydroxide media, the α -bromo derivative underwent a nucleophilic substitution generating the peracetylated sesamyl β -D-glucopyranoside. β -anomer was selectively afforded due to the neighboring participation of acetyl substituent in position 2. A byproduct was also isolated in the media, due to the β -elimination of the anomeric bromide generating a 2-acetyl glycal derivative, highlighting the low yield of the transformation. Acetyl substituents were removed by transesterification to afford expected sesamyl β -D-glucopyranoside.



Scheme 27. Synthesis of sesamyl β -D-glucopyranoside

Post-modification of PPFMA with sesamyl β -D-glucopyranoside was performed as given in Scheme 28.



Scheme 28. Post-modification of PPFMA with sesamyl β -D-glucopyranoside

The first attempt to carry out the reaction in anhydrous THF was not successful as the reaction mixture was not homogeneous, indicating that the solubility of reagents is an important factor.

Thus, a mixture of THF and DMF was used so that all reagents were soluble prior adjusting reactor to preheated 60 °C oil bath. After 96 hours of reaction, a total conversion was achieved and the reaction mixture was precipitated directly in diethyl ether. Even though the polymer was not purified to eliminate all residues from reagents and catalyst, ¹H NMR spectrum of obtained product reassemble the peaks found in PSeMA and PMGluMA as presented in Figure 110. First of all, methylenedioxy of sesamyl group is present at 5.8 ppm (-O-CH₂-O-) and the phenylic protons are observed at 6.6 ppm. Additionally, a broad range of intensities between 2.8 ppm and 4.0 ppm are assigned to protons originated from glucose moieties of the polymer. The appearance of these signals confirmed that the post-modification process was successful.

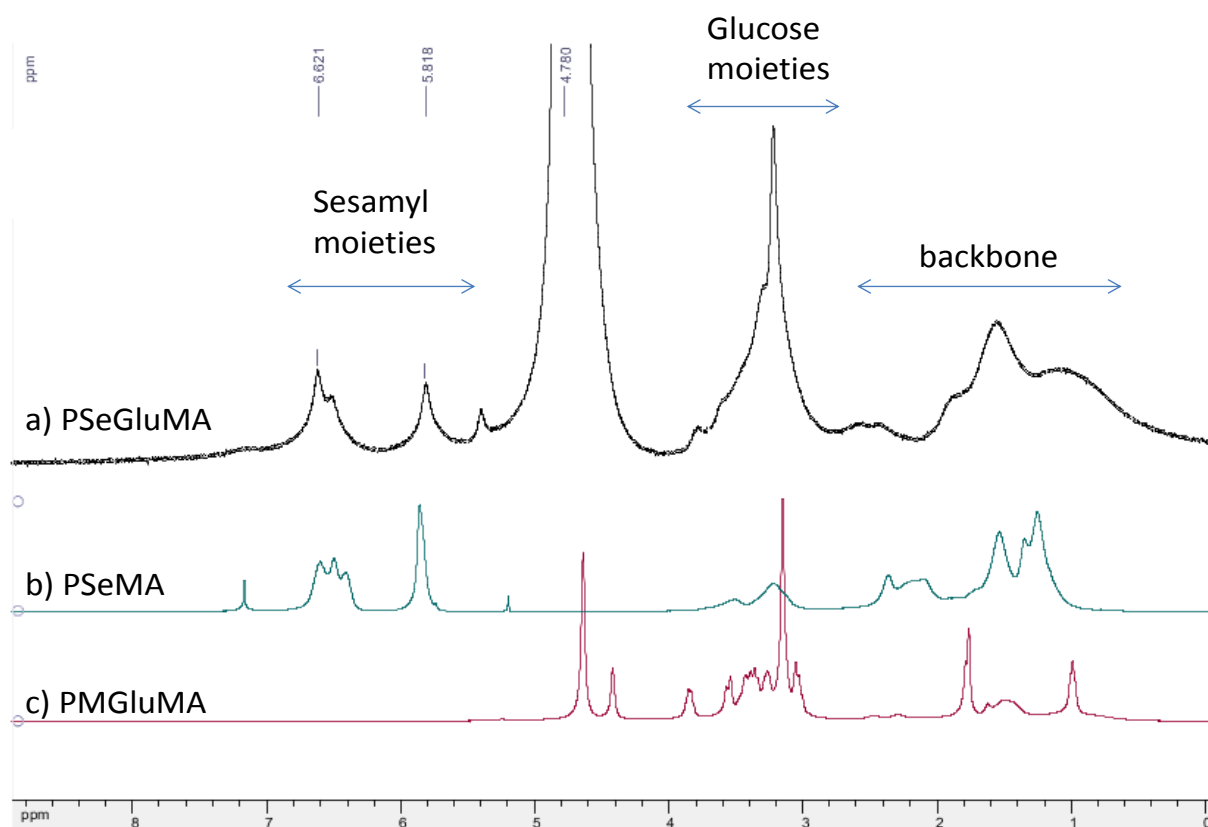


Figure 110. ¹H NMR spectra of a) PSeMA (CDCl₃, 360 MHz), b) PMGluMA (MeOD, 360 MHz), and c) PSeGluMA (MeOD, 360 MHz).

ATR FTIR of the product was done to evaluate the chemical structure of PSeGluMA. Figure 111 compares the spectrum of three polymers: PSeMA, PMGluMA and PSeGluMA.

As PSeGluMA is the polymer derived from both sesamol and D-glucopyranoside, its spectrum is composed of characteristic peaks of both PSeMA and PMGluMA. The specified peak of methylenedioxy of sesamol is clearly shown at 927 cm⁻¹ in spectra of PSeMA and PSeGluMA while this peak is absent in PMGluMA. In addition, the stretching intensity at 1484 cm⁻¹ of methylenedioxy is also observed for the two polymers derived from sesamol. On the other hand, the stretching vibration of C=O at 1729 cm⁻¹ in both PMGluMA and

PSeGluMA confirms that the ester bond is next to the sugar moieties. More importantly, a broad absorption at 3276 cm^{-1} indicates the presence of many hydroxyl groups, hence, confirming the presence of sugar moieties in PSeGluMA.

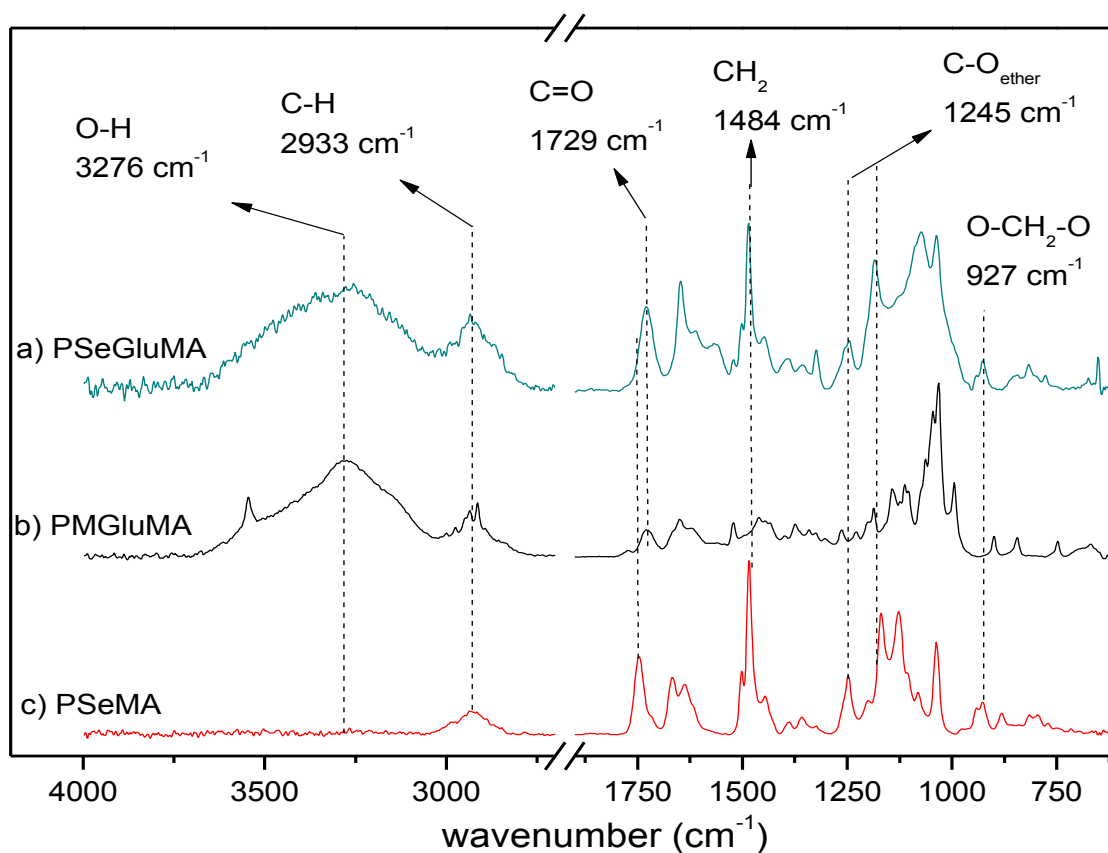


Figure 111. ATR FTIR spectra of a) PSeGluMA, b) PMGluMA, and c) PSeMA

Overall, the “crude” ^1H NMR spectrum and ATR FTIR spectrum of PSeGluMA in comparison with that of PSeMA and PMGluMA present that the post-modification of PPFMA with sesamyl β -D-glucopyranoside was successful.

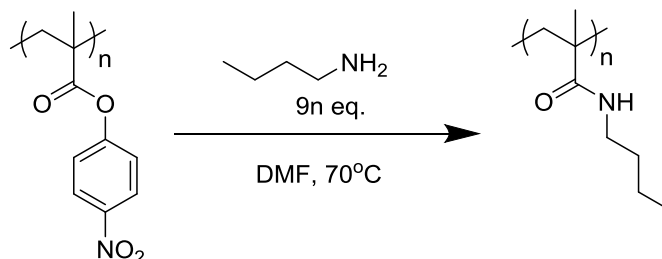
4.1.1. Conclusion

In conclusion, this section has provided results and discussion on the post-modification of PPFMA with various types of compounds containing different nucleophilic source for substitution. It is confirmed the huge possibility to prepare functional polymer from PPFMA templates with molecules of simple to complex structure.

4.2. Post-modification of PNPMA

4.2.1. Post-modification with amines

Post-modification of PNPMA was performed firstly with *n*-butylamine as presented in Scheme 29.



Scheme 29. Post-modification of PNPMA with *n*-butylamine

After 48 hours, a conversion of 100% was obtained proven by the total diminution of peaks characterized for phenylic protons at 7.3 ppm and 8.0 ppm (Figure 112b).

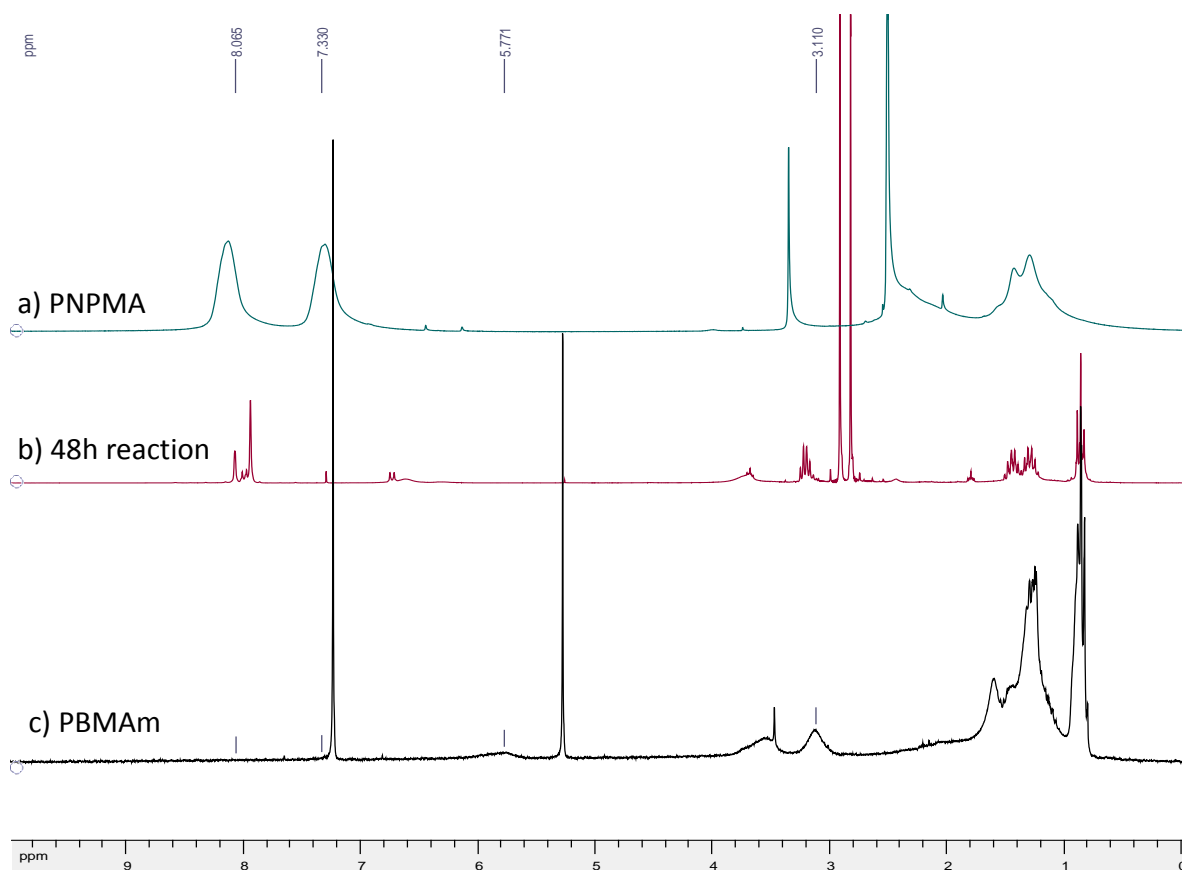


Figure 112. ¹H NMR of a) PNPMA, b) reaction mixture after 48 hours, and c) PBMAm

From Figure 112a and Figure 112c, ¹H NMR spectra of PNPMA and PBMAm are well discriminated. PNPMA is characterized by phenylic peaks at 7.3 ppm and 8.0 ppm originated

from *p*-nitrophenyl groups. On the other hand, peaks characterized for methylene adjacent to amide bond is observed between 3.0 ppm to 3.8 ppm in spectrum of PBMAm. Furthermore, the introduction of an alkyl chain as pendant groups enhances the intensity of aliphatic protons between 0.8 ppm to 2.0 ppm.

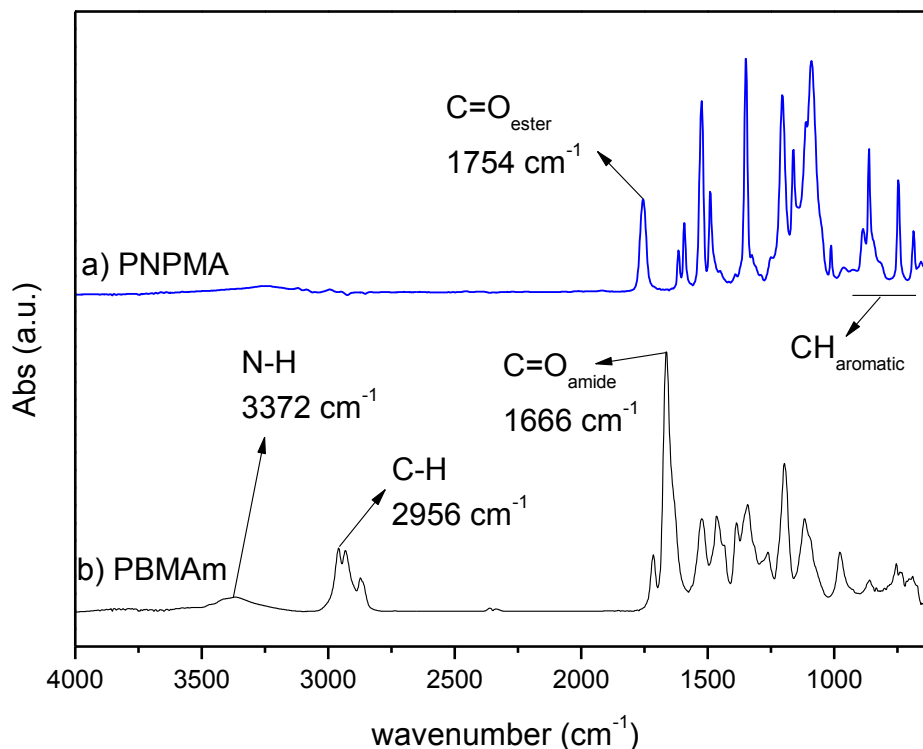


Figure 113. ATR FTIR spectrum of a) PNPMA and b) PBMAm

ATR FTIR spectra of the two materials also confirmed the change in chemical environment of the polymer before and after nucleophilic substitution: Instead of showing a vibration of C=O of NPMA at 1754 cm^{-1} , PBMAm has a vibration band of C=O at lower wavenumber of 1666 cm^{-1} due to the change from an ester to an amide bond. Moreover, the broad absorption intensity at 3372 cm^{-1} indicates the presence of an N-H bond while the peak at 2956 cm^{-1} specifies the presence of aliphatic C-H. Additionally, the C-H in aromatic ring of NPMA is specified by peaks at lower than 1000 cm^{-1} while these intense peaks disappeared in spectrum of PBMAm. These characteristic differences in the spectra of the two polymers indicate a total conversion from NPMA monomer unit to BMAM monomer unit (Figure 113).

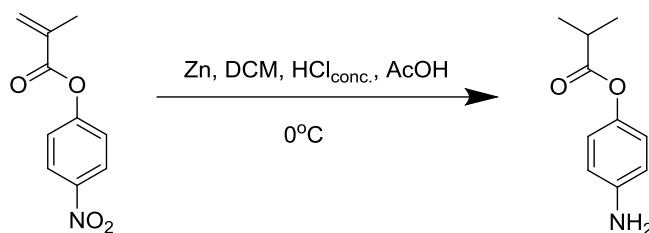
In conclusion, ^1H NMR and FTIR spectra of polymer before and after reaction clearly demonstrate the success in the nucleophilic substitution of PNPMA with *n*-butylamine.

4.2.2. Reduction of nitro groups

The reduction of nitro groups is one of attractive reactions of *p*-nitrophenyl compounds that have been widely used for numerous applications [343-345]. As the possession of aminophenyl group on polymer chain may increase the pool of reaction for post-modification,

an attempt to investigate the possibility to reduce the nitrophenyl group of NPMA as given in Scheme 30. Active hydrogen was generated *in situ* from zinc metal in mixture of acetic acid and concentrated hydrochloric acid. This approach was chosen because it is easy to perform and have also proven its efficiency in literature [346].

As nitrophenyl methacrylate is not soluble in the reaction medium, a small amount of dichloromethane was added. The reaction was carried out under heterogeneous yet fully liquid condition with vigorous stir.



Scheme 30. Reduction of nitro groups of NPMA monomer

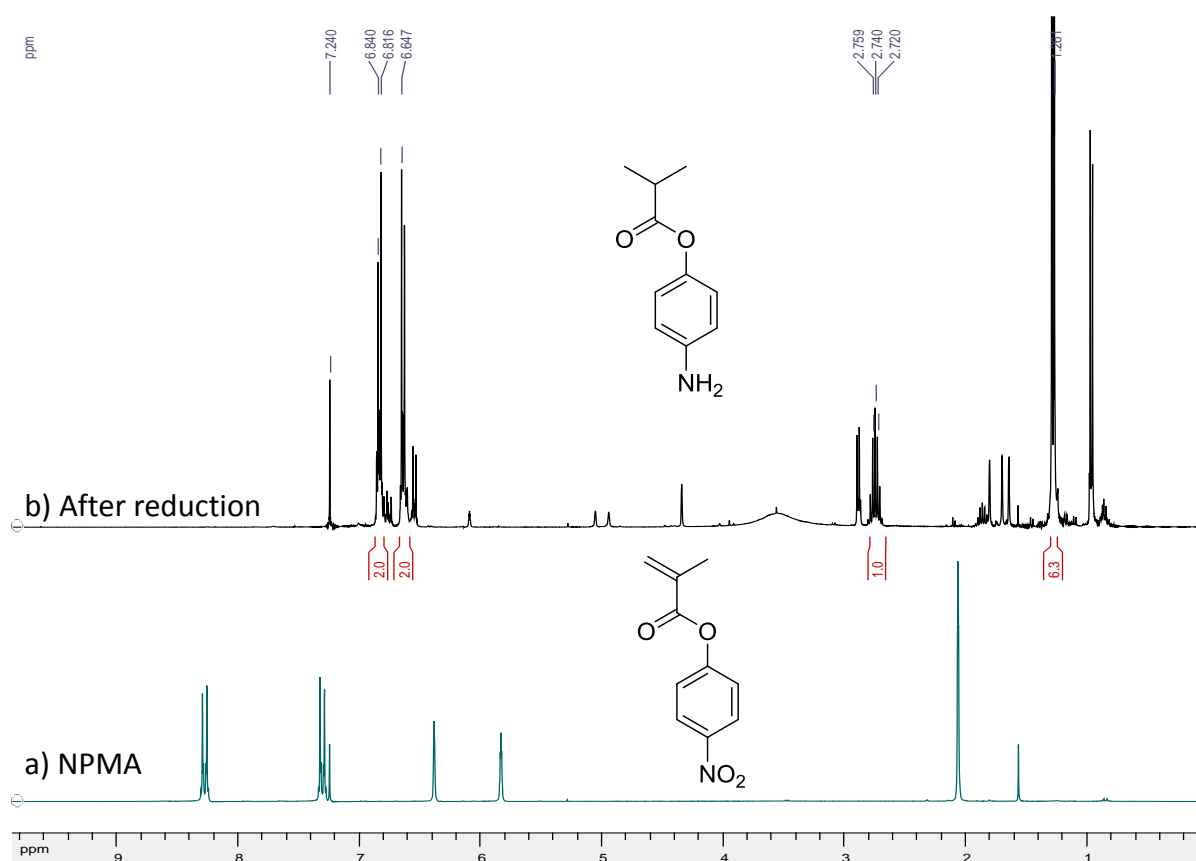
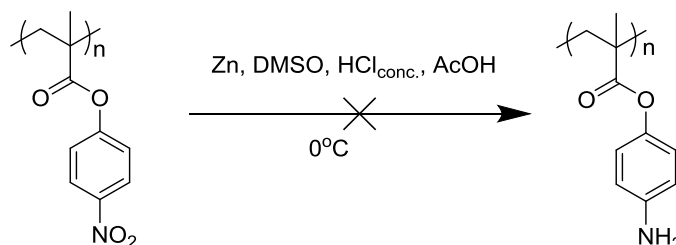


Figure 114. ¹H NMR spectrum of a) NPMA and b) product obtained after reduction of nitro groups (CDCl₃, 360 MHz).

Figure 114 shows ¹H NMR spectra of NPMA monomer and the product obtained after reduction of nitro groups. After reaction, the peaks characterized for phenylic protons of NPMA (7.3 ppm and 8.2 ppm) were disappeared. Instead, new peaks which are considered to

be phenylic protons of 4-aminophenyl compounds are present at 6.6 ppm and 6.8 ppm. Additionally, the two methylene intensity specified the double bond of NPMA were also diminished due to the reduction of alcene functions with hydrogen. The reduction of double bond was confirmed by the appearance of a peak at 2.7 ppm (R_3C-H) and the shift in position (~ 2.0 ppm to 1.2 ppm) and increase in integration of methyl peaks.



Scheme 31. Reduction of nitro groups of PNPMA

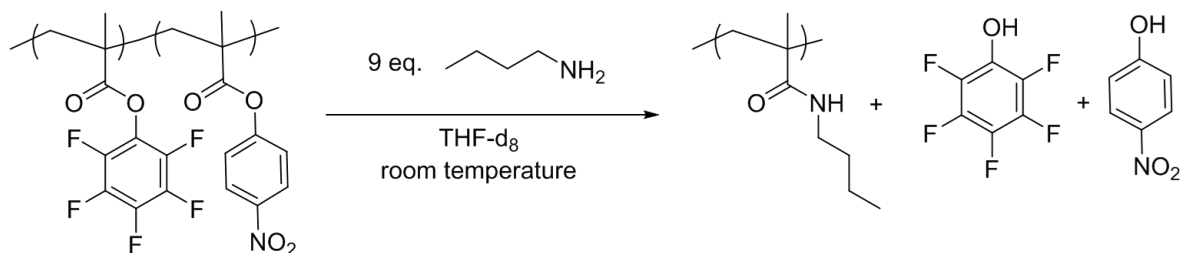
Taking advantage of the success in reduction of nitro groups of NPMA, the reduction was carried out on NPMA's polymer (Scheme 31). Like its monomer, PNPMA is not soluble in acetic acid/HCl mixture, therefore, the polymer was solubilized in DMSO prior to reaction. Unfortunately, despite of an excessive amount of DMSO used, the polymer precipitated upon introduction of concentrated HCl to reaction. The reduction was not successful probably due to the lack of solubility.

4.2.3. Conclusion

In conclusion, the success in post-modification of PNPMA with *n*-butylamine confirms the polymer reactivity towards nucleophilic substitution. Reduction of nitro groups was carried out for both monomer and polymer of NPMA. While the reaction was successful for monomer, yet the low solubility of polymer is believed to be the cause that no reduction was observed.

4.3. Post-modification of copolymers

As mentioned above, nucleophilic substitution of PNPMA and PFPMA with *n*-butylamine is easily performed. Both reactive polymers reacted to 100% conversion in large excess of the amine. Thus, copolymers of NPMA and PFPMA were also examined in the same manner to investigate the expected difference in reactivity of the two monomer units. The post-modification was carried out as given in Scheme 32.



Scheme 32. Post-modification of PFPMA-*co*-PNPMA with *n*-butylamine

Table 26 summarizes conversion of NPMA and PFPMA when the copolymers were reacted with large excess of *n*-butylamine. Conversion of NPMA was calculated from ¹H NMR spectrum while conversion of PFPMA was calculated by ¹⁹F NMR.

Table 26. Results of copolymers substitution with *n*-butylamine

	time	conversion (%) (NMR)	
		NPMA (¹ H)	PFPMA (¹⁹ F)
copo1N2F-68	24 h	54	100
copo1N1F-68	30 min	7	100
copo2N1F-68	24 h	63	100

From results listed in Table 26, it is seen that regardless of copolymer compositions, all PFPMA units have completely reacted with *n*-butylamine while NPMA was substituted partially to around 50-60% after 24 hours.

To gain deeper understanding on the reactivity of the two leaving group, a kinetic study of substitution was carried out for copo2N1F. Figure 115 presents kinetics of *n*-butylamine substitution with copo2N1F. The substitution to PFPMA moieties is much faster than substitution to NPMA. It took around 10 hours to achieve 100% conversion of PFPMA while only 50% of NPMA has been then substituted.

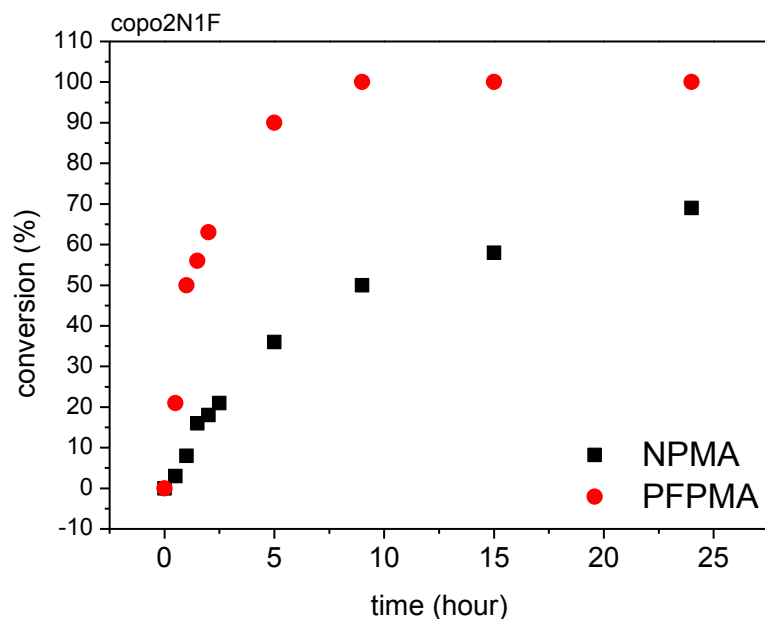
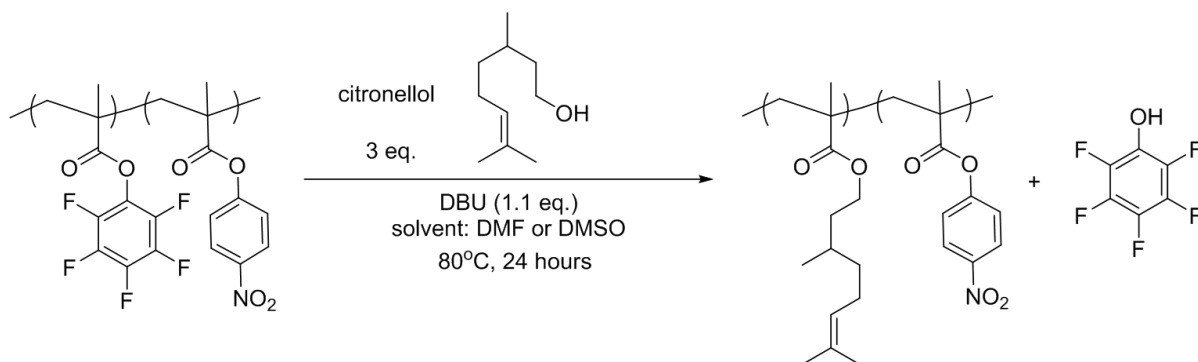


Figure 115. Kinetics of *n*-butylamine substitution with copo2N1F

These results indicate as expected that PFPMA units have higher reactivity towards nucleophilic substitution than NPMA, pentafluorophenyl is more or less two time more reactive compared to nitrophenyl group.

Another study was performed to evaluate the reactivity of the two monomer units in substitution with citronellol. Reaction conditions are as given in Scheme 33, copo1N1F was used as template.



Scheme 33. Substitution of PFPMA-*co*-PNPMA with citronellol

Figure 116 presents NMR spectra of reaction carried out in DMSO and DMF after 24 hours. Both reactions gave 95% to 100% conversion for PFPMA units, while the substitution of NPMA units only reached 21% in DMSO and 32% in DMF.

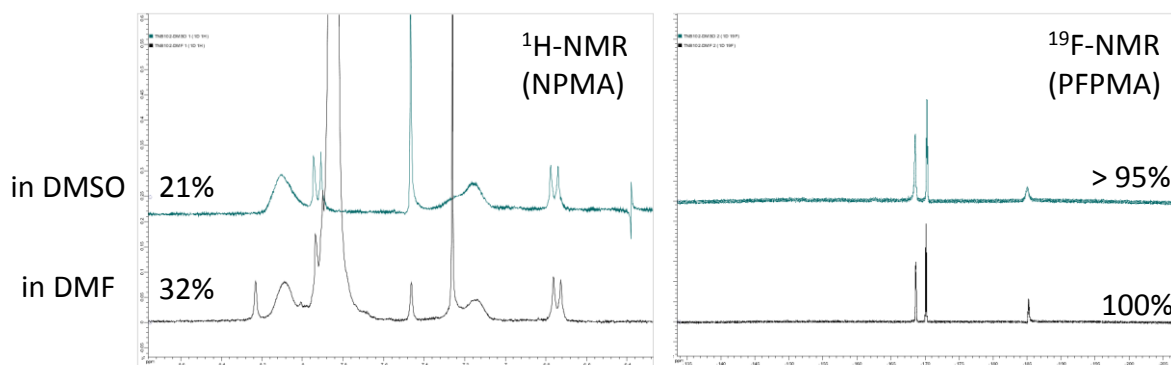


Figure 116. NMR spectra (^1H : left, ^{19}F : right) of post-modification of copo1N1F with citronellol in DMSO (top) and DMF (bottom)

Overall, the nucleophilic substitution with copolymers composed of NPMA and PFPMA units suggests that PFPMA moieties have higher reactivity than NPMA in substitution with both primary amine and primary alcohol. Further studies are needed to find the conditions in which the substitution will be totally selective towards only one type of monomer units.

4.4. Conclusion

This chapter has provided several examples and corresponding results on post-modification of different polymeric reactive templates including homopolymers and copolymers of PFPMA and NPMA. It is seen from these results that (co)polymers derived from active esters can react with different types of nucleophilic compounds, ranging from primary amine, compounds in ammonium chloride form, primary alcohol, and phenols. More importantly, we have also studied and confirmed the possibility to perform sequential and dual post-modification of PFPMA with different alcohols. These results present to be promising and indicate that, one can easily obtain copolymer of different essential oils *via* their substitution with PFPMA by careful selection of reaction conditions.

Even though the reactivity of PNPMA was less focused compared to PFPMA, evident on its reactivity in nucleophilic substitution was roughly examined, which later allowed the study on post-modification of copolymer of NPMA and PFPMA. From such studies, it is to conclude that pentafluorophenyl group has higher reactivity in nucleophilic substitution compared to *p*-nitrophenyl group. Therefore, it is of our belief that better selectivity between NPMA and PFPMA can be obtained by investigating and tuning the influence of reaction conditions like temperature, reaction stoichiometry, and medium.

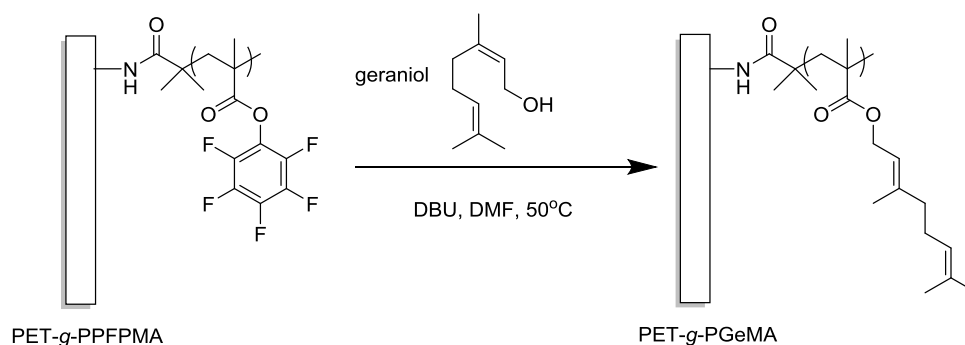
Chapter 5. Post-modification of PET-*g*-PPFPMA and bacterial adhesion on functionalized PET films

It is seen from the previous chapter that the post-modification of PPFPMA with essential oils resulted in functional polymers whose chemical structures are of great agreement with expectations. Taking advantages of large-batch setup for surface-initiated polymerization, this chapter introduces and discusses the effectiveness in chemical transformation of PPFPMA grafted on PET supports to functionalize the supporting surfaces with polymer derived from essential oils. Some

5.1. Post-modification of PET-*g*-PPFPMA

5.1.1. Post-modification of PET-*g*-PPFPMA with geraniol

PET-*g*-PPFPMA-90 films were post-modified with geraniol via transesterification in DMF at 50 °C in presence of DBU to obtain PET grafted with poly(geranyl methacrylate) (PET-*g*-PGeMA) (Scheme 34).



Scheme 34. Post-modification of PET-*g*-PPFPMA with geraniol

The first indicator of the post-modification success was the significant drop in water contact angle (from 90° to 74°) due to the replacement of pentafluorophenyl moieties by the less hydrophobic geranyl groups as shown in Figure 117.



Figure 117. Water contact angle of a) PET-*g*-PPFPMA, b) PET-*g*-PGeMA

The substitution was further confirmed by ATR FTIR (Figure 118) with the disappearance of peaks corresponding to C=O (1776 cm⁻¹), C=C (1519 cm⁻¹), C-O (1052 cm⁻¹) and C-F (995

cm^{-1}) of PFPMA. Unfortunately, the peaks originated from polymer of geranyl methacrylate could not be distinguished clearly from that of PET support due to similarity in their chemical environment. The only pronounced difference is the appearance of peaks characterized to the sp^3 C-H stretching of geranyl group at 2931 cm^{-1} and a broad peak from $2844\text{-}2892 \text{ cm}^{-1}$.

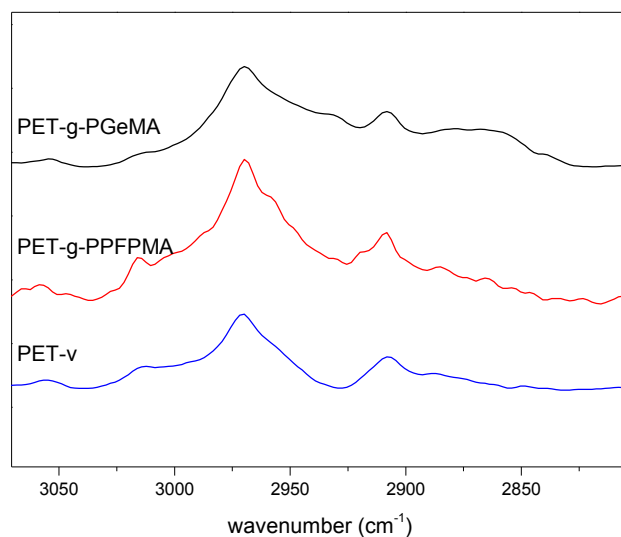
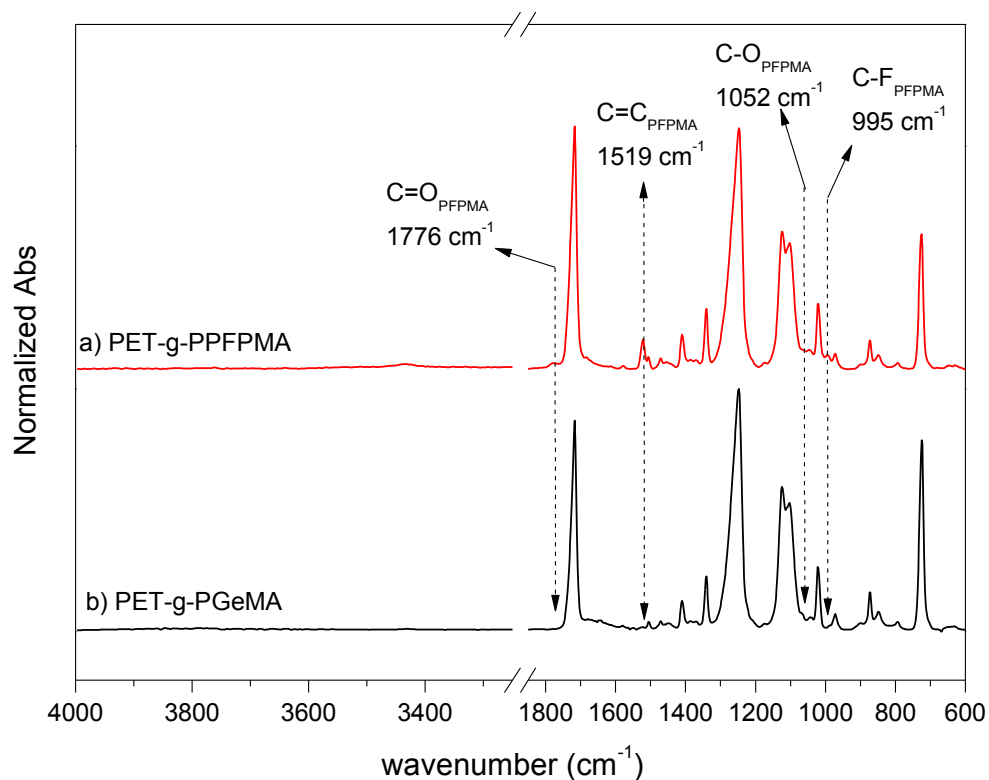


Figure 118. ATR FTIR spectra of a) PET-g-PPFPMA prior to substitution and b) PET-g-PGeMA obtained; bottom: C-H stretching between 2800 cm^{-1} and 3200 cm^{-1}

The success of post-modification is proven clearly by comparing survey spectrum of PET-g-PPFPMA and PET-g-PGeMA as in Figure 119. As discussed in 3.2.3 on surface-initiated

polymerization of PFPMA, survey spectrum of PET-g-PPFPMA shows the presence of C1s, O1s and notably an intense signal of F1s around 699 eV. After transesterification with geraniol to provide PET-g-PGeMA, the intensity of F1s almost disappeared (<1% total atomic count), indicating the removal of all fluoro-containing molecules on the modified surface. Besides O1s and C1s, around 3-4% of unknown-source N1s was also found on surface.

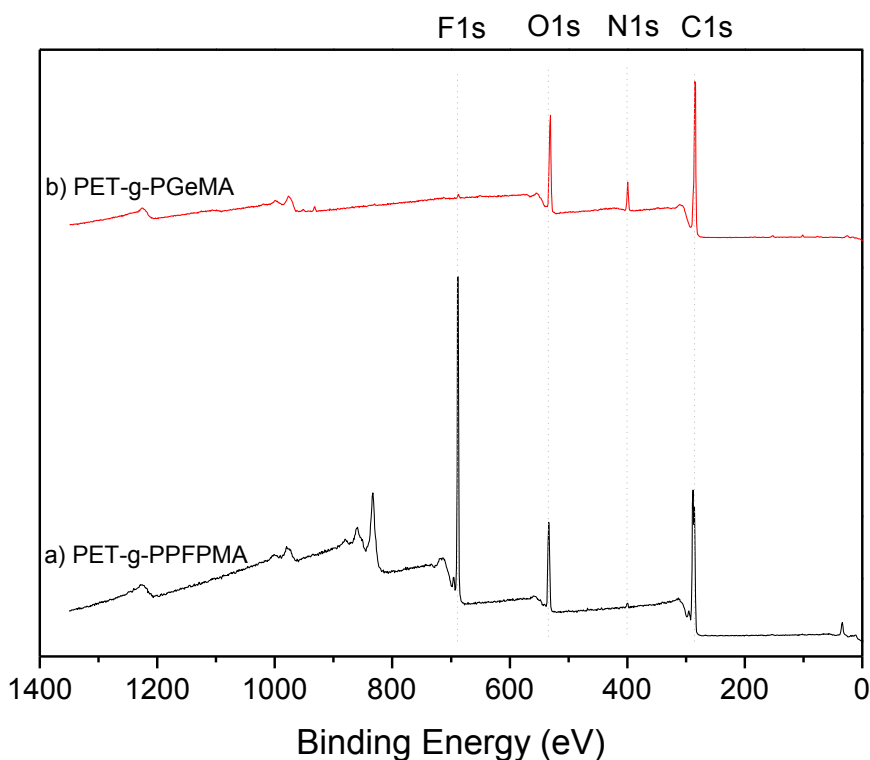


Figure 119. XPS survey spectra of a) PET-g-PPFPMA and b) PET-g-PGeMA

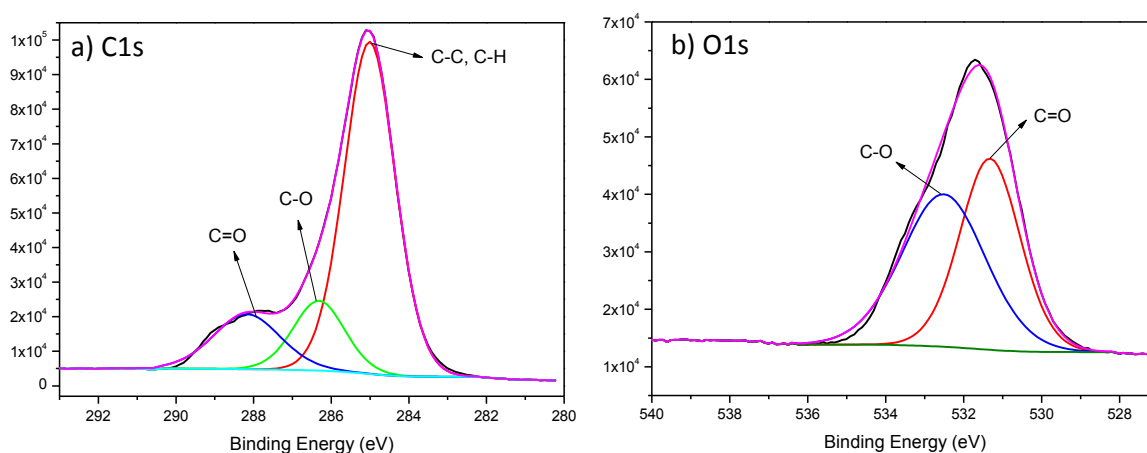


Figure 120. a) C1s and b) O1s core levels and fitting results of PET-g-PGeMA

Table 27. Fitting parameter for deconvolution of C1s and O1s core level scans in XPS measurements of PET-g-PGeMA

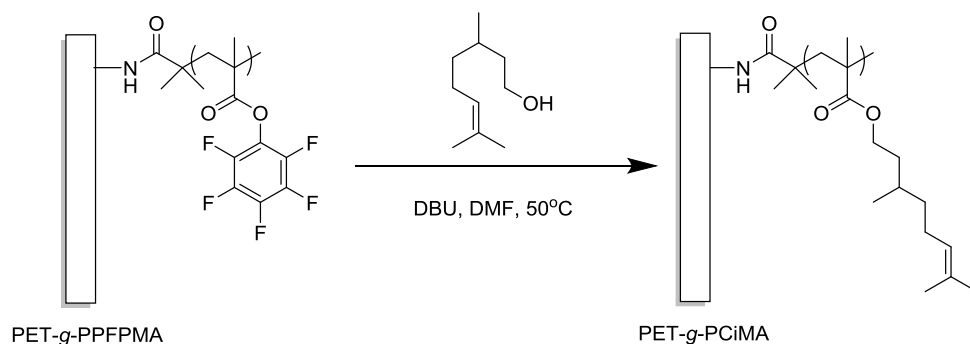
Core level	Bonding	PET-g-PGeMA		
		BE	FWHM	%
C1s (75.5 %)	C-C, C-H	285.0	1.55	70.0
	C-O	286.3	1.56	14.8
	COO	288.2	2.02	15.2
O1s (17.4 %)	C=O	532.5	1.85	50
	C-O	532.6	2.64	50

C1s and O1s core level scans as well as their deconvolution are presented in Figure 120, fitting parameters are summarized in Table 25. Both C1s and O1s of PET-g-PGeMA reassemble typical profiles of polyester. C1s core level scan of PET-g-PGeMa differs significantly from that of PET-g-PPFPMA as the most intense peak is attributed to C-C bond at 285.0 eV instead of C-F at around 287 - 288 eV. Furthermore, two other contributors characterized for ester function are found at C-O (286.3 eV) and C=O (288.2 eV). In O1s scan and deconvolution, an equal contribution of C-O (532.6 eV) and C=O (531.5 eV) confirms the ester structure. Additionally, it is to remind that both C1s and O1s core levels scan of PET-g-PPFPMA consist shakeup intensity due to the π - π^* transition. Thus, the replacement of pentafluorophenyl with geranyl groups led to the removal of π -conjugation, hence, no shakeup was recorded during C1s and O1s core level scans of PET-g-PGeMA.

Overall, these analyses confirm that the post-modification of PET-g-PPFPMA with geraniol was successful.

5.1.2. Post-modification of PET-g-PPFPMA with citronellol

The transesterification of PPFMA with citronellol was discussed in 4.1.2.1. Herein, the post-modification of reactive polymer grafted on PET surface was carried out as in Scheme 35.



Scheme 35. Post-modification of PET-g-PPFPMA with citronellol

Figure 121 shows the difference in water contact angle of PET-g-PPFPMA and its post-modified product PET-g-PCiMA. The change in hydrophobicity is obvious with a sharp decrease from $\approx 91^\circ$ to $\approx 65^\circ$. This change corresponds to the removal of non-polar pentafluorophenyl moieties and the introduction of less polar citronellyl groups.

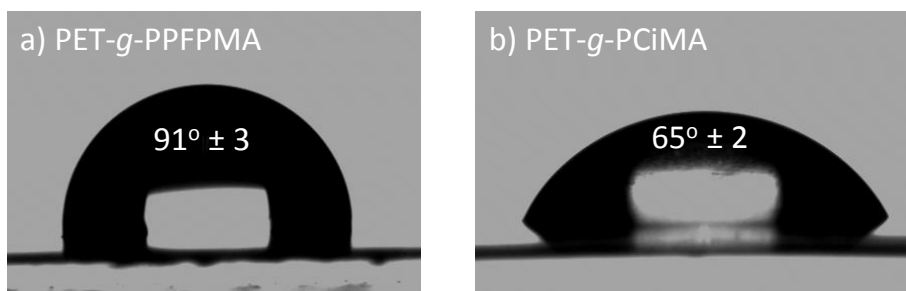


Figure 121. Water contact angle of a) PET-g-PPFPMA and b) PET-g-PCiMA

ATR FTIR spectra of PET surface before and after transesterification of PPFMA with citronellol (Figure 122) also demonstrate the success of post-modification.

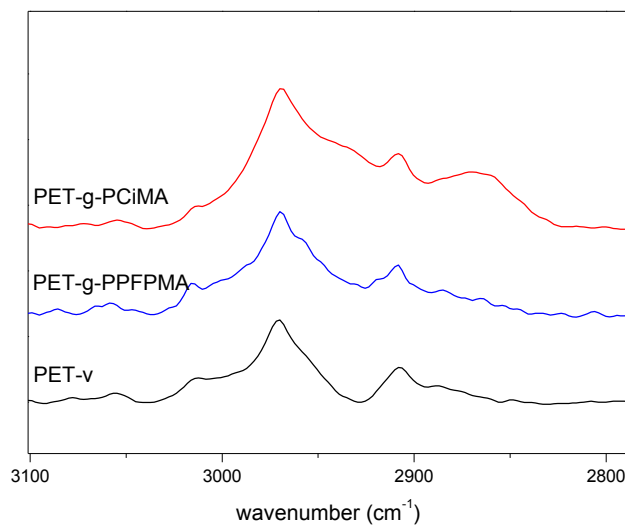
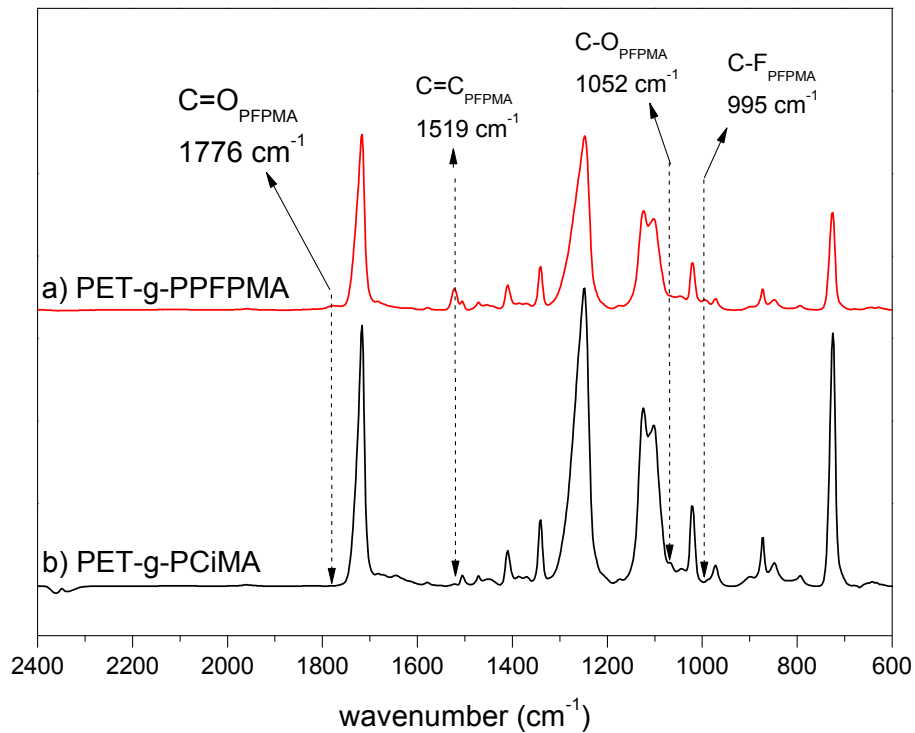


Figure 122. Top: ATR FTIR of a) PET-g-PPFPMA and b) PET-g-PCiMA; bottom: C-H stretching between 2800 cm^{-1} and 3200 cm^{-1}

There is almost no difference in FTIR spectrum of PET-g-PCiMA due to their chemical similarity except the diminution in intensity of bands characterized for PFPMA and the appearance of new C-H stretching vibration observed at around 2850 cm^{-1} and 2930 cm^{-1} , as presented in Figure 122.

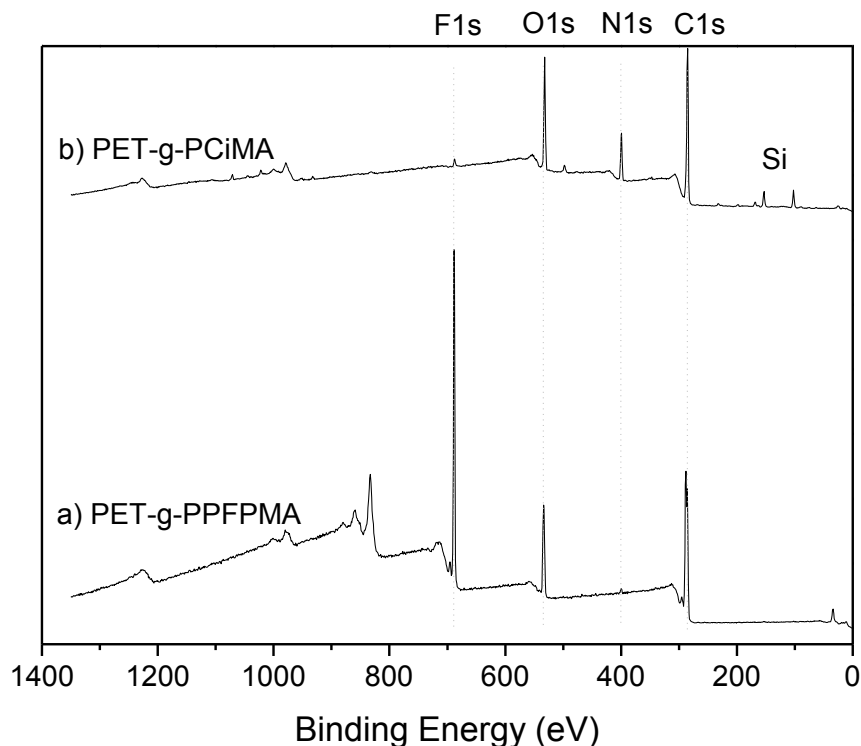


Figure 123. XPS survey spectra of a) PET-g-PPFPMA and b) PET-g-PCiMA

Similar to the case of geraniol, XPS survey spectrum of PET-g-PCiMA shows nearly complete disappearance of F1s compared to spectrum of PET-g-PPFPMA (Figure 123), confirming the removal of pentafluorophenyl moieties.

As observed in survey spectrum of this surface, C1s core level scan of PET-g-PCiMA (Figure 124a) shows a predominant intensity from carbon to carbon bonds at around 285.0 eV, which is distinctive from C-F dominance at ~288 eV of PET-g-PPFPMA. On the other hand, O1s core level scan (Figure 124b) presents to be unimodal. Unfortunately, the survey spectrum of studied PET-g-PCiMA indicates the presence of some impurities including nitrogen containing compound and, unexpectedly, silicon. While the nitrogen contamination may be attributed to residues of solvent (DMF) or base catalyst (DBU), the real source of silicon contamination is currently unknown. Deconvolution of C1s and O1s core level scans was not done because the structure of contaminants are unknown yet they take more than 12% of total atomic counts as summarized in **Table 28**.

Table 28. Atomic percentage of atoms found on PET-g-PCiMA surface

C1s	O1s	N1s	Si2p
70.2%	17.3%	6.7%	5.8%

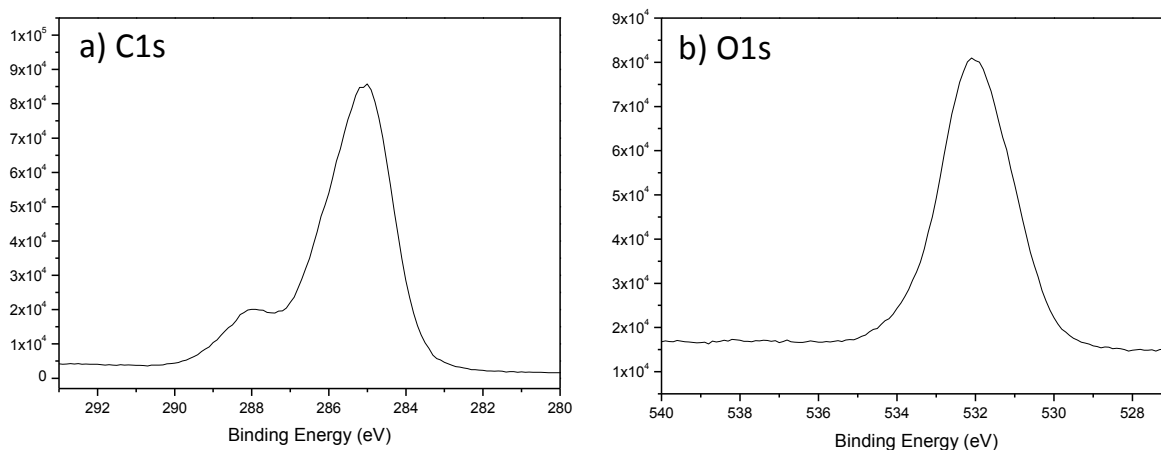
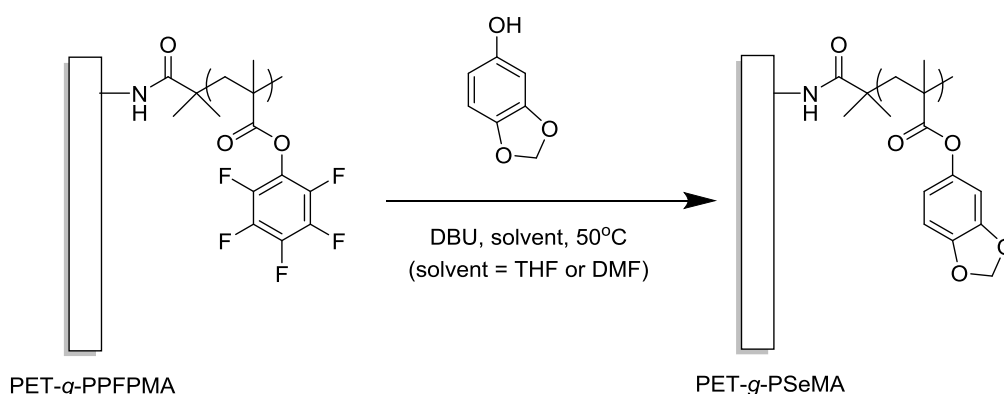


Figure 124. a) C1s core level scan and b) O1s core level scan of PET-*g*-PCiMA

5.1.3. Post-modification of PET-*g*-PPFPMA with sesamol

As described in 4.1.2.2, post-modification of PPFMA with sesamol proceeded to very high conversion. Herein, post-modification of PET-*g*-PPFPMA was carried out under conditions as given in Scheme 36.



Scheme 36. Post-modification of PET-*g*-PPFPMA with sesamol

Water contact angle on surface changed significantly before and after post-modification of PET-*g*-PPFPMA with sesamol. Starting from a hydrophobic surface of $\approx 92^\circ \pm 2$ in water contact angle, the value decreased to $\approx 56^\circ \pm 2$ once the sesamyl moieties replaced the pentafluorophenyl ones as seen in Figure 125.

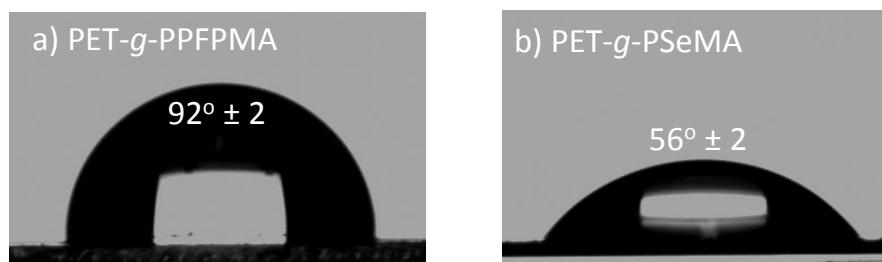


Figure 125. Water contact angle of a) PET-*g*-PPFPMA and b) PET-*g*-PSeMA

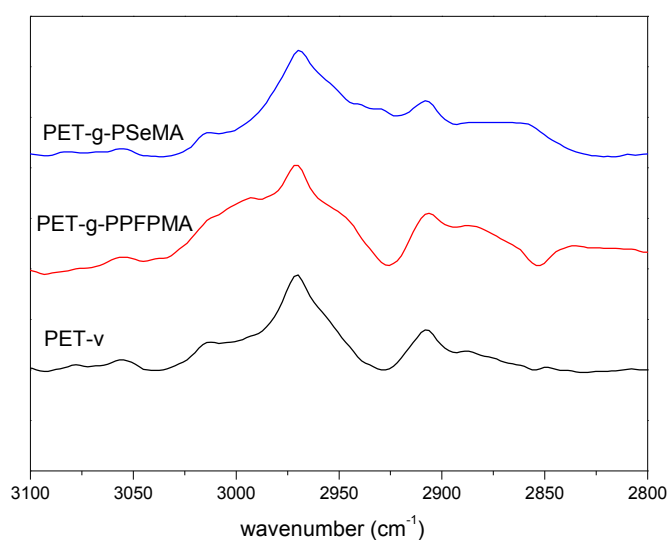
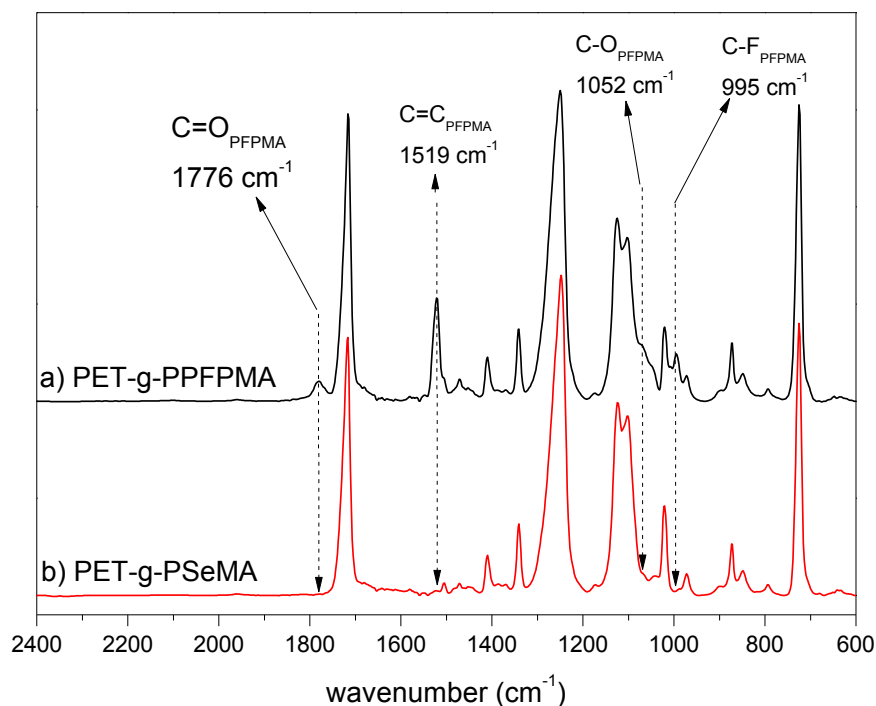


Figure 126. Top: ATR FTIR of a) PET-*g*-PPFPMA and b) PET-*g*-PSeMA; bottom: comparison of C-H stretching of PET-*v*, PET-*g*-PPFPMA and PET-*g*-PSeMA

By ATR FTIR, it is seen that the chemical transformation from pentafluorophenyl groups to sesamyl groups was complete, proven by the total diminution of PFPMA signals of PET-*g*-PSeMA compared to PET-*g*-PPFPMA (Figure 126). Similar to the case of PET-*g*-PGeMA and PET-*g*-PCiMA, the grafted polymer and the supporting surface in PET-*g*-PSeMA are both polyester, therefore, the difference in their ATR FTIR spectra is not obvious.

In good agreement with ATR FTIR in term of conversion, XPS survey spectrum of PET-*g*-SeMA retains only ~0.5% F1s residues. Interestingly as in case of PSeMA discussed

previously, the atomic percentage found on PET-*g*-SeMA matches well, *i.e.* atomic percentages of C1s, O1s and N1s are 76.9%, 19.2% and 3.3%, respectively. This result confirms that PPFMPMA transesterification in solution could be transposed to the surface.

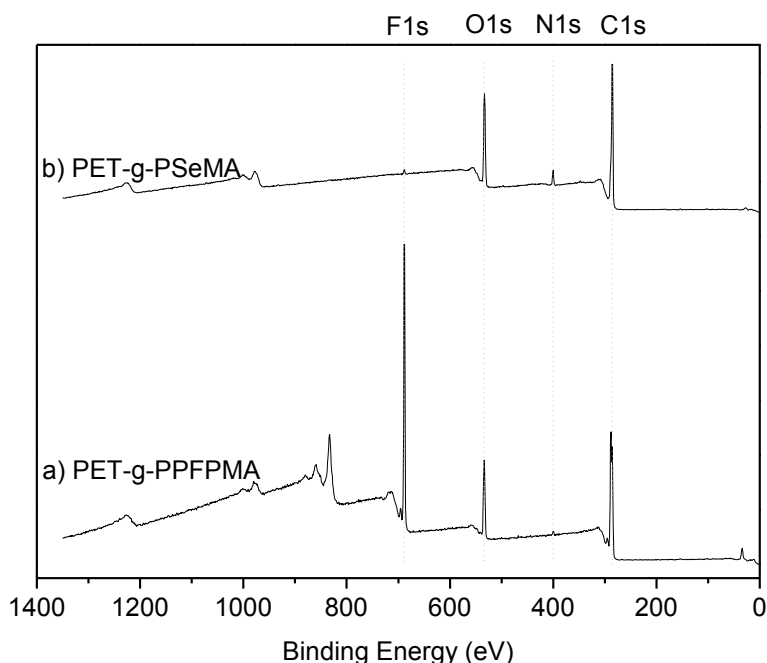


Figure 127. XPS survey spectrum of a) PET-*g*-PPFPMA and b) PET-*g*-PSeMA

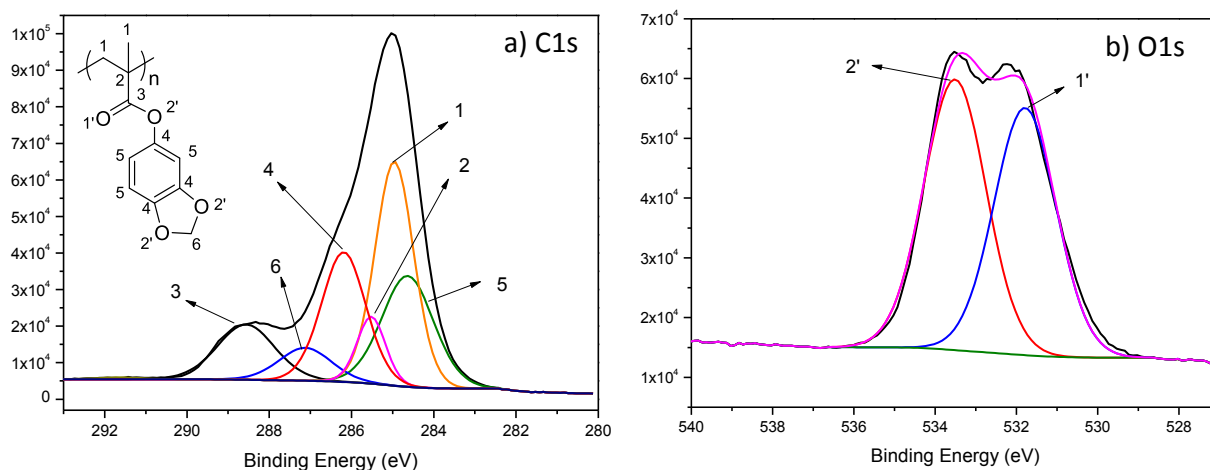


Figure 128. Core level scans and deconvolution of a) C1s and b) O1s of PET-*g*-PSeMA

Figure 128 presents core level scans and deconvolutions of C1s and O1s respectively. Table 29 summarizes fitting parameters of C1s and O1s core level scans. As studied for PSeMA, herein, the same consideration was taken into account during deconvolution process of the two core level scans. The fitting result of C1s resembles that of PSeMA with 6 contributors as presented in Figure 128a. O1s core level deconvolution of PSeMA grafted to PET support confirms the presence of C=O and C-O bond, validating the polyester structure. Moreover, the

percentage of the two bonds (47.7% C=O and 52.3% C-O) also fits well with that of unbound PSeMA.

Table 29. Fitting parameters of C1s and O1s core level scans of PET-g-PSeMA

Core level	Bonding	PET-g-PSeMA		
		BE	FWHM	%
C1s (77.3%)	C=C	284.6	1.48	21.2
	C-C, C-H	285.0	1.11	32.1
	C*-CH ₃	285.5	0.82	7.1
	C-O, C-N	286.2	1.26	21.2
	O-CH ₂ -O	287.1	1.50	6.4
	COO	288.6	1.63	11.7
	Shake up	291.6	1.22	0.3
O1s (19.3%)	C=O	531.8	1.80	47.7
	C-O	533.5	1.80	52.3

The XPS results of PSeMA synthesized in solution and grafted from surface are in agreement. Furthermore, the accordance of C1s and O1s core level of PET-g-SeMA taking consideration only PSeMA structure indicates that the supporting surface is all covered by the grafted polymer. This result is in consistence with PET-g-PPFPMA surface where the reactive polymer was also proven to cover the whole supporting film.

5.2. Bacterial adhesion on functionalized PET films

Thanks to the possibility in elaboration of multiple films at the same time using large-batch setup for surface-initiated polymerization and post-modification, sets of PET functionalized with either citronellol or sesamol derivatives have been prepared for investigation of their bacterial adhesion.

Two bacterial strains have been used for bacterial adhesion tests including *Pseudomonas aeruginosa* and *Staphylococcus aureus*.

Pseudomonas aeruginosa is a rode-shape Gram negative bacterium whose size is 0.5 μm - 0.8 μm in length and 1.5 μm - 3.0 μm in width. This strain of bacteria is motile thanks to the presence of flagella, thus, it is found in numerous substrates including soils, water, on animals and also humans. *P. aeruginosa* is among bacterial species that can quickly resist to antibiotics owing to their intrinsic resistance mechanism. This strain of bacteria is also

responsible for many nosocomial infections like device-caused infections, bloodstream or urinary tract infections [347].

Staphylococcus aureus is a sphere-shape Gram positive bacterium whose diameter is around 0.5 μm to 1.5 μm . This immotile bacterium is amongst the most dangerous staphylococcal bacteria. It often causes skin infections but can also cause pneumonia, endocarditis and even bone infections [348].

This chapter presents a few preliminary results on adhesion of these two bacteria on PET films functionalized with polymer derived from essential oils. The tests were taken in collaboration with Dr. Christophe Regeard at Institut de Biologie Intégrative de la Cellule (I2BC) – University Paris-Sud. Films of interest were placed in culture plate at desired conditions for each bacterial strain. The number of viable and cultivable bacteria was determined by enumeration of cultivable cell on LB plates and is going to be reported as colony-forming unit (CFU) per cm^2 . Each experiment was conducted with triplication and non-treated clean PET films were used as control.

5.2.1. Adhesion of bacteria on PET-g-PCiMA

Figure 129 shows comparison of number of bacteria per cm^2 when *P. aeruginosa* was exposed to pristine PET and PET-g-PCiMA. There was a slight increase in number of bacteria adhered on PET modified with PCiMA (4.0×10^6 CFU/ cm^2) compared to control PET (3.7×10^6 CFU/ cm^2).

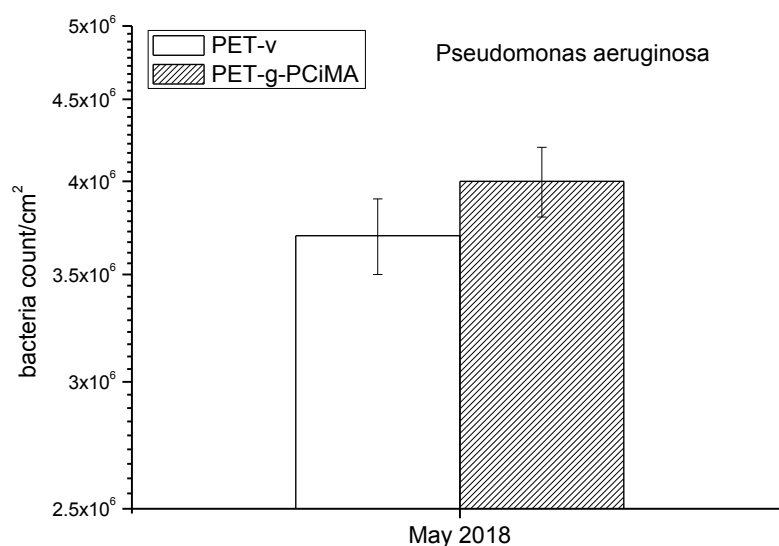


Figure 129. *Pseudomonas aeruginosa* adhesion on PET-virgin and PET-g-PCiMA

5.2.2. Adhesion of bacteria on PET-g-PSeMA

Figure 130 summarizes results obtained from adhesion tests of *P. aeruginosa* on PET-g-PSeMA. The results obtained from three individual tests are greatly deviated in number of

cells adhered to both pristine PET and PET-g-PSeMA. This event may be attributed to the difference in initial amount of bacteria in culture media. Furthermore, among the three individual tests, there are two set of results indicate that PET-g-PSeMA films promoted the adhesion of *P. aeruginosa* on surface while the other test carried out on May 2018 suggests a decrease in the number of cells attached to sesamyl grafted PET. Thus, it is unable to withdraw a Conclusion on the adhesion behavior of *P. aeruginosa* on PET-g-PSEMA.

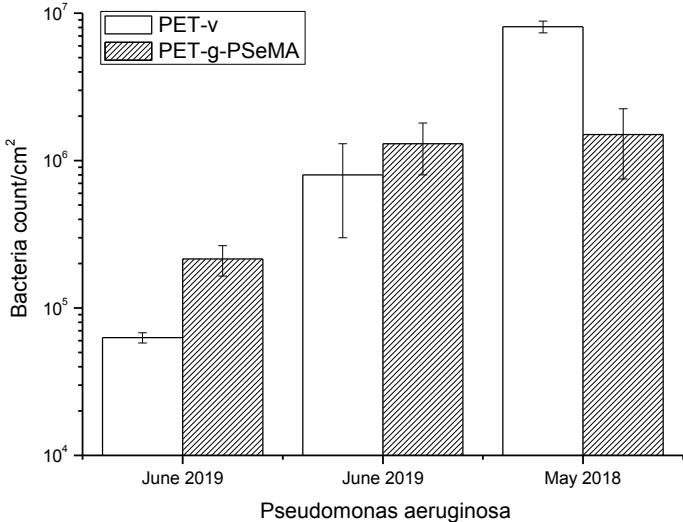


Figure 130. *Pseudomonas aeruginosa* adhesion on PET-virgin and PET-g-PSeMA

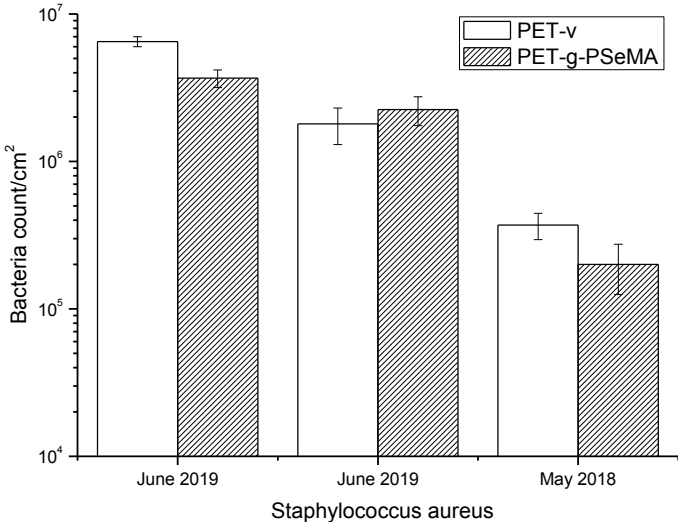


Figure 131. *Staphylococcus aureus* adhesion on PET-virgin and PET-g-PSeMA

Figure 131 presents a summary on adhesion of *Staphylococcus aureus* on pristine PET and PET-g-PSeMA. Similar to the case of *P. aeruginosa*, except for the global difference in number of cells harvested, no overall qualitative trend could be withdrawn from these results. In general, each test indicates that there is a small difference between the numbers of cells

adhered on pristine PET and PET-*g*-PSeMA. However, that variation is often in the range of error bar; thus, the difference is insignificant.

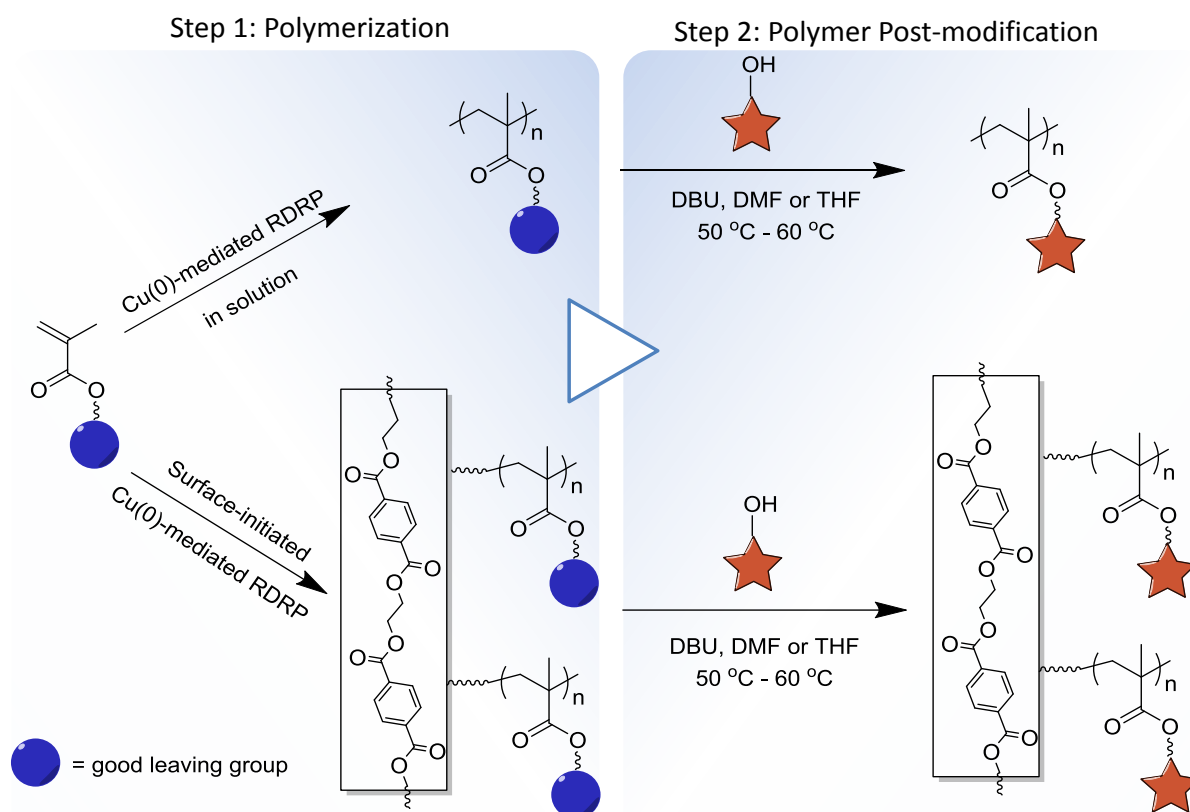
5.3. Conclusion

In conclusion, the post-modifications of PET-*g*-PPFPMA with three essential oils geraniol, citronellol and sesamol were successful and proven with water contact angle, ATR FTIR and XPS measurements. In all cases, a drop in water contact angle was observed in all cases due to the replacement of nonpolar pentafluorophenyl group with more polar ones. ATR FTIR confirms that signals of PFPMA on PET-*g*-PPFPMA disappeared after post-modification with alcohols. XPS results also validate the complete transesterification of PET-*g*-PPFPMA with these three alcohols.

The functionalized PET surfaces grafted with polymer derived from citronellol and sesamol have been tested for their bacterial adhesion properties against *Pseudomonas aeruginosa* and *Staphylococcus aureus*. Even though these functionalized surfaces were expected to have antibacterial or antiadhesion properties, biological results obtained in this research did not meet such expectations. Indeed, the adhesion of bacteria on a surface is a complicated process where not only the chemistry but also the topology, roughness and other physical properties play synergetic effect. Therefore, further studies need to be performed in order to understand other properties of functionalized PET surfaces other than water contact angle and chemistry of such films.

Chapter 6. Conclusions and Perspectives

Cu(0)-mediated Reversible Deactivation Radical Polymerization proved to be a method of choice to allow an easy preparation of polymers of active esters both in solution and on supporting PET surfaces. The elaboration of polymers derived from essential oils, either unbound or attached to a surface, was also demonstrated to be straightforward with good agreement in chemical structures of obtained and desired products. Scheme 38 summarizes major steps acquired and achieved during the course of this research.



Scheme 37. General scheme of Cu(0)-mediated RDRP of active esters and their post-modification to fabricate polymer derived from essential oils

The primary step consists of the preparation of reactive (co)polymers from two active esters PFPMA and NPMA. First of all, a detailed study on control polymerization of PFPMA by Cu(0)-mediated RDRP was examined. The found optimized conditions were proven to be robust and straightforward to obtain polymers bearing reactive esters, in a large range of molecular weight at narrowed polydispersity without losing “living” characteristics of controlled polymerization. The application of Cu(0)-mediated RDRP on PET-initiated polymerization of PFPMA was also investigated. Functionalization on surface proved to be effective, even in large scale allowing thus the preparation of a large batch of PET-g-

PPFPMA films at the same time, *i.e.* 12 films per reaction. Cu(0)-mediated RDRP was transposed to NPMA monomer, both polymerization in solution and grafting from PET surface was studied. Despite the high monomer conversion, the control of polymerization was not yet achieved and remains questionable. Furthermore, copolymerizations of PFPMA and NPMA were also considered and proved to be successful. The composition of copolymers were characterized and analyzed to confirm that the ratio between comonomer units in ratio in feed and in final products are in full agreement in solution but deviated on PET-g-P(PPFPMA-*co*-PNPMA) surface.

Secondly, polymer post-modification of obtained (co)polymers with various compounds had been proven to be efficient, easy to perform. Additionally, the structure and characteristics of obtained products were confirmed to match with expectations. It is remarkable that the post-modification of PFPMA can be done as sequential process, single or dual functionalization with several different essential oils, which are natural antibacterial or antioxidant compounds. On the other hand, the success in polymerization and post-modification of polymer of active esters in solution allowed the fabrication of different PET film grafted with polymers expected to have antiadhesion properties. Attempts to test such properties were also done against two model bacteria including *Staphylococcus aureus* and *Pseudomonas aeruginosa*. Unfortunately, all acquired tests exhibited no significant difference in adhesion of the two bacteria on pristine PET and functionalized PET.

In general, the use of reactive polymers is a promising approach to obtain diverse functional polymers and copolymers. However, there exist a few concerns that have not been validated, yet need to be considered and/or clarified in future work. First of all, thermal properties of PNPMA should be studied in deeper manner to find out the critical value from where the glass transition temperature is independent from molecular weight. From such research, the thermal property of copolymers may be explained properly. Secondly and more importantly, surface modification with PEI merits additional attention. It is realized during this dissertation that the use of branched PEI may result into interpenetrations of polyamine chains into the to-be-formed “layer” of reactive polymers. As consequence, the reaction between PEI chains and reactive polymer chains may happen, which can also be attributed to the presence of N1s in all XPS measurement of PET functionalized with essential oils. Time of flight secondary-ion mass spectrometry (ToF SIMS) can be used to clarify this issue. To avoid this potential problem, future work may consider the use of short, linear diamines or the application of ammonia plasma to introduce reactive amines on surface.

Materials and Methods

Materials

Pentafluorophenol (TCI, 98% pure), methacryloyl chloride (Sigma-Aldrich, 97% stabilized), tris(2-pyridylmethyl) amine (TPMA) (TCI, 98%), *N,N,N',N'',N''*-pentamethyldiethylenetriamine (PMDETA) (Sigma Aldrich), 1,1,4,7,10,10-hexamethyltriethylenetetramine (HMTETA) (Sigma Aldrich), and 4,4'-dinonyl-2,2'-bipyridine (dNbpy) (TCI), ethyl α -bromoisobutyrate (eBiB) (Sigma-Aldrich), methyl α -bromophenylacetate MBPA (TCI, 98%), copper (II) bromide (Sigma-Aldrich), tetrahydrofuran (THF, pure), sulfolane (Alfa Aesar, 99% pure), branched polyethyleneimine (PEI) (Sigma Aldrich) (average Mw 25 000 g.mol⁻¹), Orange II dye (TCI, >97%), were used as received. Trimethylamine (TEA) (Sigma-Aldrich, distilled over KOH under argon before used). Copper wire (Alfa Aesar, 99%, d = 1.0 mm, density \approx 7.02 g/m²) was washed with a mixture of methanol:HCl 1M (1:1 v/v), rinsed with methanol and acetone, then dried completely before used.

Methods

NMR

¹H and ¹⁹F NMR measurements were performed using either Bruker Advanced 250 MHz or 360 MHz in 5-mm NMR tubes. Spectra visualization and integration were calibrated with internal signals of solvents (δ /CDCl₃ = 7.24 ppm). NMR spectra of polymers were acquired by solubilizing 15-20 mg of polymers in appropriate solvent.

SEC

Size Exclusion Chromatography (SEC) analysis of polymers was carried out at 35 °C using THF as eluent. Polymer solution was prepared at 4 mg/mL, then filtered through 0.4 μ m TFPE filter to remove insoluble residues; 50 μ L of ready polymer solution was injected in each measurement. The separation system includes one guard column (Malvern TGuard) and two separation columns: 1) Viscotek LC3000L (300 x 8.0 mm) and 2) ViscoGEL™ GMHH r-H (300 x 7.8 mm). Intensity was recorded using a refractive index (RI) detector (Walter 410) and a multi-angle light scattering (MALS) detector (Viscotek SEC-MALS 20). A refractive index increment (dn/dc) of 0.042 mL/g was determined experimentally (see Supplementary Information) and used for the determination of absolute molecular weight using OmniSec™ 5.12.467 software distributed by Malvern Panalytical.

Copolymers of PFPMA and NPMA were also analyzed in DMF (+ LiBr, 1g.L⁻¹) at Laboratory de Chimie de Polymere (LCP) – Institut Parisien de Chimie Moléculaire – Université Pierre Marie Curie. The analyses were performed at 60°C and at a flow rate of 0.8 mL.min⁻¹ at a polymer concentration of 3 mg.mL⁻¹ filtered through 0.22 μ m. The steric

exclusion was carried out on two PSS GRAM 1000 Å columns (8 x 300 mm; separation limits: 1 to 1000 kg mol⁻¹) and one PSS GRAM 30 Å (8 x 300 mm; separation limits: 0.1 to 10 kg mol⁻¹) coupled with three detectors (Viscotek, TDA 305) including a differential refractive index (RI) detector, a viscometer detector and a light scattering (LS) detector (laser $\lambda = 670$ nm at 7° and 90°). The OmniSEC 5.12 software was used for data acquisition and data analysis. Molar masses (M_n , the number-average molar mass, M_w , the weight-average molar mass) and polydispersity indexes ($\mathcal{D} = M_w/M_n$) were calculated with a calibration curve based on narrow poly(methyl methacrylate) (PMMA) standards (from Polymer Standard Services), using only the RI detector.

Water contact angle

Static contact angle measurement was performed using a DSA100 Kruss analyser. The contact angle was measured by depositing a 3 μ L droplet of milliQ water on surface, an average contact angle was calculated from 3 droplets for each film, and errors were calculated as standard deviation.

Surface homogeneity wettability was investigated by water contact angle measurements using the sessile drop technique with a micro-goniometer (DSA100 M, Krüss, Les Ulis, France). This device deposited a deionized water droplet (300 pL) with a piezo dosing unit every 1 mm on a rectangular zone of 20 mm \times 10 mm. Droplets were monitored for 2 s with a fast CCD camera with 4 \times zoom and a 20 \times microscope objective. The angle of interest was the one obtained on the first acquisition image because of the very quick evaporation process of the small drops. The water contact angle and standard deviation were calculated as average of all captured droplets deposited on surface.

UV-Vis measurement

UV-Vis absorbance determination was carried out with Varian Cary 1E UV-Visible spectrometer using two-sided disposable 3-mL VWR® polystyrene cuvettes with light path of 10 mm.

Attenuated Total Reflectance FTIR

Absorbance of films was measured by Bruker IFS 66 equipment with an ATR module using diamond crystals of Pike technologies. 200 scans of resolution 4 cm⁻¹ were recorded between 600 cm⁻¹ to 4000 cm⁻¹. Spectra visualization and treatment were done using OPUS software; spectra integration was done using the built-in integration function of Origin® v8.0724.

X-ray Photoelectron Spectroscopy

K-alpha spectrometer from ThermoFisher, equipped with a monochromatic X-ray source (Al K-alpha, 1486.6 eV). A spot size of 400 μ m was employed; the hemispherical analyser was operated in CAE (Constant Analyzer Energy) mode, with passing energy of 200 eV, a step of

1 eV for the acquisition of survey spectra, and 50 eV and 0.2 eV for high resolution spectra. A “dual beam” flood gun was used to neutralize the charge build-up. The obtained spectra were treated by CasaXPS® version 2.3.19. A Shirley-type background subtraction was used and the peak areas were normalized using the Scofield sensitivity factors in the calculation of elemental compositions. Fitting was carried out by calibrating binding energy of C=C peak to 284.8 eV or binding energy of C-C peak to 285 eV. All line shapes were considered to be a 30/70 or 40/60 mix of Gaussian and Lorentzian distributions.

Atomic Force Microscopy

Tapping mode topography and phase imaging was accomplished using di Innova AFM Bruker with NanoDrive v8.02 software. Tapping mode images were acquired using silicon tips from Nanosensors (PPP NCSTR) with a resonance frequency ranging between 76 and 263 kHz. Image processing was performed and visualized using WSxM software [349]. RMS indicates root-mean-square roughness of obtained at focusing window of 10 μ m x 10 μ m.

Scanning Electron Microscopy (SEM)

Scanning Electron Microscopy (SEM) was performed at short working distance using a field emission gun (FEG) at low voltage (1 kV) and low current (few pA) in order to observe only the extreme surface of sample, hence, allowing the comparison with AFM images.

Elemental Analysis

Elemental analysis was performed by Service de Microanalyse at Institut de Chimie des Substances Naturelles (ICSN) - CNRS, Gif-sur-Yvette.

Experimental

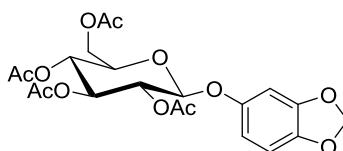
Synthesis of pentafluorophenyl methacrylate

Pentafluorophenol (24 g, 0.13 mol) was dissolved in 300 mL of anhydrous dichloromethane under moderate stream of argon. Reaction mixture was cooled down to 0 °C with an ice bath, then triethylamine (23 mL, 0.14 mol) and methacryloyl chloride (11.5 mL, 0.12 mol) were introduced dropwise subsequently *via* a tight Ar-washed syringe. After 3 hours, reaction was left at ambient temperature overnight under argon. Reaction mixture was filtered to remove insoluble solid, then washed with NaHCO₃ several times to remove excess pentafluorophenol. Organic phase was dried over MgSO₄ before distilled under vacuum at 85 °C to collect PFPMA as transparent liquid. Yield: 80%. ¹H NMR (250 MHz, CDCl₃, δ/ppm): 2.06 (s, 3H, -C*-CH₃), 5.89 (s, 1H, CH₂=C), 6.43 (s, 1H, CH₂=C). ¹⁹F NMR (250 MHz, CDCl₃, δ/ppm): -162.45 (t, 2F, meta positions), -158.14 (t, 1F, para position), -152.75 (d, 2F, ortho positions).

Synthesis of *p*-nitro methacrylate

p-nitrophenol (5 g, 0.036 mol) was dissolved in 120 mL of anhydrous dichloromethane under a flow of argon. Triethylamine (5.5 mL, 0.040 mol) was adjusted drop-wise into reaction mixture. The reaction flask was then placed on an ice bath to cool down the mixture to 0 °C before methacryloyl chloride (3.6 mL, 0.032 mol) was introduced drop-wisely via a syringe. The reaction mixture was left stirring at 0 °C for 10 minutes prior to defrost to ambient temperature. After 3 hours, the whole reaction mixture was transferred into a 500 mL separatory funnel, followed by the addition of 25 mL HCl 1M. The collected organic phase was then washed twice with 15 mL of NaOH 1M each. The collected organic phase was rinsed with 15 mL water and followed by the introduction of excess MgSO₄ to remove remaining water. The organic phase was filtered in a Buchner funnel to collect liquid phase which was then concentrated under vacuum. Dissolved the obtained solid in a minimum volume of DCM and 4-nitrophenyl methacrylate crystals were then collected by precipitation in petroleum ether. Yield: 40%. ¹H NMR (360 MHz, CDCl₃, δ ppm): 2.06 (s, 3H, -C-CH₃), 5.9 (s, 1H, CH₂=C), 6.3 (s, 1H, CH₂=C), 7.3 (d, 2H, J = 8.8 Hz, aromatic protons in ortho positions), 8.27 (d, 2H, J = 9.5 Hz, aromatic protons in meta positions).

3,4-(Methylenedioxy)phenyl 2,3,4,6-tetra-*O*-acetyl-β-D-glucopyranoside (SeAcGlu)

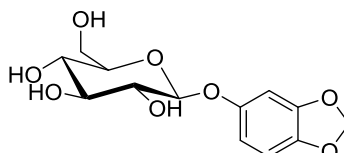


Tetrabutylammonium hydrogensulfate (1.63 g, 4.8 mmol, 1 equiv) was added at room temperature to a solution of acetobromo-α-D-glucose (2 g, 4.8 mmol) and sesamol (1.34 g, 9.7 mmol, 2 equiv) in 16 mL of CH₂Cl₂. Then, 16 mL of a NaOH aqueous solution (1 M) were added and the mixture was stirred overnight at room temperature. Ethyl acetate (90 mL) and

aqueous NaOH (1 M, 70 mL) were added to the brown solution. The organic layer was washed twice with water, dried over Na₂SO₄, filtered and concentrated *in vacuo*. The crude product was purified by flash column chromatography (EtOAc/cyclohexane: 1/2.5) to give the expected compound (640 mg, 28%) as a white solid. R_f: 0.29 (EtOAc/cyclohexane: 1/2), analytical data were in agreement with those reported.¹

¹L. Verotta, F. Orsini, F. Pelizzoni, G. Torri, C. B. Rogers *J. Nat. Prod.* **1999**, *62*, 1526-1531.

3,4-(Methylenedioxy)phenyl β-D-glucopyranoside (SeGlu)



K₂CO₃ (72 mg, 0.52 mmol, 0.2 equiv) was added to compound SeAcGlu (1.08 g, 2.3 mmol) in 24 mL of MeOH. The mixture was stirred at 30 °C and monitored by TLC until completion of the reaction. 400 mg of Dowex 50WX8 (H⁺ form) were added and the solution was stirred for 20 min at room temperature. The mixture was filtered, washed twice with MeOH and the solvent was evaporated to dryness to give compound SeGlu (686 mg, 99%) as solid. Melting point: 167-169 °C; ¹H NMR (360 MHz, CD₃OD) δ (ppm): 6.74 (d, 1H, *J* = 2.3 Hz), 6.73 (d, 1H, *J* = 8.6 Hz), 6.62 (dd, 1H, *J* = 8.6 Hz, *J* = 2.3 Hz), 5.93 (s, 2H), 4.77 (d, 1H, *J* = 7.6 Hz, H₁), 3.92 (dd, 1H, *J* = 12.0 Hz, *J* = 1.8 Hz, H_{6a}), 3.72 (dd, 1H, *J* = 12.0 Hz, *J* = 5.0 Hz, H_{6b}), 3.47-3.38 (m, 4H, H₂, H₃, H₄, H₅).

End-chain analysis by MALDI-ToF

PPFMA (M_{n,theo} = 2749 g mol⁻¹, M_{n,SEC} = 7000 g mol⁻¹, *D* = 1.07) was prepared at a concentration of 60 μM in THF. The matrix DCTB solution was prepared at a concentration of 6 mM in THF. The cationising agent, sodium trifluoroacetate (CF₃CO₂Na), was prepared at 0.7 mM in THF. The sample was prepared by mixing the polymer solution with matrix solution and cationising agent solution at a volume ratio of 1:9:1. Acquisitions were performed in reflector positive ion mode by an UltrafleXtreme mass spectrometer (Bruker Daltonics, Bremen). The laser intensity was set just above the ion generation threshold to obtain peaks with the highest possible signal-to-noise (S/N) ratio without significant peak broadening. The mass spectrometer was externally calibrated using PEG1500-3000-4000. All data were processed using the program FlexAnalysis (Bruker Daltonics, Bremen).

Typical procedure of Cu(0)-mediated RDRP of PFPMA

In a typical Cu(0)-mediated RDRP of PFPMA, where ligand (0.0136 mmol) and copper(II) bromide (CuBr₂) (0.0034 mmol), [PFPMA]₀/[initiator]₀/[ligand]₀/[CuBr₂]₀ = 100/1/0.4/0.1, and solvent (2640 μL) were taken in a 5-mL graduated glass tube then purged with a moderate stream of argon for 10-15 minutes. PFPMA (3.4 mmol) was introduced into the

reaction tube subsequently followed by the addition of a 2 cm pre-washed Cu(0) wire, then initiator (0.034 mmol) was added. Reaction was left under positive argon medium; the reactor was then sealed and placed in a preheated oil bath at 60 °C for desired period of time. At the end of the reaction, reaction mixture was diluted in dichloromethane then precipitated in cold methanol followed by filtration to collect a white solid. Kinetics of polymerization was carried out either in one-pot or by several separated batches; data was then taken as average value of different reactions carried out at the same period of time.

Typical procedure of Cu(0)-mediated RDRP of NPMA

In a typical Cu(0)-mediated RDRP of NPMA, tris(2-pyridylmethyl)amine (TPMA) (2.3 mg, 0.008 mmol) and copper(II) bromide (CuBr₂) (0.5 mg, 0.002 mmol) were taken in a 5-mL graduated glass tube. NPMA (400 mg, 2.0 mmol) was introduced into the reaction tube subsequently followed by the addition of 0.5 cm pre-washed (with a 1:1 (v/v) mixture of methanol and HCl 2M) and dried (by acetone and vacuum) metallic copper. Solvent (370 μL) was injected to the tube, which was then closed with a rubber septum and placed in a 60°C pre-heated oil bath. Until reaction mixture was stirred thoroughly, ethyl α-bromoisobutyrate (eBiB) (3.9 mg, 0.02 mmol) was added then the tube was sealed with parafilm and purged with a strong flow of argon. The reaction mixture was kept under argon until the reaction time reached, after that, reaction mixture polymers was precipitated in methanol followed by filtration to collect white solid. Yield in mass: 70%. ¹H-NMR (360 MHz, DMSO-d₅, δ): 1.0 to 1.8 (br, 3H, -C-CH₃), 7.2 to 7.7 (br, 2H, aromatic protons in ortho positions), 8.0 to 8.5 (br, 2H, aromatic proton in ortho positions). Note: the peak(s) characterize for -CH₂- in polymer backbone overlap(s) with peaks of DMSO-d₅ (δ = 2.0 to 3.0).

***In situ* chain extension of PFPMA-Br**

In a reactor, dnNbp_y (0.0136 mmol) and copper(II) bromide (CuBr₂) (0.0034 mmol) were solubilized in 990 μL THF, then 330 μL of sulfolane was added. The complex mixture was degassed for 10 minutes under a moderate stream of argon, then PFPMA (330 μL) was injected followed by the addition of 1-cm prewashed Cu(0) wire. The initiator MBPA (13.5 μL) was introduced at last, the reaction was sealed under slight positive argon medium. The reactor was immersed in an oil bath preheated at 60 °C. After 6 hours, 200 μL of reaction mixture was withdrawn using an air-tight Ar-washed syringe for further characterizations. The monomer conversion was determined to be 89%. Then, a mixture of 1500 μL PFPMA, 1500 μL THF, 500 μL sulfolane, which was degassed by medium argon flow, was injected to reactor via an air-tight argon-washed syringe. The reaction reached 69% monomer conversion after 18 hours. The polymer was then precipitated in cold methanol and filtered under vacuum.

Typical procedure for copolymerization by Cu(0)-mediated RDRP

Prior to use, a Cu (0) wire of 1cm was washed by HCl 1M/MeOH (1:1 v/v), rinsed with acetone and dried under vacuum. In a round bottom flask, NPMA at given weight was

dissolved in 1320 μL THF, then a mixture of TPMA (4.3 mg, 0.015 mmol) and CuBr_2 (0.8 mg, 3.6×10^{-3} mmol) in 660 μL of sulfolane was introduced, followed by the introduction of PFPMA. The mixture was degassed for 15 minutes under argon. Cu^0 and eBiB (5.0 μL , 3.4×10^{-5} mmol) were introduced respectively. The flask was sealed by a rubber septum and parafilm before immersed in a preheated oil bath at 60 $^\circ\text{C}$. The reaction was stopped at desired time. Reaction mixture was passed through a basic aluminum column with DCM as solvent. The collected solution was then concentrated and precipitated in excess MeOH. Further purification was done by redissolution of copolymers in THF, reprecipitation in excess MeOH and dry under high vacuum at room temperature.

Preparation of PET-NH₂ film by aminolysis

PET films of 1 cm x 2 cm were cleaned with EtOH:H₂O (1:1 vol.) by shaking for 15 minutes then washed with acetone and dried under vacuum. Dry films were immersed in a solution of PEI 5% w/w in DMSO in a 50 $^\circ\text{C}$ preheated water bath. After 6 hours, films were washed with excess DMSO by shaking at 200 rpm overnight. Films were then cleaned with excess deionized water until no absorption under UV light at 214 nm was detected, indicating the complete removal of non-specific attached PEI and DMSO. Finally, films were subsequently rinsed with acetone and dried under vacuum at room temperature.

UV-Vis titration of amino groups by orange II dye

The titration of amino groups on PET surface was done as described in literature by the use of orange II dye [327]. Briefly, each film was immersed in 2 mL of orange II dye in acidic water (pH 3, dye concentration 15 $\text{mg}\cdot\text{mL}^{-1}$) for 45 minutes at 40 $^\circ\text{C}$. Non-specific interaction dye was removed by subsequently washing films in acidic water (pH 3). Detachment of adsorbed dye was performed by dipping films in basic water (pH 12) for a few minutes, solution of detached dyes was adjusted to pH 3 using concentrated HCl. Absorbance was measured between 350 - 600 nm, maximum absorbance at 484 nm was recorded and the amount of amino groups was reported as number of group per nm^2 .

A calibration curve was obtained using Orange II dye solution in acidic water (pH 3) at several dye concentrations of 9×10^{-4} , 18×10^{-4} , 27×10^{-4} , 36×10^{-4} and 72×10^{-4} $\text{mg}\cdot\text{mL}^{-1}$ to evaluate the wavelength-dependent molar absorptivity coefficient (ϵ) of $51.3 \text{ M}^{-1}\text{cm}^{-1}$.

Immobilization of initiator (PET-Br films)

2 films were placed face-to-face in a special designed mini reactor. In a pear-shaped flask, 6 mini-reactors (12 films) were placed vertically. The reactor was purged with a strong argon stream, and then 35 mL of anhydrous diethylether was introduced via an air-tight syringe. 5 mL of triethylamine (0.036 mmol) was injected at 0 $^\circ\text{C}$, followed by 3.75 mL of α -bromoisobutyryl bromide (0.03 mmol) dropwise. The reaction was kept at 0 $^\circ\text{C}$ for 3 hours, and then left overnight at room temperature. Films were removed from solution and washed

several times with excess amount of dichloromethane, acetone and water then dried under vacuum.

Surface-initiated Cu(0)-mediated radical polymerization of PFPMA

For surface of **PET-g-PPFPMA-110** and **PET-g-PPFPMA-127**: in a modified 10 mL round-bottom vial, 2 films were placed face-to-face, then 2 mL of DMSO:Sulfolane (1:4 vol.) containing 3.5 mg of TPMA and 0.8 mg of CuBr₂ was injected *via* an air-tight syringe. Reactor was then purged with a mediate argon stream for 5 minutes, then 660 µL of PFPMA (3.4 mmol) and a prewashed U-shaped Cu(0) wire were introduced (total 2.5 cm). The reactor was then capped, sealed with parafilm and placed in a 60 °C preheated oil bath for 24 hours (PET-g-PPFPMA-110) and 72 hours (PET-g-PPFPMA-127). Films were removed from solution and washed with excess amount of dichloromethane, acetone and water several times, then dried and stored under vacuum prior to analysis.

Large batch reaction (PET-g-PPFPMA-90): 43.0 mg of TPMA (0.148 mmol) and 8.0 mg of CuBr₂ (0.036 mmol) were dissolved in a mixture of 6 mL DMSO and 24 mL sulfolane in a 50 mL eggplant-shaped flask. 12 films in 6 mini-reactors were then arranged vertically in the flask, each mini-reactor also contained a U-shaped Cu⁰ wire (total 5 cm). 5 mL of PFPMA (22.03 mmol) was injected *via* an air-tight syringe. The flask was then purged with a modest flow of argon for 15 minutes. The reaction was carried out in a 60 °C preheated oil bath for 24 hours. Films were then washed with excess amount of dichloromethane, acetone and water several times, then dried and stored under vacuum prior to analysis.

Typical post-modification of PFPMA in solution

250 mg of PFPMA (~1.0 mmol of pentafluorophenyl moieties) in a round-bottomed flask was dissolved in 1mL of anhydrous THF under a moderate stream of argon. A desired equivalent of dry alcohol or amine was then rapidly introduced into flask followed by the addition of DBU. The flask was then sealed under argon and immersed in an oil bath at 60 °C. After reaching desired reaction time, the polymer was collected by direct precipitation in cold methanol or proper ethers (diethylether or petroleum ether).

Typical post-modification of PET-g-PPFPMA-90

Post-modification of PET-g-PPFPMA-90 in general was carried out in the setup as given in 3.2. Two films were placed back-to-back in a minireactor, 6 reactors were aligned vertically in a flask. Then an excess amount of alcohol/amine (3.5 mmol) was added to reactor. 40-mL of anhydrous solvent (THF or DMF) was introduced *via* air-tight syringe under argon. 3.5 mmol of DBU was injected. The flask was immerse in pre-heated oil bath of 50-60 °C. After 24 hours, films were taken out and washed several times with copious amount of THF, water, ethanol and acetone before drying in vacuum at room temperature.

References

1. K. H.-M. Philippe Cavalié, *Evolution des consommations d'antibiotiques en France entre 2000 et 2015*, 2017.
2. R. M. Donlan, *Emerging infectious diseases*, 2002, **8**, 881-890.
3. H. H. Tuson and D. B. Weibel, *Soft matter*, 2013, **9**, 4368-4380.
4. H. Vlamakis, Y. Chai, P. Beauregard, R. Losick and R. Kolter, *Nature Reviews Microbiology*, 2013, **11**, 157.
5. J. Ma, Y. Sun, K. Gleichauf, J. Lou and Q. Li, *Langmuir*, 2011, **27**, 10035-10040.
6. E. P. Ivanova, J. Hasan, H. K. Webb, V. K. Truong, G. S. Watson, J. A. Watson, V. A. Baulin, S. Pogodin, J. Y. Wang and M. J. Tobin, *Small*, 2012, **8**, 2489-2494.
7. D. R. Orvos, D. J. Versteeg, J. Inauen, M. Capdevielle, A. Rothenstein and V. Cunningham, *Environmental Toxicology and Chemistry: An International Journal*, 2002, **21**, 1338-1349.
8. A. B. Dann and A. Hontela, *Journal of applied toxicology*, 2011, **31**, 285-311.
9. S. Langsrud, M. S. Sidhu, E. Heir and A. L. Holck, *International Biodeterioration & Biodegradation*, 2003, **51**, 283-290.
10. G. Sundheim, S. Langsrud, E. Heir and A. Holck, *International Biodeterioration & Biodegradation*, 1998, **41**, 235-239.
11. W. A. Rutala, M. M. Stiegel, F. A. Sarubbi and D. J. Weber, *Infection Control & Hospital Epidemiology*, 1997, **18**, 417-421.
12. A. Bridier, R. Briandet, V. Thomas and F. Dubois-Brissonnet, *Biofouling*, 2011, **27**, 1017-1032.
13. F. Siedenbiedel and J. C. Tiller, *Polymers*, 2012, **4**, 46.
14. S. Jeon, J. Lee, J. Andrade and P. De Gennes, *Journal of colloid and interface science*, 1991, **142**, 149-158.
15. J. Li, D. Tan, X. Zhang, H. Tan, M. Ding, C. Wan and Q. Fu, *Colloids and Surfaces B: Biointerfaces*, 2010, **78**, 343-350.
16. B. Dong, H. Jiang, S. Manolache, A. C. L. Wong and F. S. Denes, *Langmuir*, 2007, **23**, 7306-7313.
17. V. Hynninen, L. Vuori, M. Hannula, K. Tapio, K. Lahtonen, T. Isoniemi, E. Lehtonen, M. Hirsimäki, J. J. Toppari, M. Valden and V. P. Hytönen, *Scientific Reports*, 2016, **6**, 29324.
18. T. Ekblad, G. Bergström, T. Ederth, S. L. Conlan, R. Mutton, A. S. Clare, S. Wang, Y. Liu, Q. Zhao, F. D'Souza, G. T. Donnelly, P. R. Willemsen, M. E. Pettitt, M. E. Callow, J. A. Callow and B. Liedberg, *Biomacromolecules*, 2008, **9**, 2775-2783.
19. E. Ostuni, R. G. Chapman, R. E. Holmlin, S. Takayama and G. M. Whitesides, *Langmuir*, 2001, **17**, 5605-5620.
20. Q. Yang, C. Kaul and M. Ulbricht, *Langmuir*, 2010, **26**, 5746-5752.
21. L. Pérez-Álvarez, L. Ruiz-Rubio, I. Azua, V. Benito, A. Bilbao and J. L. Vilas-Vilela, *European Polymer Journal*, 2019, **112**, 31-37.
22. J. C. Kim, Y. Rho, G. Kim, M. Kim, H. Kim, I. J. Kim, J. R. Kim and M. Ree, *Polymer Chemistry*, 2013, **4**, 2260-2271.
23. S. Chen, L. Li, C. Zhao and J. Zheng, *Polymer*, 2010, **51**, 5283-5293.

24. W. K. Cho, B. Kong and I. S. Choi, *Langmuir*, 2007, **23**, 5678-5682.
25. Y.-F. Yang, Y. Li, Q.-L. Li, L.-S. Wan and Z.-K. Xu, *Journal of Membrane Science*, 2010, **362**, 255-264.
26. W. Li, Q. Liu and L. Liu, *Journal of Biomaterials Science, Polymer Edition*, 2014, **25**, 1730-1742.
27. J. Zheng, L. Li, H.-K. Tsao, Y.-J. Sheng, S. Chen and S. Jiang, *Biophysical journal*, 2005, **89**, 158-166.
28. S. Herrwerth, W. Eck, S. Reinhardt and M. Grunze, *Journal of the American Chemical Society*, 2003, **125**, 9359-9366.
29. S. Jeon and J. Andrade, *Journal of Colloid and Interface Science*, 1991, **142**, 159-166.
30. B. J. Privett, J. Youn, S. A. Hong, J. Lee, J. Han, J. H. Shin and M. H. Schoenfish, *Langmuir*, 2011, **27**, 9597-9601.
31. J. Bruzaud, J. Tarrade, E. Celia, T. Darmanin, E. Taffin de Givenchy, F. Guittard, J.-M. Herry, M. Guilbaud and M.-N. Bellon-Fontaine, *Materials Science and Engineering: C*, 2017, **73**, 40-47.
32. L. R. Freschauf, J. McLane, H. Sharma and M. Khine, *PLoS One*, 2012, **7**, e40987.
33. E. Fadeeva, V. K. Truong, M. Stiesch, B. N. Chichkov, R. J. Crawford, J. Wang and E. P. Ivanova, *Langmuir*, 2011, **27**, 3012-3019.
34. F. Gelman, K. Lewis and A. M. Klibanov, *Biotechnology letters*, 2004, **26**, 1695-1700.
35. J. Haldar, J. Chen, T. M. Tumpey, L. V. Gubareva and A. M. Klibanov, *Biotechnology letters*, 2008, **30**, 475-479.
36. S. A. Koplín, S. Lin and T. Domanski, *Biotechnology progress*, 2008, **24**, 1160-1165.
37. J. Lin, S. Qiu, K. Lewis and A. M. Klibanov, *Biotechnology Progress*, 2002, **18**, 1082-1086.
38. T. He and V. Chan, *Journal of Biomedical Materials Research Part A*, 2010, **95A**, 454-464.
39. J. Xu, X. Feng, P. Chen and C. Gao, *Journal of Membrane Science*, 2012, **413-414**, 62-69.
40. W.-Z. Qiu, Z.-S. Zhao, Y. Du, M.-X. Hu and Z.-K. Xu, *Applied Surface Science*, 2017, **426**, 972-979.
41. T. Kruk, K. Szczepanowicz, D. Kręgiel, L. Szyk-Warszyńska and P. Warszyński, *Colloids and Surfaces B: Biointerfaces*, 2016, **137**, 158-166.
42. J. Hernandez-Montelongo, E. G. Lucchesi, V. F. Nascimento, C. G. França, I. Gonzalez, W. A. A. Macedo, D. Machado, M. Lancellotti, A. M. Moraes, M. M. Beppu and M. A. Cotta, *Materials Science and Engineering: C*, 2017, **71**, 718-724.
43. M. Gultekinoglu, Y. Tunc Sarisozen, C. Erdogdu, M. Sagioglu, E. A. Aksoy, Y. J. Oh, P. Hinterdorfer and K. Ulubayram, *Acta Biomaterialia*, 2015, **21**, 44-54.
44. D. Roy, J. S. Knapp, J. T. Guthrie and S. Perrier, *Biomacromolecules*, 2008, **9**, 91-99.
45. X. Liu, H. Zhang, Z. Tian, A. Sen and H. R. Allcock, *Polymer Chemistry*, 2012, **3**, 2082-2091.
46. H. Dong, J. Huang, R. R. Koepsel, P. Ye, A. J. Russell and K. Matyjaszewski, *Biomacromolecules*, 2011, **12**, 1305-1311.
47. L.-A. B. Rawlinson, S. M. Ryan, G. Mantovani, J. A. Syrett, D. M. Haddleton and D. J. Brayden, *Biomacromolecules*, 2009, **11**, 443-453.
48. F. Xu, S. Yuan, S. Pehkonen, E. Kang and K. Neoh, *NanoBiotechnology*, 2006, **2**, 123-134.
49. J. C. Tiller, S. B. Lee, K. Lewis and A. M. Klibanov, *Biotechnology and Bioengineering*, 2002, **79**, 465-471.

50. J. Thome, A. Holländer, W. Jaeger, I. Trick and C. Oehr, *Surface and Coatings Technology*, 2003, **174-175**, 584-587.
51. J. Guo, J. Qin, Y. Ren, B. Wang, H. Cui, Y. Ding, H. Mao and F. Yan, *Polymer Chemistry*, 2018, **9**, 4611-4616.
52. L.-H. Yin, B. Ran, T.-J. Hu, C. Yang, J.-J. Fei and Y.-H. Li, *RSC Advances*, 2017, **7**, 6006-6012.
53. S. Burt, *International journal of food microbiology*, 2004, **94**, 223-253.
54. L. Nedorostova, P. Kloucek, L. Kokoska, M. Stolcova and J. Pulkrabek, *Food control*, 2009, **20**, 157-160.
55. J. Gutierrez, C. Barry-Ryan and P. Bourke, *International journal of food microbiology*, 2008, **124**, 91-97.
56. F. A. Al-Bayati, *Journal of ethnopharmacology*, 2008, **116**, 403-406.
57. A. Govaris, N. Solomakos, A. Pexara and P. Chatzopoulou, *International journal of food microbiology*, 2010, **137**, 175-180.
58. D. D. Jayasena and C. Jo, *Trends in Food Science & Technology*, 2013, **34**, 96-108.
59. A. Guarda, J. F. Rubilar, J. Miltz and M. J. Galotto, *International journal of food microbiology*, 2011, **146**, 144-150.
60. M. Peltzer, J. Wagner and A. Jiménez, *Food Additives & Contaminants: Part A*, 2009, **26**, 938-946.
61. S. A. Burt and R. D. Reinders, *Letters in applied microbiology*, 2003, **36**, 162-167.
62. M. Moraes-Lovison, L. F. Marostegan, M. S. Peres, I. F. Menezes, M. Ghiraldi, R. A. Rodrigues, A. M. Fernandes and S. C. Pinho, *LWT*, 2017, **77**, 233-240.
63. I. Liakos, L. Rizzello, D. J. Scurr, P. P. Pompa, I. S. Bayer and A. Athanassiou, *International journal of pharmaceutics*, 2014, **463**, 137-145.
64. A. Nostro, R. Scaffaro, M. D'Arrigo, L. Botta, A. Filocamo, A. Marino and G. Bisignano, *Applied microbiology and biotechnology*, 2012, **96**, 1029-1038.
65. P. Persico, V. Ambrogi, C. Carfagna, P. Cerruti, I. Ferrocino and G. Mauriello, *Polymer Engineering & Science*, 2009, **49**, 1447-1455.
66. B. Lepoittevin, X. Wang, J.-P. Baltaze, H. Liu, J.-M. Herry, M.-N. Bellon-Fontaine and P. Roger, *European Polymer Journal*, 2011, **47**, 1842-1851.
67. S. Bedel, B. Lepoittevin, L. Costa, O. Leroy, D. Dragoë, J. Bruzard, J.-M. Herry, M. Guilbaud, M.-N. Bellon-Fontaine and P. Roger, *Journal of Polymer Science Part A: Polymer Chemistry*, 2015, **53**, 1975-1985.
68. H. Salmi-Mani, G. Terreros, N. Barroca-Aubry, C. Aymes-Chodur, C. Regeard and P. Roger, *European Polymer Journal*, 2018, **103**, 51-58.
69. M. Ruiz-Rico, É. Pérez-Esteve, A. Bernardos, F. Sancenón, R. Martínez-Máñez, M. D. Marcos and J. M. Barat, *Food Chemistry*, 2017, **233**, 228-236.
70. L. Luo, G. Li, D. Luan, Q. Yuan, Y. Wei and X. Wang, *ACS Applied Materials & Interfaces*, 2014, **6**, 19371-19377.
71. S. Thomas and P. Visakh, *Handbook of Engineering and Specialty Thermoplastics, Volume 3: Polyethers and Polyesters*, John Wiley & Sons, 2011.
72. S. Pira, *The Future of PET Packaging to 2021*, 2016.
73. Y. Liu, R. Luo, F. Shen, L. Tang, J. Wang and N. Huang, *Applied Surface Science*, 2015, **328**, 163-169.

74. G. Marcelo and M. Fernández-García, *RSC Advances*, 2014, **4**, 11740-11749.
75. O. Zvarec, S. Purushotham, A. Masic, R. V. Ramanujan and A. Miserez, *Langmuir*, 2013, **29**, 10899-10906.
76. W.-H. Zhou, C.-H. Lu, X.-C. Guo, F.-R. Chen, H.-H. Yang and X.-R. Wang, *Journal of Materials Chemistry*, 2010, **20**, 880-883.
77. S. Suárez-García, J. Sedó, J. Saiz-Poseu and D. Ruiz-Molina, *Biomimetics*, 2017, **2**, 22.
78. S. Moulay, *Polymer Reviews*, 2014, **54**, 436-513.
79. D. Hong, K. Bae, S.-P. Hong, J. H. Park, I. S. Choi and W. K. Cho, *Chemical communications*, 2014, **50**, 11649-11652.
80. R. Subair, B. P. Tripathi, P. Formanek, F. Simon, P. Uhlmann and M. Stamm, *Chemical Engineering Journal*, 2016, **295**, 358-369.
81. Z. Xu, K. Miyazaki and T. Hori, *Applied Surface Science*, 2016, **370**, 243-251.
82. J. Ryu, S. H. Ku, H. Lee and C. B. Park, *Advanced Functional Materials*, 2010, **20**, 2132-2139.
83. M. Sureshkumar and C.-K. Lee, *Carbohydrate polymers*, 2011, **84**, 775-780.
84. J. Ou, J. Wang, S. Liu, J. Zhou, S. Ren and S. Yang, *Applied Surface Science*, 2009, **256**, 894-899.
85. X. Liu, J. Cao, H. Li, J. Li, Q. Jin, K. Ren and J. Ji, *ACS nano*, 2013, **7**, 9384-9395.
86. H. Karkhanechi, R. Takagi and H. Matsuyama, *Desalination*, 2014, **337**, 23-30.
87. W. Wang, W. Cheng, M. Tian, H. Zou, L. Li and L. Zhang, *Electrochimica Acta*, 2012, **79**, 37-45.
88. Y. Zhou, L. Jiang, Y. Guo, Z. Sun, Z. Jiang, S. Chen, J. Ma and S. Jerrams, *Textile Research Journal*, 2019, **0**, 0040517519826893.
89. L. Li and H. Li, *Materials Research Innovations*, 2015, **19**, S8-174-S178-179.
90. C. Zhao, L. Xing, J. Xiang, L. Cui, J. Jiao, H. Sai, Z. Li and F. Li, *Particuology*, 2014, **17**, 66-73.
91. H. Niu, S. Wang, T. Zeng, Y. Wang, X. Zhang, Z. Meng and Y. Cai, *Journal of Materials Chemistry*, 2012, **22**, 15644-15653.
92. A. Y. Fadeev and T. J. McCarthy, *Langmuir*, 1998, **14**, 5586-5593.
93. H. Poortavasoly, M. Montazer and T. Harifi, *Materials Science and Engineering: C*, 2016, **58**, 495-503.
94. B. Lepoittevin, L. Costa, S. Pardoue, D. Dragoé, S. Mazerat and P. Roger, *Journal of Polymer Science Part A: Polymer Chemistry*, 2016, **54**, 2689-2697.
95. B. Loïc, M. Thierry, L. Bénédicte and R. Philippe, *Journal of Polymer Science Part A: Polymer Chemistry*, 2007, **45**, 2172-2183.
96. H. Zahn and H. Pfeifer, *Polymer*, 1963, **4**, 429-432.
97. M. Maaz, T. Elzein, A. Bejjani, N. Barroca-Aubry, B. Lepoittevin, D. Dragoé, S. Mazerat, B. Nsouli and P. Roger, *Journal of Colloid and Interface Science*, 2017, **500**, 69-78.
98. S. Noel, B. Liberelle, A. Yogi, M. J. Moreno, M. N. Bureau, L. Robitaille and G. De Crescenzo, *Journal of Materials Chemistry B*, 2013, **1**, 230-238.
99. A. Utrata-Wesołek, W. Wałach, M. Bochenek, B. Trzebicka, J. Anioł, A. L. Sieroń, J. Kubacki and A. Dworak, *European Polymer Journal*, 2018, **105**, 313-322.

100. A. Boulares-Pender, A. Prager, S. Reichelt, C. Elsner and M. R. Buchmeiser, *Journal of Applied Polymer Science*, 2011, **121**, 2543-2550.
101. L. N. Bui, M. Thompson, N. B. McKeown, A. D. Romaschin and P. G. Kalman, *Analyst*, 1993, **118**, 463-474.
102. M. Monier and D. A. Abdel-Latif, *Journal of Hazardous Materials*, 2013, **250-251**, 122-130.
103. S. L. Fávaro, A. F. Rubira, E. C. Muniz and E. Radovanovic, *Polymer Degradation and Stability*, 2007, **92**, 1219-1226.
104. W. Chen and T. J. McCarthy, *Macromolecules*, 1998, **31**, 3648-3655.
105. V. Muthuvijayan, J. Gu and R. S. Lewis, *Acta Biomaterialia*, 2009, **5**, 3382-3393.
106. J. Bucheňska, *Journal of Applied Polymer Science*, 1997, **65**, 967-977.
107. P. A. Ramires, L. Mirengi, A. R. Romano, F. Palumbo and G. Nicolardi, *Journal of Biomedical Materials Research*, 2000, **51**, 535-539.
108. J. Sun, L. Yao, Z. Gao, S. Peng, C. Wang and Y. Qiu, *Surface and Coatings Technology*, 2010, **204**, 4101-4106.
109. I. Junkar, A. Vesel, U. Cvelbar, M. Mozetič and S. Strnad, *Vacuum*, 2009, **84**, 83-85.
110. L. Yang, J. Chen, Y. Guo and Z. Zhang, *Applied Surface Science*, 2009, **255**, 4446-4451.
111. K. N. Pandiyaraj, V. Selvarajan, R. Deshmukh and C. Gao, *Vacuum*, 2008, **83**, 332-339.
112. N. Recek, M. Jaganjac, M. Kolar, L. Milkovic, M. Mozetič, K. Stana-Kleinschek and A. Vesel, *Molecules*, 2013, **18**, 12441-12463.
113. E. Amanatides, D. Mataras, M. Katsikogianni and Y. Missirlis, *Surface and Coatings Technology*, 2006, **200**, 6331-6335.
114. S. Pelagade, N. Singh, A. Qureshi, R. Rane, S. Mukherjee, U. Deshpande, V. Ganesan and T. Shripathi, *Nuclear Instruments and Methods in Physics Research Section B: Beam Interactions with Materials and Atoms*, 2012, **289**, 34-38.
115. J. Lai, B. Sunderland, J. Xue, S. Yan, W. Zhao, M. Folkard, B. D. Michael and Y. Wang, *Applied Surface Science*, 2006, **252**, 3375-3379.
116. T.-S. Cheng, H.-T. Lin and M.-J. Chuang, *Materials Letters*, 2004, **58**, 650-653.
117. J. Lei, L. Yang, Y. Zhan, Y. Wang, T. Ye, Y. Li, H. Deng and B. Li, *Colloids and Surfaces B: Biointerfaces*, 2014, **114**, 60-66.
118. K.-S. Chen, J.-C. Tsai, C.-W. Chou, M.-R. Yang and J.-M. Yang, *Materials Science and Engineering: C*, 2002, **20**, 203-208.
119. F. C. Loh, K. L. Tan, E. T. Kang, Y. Uyama and Y. Ikada, *Polymer*, 1995, **36**, 21-27.
120. M.-R. Yang, K.-S. Chen, J.-C. Tsai, C.-C. Tseng and S.-F. Lin, *Materials Science and Engineering: C*, 2002, **20**, 167-173.
121. J. Casimiro, B. Lepoittevin, C. Boisse-Laporte, M.-G. Barthés-Labrousse, P. Jegou, F. Brisset and P. Roger, *Plasma Chemistry and Plasma Processing*, 2012, **32**, 305-323.
122. L. Bech, B. Lepoittevin, A. El Achhab, E. Lepleux, L. Teulé-Gay, C. Boisse-Laporte and P. Roger, *Langmuir*, 2007, **23**, 10348-10352.
123. E. Uchida, Y. Uyama and Y. Ikada, *Journal of Applied Polymer Science*, 1990, **41**, 677-687.
124. Y.-W. Song, H.-S. Do, H.-S. Joo, D.-H. Lim, S. Kim and H.-J. Kim, *Journal of Adhesion Science and Technology*, 2006, **20**, 1357-1365.
125. N. H. Mohamed, T. Bahners, A. Wego, J. S. Gutmann and M. Ulbricht, *Applied Surface Science*, 2012, **259**, 261-269.

126. L. M. Beckley, T. J. Lewis and D. M. Taylor, *Journal of Physics D: Applied Physics*, 1976, **9**, 1355-1365.
127. D. M. Taylor, *Journal of Physics D: Applied Physics*, 1976, **9**, 2269-2279.
128. I. Prosyčėvas, J. Puišo, S. Tamulevičius, A. Juraitis, M. Andrulevičius and B. Čyžiūtė, *Thin Solid Films*, 2006, **495**, 118-123.
129. W. Qiu, U. W. Paetzold, R. Gehlhaar, V. Smirnov, H.-G. Boyen, J. G. Tait, B. Conings, W. Zhang, C. B. Nielsen, I. McCulloch, L. Froyen, P. Heremans and D. Cheyns, *Journal of Materials Chemistry A*, 2015, **3**, 22824-22829.
130. G. Burillo, L. Tenorio, E. Bucio, E. Adem and G. P. Lopez, *Radiation Physics and Chemistry*, 2007, **76**, 1728-1731.
131. J. Wang, G. A. Botton, M. M. West and A. P. Hitchcock, *The Journal of Physical Chemistry B*, 2009, **113**, 1869-1876.
132. N. Singh, A. Sharma and D. K. Avasthi, *Nuclear Instruments and Methods in Physics Research Section B: Beam Interactions with Materials and Atoms*, 2003, **206**, 1120-1123.
133. J.-W. Han, H.-J. Kang, J.-H. Kim and D.-S. Seo, *Japanese Journal of Applied Physics*, 2006, **45**, L827-L829.
134. A. C. Rinkenauer, S. Schubert, A. Traeger and U. S. Schubert, *Journal of Materials Chemistry B*, 2015, **3**, 7477-7493.
135. B. Lepoittevin, S. Bedel, D. Dragoé, J. Bruzaud, M.-G. Barthés-Labrousse, S. Mazerat, J.-M. Herry, M.-N. Bellon-Fontaine and P. Roger, *Progress in Organic Coatings*, 2015, **82**, 17-25.
136. X. Jin, J. Yuan and J. Shen, *Colloids and Surfaces B: Biointerfaces*, 2016, **145**, 275-284.
137. F. Chen, Z. Shi, K. G. Neoh and E. T. Kang, *Biotechnology and Bioengineering*, 2009, **104**, 30-39.
138. R. Kaur and S. Liu, *Progress in Surface Science*, 2016, **91**, 136-153.
139. M. Khan, J. Yang, C. Shi, J. Lv, Y. Feng and W. Zhang, *Acta Biomaterialia*, 2015, **20**, 69-81.
140. I. Willner, *Science*, 2002, **298**, 2407-2408.
141. Z. Zhang, S. Yuan, X. Zhu, K. Neoh and E. Kang, *Biosensors and Bioelectronics*, 2010, **25**, 1102-1108.
142. T. K. Tam, J. Zhou, M. Pita, M. Ornatska, S. Minko and E. Katz, *Journal of the American Chemical Society*, 2008, **130**, 10888-10889.
143. O. Parlak, M. Ashaduzzaman, S. B. Kollipara, A. Tiwari and A. P. Turner, *ACS applied materials & interfaces*, 2015, **7**, 23837-23847.
144. P. Wan and X. Chen, *ChemElectr oChem*, 2014, **1**, 1602-1612.
145. K. R. Reddy, B. C. Sin, K. S. Ryu, J.-C. Kim, H. Chung and Y. Lee, *Synthetic Metals*, 2009, **159**, 595-603.
146. S. Tugulu, P. Silacci, N. Stergiopulos and H.-A. Klok, *Biomaterials*, 2007, **28**, 2536-2546.
147. H. Wu, G. Yu, L. Pan, N. Liu, M. T. McDowell, Z. Bao and Y. Cui, *Nature communications*, 2013, **4**, 1943.
148. S. Porel, S. Singh, S. S. Harsha, D. N. Rao and T. Radhakrishnan, *Chemistry of Materials*, 2005, **17**, 9-12.
149. A. Korchev, M. Bozack, B. Slaten and G. Mills, *Journal of the American Chemical Society*, 2004, **126**, 10-11.

150. S. Gupta, M. Agrawal, M. Conrad, N. A. Hutter, P. Olk, F. Simon, L. M. Eng, M. Stamm and R. Jordan, *Advanced Functional Materials*, 2010, **20**, 1756-1761.
151. F. Costantini, W. P. Bula, R. Salvio, J. Huskens, H. J. Gardeniers, D. N. Reinhoudt and W. Verboom, *Journal of the American Chemical Society*, 2009, **131**, 1650-1651.
152. F. Costantini, E. M. Benetti, R. M. Tiggelaar, H. J. Gardeniers, D. N. Reinhoudt, J. Huskens, G. J. Vancso and W. Verboom, *Chemistry—A European Journal*, 2010, **16**, 12406-12411.
153. H. Ma, M. S. Liu and A. K. Y. Jen, *Polymer International*, 2009, **58**, 594-619.
154. H. J. Snaith, G. L. Whiting, B. Sun, N. C. Greenham, W. T. Huck and R. H. Friend, *Nano letters*, 2005, **5**, 1653-1657.
155. G. L. Whiting, H. J. Snaith, S. Khodabakhsh, J. W. Andreasen, D. W. Breiby, M. M. Nielsen, N. C. Greenham, R. H. Friend and W. T. Huck, *Nano letters*, 2006, **6**, 573-578.
156. T. M. Fulghum, P. Taranekekar and R. C. Advincula, *Macromolecules*, 2008, **41**, 5681-5687.
157. J. C. Pinto, G. L. Whiting, S. Khodabakhsh, L. Torre, A. Rodríguez, R. M. Dalglish, A. M. Higgins, J. W. Andreasen, M. M. Nielsen and M. Geoghegan, *Advanced Functional Materials*, 2008, **18**, 36-43.
158. D. Maillard, S. K. Kumar, A. Rungta, B. C. Benicewicz and R. E. Prud'homme, *Nano letters*, 2011, **11**, 4569-4573.
159. V. Goel, J. Pietrasik, H. Dong, J. Sharma, K. Matyjaszewski and R. Krishnamoorti, *Macromolecules*, 2011, **44**, 8129-8135.
160. C. Perruchot, M. Khan, A. Kamitsi, S. v. Armes, T. Von Werne and T. Patten, *Langmuir*, 2001, **17**, 4479-4481.
161. X. Ye, C. Zhu, P. Ercius, S. N. Raja, B. He, M. R. Jones, M. R. Hauwiller, Y. Liu, T. Xu and A. P. Alivisatos, *Nature communications*, 2015, **6**, 10052.
162. B. G. Van Ravensteijn and W. K. Kegel, *Polymer Chemistry*, 2016, **7**, 2858-2869.
163. B. Liu, W. Wei, X. Qu and Z. Yang, *Angewandte Chemie International Edition*, 2008, **47**, 3973-3975.
164. B. Xin and J. Hao, *Chemical Society Reviews*, 2010, **39**, 769-782.
165. E. Svetushkina, N. Pureskiy, L. Ionov, M. Stamm and A. Synytska, *Soft Matter*, 2011, **7**, 5691-5696.
166. S. Minko, M. Müller, M. Motornov, M. Nitschke, K. Grundke and M. Stamm, *Journal of the American Chemical Society*, 2003, **125**, 3896-3900.
167. J. A. Howarter and J. P. Youngblood, *Advanced materials*, 2007, **19**, 3838-3843.
168. O. Azzaroni, A. A. Brown and W. T. Huck, *Advanced Materials*, 2007, **19**, 151-154.
169. K. Yu and Y. Han, *Soft Matter*, 2009, **5**, 759-768.
170. J. L. Paris, M. V. Cabañas, M. Manzano and M. Vallet-Regí, *ACS nano*, 2015, **9**, 11023-11033.
171. K. Matyjaszewski, *Macromolecules*, 2012, **45**, 4015-4039.
172. G. Moad, E. Rizzardo and S. H. Thang, *Polymer*, 2008, **49**, 1079-1131.
173. M. Baum and W. J. Brittain, *Macromolecules*, 2002, **35**, 610-615.
174. G. Gody, C. Rossner, J. Moraes, P. Vana, T. Maschmeyer and S. Perrier, *Journal of the American Chemical Society*, 2012, **134**, 12596-12603.
175. Q. Peng, D. M. Lai, E. Kang and K. Neoh, *Macromolecules*, 2006, **39**, 5577-5582.
176. Y. Zhao and S. Perrier, *Macromolecules*, 2006, **39**, 8603-8608.

177. Y. Zhao and S. Perrier, 2007.
178. M. H. Stenzel, L. Zhang and W. T. Huck, *Macromolecular rapid communications*, 2006, **27**, 1121-1126.
179. B. M. Cash, L. Wang and B. C. Benicewicz, *Journal of Polymer Science Part A: Polymer Chemistry*, 2012, **50**, 2533-2540.
180. N. S. Lee and K. L. Wooley.
181. V. Ladmiral, T. Morinaga, K. Ohno, T. Fukuda and Y. Tsujii, *European Polymer Journal*, 2009, **45**, 2788-2796.
182. R. B. Grubbs, *Polymer Reviews*, 2011, **51**, 104-137.
183. J. O. Zoppe, N. C. Ataman, P. Mocny, J. Wang, J. Moraes and H.-A. Klok, *Chemical reviews*, 2017, **117**, 1105-1318.
184. K. M. Wei Tang, *Macromolecules*, 2007, **40**, 7.
185. Y. Kwak and K. Matyjaszewski, *Macromolecules*, 2008, **41**, 6627-6635.
186. W. Tang, Y. Kwak, W. Braunecker, N. V. Tsarevsky, M. L. Coote and K. Matyjaszewski, *Journal of the American Chemical Society*, 2008, **130**, 10702-10713.
187. A. K. Nanda and K. Matyjaszewski, *Macromolecules*, 2003, **36**, 1487-1493.
188. K. Matyjaszewski, H.-j. Paik, P. Zhou and S. J. Diamanti, *Macromolecules*, 2001, **34**, 5125-5131.
189. N. Bortolamei, A. A. Isse, A. J. D. Magenau, A. Gennaro and K. Matyjaszewski, *Angewandte Chemie International Edition*, 2011, **50**, 11391-11394.
190. W. A. Braunecker, N. V. Tsarevsky, A. Gennaro and K. Matyjaszewski, *Macromolecules*, 2009, **42**, 6348-6360.
191. N. Bortolamei, A. A. Isse, V. B. Di Marco, A. Gennaro and K. Matyjaszewski, *Macromolecules*, 2010, **43**, 9257-9267.
192. A. J. D. Magenau, N. C. Strandwitz, A. Gennaro and K. Matyjaszewski, *Science*, 2011, **332**, 81-84.
193. D. Konkolewicz, K. Schröder, J. Buback, S. Bernhard and K. Matyjaszewski, *ACS Macro Letters*, 2012, **1**, 1219-1223.
194. W. Jakubowski, K. Min and K. Matyjaszewski, *Macromolecules*, 2006, **39**, 39-45.
195. A. Anastasaki, V. Nikolaou, G. Nurumbetov, P. Wilson, K. Kempe, J. F. Quinn, T. P. Davis, M. R. Whittaker and D. M. Haddleton, *Chemical reviews*, 2015, **116**, 835-877.
196. S. Harrisson, P. Couvreur and J. Nicolas, *Macromolecules*, 2012, **45**, 7388-7396.
197. D. Konkolewicz, Y. Wang, M. Zhong, P. Krys, A. A. Isse, A. Gennaro and K. Matyjaszewski, *Macromolecules*, 2013, **46**, 8749-8772.
198. D. Konkolewicz, Y. Wang, P. Krys, M. Zhong, A. A. Isse, A. Gennaro and K. Matyjaszewski, *Polymer Chemistry*, 2014, **5**, 4396-4417.
199. F. Lorandi, M. Fantin, A. A. Isse and A. Gennaro, *Polymer*, 2015, **72**, 238-245.
200. G. Lligadas, B. M. Rosen, M. J. Monteiro and V. Percec, *Macromolecules*, 2008, **41**, 8360-8364.
201. D. Konkolewicz, P. Krys, J. R. Góis, P. V. Mendonça, M. Zhong, Y. Wang, A. Gennaro, A. A. Isse, M. Fantin and K. Matyjaszewski, *Macromolecules*, 2014, **47**, 560-570.
202. N. H. Nguyen and V. Percec, *Journal of Polymer Science Part A: Polymer Chemistry*, 2011, **49**, 4227-4240.

203. Y. Gao, T. Zhao and W. Wang, *RSC Advances*, 2014, **4**, 61687-61690.
204. B. M. Rosen, X. Jiang, C. J. Wilson, N. H. Nguyen, M. J. Monteiro and V. Percec, *Journal of Polymer Science Part A: Polymer Chemistry*, 2009, **47**, 5606-5628.
205. X. H. Liu, G. B. Zhang, B. X. Li, Y. G. Bai and Y. S. Li, *Journal of Polymer Science Part A: Polymer Chemistry*, 2010, **48**, 5439-5445.
206. L. Xue, Z. Lyu, X. Shi, Z. Tang, G. Chen and H. Chen, *Macromolecular Chemistry and Physics*, 2014, **215**, 1491-1497.
207. P. i. V. M. Joana P. Mendes, Pedro Maximiano, Carlos M. R. Abreu, and A. e. C. S. a. J. F. J. C. Tamaz Guliashvili, *RSC Advances*, 2016, **6**, 9598.
208. P. Krys, Y. Wang, K. Matyjaszewski and S. Harrisson, *Macromolecules*, 2016, **49**, 2977-2984.
209. K. F. Augustine, T. G. Ribelli, M. Fantin, P. Krys, Y. Cong and K. Matyjaszewski, *Journal of Polymer Science Part A: Polymer Chemistry*, 2017, **55**, 3048-3057.
210. D. Jenkins Aubrey, G. Jones Richard and G. Moad, *Journal*, 2009, **82**, 483.
211. R. Whitfield, A. Anastasaki, G. R. Jones and D. M. Haddleton, *Polymer Chemistry*, 2018, **9**, 4395-4403.
212. G. R. Jones, R. Whitfield, A. Anastasaki, N. Risangud, A. Simula, D. J. Keddie and D. M. Haddleton, *Polymer Chemistry*, 2018, **9**, 2382-2388.
213. M. Enayati and A. Abbaspourrad, *Polymer*, 2018, **153**, 464-473.
214. G. R. Jones, Z. Li, A. Anastasaki, D. J. Lloyd, P. Wilson, Q. Zhang and D. M. Haddleton, *Macromolecules*, 2016, **49**, 483-489.
215. J. R. G. Francisco Catalao, A. S. M. Trino, Armenio C. Serra and Jorge F. J. Coelho, *Polym. Chem.*, 2015, **6**.
216. P. V. Mendonca, D. Konkolewicz, S. E. Averick, A. C. Serra, A. V. Popov, T. Guliashvili, K. Matyjaszewski and J. F. J. Coelho, *Polymer Chemistry*, 2014, **5**, 5829-5836.
217. A. Simula, V. Nikolaou, F. Alsubaie, A. Anastasaki and D. M. Haddleton, *Polymer Chemistry*, 2015, **6**, 5940-5950.
218. C. Boyer, A. H. Soeriyadi, P. B. Zetterlund and M. R. Whittaker, *Macromolecules*, 2011, **44**, 8028-8033.
219. F. Alsubaie, A. Anastasaki, P. Wilson and D. M. Haddleton, *Polymer Chemistry*, 2014, **6**, 406-417.
220. L. Xue, Z. Lyu, X. Shi, Z. Tang, G. Chen and H. Chen, *Macromolecular Chemistry and Physics*, 2014, **215**, 1491-1497.
221. J. Laun, M. Vorobii, A. de los Santos Pereira, O. Pop-Georgievski, V. Trouillet, A. Welle, C. Barner-Kowollik, C. Rodriguez-Emmenegger and T. Junkers, *Macromolecular rapid communications*, 2015, **36**, 1681-1686.
222. M. Vorobii, A. de los Santos Pereira, O. Pop-Georgievski, N. Y. Kostina, C. Rodriguez-Emmenegger and V. Percec, *Polymer Chemistry*, 2015, **6**, 4210-4220.
223. M. A. Ver Meer, B. Narasimhan, B. H. Shanks and S. K. Mallapragada, *ACS Applied Materials & Interfaces*, 2009, **2**, 41-47.
224. T. Zhang, Y. Du, F. Müller, I. Amin and R. Jordan, *Polymer Chemistry*, 2015, **6**, 2726-2733.
225. X.-J. Shi, G.-J. Chen, Y.-W. Wang, L. Yuan, Q. Zhang, D. M. Haddleton and H. Chen, *Langmuir*, 2013, **29**, 14188-14195.

226. M. Maaz, T. Elzein, D. Dragoe, A. Bejjani, N. Jarroux, C. Poulard, N. Aubry-Barroca, B. Nsouli and P. Roger, *Journal of Materials Science*, 2019, **54**, 1184-1196.
227. S. Ding, J. A. Floyd and K. B. Walters, *Journal of Polymer Science Part A: Polymer Chemistry*, 2009, **47**, 6552-6560.
228. E. Turan and T. Caykara, *Reactive and Functional Polymers*, 2011, **71**, 1089-1095.
229. T. Zhang, E. M. Benetti and R. Jordan, *ACS Macro Letters*, 2019, DOI: 10.1021/acsmacrolett.8b00912, 145-153.
230. Y. Che, T. Zhang, Y. Du, I. Amin, C. Marschelke and R. Jordan, *Angewandte Chemie International Edition*, 2018, **57**, 16380-16384.
231. X. Chen, L. Yuan, P. Yang, J. Hu and D. Yang, *Journal of Polymer Science Part A: Polymer Chemistry*, 2011, **49**, 4977-4986.
232. Y. Deng, J. Z. Zhang, Y. Li, J. Hu, D. Yang and X. Huang, *Journal of Polymer Science Part A: Polymer Chemistry*, 2012, **50**, 4451-4458.
233. W. Yan, M. Fantin, S. Ramakrishna, N. D. Spencer, K. Matyjaszewski and E. M. Benetti, *ACS Applied Materials & Interfaces*, 2019, **11**, 27470-27477.
234. J. O. Zoppe, Y. Habibi, O. J. Rojas, R. A. Venditti, L.-S. Johansson, K. Efimenko, M. Österberg and J. Laine, *Biomacromolecules*, 2010, **11**, 2683-2691.
235. J. O. Zoppe, R. A. Venditti and O. J. Rojas, *Journal of colloid and interface science*, 2012, **369**, 202-209.
236. U. D. Hemraz, A. Lu, R. Sunasee and Y. Boluk, *Journal of colloid and interface science*, 2014, **430**, 157-165.
237. Y. Zou, J. N. Kizhakkedathu and D. E. Brooks, *Macromolecules*, 2009, **42**, 3258-3268.
238. B. F. L. Lai, A. L. Creagh, J. Janzen, C. A. Haynes, D. E. Brooks and J. N. Kizhakkedathu, *Biomaterials*, 2010, **31**, 6710-6718.
239. V. Chabrol, D. Léonard, M. Zorn, B. Reck, F. D'Agosto and B. Charleux, *Macromolecules*, 2012, **45**, 2972-2980.
240. J. Yuan, L. Wang, L. Zhu, M. Pan, W. Wang, Y. Liu and G. Liu, *Langmuir*, 2015, **31**, 4087-4095.
241. C. Zhou, H. Song, J. L. C. Loh, J. She, L. Deng and B. Liu, *Journal of Biomaterials Science, Polymer Edition*, 2018, **29**, 2106-2123.
242. T. Tischer, C. Rodriguez-Emmenegger, V. Trouillet, A. Welle, V. Schueler, J. O. Mueller, A. S. Goldmann, E. Brynda and C. Barner-Kowollik, *Advanced Materials*, 2014, **26**, 4087-4092.
243. M. Kopeć, J. Spanjers, E. Scavo, D. Ernens, J. Duvigneau and G. Julius Vancso, *European Polymer Journal*, 2018, **106**, 291-296.
244. S. Chen, N. Hori, M. Kajiyama and A. Takemura, *Journal of Applied Polymer Science*, 2019, **0**, 48246.
245. W. A. Cunningham, *Journal of Chemical Education*, 1935, **12**, 120.
246. R. E. Oesper, *Journal of Chemical Education*, 1929, **6**, 677.
247. K. A. Günay, P. Theato and H.-A. Klok, *Journal of Polymer Science Part A: Polymer Chemistry*, 2013, **51**, 1-28.
248. E. Blasco, M. B. Sims, A. S. Goldmann, B. S. Sumerlin and C. Barner-Kowollik, *Macromolecules*, 2017, **50**, 5215-5252.
249. P. Ferruti, A. Bettelli and A. Fere, *Polymer*, 1972, **13**, 462-464.

250. M.-N. Erout, A. Troesch, C. Pichot and P. Cros, *Bioconjugate chemistry*, 1996, **7**, 568-575.
251. L. E. Strong and L. L. Kiessling, *Journal of the American Chemical Society*, 1999, **121**, 6193-6196.
252. M. Mammen, G. Dahmann and G. M. Whitesides, *Journal of medicinal chemistry*, 1995, **38**, 4179-4190.
253. A. Godwin, M. Hartenstein, A. H. E. Müller and S. Brocchini, *Angewandte Chemie International Edition*, 2001, **40**, 594-597.
254. Z. Hu, Y. Liu, C. Hong and C. Pan, *Journal of applied polymer science*, 2005, **98**, 189-194.
255. S. Monge and D. M. Haddleton, *European polymer journal*, 2004, **40**, 37-45.
256. S. Parvin, J. Matsui, E. Sato and T. Miyashita, *Journal of colloid and interface science*, 2007, **313**, 128-134.
257. S. V. Orski, A. A. Poloukhtine, S. Arumugam, L. Mao, V. V. Popik and J. Locklin, *Journal of the American Chemical Society*, 2010, **132**, 11024-11026.
258. A. Favier, F. D'Agosto, M.-T. Charreyre and C. Pichot, *Polymer*, 2004, **45**, 7821-7830.
259. M. J. Yanjarappa, K. V. Gujraty, A. Joshi, A. Saraph and R. S. Kane, *Biomacromolecules*, 2006, **7**, 1665-1670.
260. E. N. Savariar and S. Thayumanavan, *Journal of Polymer Science Part A: Polymer Chemistry*, 2004, **42**, 6340-6345.
261. P. Relógio, M.-T. Charreyre, J. P. S. Farinha, J. M. Martinho and C. Pichot, *Polymer*, 2004, **45**, 8639-8649.
262. S. R. A. Devenish, J. B. Hill, J. W. Blunt, J. C. Morris and M. H. G. Munro, *Tetrahedron Letters*, 2006, **47**, 2875-2878.
263. S. Y. Wong and D. Putnam, *Bioconjugate Chemistry*, 2007, **18**, 970-982.
264. L. Kisfaludy, M. Löw, O. Nyéki, T. Szirtes and I. Schön, *Justus Liebigs Annalen der Chemie*, 1973, **1973**, 1421-1429.
265. M. Eberhardt and P. Théato, *Macromolecular rapid communications*, 2005, **26**, 1488-1493.
266. M. Eberhardt, R. Mruk, R. Zentel and P. Théato, *European Polymer Journal*, 2005, **41**, 1569-1575.
267. L. Nuhn, S. Hartmann, B. Palitzsch, B. Gerlitzki, E. Schmitt, R. Zentel and H. Kunz, *Angewandte Chemie International Edition*, 2013, **52**, 10652-10656.
268. D. Varadharajan and G. Delaittre, *Polymer Chemistry*, 2016, **7**, 7488-7499.
269. K. Nilles and P. Theato, *European Polymer Journal*, 2007, **43**, 2901-2912.
270. G. Moad, E. Rizzardo and S. H. Thang, *Polymer International*, 2011, **60**, 9-25.
271. J.-M. Noy, A.-K. Friedrich, K. Batten, M. N. Bhebhe, N. Busatto, R. R. Batchelor, A. Kristanti, Y. Pei and P. J. Roth, *Macromolecules*, 2017, **50**, 7028-7040.
272. A. Das and P. Theato, *Macromolecules*, 2015, **48**, 8695-8707.
273. P. R. Bachler, K. E. Forry, C. A. Sparks, M. D. Schulz, K. B. Wagener and B. S. Sumerlin, *Polymer Chemistry*, 2016, **7**, 4155-4159.
274. Y. Zhu, J.-M. Noy, A. B. Lowe and P. J. Roth, *Polymer Chemistry*, 2015, **6**, 5705-5718.
275. G. Wilaiporn, Z. Hui, K. Suda, T. Patrick and H. V. P., *Journal of Polymer Science Part A: Polymer Chemistry*, 2015, **53**, 1103-1113.
276. P. A. Woodfield, Y. Zhu, Y. Pei and P. J. Roth, *Macromolecules*, 2014, **47**, 750-762.

277. C. Boyer and T. P. Davis, *Chemical Communications*, 2009, DOI: 10.1039/B910296E, 6029-6031.
278. P. J. Roth, K. T. Wiss, R. Zentel and P. Theato, *Macromolecules*, 2008, **41**, 8513-8519.
279. M. I. Gibson, E. Fröhlich and H. A. Klok, *Journal of Polymer Science Part A: Polymer Chemistry*, 2009, **47**, 4332-4345.
280. M. Beija, Y. Li, A. B. Lowe, T. P. Davis and C. Boyer, *European Polymer Journal*, 2013, **49**, 3060-3071.
281. J. Xu, S. Shanmugam, H. T. Duong and C. Boyer, *Polymer Chemistry*, 2015, **6**, 5615-5624.
282. K. Nilles and P. Theato, *Journal of Polymer Science Part A: Polymer Chemistry*, 2010, **48**, 3683-3692.
283. H. Son, J. Ku, Y. Kim, S. Li and K. Char, *Biomacromolecules*, 2018, **19**, 951-961.
284. B. Couturaud, P. G. Georgiou, S. Varlas, J. R. Jones, M. C. Arno, J. C. Foster and R. K. O'Reilly, *Macromolecular rapid communications*, 2019, **40**, 1800460.
285. A. Das and P. Theato, *Chemical Reviews*, 2016, **116**, 1434-1495.
286. N. K. Singha, M. I. Gibson, B. P. Koiry, M. Danial and H.-A. Klok, *Biomacromolecules*, 2011, **12**, 2908-2913.
287. Y. Lee, Doctor of Philosophy, Seoul University, 2016.
288. Y. Lee, J. Pyun, J. Lim and K. Char, *Journal of Polymer Science Part A: Polymer Chemistry*, 2016, **54**, 1895-1901.
289. L. Q. Xu, K.-G. Neoh, E.-T. Kang and G. D. Fu, *Journal of Materials Chemistry A*, 2013, **1**, 2526-2532.
290. X. S. Li, L. H. Gan and Y. Y. Gan, *Polymer*, 2008, **49**, 1879-1884.
291. P. Rejmanová, J. Labský and J. Kopeček, *Die Makromolekulare Chemie*, 1977, **178**, 2159-2168.
292. J. Labský and J. Kálal, *European Polymer Journal*, 1979, **15**, 167-171.
293. S. Thamizharasi, P. Gnanasundaram and S. Balasubramanian, *Journal of Macromolecular Science—Pure and Applied Chemistry*, 1998, **35**, 1835-1852.
294. S. Thamizharasi, P. Gnanasundaram and S. Balasubramanian, *Journal of applied polymer science*, 2003, **88**, 1817-1824.
295. S. Thamizharasi, P. Gnanasundaram, K. V. Rao and A. V. R. Reddy, *European polymer journal*, 1996, **32**, 105-109.
296. I. Pulko, M. Sandholzer, M. Kolar, C. Slugovc and P. Krajnc, *Tetrahedron Letters*, 2010, **51**, 5827-5829.
297. S. Thamizharasi, P. Gnanasundaram and B. Reddy, *Journal of applied polymer science*, 1997, **65**, 1285-1291.
298. T. Narasimhaswamy, N. T. Murthy, S. C. Sumathi and B. S. R. Reddy, *Die Angewandte Makromolekulare Chemie*, 1993, **213**, 21-32.
299. T. Narasimhaswamy, S. C. Sumathi, B. S. R. Reddy and G. D. Devasagayam, *Polymer International*, 1992, **27**, 75-80.
300. R. Ruschel Campedelli, M. H. Keller, G. Pinheiro, C. E. M. Campos, L. Zaramello and B. Silveira de Souza, *The Journal of Organic Chemistry*, 2019, DOI: 10.1021/acs.joc.9b01122.
301. Y. Liu, L. Wang and C. Pan, *Macromolecules*, 1999, **32**, 8301-8305.

302. Y.-C. Hu, Y. Liu and C.-Y. Pan, *Journal of Polymer Science Part A: Polymer Chemistry*, 2004, **42**, 4862-4872.
303. J. Hwang, R. C. Li and H. D. Maynard, *Journal of Controlled Release*, 2007, **122**, 279-286.
304. J. Warneke, Z. Wang, M. Zeller, D. Leibfritz, M. Plaumann and V. A. Azov, *Tetrahedron*, 2014, **70**, 6515-6521.
305. J. P. Mendes, F. Branco, C. M. R. Abreu, P. V. Mendonça, A. C. Serra, A. V. Popov, T. Guliashvili and J. F. J. Coelho, *ACS Macro Letters*, 2014, **3**, 858-861.
306. N. H. Nguyen, B. M. Rosen, G. Lligadas and V. Percec, *Macromolecules*, 2009, **42**, 2379-2386.
307. M. E. Levere, N. H. Nguyen, X. Leng and V. Percec, *Polymer Chemistry*, 2013, **4**, 1635-1647.
308. U. Domańska, W. C. Moollan and T. M. Letcher, *Journal of Chemical & Engineering Data*, 1996, **41**, 261-265.
309. Y. Zhang, Y. Wang, C.-h. Peng, M. Zhong, W. Zhu, D. Konkolewicz and K. Matyjaszewski, *Macromolecules*, 2012, **45**, 78-86.
310. Y. Lee, S. Hanif, P. Theato, R. Zentel, J. Lim and K. Char, *Macromolecular Rapid Communications*, 2015, **36**, 1089-1095.
311. T. Pintauer, J. Qiu, G. Kickelbick and K. Matyjaszewski, *Inorganic chemistry*, 2001, **40**, 2818-2824.
312. G. Kickelbick, T. Pintauer and K. Matyjaszewski, *New Journal of Chemistry*, 2002, **26**, 462-468.
313. N. Chan, M. F. Cunningham and R. A. Hutchinson, *Polymer Chemistry*, 2012, **3**, 486-497.
314. L. Charles, *Mass spectrometry reviews*, 2014, **33**, 523-543.
315. N. K. Singha, S. Rimmer and B. Klumperman, *European polymer journal*, 2004, **40**, 159-163.
316. H. Sato, Y. Ishii, H. Momose, T. Sato and K. Teramoto, *Mass Spectrom (Tokyo)*, 2013, **2**, A0014-A0014.
317. X. Jiang, B. M. Rosen and V. Percec, *Journal of Polymer Science Part A: Polymer Chemistry*, 2010, **48**, 2716-2721.
318. S. Harrisson and J. Nicolas, *ACS Macro Letters*, 2014, **3**, 643-647.
319. K. A. Gunay, N. Schuwer and H.-A. Klok, *Polymer Chemistry*, 2012, **3**, 2186-2192.
320. F. D. Jochum and P. Theato, *Polymer*, 2009, **50**, 3079-3085.
321. L. Francesch, S. Borros, W. Knoll and R. Förch, *Langmuir*, 2007, **23**, 3927-3931.
322. H. Teng, L. Yang, F. Mikes, Y. Koike and Y. Okamoto, *Polymers for Advanced Technologies*, 2007, **18**, 453-457.
323. K. Koike, T. Kado, Z. Satoh, Y. Okamoto and Y. Koike, *Polymer*, 2010, **51**, 1377-1385.
324. R. SOLTANMORADĪ and M. H. NASĪRTABRĪZĪ, *Cumhuriyet Üniversitesi Fen-Edebiyat Fakültesi Fen Bilimleri Dergisi*, 2015, **36**, 1664-1673.
325. T. G. F. Jr. and P. J. Flory, *Journal of Applied Physics*, 1950, **21**, 581-591.
326. J. M. G. Cowie and P. M. Toporowski, *European Polymer Journal*, 1968, **4**, 621-625.
327. S. Noel, B. Liberelle, L. Robitaille and G. De Crescenzo, *Bioconjugate Chemistry*, 2011, **22**, 1690-1699.
328. S. Yamamoto, M. Ejaz, Y. Tsujii, M. Matsumoto and T. Fukuda, *Macromolecules*, 2000, **33**, 5602-5607.

329. T. Wu, K. Efimenko and J. Genzer, *Journal of the American Chemical Society*, 2002, **124**, 9394-9395.
330. D. Quéré, *Physica A: Statistical Mechanics and its Applications*, 2002, **313**, 32-46.
331. B. Deng, E. F. Palermo and Y. Shi, *Polymer*, 2017, **129**, 105-116.
332. S. Turgman-Cohen and J. Genzer, *Journal of the American Chemical Society*, 2011, **133**, 17567-17569.
333. H. Liu, B. Lepoittevin, C. Roddier, V. Guerineau, L. Bech, J.-M. Herry, M.-N. Bellon-Fontaine and P. Roger, *Polymer*, 2011, **52**, 1908-1916.
334. N. Erkan, G. Ayranci and E. Ayranci, *Food chemistry*, 2008, **110**, 76-82.
335. I. P. Kaur and A. Saini, *Mutation Research/Genetic Toxicology and Environmental Mutagenesis*, 2000, **470**, 71-76.
336. R. Joshi, M. S. Kumar, K. Satyamoorthy, M. Unnikrisnan and T. Mukherjee, *Journal of agricultural and food chemistry*, 2005, **53**, 2696-2703.
337. S. Sharma and I. P. Kaur, *International journal of dermatology*, 2006, **45**, 200-208.
338. A. Kuhad and K. Chopra, *Experimental brain research*, 2008, **185**, 411-420.
339. G. J. Kapadia, M. A. Azuine, H. Tokuda, M. Takasaki, T. Mukainaka, T. Konoshima and H. Nishino, *Pharmacological Research*, 2002, **45**, 499-505.
340. S. G. Khokarale and J.-P. Mikkola, *RSC Advances*, 2018, **8**, 18531-18541.
341. M. Mirghani, Y. C. Man, S. Jinap, B. Baharin and J. Bakar, *Journal of the American Oil Chemists' Society*, 2003, **80**, 1-4.
342. J. Xu, F. Zhou, B.-P. Ji, R.-S. Pei and N. Xu, *Letters in Applied Microbiology*, 2008, **47**, 174-179.
343. D. J. Guo and H. L. Li, *Carbon*, 2005, **43**, 1259-1264.
344. C. Zhou, S. Zhang, M. Nanamori, Y. Zhang, Q. Liu, N. Li, M. Sun, J. Tian, P. P. Ye, N. Cheng, R. D. Ye and M.-W. Wang, *Molecular Pharmacology*, 2007, **72**, 976.
345. S. S. C. Yu, E. S. Q. Tan, R. T. Jane and A. J. Downard, *Langmuir*, 2007, **23**, 11074-11082.
346. J. Geiger, N. Barroca and R. R. Schmidt, *Synlett*, 2004, **2004**, 0836-0840.
347. A. Potron, L. Poirel and P. Nordmann, *International Journal of Antimicrobial Agents*, 2015, **45**, 568-585.
348. S. Y. C. Tong, J. S. Davis, E. Eichenberger, T. L. Holland and V. G. Fowler, *Clinical Microbiology Reviews*, 2015, **28**, 603.
349. I. Horcas, R. Fernández, J. M. Gómez-Rodríguez, J. Colchero, J. Gómez-Herrero and A. M. Baro, *Review of Scientific Instruments*, 2007, **78**, 013705.

Modifications de polymères et de surfaces à visées antibactériennes

La contamination microbienne des surfaces est l'une des préoccupations majeures des secteurs d'activités comme l'industrie agro-alimentaire, la santé publique et les milieux hospitaliers. Face aux problèmes de santé publique liés à contamination bactérienne sur les surfaces, la préparation de surfaces aux propriétés antibactériennes est devenue un intérêt de recherche majeur pour de nombreux scientifiques et ce, dans de nombreux domaines de recherches. Du point de vue de la chimie, des matériaux et de la microbiologie, la fonctionnalisation des surfaces de matériaux polymères préexistants sans altérer leur propriété initiale est une solution séduisante. Pour cela, développer des nouveaux matériaux antibactériens/antifouling où la surface serait fonctionnalisée par des polymères antimicrobiens, greffés de manière robuste *i.e.* de façon covalente représente une solution idéale. Afin de faciliter et d'accélérer le processus de criblage, il est proposé dans ce travail une nouvelle approche pour obtenir des polymères ayant des propriétés antimicrobiennes à la fois en solution et à partir de la surface. Ce travail comprend une étude de (co)-polymérisations contrôlées d'esters actifs servant d'intermédiaires pouvant être post-modifiés pour synthétiser des polymères d'intérêts présentant les caractéristiques antimicrobiennes attendues.

La thèse présentée est un contenu de 6 chapitres. Le premier chapitre est consacré à une étude bibliographique en lien avec le sujet développé. Le chapitre 2 concerne la polymérisation en solution des deux méthacrylates sélectionnés : le méthacrylate de pentafluorophényle (PFMA) et méthacrylate de para-nitrophényle (NPMA). Le chapitre 3 décrit la polymérisation amorcée en surface des mêmes monomères esters actifs sur des surfaces de poly (téréphtalate d'éthylène) (PET). Les résultats de polymérisation présentés dans les chapitres 2 et 3 sont conséquents. Plusieurs techniques expérimentales ont été utilisées pour caractériser les matériaux obtenus et une discussion critique a été menée dans tous les cas. Une analyse minutieuse des résultats a permis de montrer que la polymérisation radicalaire contrôlée des esters actifs en présence de cuivre (0)/cuivre (II) était possible. En suit, les chapitres 4 et 5 décrivent les réactions post-polymérisation effectuées sur les polyméthacrylates précédemment synthétisés et sur les PET greffés par des polyméthacrylates, respectivement. Le PPFMA a ainsi été mis en réaction avec des amines, des alcools dérivés d'huiles essentielles et des saccharides. Des dérivés d'huiles essentielles ont également été considérés puisque les polymères ont été modifiés par du sesamol, geraniol, ou la combinaison des deux. Les produits obtenus ont été caractérisés par chromatographie d'exclusion stérique, spectroscopie infrarouge et XPS. Les différentes techniques de caractérisation ont permis de montrer que les réactions de post-polymérisation fonctionnaient très bien avec des taux de conversion toujours supérieurs à 90%. Le PNPMA a également été modifié par la *n*-butylamine. Enfin, les copolymères préparés à partir des deux esters actifs

ont pu être modifiés en présence de *n*-butylamine et les résultats obtenus ont permis de prouver que le groupement pentafluorophényle était plus réactif que le *p*-nitrophényle. Le chapitre 5 décrit la modification des polymères PFPMA greffés en surface du PET. Ces surfaces modifiées ont été testées contre deux bactéries modèles telles que *Staphylococcus aureus* et *Pseudomonas aeruginosa*.

En résumé, ce travail démontre que la polymérisation radicalaire contrôlée en présence de Cu(0)/Cu(II) est une technique appropriée qui permet de préparer facilement des (co)-polymères réactifs, en solution mais aussi à partir de surface de poly (téréphtalate d'éthylène), communément appelé PET. Dans un premier temps, nous aborderons l'étude de la polymérisation contrôlée du PFPMA, avec son optimisation en solution, puis à partir de surface du PET porteuse de groupement d'amorçage. De plus, la polymérisation du NPMA sera également examinée, ainsi que la copolymérisation des deux esters actifs là-encore par polymérisation de type contrôlée en présence de Cu(0)/Cu(II). La post-modification des polymères activés est ensuite présentée. La post-modification s'est révélée efficace et facile à mettre en œuvre. La structure et les caractéristiques des polymères obtenus ont été analysées et confirmées. Il est à noter que la post-modification a pu être effectuée par un processus séquentiel avec une fonctionnalisation simple ou avec plusieurs huiles essentielles, qui possèdent des propriétés naturelles antibactériennes ou antioxydantes. Différents films de PET ont été modifiés, des polymères aux propriétés anti-adhérentes ont été greffés par cette même méthodologie. Ces surfaces modifiées ont été testées contre deux bactéries modèles afin de déterminer si les modifications de surface ont conféré au film de PET les propriétés biologiques attendues.

Titre : Modifications de polymères et de surfaces à visées antibactériennes

Mots clés : polymérisation contrôlée, polymères réactifs, molécules bio-sourcées, antibactérien, anti-biofilm

Résumé : La contamination microbienne des surfaces est l'une des préoccupations majeures des secteurs d'activités comme l'industrie agro-alimentaire, la santé publique et les milieux hospitaliers. Face aux problèmes de santé publique liés à contamination bactérienne sur les surfaces, la préparation de surfaces aux propriétés antibactériennes est devenue un intérêt de recherche majeur pour de nombreux scientifiques et ce, dans de nombreux domaines de recherches. Du point de vue de la chimie, des matériaux et de la microbiologie, la fonctionnalisation des surfaces de matériaux polymères préexistants sans altérer leur propriété initiale est une solution séduisante. Pour cela, développer des nouveaux matériaux antibactériens/antifouling où la surface serait fonctionnalisée par des polymères antimicrobiens, greffés de manière robuste *i.e.* de façon covalente représente une solution idéale. Afin de faciliter et d'accélérer le processus de criblage, il est proposé dans ce travail une nouvelle approche pour obtenir des polymères ayant des propriétés antimicrobiennes à la fois en solution et à partir de la surface. Ce travail comprend une étude de (co)-polymérisations contrôlées d'esters actifs servant d'intermédiaires pouvant être post-modifiés pour synthétiser des polymères d'intérêts présentant les caractéristiques antimicrobiennes attendues.

Ce travail démontre que la polymérisation radicalaire contrôlée en présence de Cu(0)/Cu(II) est une technique appropriée qui permet de préparer facilement des (co)-polymères réactifs, en solution mais aussi à partir de surface de poly (téréphtalate d'éthylène), communément appelé PET. Dans un premier temps, nous aborderons l'étude de la polymérisation contrôlée du méthacrylate de pentafluorophényle (PFPMA), avec son optimisation en solution, puis à partir de surface du PET porteuse de groupement d'amorçage. De plus, la polymérisation du méthacrylate de p-nitrophényle (NPMA) sera également examinée, ainsi que la copolymérisation des deux esters actifs là-encore par polymérisation de type contrôlée en présence de Cu(0)/Cu(II). La post-modification des polymères activés est ensuite présentée. La post-modification s'est révélée efficace et facile à mettre en œuvre. La structure et les caractéristiques des polymères obtenus ont été analysées et confirmées. Il est à noter que la post-modification a pu être effectuée par un processus séquentiel avec une fonctionnalisation simple ou avec plusieurs huiles essentielles, qui possèdent des propriétés naturelles antibactériennes ou antioxydantes. Différents films de PET ont été modifiés, des polymères aux propriétés anti-adhérentes ont été greffés par cette même méthodologie. Ces surfaces modifiées ont été testées contre deux bactéries modèles telles que *Staphylococcus aureus* et *Pseudomonas aeruginosa* afin de déterminer si les modifications de surface ont conféré au film de PET les propriétés biologiques attendues.

Title: Polymer and surface modifications for antibacterial purposes

Keywords: Controlled polymerization, reactive polymer, bio-based molecules, antibacterial, anti-biofilm

Abstract: Microbial contamination on surfaces has become major concern in various areas including industrial process as well as public health and hospitalization. Being aware of several problems causing by adherence and attachment of bacteria on a surface, preparation of antibacterial surface has become a global research interest for researchers in many domains. From the chemistry integrated with material science and microbiology point of view, functionalization of existing polymeric material surfaces is an attractive solution. In this domain, the surface functionalized with covalently grafted antimicrobial polymers represents an ideal solution. In order to facilitate the screening process, it is proposed in this particular research a new approach to obtain polymers with antimicrobial properties both in solution and from surface. The present approach includes a study in controlled (co)polymerization of active ester(s) serving as intermediate templates that can be eventually modified by polymer post-modification process to fabricate polymer of interest with expected antimicrobial characteristics.

In general, it is demonstrated herein that the use of Cu(0)-mediated reversible deactivation radical polymerization (RDRP) is a suitable technique that allows facile preparation of reactive (co)polymers in solution and from surface of poly(ethylene terephthalate). First of all, this thesis focused on the study of controlled polymerization of pentafluorophenyl methacrylate (PFPMA) which appeared to be challenging. Furthermore, along with the optimization of polymerization in solution was the investigation of surface-initiated polymerization of this monomer from PET surface. Besides, polymerization of p-nitrophenyl methacrylate (NPMA) and copolymerization of the two active esters by Cu(0)-mediated RDRP were also examined. In addition, polymer post-modification of obtained (co)polymers with various compounds had been proven to be efficient and easy to perform. The structure and characteristics of obtained products were confirmed to match with expectations. It is remarkable that the post-modification can be done as sequential process, single or dual functionalization with several different essential oils, which are natural antibacterial or antioxidant compounds. On the other hand, the success in polymerization and post-modification of polymer of active esters in solution allowed the fabrication of different PET film grafted with polymers that are envisaged to have antiadhesion properties. Attempts to test such properties were also done against two model bacteria including *Staphylococcus aureus* and *Pseudomonas aeruginosa* to investigate if expectations are valid.